Durham University

Durham E-Theses

Novel Organometallic Mixed Valence Complexes

NEIL JOHN BROWN

How to cite:

BROWN, NEIL JOHN (2010) Novel Organometallic Mixed Valence Complexes. Doctoral thesis, Durham University.

Use policy

The full-text may be used and/or reproduced, and given to third parties in any format or medium, without prior permission or charge, for personal research or study, educational, or not-for-profit purposes provided that:

- a full bibliographic reference is made to the original source
- a https://etheses.durham.ac.uk/id/eprint/417/ is made to the metadata record in Durham E-Theses
- the full-text is not changed in any way

The full-text must not be sold in any format or medium without the formal permission of the copyright holders.

Please consult the full Durham E-Theses policy for further details.

Academic Support Office, The Palatine Centre, Durham University, Stockton Road, Durham, DH1 3LE
e-mail: e-theses.admin@durham.ac.uk Tel: +44 0191 334 6107
https://etheses.durham.ac.uk

Statement of Copyright

The copyright of this thesis rests with the author. No quotation from it should be published in any form, including electronic and the internet, without the author's prior written consent and information derived from it should be acknowledged appropriately.

Declaration

The work described in this thesis was carried out at the University of Durham, Department of Chemistry, between October 2007 and September 2010. All the work is that of the author unless stated otherwise, and it has not been submitted for a degree at this or any other university.

Memorandum

Part of this work has been the subject of the following published articles:

Electronic interaction between and through covalently-bonded polymetallic complexes.

P.J. Low, N.J. Brown. *J. Cluster Sci., doi:10.1007/s10876-010-0328-4.*

Spectroscopic properties and electronic structure of the cycloheptatrienyl molybdenum alkynyl complexes $[Mo(C{\equiv}CR)(Ph_2PCH_2CH_2PPh_2)(\eta\text{-}C_7H_7)]^{n+}$ (n = 0 or 1; R = Bu^t, Fc, CO_2Me, or C_6H_4-4-X, X = NH_2, OMe, Me, H, CHO, CO_2Me).

N.J. Brown, D. Collison, R. Edge, E.C. Fitzgerald, M. Helliwell, J.A.K. Howard, H.N. Lancashire, P.J. Low, J.J.W. McDouall, J. Raftery, C.A. Smith, D.S. Yufit, M.W. Whiteley. *Organometallics,* 2010, **29**, 1261.

Metal Stabilised diynyl radical: structure and reactivity of $Mo(C{\equiv}CC{\equiv}CSiMe_3)L_2(\eta\text{-}C_7H_7)]^{\cdot+}$ (L_2 = 2,2'-bipyridine or dppe).

N.J. Brown, D. Collison, R. Edge, E.C. Fitzgerald, P.J. Low, M. Helliwell, Y.T. Ta, M.W. Whiteley. *Chem. Commun.,* 2010, **46**, 2253.

The synthesis and structures of mono- and di-bromovinylidenes.

N.J. Brown, M.A. Fox, M.E. Smith, D.S. Yufit, J.A.K. Howard, P.J. Low. *J. Organomet. Chem.,* 2009, **694**, 4042.

The preparation and characterization of ruthenium cyanovinylidene complexes.

N.J. Brown, P.K. Eckert, M.A. Fox, D.S. Yufit, J.A.K. Howard and P.J. Low. *Dalton Trans.,* 2008, 433.

Part of this work has been the subject of the following presentations:

39th International Coordination Chemistry Conference

Adelaide, Australia: July 2010

Poster entitled: Cyanoligand chemistry: A versatile synthesis of cyanovinylidenes to cyanoacetylides

24th International Conference of Organometallic Chemistry

Taipei, Taiwan: July 2010

Poster entitled: A bis-ethynylcarborane bridged bimetallic molybdenum complex: In search of 'genuine' organometallic mixed valency

Universities of Scotland Inorganic Chemistry Conference

University of Durham: England. July 2010

Poster entitled: A bis-ethynylcarborane bridged bimetallic molybdenum complex: In search of 'genuine' organometallic mixed valency

Synthetic Seminar Series

University of Durham, England: December 2009

Lecture entitled: Monometallic and bimetallic molybdenum acetylide complexes

Universities of Scotland Inorganic Chemistry Conference

Heriot-Watt University, Scotland: September 2009

Lecture entitled: Synthesis, spectroscopic properties and electronic structure of a series of molybdenum acetylide complexes

EPR User Service Meeting

University of Manchester, England: May 2009

Poster entitled: Spectroscopic properties and electronic structure of cycloheptatrienyl molybdenum alkynyl complexes

5th Chianti Electrochemistry Meeting

University of Sienna, Italy: July 2008

Poster entitled: Synthetic, spectroelectrochemical and computational studies of electron-rich acetylide complexes $Mo(C{\equiv}CC_6H_4X)(dppe)(\eta^7\text{-}C_7H_7)$ and $Ru(C{\equiv}CC_6H_4X)(bipy)(\eta^5\text{-}C_5Me_5)$

Abstract

Organometallic mixed valence complexes have been studied extensively over the past 30 years providing many synthetic and theoretical challenges. This thesis has sought to provide the field with a unique family of mixed valence complexes through which theories of electron transfer in weakly coupled systems can be tested. The metal fragment Mo(dppe)(η^7-C_7H_7) is unique amongst its half-sandwich counterparts providing low formal oxidation states and a well resolved EPR signal and forms the basis of these studies.

Before undertaking a study of the electronic structure of [{(Mo(dppe)(η^7-C_7H_7)}$_2${μ-C≡CXC≡C}]$^{n+}$ systems, and associated issues regarding mixed valence characteristics and carbon-chain mediated metal-metal interactions, mono-metallic molybdenum acetylide complexes that serve as model systems were studied in detail and their electronic structure fully rationalised. Thus, in Chapter two, a range of *para* substituted molybdenum aryl acetylides, Mo(C≡CC_6H_4X-4)(dppe)(η^7-C_7H_7), featuring a range of electron-donating and -withdrawing substituents, are described. These compounds have been studied using a range of spectroscopic, crystallographic, electrochemical, spectroelectrochemical, and computational techniques establishing metal centred oxidation character. This is a consequence of cycloheptatrienyl ring destabilising the filled d_{z2} metal d-orbtial which then forms the HOMO. The poor symmetry match of this d_{z2} orbital and the alkynyl π-system effectively decouples the molybdenum fragment from the alkynyl substituent.

As a precursor to the synthesis and understanding of bi-metallic complexes containing all-carbon bridging moieties, a series of mono-metallic compounds containing diynyl and triynyl ligands have been studied in Chapter three. The subsequent elucidation of the influence of the length of the carbon chain on the electronic structure has been studied using a combination of spectroelectrochemical and computational techniques. These studies reveal that the length of the carbon chain, and the identity of the supporting ligand, (bipyridine or dppe) increases the chain character of the frontier orbitals.

Homo-bimetallic complexes containing a bis(ethynyl) substituted *para*-carborane bridging moiety were synthesised (Chapter four) together with the monometallic complex $Mo(C{\equiv}CC_2B_{10}H_{11})(dppe)(\eta^7\text{-}C_7H_7)$. The mono-metallic complex was first synthesised and studied to establish how the ethynyl carborane affects the electronic structure of the $Mo(dppe)(\eta^7\text{-}C_7H_7)$ centre and the nature of interaction between the molybdenum centre, the ethynyl fragment and the carborane cage. This preliminary work was followed by the synthesis of the bimetallic complex, $[\{Mo(dppe)(\eta^7\text{-}C_7H_7)\}_2\{\mu\text{-}C{\equiv}C(C_2B_{10}H_{10})C{\equiv}C\}]$. Using a range of spectroscopic, spectroelectrochemical and computational techniques the electronic structure, and charge transfer process of $[\{Mo(dppe)(\eta^7\text{-}C_7H_7)\}_2\{\mu\text{-}C{\equiv}C(C_2B_{10}H_{10})C{\equiv}C\}]^{n+}$ (n = 0, 1 or 2) have been explored. The monocation $[\{Mo(dppe)(\eta^7\text{-}C_7H_7)\}_2\{\mu\text{-}C{\equiv}C(C_2B_{10}H_{10})C{\equiv}C\}]^{+}$ has shown to be a genuine example of a valence trapped, weakly coupled mixed valence complex allowing conventional descriptions of the intervalence transition to be compared with TD-DFT based interpretations.

The literature surrounding the area of poly-carbon ligand chemistry indicates that the butadiyndiyl bridging moiety is an efficient conduit for electron transfer, due to its two orthogonal π-systems that span across the entirety of the ligand, leading to systems which are generally delocalised. An investigation of the mixed valence complex, $[\{Mo(dppe)(\eta^7\text{-}C_7H_7)\}_2(\mu\text{-}C{\equiv}CC{\equiv}C)]^+$ reveals a weakly coupled, localised mixed valence electronic structure, which is unique amongst its poly-carbon counterparts (Chapter five). Through using a range of spectroscopic timescales (EPR /IR /UV /vis) the rate of electron transfer has been estimated. To fully account for the number of transitions in the NIR region and the shape of the resulting absorption bands, it is necessary to employ a three state approximation (which explicity indicates the bridge state) when describing the electron transfer process.

The complex $[\{Mo(dppe)(\eta^7\text{-}C_7H_7)\}_2\{\mu\text{-}C{\equiv}C(C_6H_4)C{\equiv}C\}]^{n+}$ has been studied using a range of spectroscopic, electrochemical and computational methods to establish the nature and rate of electron transfer of the mixed valence complex (Chapter six). It has been demonstrated that the 1,4-diethynylbenzene bridge mixes more efficiently with the $Mo(dppe)(\eta^7\text{-}C_7H_7)$ than the 1,3-butadiyndiyl bridge. Spectroscopic analysis revealed a moderately coupled, localised mixed valence complex, where the rate of electron transfer is much faster than the diynyl complex but not faster than the infrared spectroscopy timescale. The application of the three state model in the description of the charge transfer process allows the increased electron transfer rate to be explained through the increased mixing of the bridge with the $Mo(dppe)(\eta^7\text{-}C_7H_7)$ moiety, characterised by the lowering of the LMCT transition in comparison to carboranyl and diynyl containing complexes.

Metal complexes containing the cyanoacetylide moiety, C≡CC≡N, have been known for several decades, but despite the obvious synthetic advantages of cyanoacetylide as a bridging moiety compared to a butadiyndiyl bridge, C≡CC≡C, the C≡CC≡N ligand has been largely ignored. Chapter seven summarises attempts made to provide a convenient route to complexes containing the cyanoacetylide moiety so that a greater variety bimetallic complexes can be synthesised, thus allowing the investigation of the charge transfer characteristics of $[\{L_xM\}(\mu\text{-}C{\equiv}CC{\equiv}N)\{ML_x\}]^{n+}$ complexes. Reactions of cyanogen bromide with metal acetylide complexes yield novel mono- and di-bromovinylidenes rather than cyano containing complexes. The cyanation reagent of choice is 1-cyano-4-dimethylaminopyridinium tetrafluoroborate ($[CAP]BF_4$) which allows the ready synthesis of mono- and di-cyanovinylidenes, as well as the synthesis of cyanoacetylide containing complexes. The cyanating agent $[CAP]BF_4$ is able to cyanate a range of metal acetylides, thus expanding the number of potential bimetallic complexes. The hetero-bimetallic complex $[\{Fe(dppe)(\eta^5\text{-}C_5H_5)\}(\mu\text{-}C{\equiv}CC{\equiv}N)\{Mo(dppe)(\eta^7\text{-}C_7H_7)\}]PF_6$ has been synthesised and studied using a range of techniques and has demonstrated that the cyanoacetylide bridge promotes a more delocalised electronic structure for dicationic complexes than is found for the other ethynyl based ligands described in this thesis.

Acknowledgements

Firstly, I would like to thank Dr. Paul J. Low for giving me the opportunity to carry out my research under his supervision and for his advice throughout my PhD. I would also like to extend my gratitude to Dr. Mark W. Whiteley for the fruitful collaborations and for his expertise in the handling of the often troublesome Mo(dppe)(η^7-C_7H_7) containing complexes. Thanks also to EPRSC for funding my PhD studentship.

I would also like to thank the current and former members of the Low group for their support over the years, in particular Dr. Julian D. Farmer, Miss Wing Y. Man and Mrs. Ella A. Long. For both training and advice on computational, spectroelectrochemical and synthetic techniques, regarding carborane chemistry, I am grateful to Dr. Mark A. Fox. I would like to thank Dr. Emma C. Fitzgerald and Miss. Hannah N. Lancashire from the Whiteley group and Dr. Ruth Edge from the National EPR centre, for their expertise concerning EPR spectroscopy and help in syntheses of the bi-metallic complexes. Thanks also to Dr. Dima S. Yufit for all the crystallography work carried out in the thesis and Dr. Andy Beeby and Dr. Lucas Applegarth for conducting the Raman spectroscopy experiments.

I would like to thank my family, especially my Mum, Dad and Kelly, and friends for their support and patience throughout my PhD. I also would like to thank my girlfriend Emma for spending days proof reading this thesis and always being there when I needed her most. Finally I would like to dedicate this thesis to my Gran.

Abbreviations

º	degrees
ºC	degrees Celsius
α	alpha
β	beta
δ	chemical shift
Δ	reflux / difference
ΔE	potential difference
ε	molar extinction coefficient
λ	wavelength
Å	angstrom
A	absorption
Ar	aryl
B	bridge
bipy	bipyridine
br	broad
Bu	butyl
^{t}Bu	tertiary butyl
B3LYP	Becke 3-parameter Lee-Yang-Parr
ca.	circa
cm	centimetres
cm^{-1}	wavenumbers (reciprocal centimetres)
CN	cyano
CV	cyclic voltammetry
d	doublet
dd	doublet of doublets
DFT	Density Functional Theory
dHpe	1,2-diphosphinoethane
dppe	1,2-bis(diphenylphosphino)ethane
E	potential
$E_{1/2}$	half-wave potential

EC	electrochemical
ES	electrospray
Et	ethyl
eV	electronvolts
F	Faraday constant
Fc	ferrocene
h	hour(s)
H_{ab}	Hamiltonian coupling constant
HF	Hartree Fock
HOMO	highest occupied molecular orbital
HOSO	highest occupied spin orbital
Hz	hertz
I	current
IR	infra-red
IVCT	intervalence charge transfer
K_c	comproportional constant
J	Joules
$^{n}J_{AB}$	n bound coupling constant between nuclei A and B
L	generic 2 electron ligand
LANL2DZ	Los Alamos National Laboratory double-ζ
LMCT	ligand-to-metal charge transfer
LUMO	lowest unoccupied molecular orbital
LUSO	lowest unoccupied spin orbital
m	medium
m	multiplet
M	metal / molarity
M	molecular ion
m/z	mass per unit charge
MALDI	Matrix-assisted laser desorption/ionisation
Me	methyl
MeCN	acetonitrile
MeOH	methanol
mg	milligrams
min	minutes

mL	millilitres
MLCT	metal-to-ligand charge transfer
mmol	millimoles
MO	molecular orbital
MPW1K	modified Perdew-Wang 1-parameter model for kinetics
mV	millivolts
MV	mixed-valence
$^{n}Bu_4NPF_6$	tetrabutylammonium hexafluorophosphate
NIR	near-infra-red
nm	nanometres
NMR	nuclear magnetic resonance
NO_2	nitrile
OAc	acetoxy
OMe	methoxy
Ph	phenyl
PPh_3	triphenylphosphine
ppm	part per million
^{i}Pr	isopropyl
q	quintet
R	general organic group
rt	room temperature
s^{-1}	reciprocal seconds
s	singlet (NMR)
s	strong (IR)
sh	shoulder
$SiMe_3$	trimethylsilyl group
SOMO	Singly Occupied Molecular Orbital
t	triplet
TD-DFT	Time Dependent Density Functional Theory
THF	tetrahydrofuran
TLC	thin layer chromatography
TMS	trimethylsilyl
TMSA	trimethylsilylacetylene
Tol	*para*- tolyl $C_6H_4CH_3$

UV-vis-NIR	ultraviolet-visible
V	volt(s)
w	weak
X	halide /substituents

Table of Contents

Chapter 1: Introduction

Chapter 2: Cycloheptatrienyl Molybdenum Alkynyl Complexes

Chapter 3: Molybdenum complexes bearing diynyl and triynyl ligands

Chapter 4: Cycloheptatrienyl Molybdenum Complexes of C,C'-Bis(ethynyl)carboranes

Chapter 5: Synthesis, Spectroscopy and Electronic Structure of $[\{Mo(dppe)(\eta^7\text{-}C_7H_7)\}_2(\mu\text{-}C{\equiv}CC{\equiv}C)]^{n+}$ (n = 0, 1, 2)

Chapter 6: Synthesis, Spectroscopy and Electronic Structure of $[\{Mo(dppe)(\eta^7\text{-}C_7H_7)\}_2\{\mu\text{-}C{\equiv}C(C_6H_4)C{\equiv}C\}]^{n+}$ (n = 0, 1, 2)

Chapter 1: Introduction

The exchange of electrons within and between chemical species is a fundamental process which underpins many physical and biological processes, ranging from the industrial refinement of aluminum using bulk electrolysis, to the movement of electrons within the photosystems of plants. As such, the study and exploitation of intra- and inter-molecular electron transfer is implicit in many different fields including the development of molecular devices,[1] the generation of luminescent materials and polymers,[2] understanding of biological processes such as ion pumps[3] and protein catalysis,[4] and the harnessing of solar energy.[5] Of particular interest to chemists is the transfer of a single electron between two sites in which no bonds are broken or formed, a process that may be regarded as the simplest form of electron transfer. In order to understand this phenomenon many varied techniques have been employed, such as the syntheses of model complexes in different formal oxidation states, ultra-fast and time-resolved spectroscopic techniques, Mössbauer spectroscopy, EPR spectroscopy and Stark spectroscopy. These various experimental results are supported by an equally diverse range of pure mathematical/theoretical treatments. The development and refinement of single electron transfer theory has been reviewed in several informative articles by prominent academics in the field.[6] Nevertheless, an overview of the primary elements of electron transfer processes, models and chemistry is given here in order for the reader to acquaint themselves with the concepts and, more importantly, the methods for investigating this fascinating process.

1.1 Single Electron Transfer Theory

The Franck-Condon principle, which states that the nuclear motion is always much slower than the electronic motion, at 10^{-13} s and 10^{-15} s respectively,[7] is essential to the understanding of electron transfer, whether by an inner-sphere or outer-sphere pathway. If an electron is spontaneously transferred from a site **A** to another site **B** in the same molecule, the product state will feature the two centres in the equilibrium geometry associated with the oxidation states prior to electron transfer, and thus be vibrationally excited (Figure 1). This spontaneous pathway is forbidden on the grounds of energy conservation. Thus, in the ground state for the electron transfer to take place the solvent must re-orientate and the nuclear configuration (including all translational, rotational and vibrational coordinates of the system as a whole) must re-arrange to allow an intermediate geometry (Figure 1, lower pathway) prior to the transfer of an electron from redox site **A** (Figure 1, state **X**) to redox site **B** (Figure 1, state **Y**). When **A** and **B** are chemically identical centres and differ only in their net oxidation state, there is no net change in the free energy of the complex after electron transfer has taken place. The inner and outer sphere reorganisation factors constitute an activation barrier, which is related to the reorganisation energy for the electron transfer process.

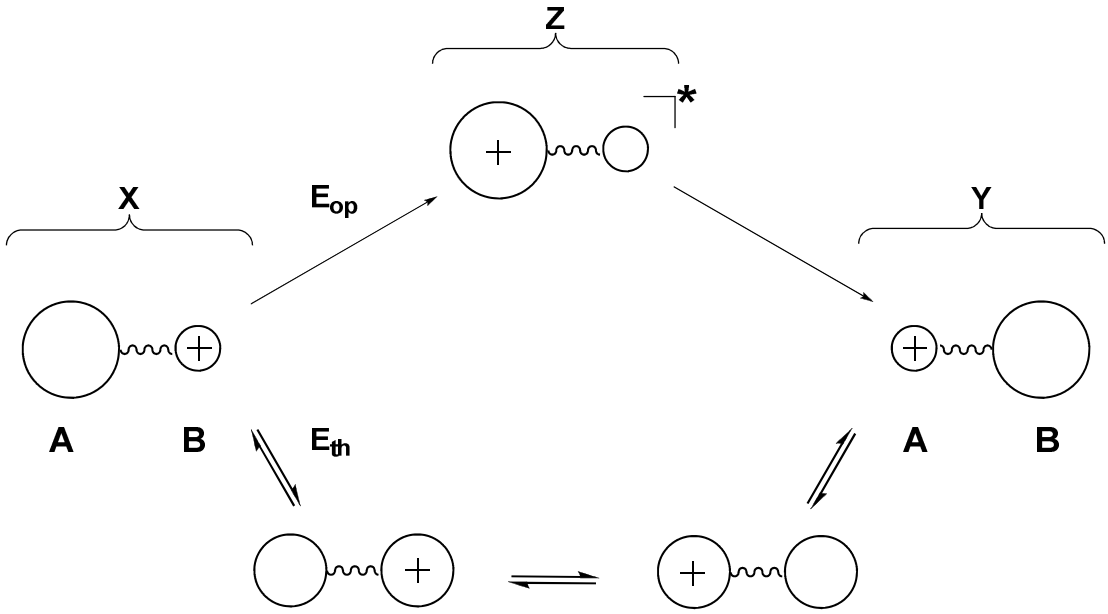

Figure 1: Schematic of single electron transfer between sites A and B, detailing thermal (E_{th}) and optical (E_{op}) routes. Where X, Y and Z refer to initial, final and transfer electronic states.

The simplest model devised to describe electron transfer is to consider a symmetrical system where the redox sites, **A** and **B**, are identical except for their respective oxidation states. This model has been termed the 'two state approximation' which has been considered in detail by Marcus and Hush and has been elaborated upon by others.[8] In its simplest model form the initial and final states, **X** and **Y**, can be described as two wavefunctions, $\psi_{\mathbf{X}}$ and $\psi_{\mathbf{Y}}$, and described in terms of free energy curves (Figure 2), which include the energies of the surrounding medium, when compared to a reaction coordinate which describes the nuclear configuration, nominally zero and one (**X** and **Y** respectively). When there is no interaction between the two sites **A** and **B**, the states **X** and **Y** do not mix and as such there is no electronic state or energetic pathway to facilitate the electron transfer between sites **A** and **B**.

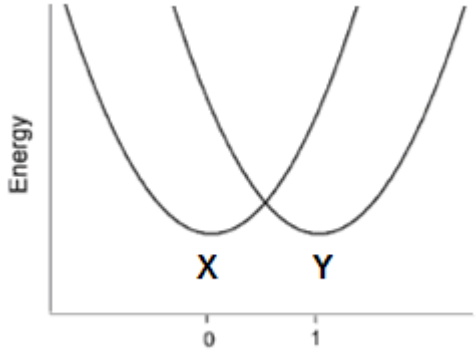

Figure 2: Potential energy plot of two non-interacting surfaces. Adapted figure from ref [6i] (Reproduced by permission of The Royal Society of Chemistry (RSC))

When there is a weak interaction between sites **A** and **B,** the two wavefunctions describing the initial and final states can mix, with the product states arising from linear combinations ψ_X and ψ_Y.

$$\psi_Z = C_X\psi_X + C_Y\psi_Y$$
$$\psi_{XY} = C_X\psi_Y - C_Y\psi_X$$

This gives rise to ground and excited adiabatic states (Figure 3). The ground state combination, **XY**, is characterised by two minimum, which correspond to initial state **X** and the final state **Y**. The barrier between these minimum gives rise to the description of the system in terms of localised valency at redox sites **A** and **B**.

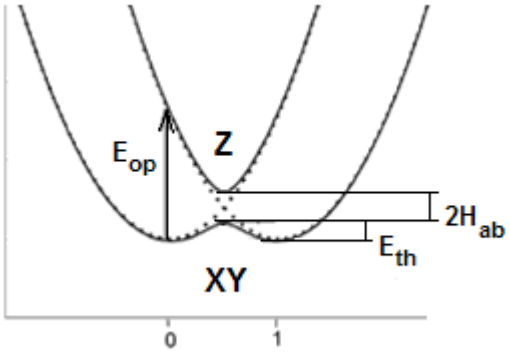

Figure 3: Marcus-Hush potential energy plot showing the interaction of states X and Y, resulting in the adiabatic state XY and Z. Adapted figure from ref [6i] (Reproduced by permission of The Royal Society of Chemistry (RSC))

From Figure 3, two pathways can be envisaged for electron transfer which relate to the upper and lower pathways in Figure 1. The first is a thermal (ground state) pathway for which the thermal barrier (E_{th}) must be overcome and provides the activation energy needed to re-arrange the complex into the requisite transition state. The second is an optical pathway which goes via the excited electronic state **Z** (Figure 1 and Figure 3) and requires a photon of energy ($h\nu = E_{op}$) which is equivalent to the reorganisational energy ($\lambda = E_{op}$). The two potential energy curves, **XY** and **Z**, are related to each other by an electronic coupling matrix element ($2H_{ab}$) which increases as the interaction between the two sites **A** and **B**.

In layman terms, complexes which can be described using this two-state model are generally termed mixed valence complexes (**MV**) which contain redox sites equivalent to the model sites **A** and **B**. Electrochemical methods are often used to determine the redox agents appropriate for generating the **MV** state from the homovalent precursor,[9] as well as to establish the thermodynamic stability of the product **MV** state, or, in the case of electrosynthesis or spectroelectrochemical methods, to define the potential necessary to generate the state of interest.

$$\mathbf{A\,B} \overset{E_1}{\rightleftharpoons} \mathbf{A^+\,B} \longleftrightarrow \mathbf{A\,B^+} \overset{E_2}{\rightleftharpoons} \mathbf{A^+\,B^+}$$

$$\Delta E_{1/2} = E_2 - E_1$$

Electrochemical techniques have been used extensively to monitor the progress of multi-electron processes, in which the $\Delta E_{1/2}$ values have been used, albeit not always wisely, as a guide to the degree of electronic interaction between the systems.[10] The mixed valence system ($\mathbf{A^+\,B} \leftrightarrow \mathbf{A\,B^+}$) is formed from the removal of a single electron

from the system (**A B**) at a potential E_1. Upon removal of a second electron at a potential E_2 the doubly oxidised system ($\mathbf{A^+ B^+}$) is formed.

$$[\mathbf{A\ B}] + [\mathbf{A^+\ B^+}] \underset{K_c}{\rightleftharpoons} 2[\mathbf{A^+\ B}]$$

$$K_c = \frac{[\mathbf{A^+B}]^2}{[\mathbf{AB}][\mathbf{A^+B^+}]}$$

$$K_c = \exp\left(\frac{\Delta E_{1/2} F}{RT}\right)$$

The difference between these formal potentials (E_1 and E_2) $\Delta E_{1/2}$ is that they are related to the comproportionation constant (K_c) which reflects the thermodynamic stability of a mixed valence state with respect to disproportionation. Using simple electrostatic arguments, the magnitude of $\Delta E_{1/2}$ and K_c should directly reflect the degree of electronic coupling between the two redox sites. If the two sites ($\mathbf{A^+\ B}$) are interacting strongly, the removal of an electron from the **MV** state will be thermodynamically unfavourable, as the site **B** experiences the charge at $\mathbf{A^+}$, thus causing an anodic shift in the potential of E_2 relative to E_1. Conversely, if two centres are weakly interacting, the removal of the electron from the **MV** state will be much easier. Therefore the $\Delta E_{1/2}$ value will be small and will be limited by a small statistical factor, 35.6 mV (K_c = 4 at 298 K).[11] The difficulties in extending this rather simplistic intereptation to 'real' systems are highlighted below.

Spectroscopically, a system which can be described using the two state model will have a characteristically identifiable transition usually in the NIR region of the spectrum, corresponding to E_{op}, which is termed an intervalence charge transfer transition (IVCT). Ideally the transition will take the form of a weak symmetric Gaussian shaped band, the energy of which will directly correspond to the E_{op} energy. From the transition band

parameters (half height band width, $\Delta\nu_{1/2}$, energy, E_{IVCT} or ν, and intensity, ε), the theoretical band width of the IVCT is calculated (Figure 4).

$$\Delta\nu_{1/2} = (2310\upsilon_{\max})^{1/2}$$

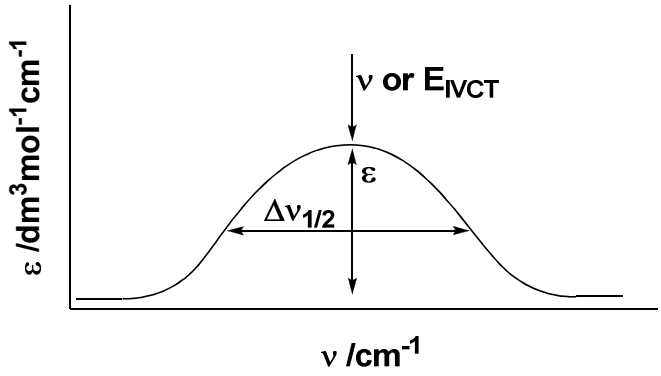

Figure 4: Model NIR band showing the band parameters.

The electronic coupling parameter (H_{ab}) can be calculated as below:

$$H_{ab} = \frac{\sqrt{(4.2\times10^{-4})\varepsilon\Delta\nu_{1/2}E_{IVCT}}}{r}$$

This shows how the electronic coupling of the two electronic states, **XY** and **Z** relates to the IVCT transition.[12] Combining the spectroscopic data allows the rate of electron transfer to be calculated.

$$\Delta G = \frac{(\lambda - 2H_{ab})^2}{4\lambda}$$

$$k_{ET} = \nu_{1/2}\exp-\left(\frac{\Delta G}{4RT}\right)$$

However, these equations correspond to a very specific system where the two redox sites, **A** and **B**, have a very weak electronic interaction, hence have a small H_{ab} value.

When the interaction between **A** and **B** increases (so there are larger values of H_{ab}) the shape of the ground state potential energy curve, **XY**, changes and it causes the two

wells in the curve to collapse into a single well in extreme limits. Therefore, in the strongly coupled limit, the identity of the initial and final states are lost and the above equations no longer apply. Therefore, the E_{op} (the optical energy needed for a transition to occur between the **XY** and **Z** states) becomes equal to $2H_{ab}$. When this ground state is achieved it is termed delocalised, and the optical transition is characterised by an intense, sharp band in the NIR region.

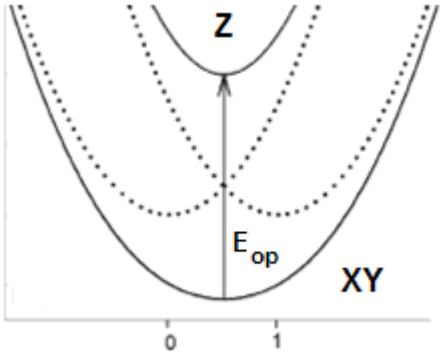

Figure 5: Potential energy plot for a delocalised system. Adapted figure from ref [6i] (Reproduced by permission of The Royal Society of Chemistry (RSC))

Robin and Day devised a classification system for **MV** complexes based upon the nature of the ground state.[13] For Class I complexes there are no interactions between states **X** and **Y** (Figure 2). Class II complexes instead have intermediate electronic coupling, and a localised ground state (Figure 3). A classical example of this is Wolffram's Red, $[Pt(etn)_4][Pt(etn)_4Cl_2]$-$Cl_4.4H_2O$, (etn = ethylamine). Class III complexes have a delocalised ground state (Figure 5), which has led to some debate as to whether or not these systems are mixed valence, or if they are better described as delocalised or averaged valence systems. Using optical spectroscopy the difference between Class II and III can be further characterised by the solvatochromic nature of the band. The localised nature of Class II compounds means that the IVCT bands exhibit strong solvatochromic band behaviour and genuine charge transfer character. In

contrast, the NIR bands associated with Class III compounds are solvent independent, as is to be expected for a delocalised system.

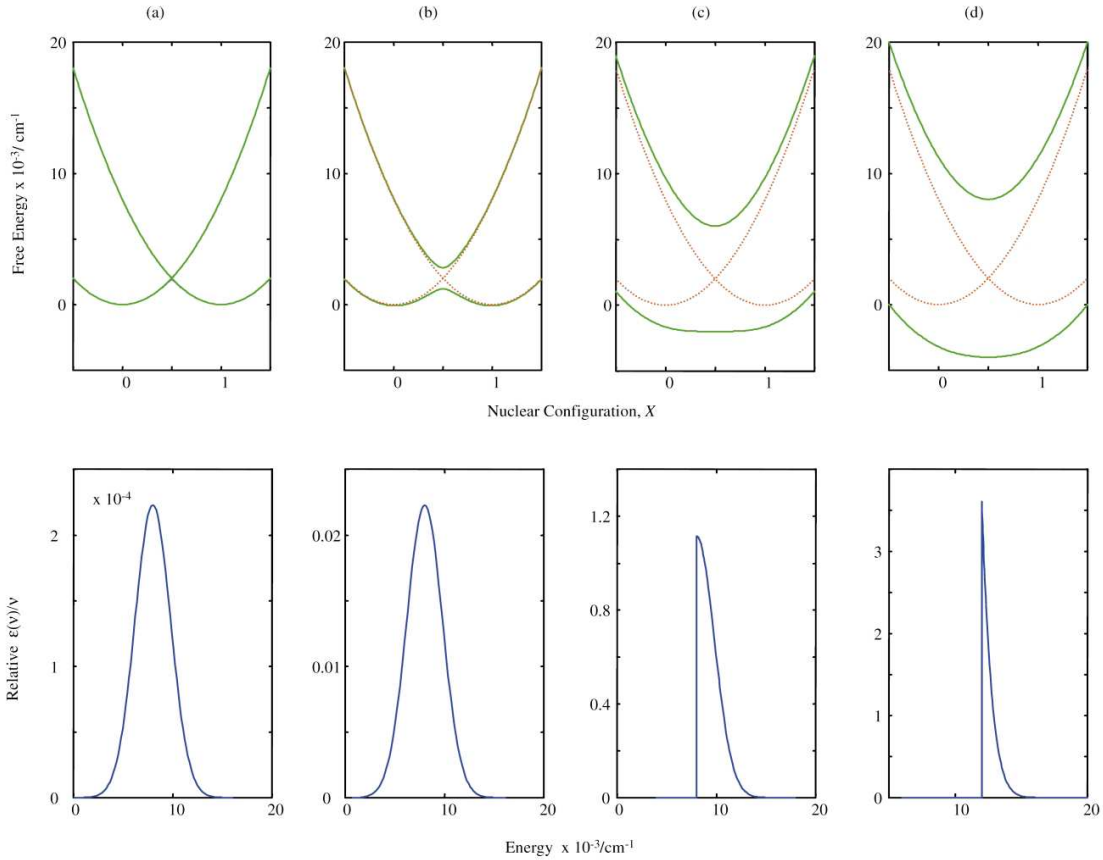

Figure 6: Simulated NIR transitions and corresponding potential energy surface plots. From (a) to (d) the electronic coupling parmeter is increasing. Where H_{ab} increases from 80 (a) to 6000 (d). Reproduced from ref [22c]. (Reproduced by permission of The Royal Society of Chemistry (RSC))

The classes therefore describe the extremes of interaction. Either a weakly interacting, localised behaviour of two sites is exhibited (Class II) or a completely delocalised system is observed where there are no longer two sites (Class III). However as Figure 6 shows, the degree of interaction is a sliding scale between the two extremes set out between limits of the descriptions of Class II and Class III systems. The generality of the Class II and Class III descriptions has given rise to the subsequent development of

sub classes, such as class IIA, class IIB, class IIIA and class IIIB, which more precisely define the degrees of intermediate coupling.

The difficulties encountered in arriving at the descriptions of **MV** systems is exemplified by the complexities experienced in determining the degree of electronic interaction using electrochemical methods. For a weakly coupled system, where the redox sites retain some identity, the $\Delta E_{1/2}$ value will be sensitive not only to electrostatic and solvation factors, but also to ion-pairing interactions, reorganisation energies, the π-donor/acceptor character of the bridge and ancillary ligands, anti-ferrromagnetic exchange contributions and resonance stabilisation energies. Only this final term pertains information about the electron transfer process. The situation becomes even more complex as the coupling between the two redox sites becomes stronger and alongside this the role the bridge plays in mediating the interaction between the sites becomes more important. For a system which is fully delocalised an inversion of the electrochemical potentials may be observed, i.e. E_2 occurs at a lower potential than E_1, indicating that the removal of the second electron is much easier than the first. This generally occurs when the localisation of charge in the doubly oxidised species is such that the reduction in the electrostatic repulsion and stabilisation of the charge by solvation increases the stability of the system.

It has also been demonstrated that notable changes in the value of $\Delta E_{1/2}$ will occur with the variation of the supporting anion and dielectric. Carefully controlled experiments, by systematic variation of the supporting anion, show that by using a weakly coordinating anion, such as $[B(C_6F_5)_4]^-$, one is able to stabilise charge in the system by ion-pairing, and the $\Delta E_{1/2}$ value can be increased. This is in contrast to more

coordinating anions, such as Cl^-.[14] The donor and acceptor properties of the solvent also show similar effects, where non-polar solvents serve to reduce the $\Delta E_{1/2}$ value.[15] Electrochemical determination of electron coupling within a series compound can be achieved,[16] but only under the strictest of conditions. These include that the site of oxidation must be directly attributable to end groups and there must be no bridge involvement. Subsequently, by varying the bridging moiety an assessment of the electronic coupling can be made.[17] These criteria are often difficult to attain, therefore accurately determining the intricate dynamics of the electron transfer make the $\Delta E_{1/2}$ and K_c parameters unreliable as primary methods to assess the electronic structure of the electron transfer system.

Upon changing to an asymmetric system, where **A** and **B** are not of the same identity, the minimum point of the wells of the **X** and **Z** electronic potential energy curves differ in energy (Figure 7). As such the energy of the transition observed experimentally is no longer equal to the re-organisational energy (λ or E_{op} in a symmetrical system) and the equations described above can no longer be used directly to estimate the characteristics of the electron transfer system. Instead the E_{op} value is the sum of the experimentally observed optical transition plus the ΔG^o of the system, which can be determined from electrochemical measurements (Figure 7).[18]

$$\Delta G^o = -RT \ln K_c$$

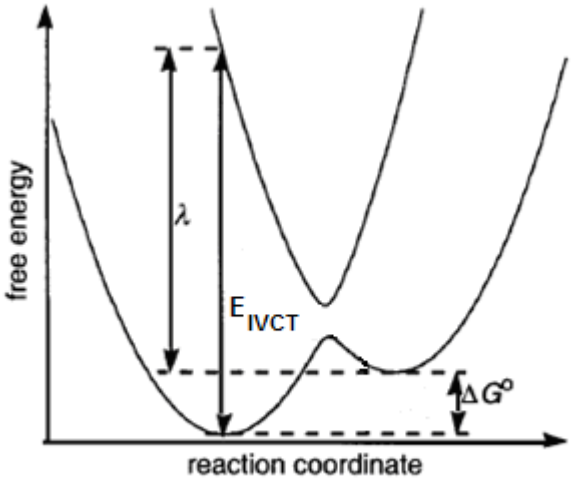

Figure 7: Asymmetric single electron transfer system. Reprinted with permission ref [14b] © 2010 American Chemical Society..

Improvements upon the two state model were driven by the ever diverse and complex compounds being synthesised by chemists. A significant step forward was made with the development of the PKS model,[19] which elegantly introduced the vibronic mode of the system coupled with the optical electron transfer process and was essentially a linear response model.[20] The model served to more accurately reflect the IVCT energy and the shape of the IVCT bands in strongly coupled complexes, such as the Creutz-Taube ion.

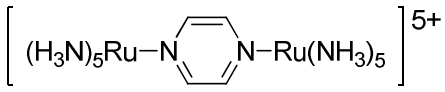

Figure 8: The Creutz-Taube ion.

Although the method was criticised by several leaders in the field,[6e] the model served as a platform for other models to be developed based upon the inclusion of multiple vibronic motions, along both asymmetric and symmetric coordinates of the complex (Figure 9).[21]

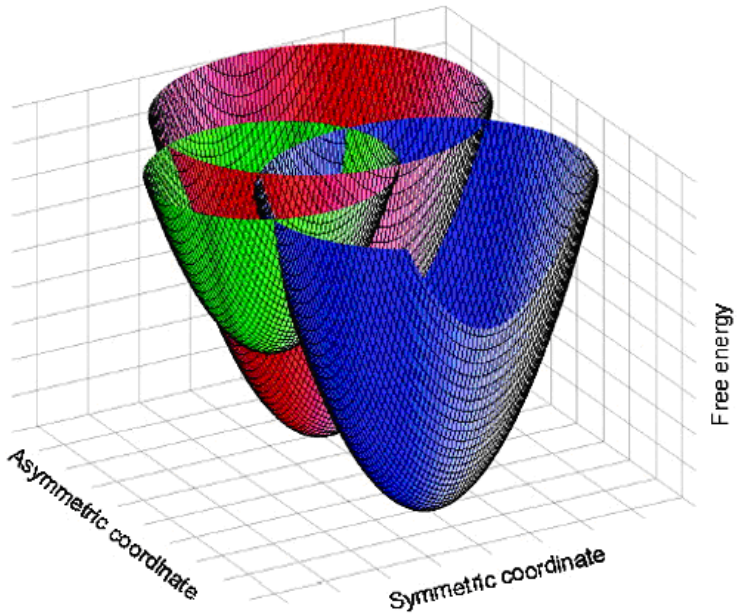

Figure 9: Three dimensional two state approximation in asymmetric and symmetric coordinate planes. Reprinted with permission ref [24] © 2010 American Chemical Society.

A further advancement, asides from the inclusion of vibronic coordinates of the system, occurred with the addition of an extra potential energy state, which highlights the influence of the bridging moiety upon the electron transfer process. This is particularly important in many organometallic mixed valence systems, where the bridging moiety can be heavily involved in the electron transfer process as a consequence of metal/bridge mixing. The simplest way to demonstrate this is through the adaptation of the two state potential energy plot, where the third diabatic state is labeled **W** (Figure 10). The implication of this is the addition of an MLCT /LMCT transition between the ground state and the bridging state in addition to the IVCT transition. This rationalises the complex NIR bands seen for many mixed valence organometallic complexes, showing that as the mixing between the redox site and the bridge increases, the intensity of the IVCT band increases (as well as becoming more asymmetric in shape) and the intensity of the MLCT /LMCT band decreases (Figure 11).[22]

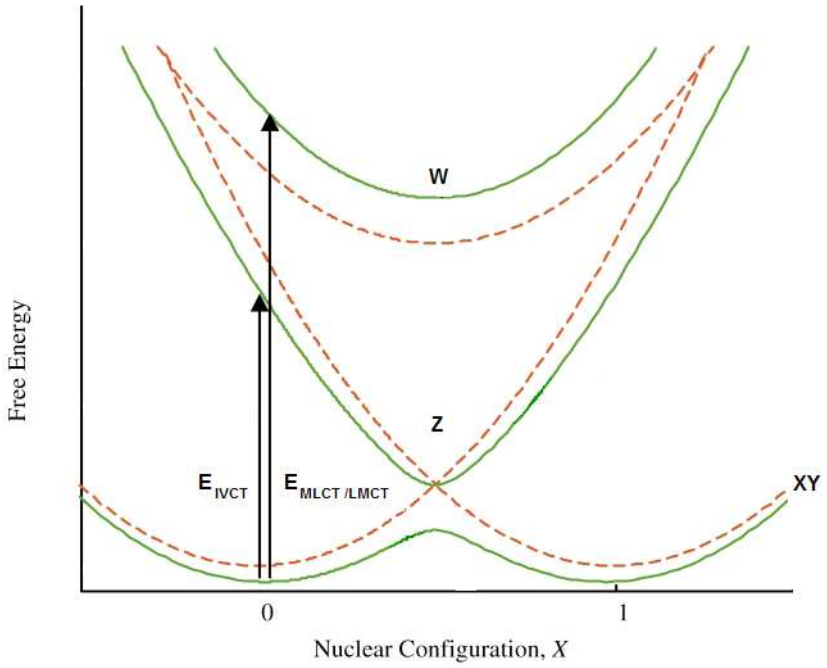

Figure 10: Three state description of an electron transfer system. Adapted figure from ref [22c] (Reproduced by permission of The Royal Society of Chemistry)

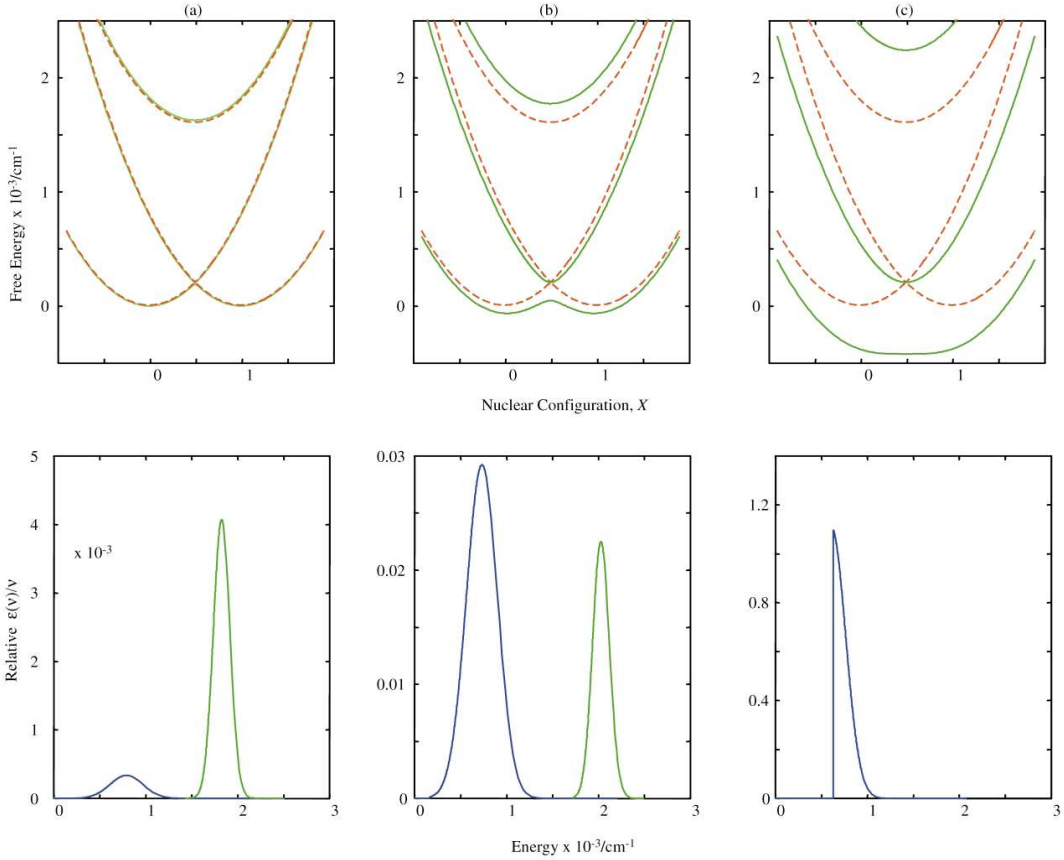

Figure 11: Simulated IVCT (blue) and MLCT (green) transistions and the corresponding three state potential energy plots. From (a) to (c) the electronic coupling parameter is increasing from 1130 (a) to 8000 (c). Reproduced from [ref 22c]. (Reproduced by permission of The Royal Society of Chemistry)

An extension of this model has included the addition of extra potential states in order to model the experimental results more accurately, leading to the creation of four state models.[22a] Multi-state models have been proposed for cluster systems,[23] as both the bridging moiety and the ancillary cluster ligands (for example [{$Ru_3O(\mu\text{-}OAc)_6$}(CO)(L)(μ-BL){$Ru_3O(\mu\text{-}OAc)_6$}(CO)(L)] (where BL = bridging ligand, and L = tunable ancillary ligand) affect the electronic interaction between the two redox sites.

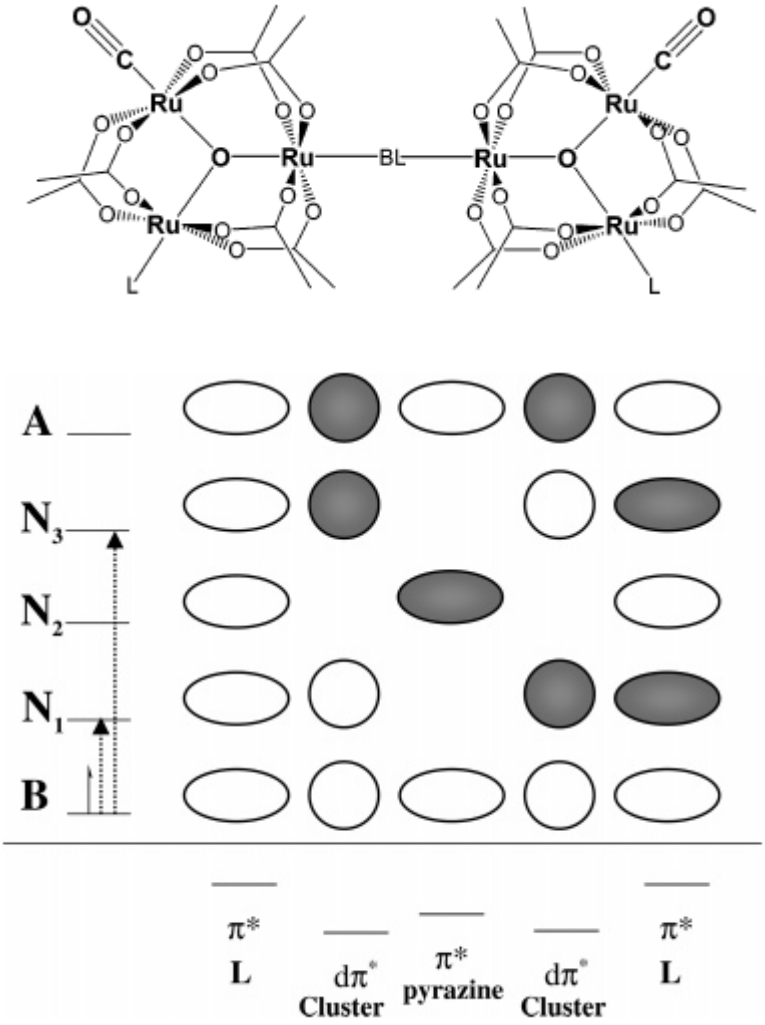

Figure 12: Proposed five state description of electron transfer systems in [{$Ru_3O(\mu\text{-}OAc)_6$}(CO)(L)(μ-BL){$Ru_3O(\mu\text{-}OAc)_6$}(CO)(L)]. Reprinted with permission ref [23] © 2010 American Chemical Society.

As suggested by the three state approximation of electron transfer, an MLCT transition is possible between the ground state and the bridging state. This is also subject to the nature of the electronic ground state, hence it is useful for describing the electron transfer system. Transitions in the UV/vis region of the spectrum, which are distinct from the lower energy NIR region in which IVCT bands are usually found, can also play an important role in determining the electronic structure of electron transfer systems, although such data is rarely interpreted in this way. Research in this area has concentrated on $[\{(^{t}BuCO_2)_3MM\}_2(\mu\text{-}O_2CCO_2)]^+$ (where MM = Mo_2, MoW and W_2) and, in relation to the IT transition, has demonstrated the MLCT transitions dependence on solvent media. This has led to an additional "class" of electron transfer system, (Class IV) being proposed, which is defined as a system that shows both the MLCT and IVCT transitions as being solvent independent and having little vibronic coupling.[24]

Vibrational spectroscopy (infrared and Raman) can provide important structural and electronic information about both the ground state and excited states of the system. This is provided that there are suitable vibrational probes, for example $\nu(C\equiv C)$ and $\nu(C\equiv O)$, which are sensitive to structural and electronic changes about their respective anchor points, i.e. the redox centres or the bridging moiety. Infrared and Raman spectroscopy are complementary techniques, both of which are dependant upon the symmetry point group of the system, yet they originate from different phenomena. Infrared spectroscopy examines the change in local dipole moments arising from moving between discrete vibrational levels within the ground state electronic structure. Non-resonance Raman scattering requires the complex to interact with the incident light (normally from a laser source) causing the formation of a very short-lived (when compared to the absorption of a photon) virtual state. When the energy of the

subsequent inelastic scattered photon is different to that of the incident light, Stokes and anti-Stokes scattering is observed (Raman scattering). The formation of the virtual state (which is a state where the electron cloud has been distorted or polarised) and the collection of the scattered photons allows the polarisability of the system to be studied. Resonance Raman spectroscopy uses the energy of the incident light absorbed to form an excited electronic state in which the virtual state is formed. The increased change in polarisation (which can be shown using Kramer Heisenberg Dirac expression) as a result of this resonance produces much more intense Raman scattering (where $I = Kl\alpha^2\omega^4$. Where I is the intensity of the Raman scattering and α is the polarisability of the electrons). As such, changes in bond polarisation which are coupled to this excited state, experience resonance enhancement in comparison to those which are not.[25]

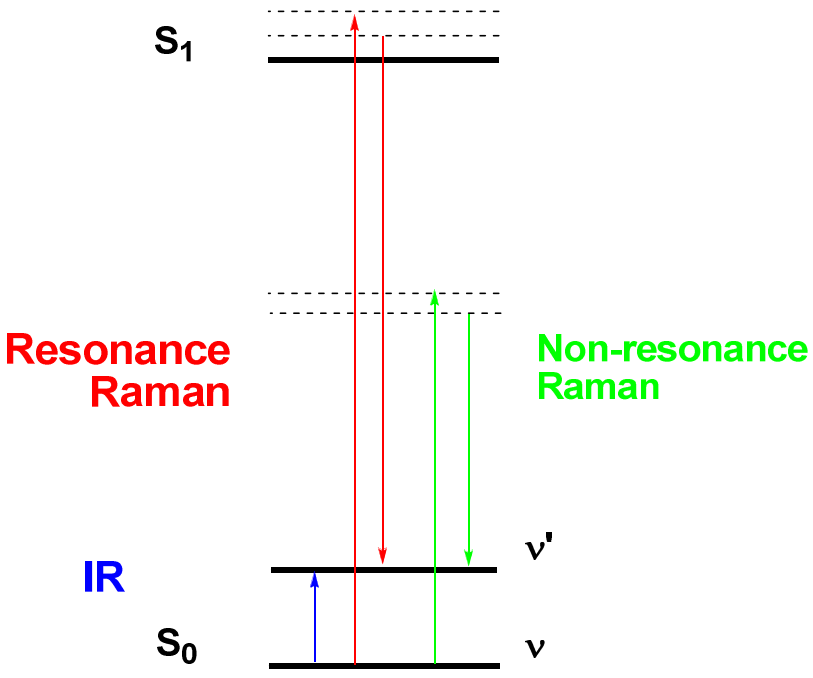

Figure 13: Schematic detailing the difference between normal and resonance Raman and infrared spectroscopy (S is used to denote electronic states within a system and ν is used to denote discrete vibration levels within an electronic state.)

Intramolecular electron transfer for symmetrical systems in solution takes place at around 10^{12} to 10^{13} s. This is similar to the timescale of infrared spectroscopy for similar transfers, making the spectroscopy ideal for identifying the nature of the ground state in rapidly exchanging systems.[26] For example, the mixed valence system $[\{Ru_3(\mu_3\text{-}O)(\mu\text{-}CH_3CO_2)_6(CO)L\}_2(\mu\text{-}Bpy)]^{-1}$ (L = dmap, py and cpy) has shown that by increasing the electronic coupling parameter, thus making the ground state more delocalised, the ν(C≡O) stretching modes begin to coalesce into a single band.[27] In contrast to this, lowering the coupling parameter leads to the localisation of the ground state into two distinct wells (for example in Figure 3). Such conclusions are also displayed by the extra "exchange" intensity seen for the ν(C≡O) stretching modes, which has been shown to be a property of interwell exchange rather than intrawell exchange, i.e. for delocalised ground states.[28] A certain degree of asymmetry or added intensity has been noted for stretching modes which are associated with the bridging moiety in electron transfer systems with a localised ground state, for example the ring stretching mode of the bridging ligand is of unusually high intensity for $[\{Os(Cl)(Bpy)_2\}_2(\mu\text{-}pz)]^{3+}$.[29]

Resonance Raman spectroscopy provides a convenient probe for specific electronic transitions, which makes it an useful tool for investigating electron transfer processes, as it links electronic transitions with the vibronic motion of the complex along the reaction (i.e. electron transfer) pathway. Despite this, very few resonance Raman studies, where the IVCT transitions are directly excited, have been conducted using organometallic complexes. This is owing to the lack of readily available lasers of sufficient power that are 1100 nm or longer wavelengths.[30] Nevertheless, a significant body of recent work with organic mixed valence complexes has been studied (where the

IT transitions are much higher in energy), for example with *p*-phenylenediamine radical cations.[31] Such studies have shown the coupling of both symmetric and asymmetric vibrational modes, involving the bridging and pendant portions of the molecule, to the IVCT transition.

Many of the mixed valence complexes designed to study electron transfer rely on metal moieties as the redox centres, which adds an extra degree of complexity to the models previously described. The identity of the metal centre and the arrangement of the ancillary ligands can cause the splitting of the metal d-orbitals, either due to the large spin-orbit coupling of the metal centre, the low-symmetry of the metal moiety or the pronounced ligand-field asymmetry.[32]

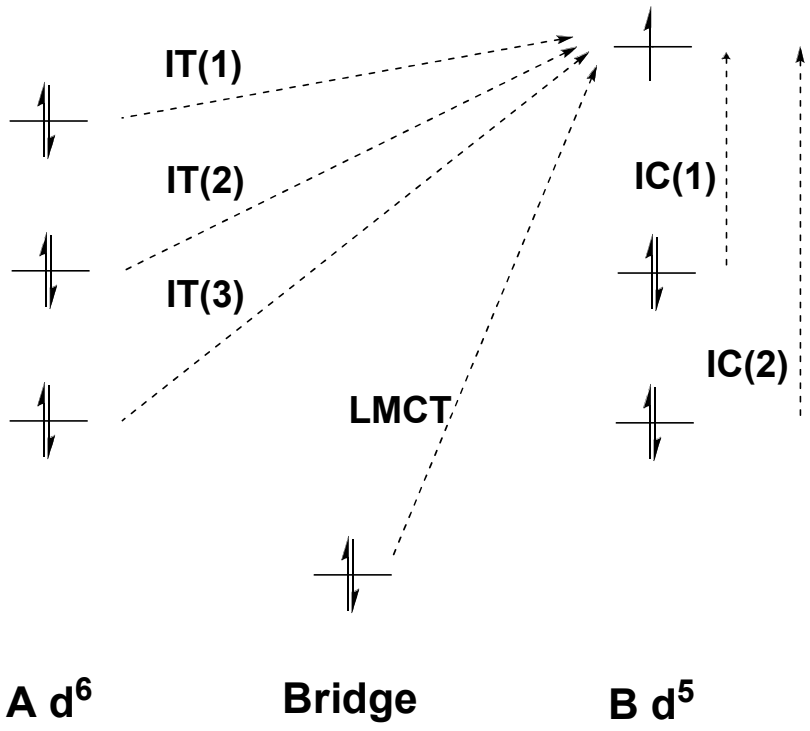

Figure 14: Single electron transfer in transition metal containing systems.

The splitting of metal d-orbitals can give rise to as many as three IVCT transitions originating from each of the filled metal d-orbitals, and also interconfigurational transitions (IC) on the oxidised centre. The inclusion of a bridge to metal charge transition (LMCT) can also be important, as its energy is dependent upon the relative energies of the bridge and the redox moieties.[33]

The difference in energies of the IT transitions are dependent upon the spin-orbit coupling of the metal centre and the electronic asymmetry of the system. Increasing either will cause the energy difference between the filled metal d-orbitals to widen, therefore spreading the IT transitions over wider range of energies. This leads to significant overlap of the IT transitions for systems containing first and second row transition metals (for example iron and ruthenium) creating difficulty when determining the lowest energy IT transition. Moreover, increasing the spin-orbit coupling value of the metal centre has an additional effect of increasing the intensity and decreasing the energy of the IC transitions.

As for many areas of chemistry, computational chemistry can provide useful insight into the electronic structure. As such, it is becoming an increasingly useful tool for understanding the cumulative roles of the individual components of the system in the electron transfer process.

1.3 Computational Analysis of Electron Transfer Systems

The previous sections have demonstrated the potential complexity of the electron transfer process and the dependence of this phenomenon and related spectroscopic

properties, not only on the nature of the redox sites, but also of the bridging moieties, solvent media and ancillary ligands. As such, it has only been relatively recently that computational techniques of sufficient accuracy and complexity have been employed to rationalise the electronic structure of electron transfer systems.

Quantum mechanical treatment of molecular systems can be described by two different variables, either the *ab initio* electronic wavefunction or by density functional theory techniques (DFT). Describing the electronic structure as a wavefunction can be carried out quickly using Hatree-Fock (HF), INDO and ZINDO techniques, however these techniques sometimes lack the accuracy needed to describe an electron transfer system. More accurate wavefunction based techniques are available and include those such as configuration interaction (CI), multi-reference CI (MRCI), complete active space techniques (CASSCF), and couple-cluster methods (CC). Although these *ab initio* techniques are very accurate, as the methods examine the wavefunctions of systems, they are very computationally intensive. Consequently, they have only been applied to small systems.[34]

Density functional techniques are now far more commonly used for calculating the electronic structure of transition metal complexes, as the computational cost scales well with the size of the system. In addition, the accuracy obtained for small systems is comparable to *ab initio* methods. DFT methods are conceptually different to *ab initio* techniques with regards to the fact that the ground state energy, and all ground state properties, are determined by the electron density (Hohenberg-Kohn theorem).[35] This allows the lowest state of a given symmetry or spin multiplicity to be calculated for open- and closed-shell systems,[36] both of which make use of the Kohn-Sham

approach.[37] Hybrid-DFT techniques have been developed which comprise of differing portions of both HF character and pure DFT character (for example BLYP). These have been used as an alternative to describing more complex transition metal containing systems. TD-DFT techniques allow the interpretation of the electronic spectra of systems, and is based upon the response of the ground state electron density to an oscillating optical field.

An important aspect of *ab initio*, DFT and hybrid-DFT techniques, especially for experimental chemists, is that the results of the calculations can be communicated in terms of molecular orbitals rather than pure mathematical results. The variety of functionals and basis sets available to compute the electronic structure of transition metal complexes is extensive, giving access to a large series of tools through which to describe these systems.[38]

Despite this, computational modeling of electron transfer systems involving two or more transition metals is fraught with difficulty, not only due to the number of core electrons involved in the metal centres, but also due to the inherent inaccuracies of open-shell approximations, which tend to produce excessively delocalised charge distributions when common hybrid-functionals (such as B3LYP) are used.[39] This is due to the localised nature of DFT functionals which cannot describe long-range electron-hole separation. This intrinsic property generally leads to TD-DFT predictions of the NIR region to be in poor agreement with experimental results, as it tends to over-estimate the intensity of more localised transitions, such as LMCT /MLCT.

To counteract this, a series of range-separated hybrid functionals and local hybrid functionals have been devised. These act to separate the electron interaction into long-, medium- and short-range interactions, such as CAM-B3LYP[40] and HSE.[41] However, they have not yet been widely applied to complex electron transfer systems containing transition metals. In addition, constrained DFT and CDFT methods have been successful in modeling the electronic interaction between linked ferrocene moieties.[42] Although the theory behind this method is mathematically complex, as a simple analogy to TD-DFT, CDFT does not calculate all the excited states, instead constraining itself to states which are ground states of an alternative external potential, i.e. the system is tuned to only view the excited states which are relevant to the electron transfer process.[43]

Regardless of the apparent drawbacks of using solely hybrid functionals to describe electron transfer systems, those which can be readily employed using the Gaussian suite[44] have been used extensively to describe electron transfer systems. Some success has been found with the application of a modified B3LYP hybrid-functional (where the ratio of HF to pure DFT character of the hybrid functional has been altered to reduce the delocalisation of charge in the MV system) to triarylamine systems, especially when solvation models, polarisable continuum model (COSMO) and IEF-PCM models, are included in TD-DFT calculations.[45] In addition, using the hybrid-functional MPW1K, the NIR region of $[\{Ru(dppe)(\eta^5\text{-}C_5Me_5)\}_2\{\mu\text{-}C{\equiv}C(C_2B_{10}H_{10})C{\equiv}C\}]^+$ was successfully modeled using TD-DFT techniques.[46]

1.4 Thesis Outline

As described in this introduction, single electron transfer reactions comprise a multi-faceted genre of science, with a combination of synthetic, theoretical chemistry, electrochemistry, spectroscopy and computational techniques used in order to rationalise the electronic structure of complexes that display intramolecular electron transfer.

This thesis will examine a closely related series of homo-bimetallic complexes of the general formula $[\{Mo(dppe)(\eta^7\text{-}C_7H_7)\}_2(\mu\text{-}C{\equiv}CXC{\equiv}C)]^+$, (where X = bond, C_6H_4, and $C_2B_{10}H_{10}$). The unique redox character, highly resolved EPR signal and unique interaction of the metal d and cyclic carbon π-orbitals of the cycloheptatrienyl containing metal fragment, $Mo(dppe)(\eta^7\text{-}C_7H_7)$, have been used to explore single electron transfer in an organometallic mixed valence system.

In order to fully rationalise the interaction of the $Mo(dppe)(\eta^7\text{-}C_7H_7)$ fragment with the carbon chain, Chapters two and three will examine the effect that changing the acetylide moiety to a longer polyynyl ligand has upon the electronic structure of the metal moiety. Chapters four, five and six will examine the electron transfer properties of homo-bimetallic complexes containing the $Mo(dppe)(\eta^7\text{-}C_7H_7)$ fragment, in order to assess the effect of the bridging moiety on electron transfer. Finally Chapter seven will explore the synthesis and application of the cyanoacetylide moiety in electron transfer systems, using the $Mo(dppe)(\eta^7\text{-}C_7H_7)$ fragment as a probe into its character. This systematic approach to studying electron transfer within a series of homo-bimetallic complexes will provide a framework for the study of these complexes, and a

demonstration of the application of techniques and theories to enable the thorough study of electron transfer in transitional metal complexes.

1.5 References

[1] For examples refer to (a) W.Y. Kim, Y.C. Choi, S.K. Choi, S.K. Min, Y. Cho, K.S. Kim, *Chem. Soc. Rev.,* 2009, **38**, 2319. (b) C. Rovira, *Chem. Rev.,* 2004, **104**, 5289. (c) P.J. Low, *Dalton. Trans.,* 2005, 2821.
[2] For examples refer to (a) A. Harriman, L.J. Mallon, K.J. Elliot, A. Haefele, G. Ulrich, R. Ziessel, *J. Am. Chem. Soc.,* 2009, **131**, 13375.
[3] For examples refer to (a) J. Heberie, J. Fitter, H.J. Sass, G. Buidt, *Biophys. Chem.,* 2000, **85**, 229.
[4] For examples refer to (a) P.G. Falkowski, T. Fenchel, E.F. Delong, *Science,* 2008, **320**, 1034.
[5] For examples refer to (a) P.V. Kamat, *Chem. Rev.,* 1993, **93**, 267. (b) D. Gust, T.A. Moore, A.L. Moore, *Acc. Chem. Res.,* 2001, **34**, 40.
[6] (a) R.A. Marcus, *Adv. Chem. Phys.,* 1999, **1**, 1. (b) N. Sutin, *Adv. Chem. Phys.,* 1999, **1**, 7. (c) C. Creutz, *Prog. Inorg. Chem.,* 1983, **30**, 1. (d) N. Sutin, C. Creutz, *J. Chem. Ed.,* 1983, **60**, 809. (e) J.R. Reimers, N.S. Hush, *Chem. Phys.,* 1996, **208**, 177. (f) R.A. Marcus, *Annu. Rev. Phys. Chem.,* 1964, **15**, 155. (g) R.J.H. Clark, *Chem. Soc. Rev.,* 1984, **13**, 219. (h) P.J. Low, N.J. Brown, *J. Cluster. Sci.,* 2010, *doi:10.1007/s10876-010-0328-4*. (i) D.M. D'Alessandro, F.R. Keene, *Chem. Soc. Rev.,* 2006, **35**, 424.
[7] W.F. Libby, *J. Phys. Chem.,* 1952, **56**, 863.
[8] R.A. Marcus, *Rev. Mod. Phys.,* 1993, **65**, 599.
[9] N.G. Connelly, W.E. Geiger, *Chem. Rev.,* 1996, **96**, 877.
[10] (a) M.D. Ward, *Chem. Soc. Rev.,* 1995, 121. (b) D. Astruc, *Acc. Chem. Res.,* 1997, **30**, 383. (c) S. Barlow, D. O'Hare, *Chem. Rev.,* 1997, **97**, 637.
[11] (a) J.B. Flannagan, S. Margel, A.J. Bard, F.C. Anson, *J. Am. Chem. Soc.,* 1978, **100**, 4248. (b) F. Ammar, J.M. Saveant, *J. Electroanal. Chem.,* 1973, **68**, 215.
[12] (a) N.S. Hush, *Prog. Inorg. Chem.,* 1967, **8**, 391. (b) N.S. Hush, *Electrochim. Acta,* 1968, **13**, 1005.
[13] M.B. Robin, P. Day, *Adv. Inorg. Radiochem.,* 1967, **10**, 247.
[14] (a) F. Barriere, N. Camire, W.E. Geiger, U.T. Mueller-Westerhoff, R. Sanders, *J. Am. Chem. Soc.,* 2002, **124**, 7262. (b) A. Nafady, T.T. Chin, W.E. Geiger, *Organometallics,* 2006, **25**, 1654.
[15] F. Barriere, W.E. Geiger, *J. Am. Chem. Soc.,* 2006, **128**, 3980.
[16] C.G. Atwood, W.E. Geiger, *J. Am. Chem. Soc.,* 2000, **122**, 5477.
[17] (a) K. Kalyanasundaram, Md. K Nazeeruddin, *Inorg. Chim. Acta,* 1994, **226**, 213. (b) S. Frohanpfel, B.E. Woodworth, H.H. Thorp, J.L. Templeton, *J. Phys. Chem. A.,* 1998, **102**, 5664.
[18] (a) A, Caballero, A. Espinosa, A. Tarraga, P. Molina, *J. Org. Chem.,* 2007, **72**, 6924. (b) S. Barlow, *Inorg. Chem.,* 2001, **40**, 7047.
[19] S.B. Piepho, E.R. Krausz, P.N. Schatz, *J. Am. Chem. Soc.,* 1978, **10**, 2996.
[20] M.J. Rice, *Phys. Rev. Letters,* 1976, **37**, 36.

[21] (a) J. Ko, M.J. Ondrechen, *Chem. Phys. Letters.,* 1984, **112**, 507. (b) Z. Gasyna, P.N. Schatz, M.E. Boyle, *J. Phys. Chem.,* 1995, **99**, 10159. (c) K Boukheddaden, J. Linares, S. Galam, F. Varret, *Chem. Phys.,* 1994, **180**, 43.
[22] (a) B.S. Brunschwig, N. Sutin, *Coord. Chem. Rev.,* 1999, **187**, 233. (b) J-P. Launay, C. Coudret, C. Hortholary, *J. Phys. Chem. B.,* 2007, **111**, 6788. (c) B.S. Brunschwig, C. Creutz, N. Sutin, *Chem. Soc. Rev.,* 2002, **31**, 168.
[23] J.C. Salsman, S. Ronco, C.H. Londergan, C.P. Kubiak, *Inorg. Chem.,* 2006, **45**, 547.
[24] B.J. Lear, M.H. Chisholm, *Inorg. Chem.,* 2009, **48**, 10945.
[25] E. Smith, G. Dent (2005) Modern Raman Spectroscopy A Practical Appraoch (Wiley).
[26] M.C. DeRosa, C.A. White, C.E.B. Evans, R.J. Crutchley, *J. Am. Chem. Soc.,* 2001, **123**, 1396.
[27] (a) T.Ito, T. Hamaguchi, H. Nagino, T. Yamaguchi, H. Kido, I.S. Zavarine, T. Richmond, J. Washington, C.P. Kubiak, *J. Am. Chem. Soc.,* 1999, **121**, 4625. (b) T. Ito, T. Hamaguchi, H. Nagino, T. Yamaguchi, J. Washington, C.P. Kubiak, *Science,* 1997, **277**, 660. (c) C.H. Londergan, J.C. Salsman, B.J. Lear, C.P. Kubiak, *Chem. Phys.,* 2006, **324**, 57.
[28] (a) W.C. Watkins, T. Jaeger, C.E. Kidd, S. Fortier, M.C. Baird, G. Kiss, G.C. Roper, C.D. Hoff, *J. Am. Chem. Soc.,* 1992, **114**, 907. (b) J.J. Turner, C.M. Gordon, S.M. Howdle, *J. Phys. Chem.,* 1995, **99**, 17532. (c) K.A. Wood, H.L. Strauss, *J. Phys. Chem.,* 1990, **94**, 5677.
[29] K.D. Demadis, G.A. Neyhart, E.M. Kober, T.J. Meyer, *J. Am. Chem. Soc.,* 1998, **120**, 7121.
[30] V. Petrov, J.T. Hupp, C. Mottley, L.C. Mann, *J. Am. Chem. Soc.,* 1994, **116**, 2171.
[31] S.E. Bailey, J.I. Zink, S.F. Nelsen, *J. Am. Chem. Soc.,* 2003, **125**, 5939.
[32] (a) K.D. Demadis, C.M. Hartshorn, T.J. Meyer, *Chem. Rev.,* 2001, **101**, 2655. (b) J.J. Concepcion, D.M. Dattelbaum, T.J. Meyer, R.C. Rocha, *Phil. Trans. R. Soc. A.,* 2008, **366**, 163.
[33] R.C. Rocha, F.N. Rein, H. Jude, A.P. Shreve, J.J. Concepcion, T.J. Meyer, *Agnew Chem. Int. Ed.,* 2008, **47**, 503.
[34] C. Lambert, S. Amthor, J. Schelter, *J. Phys. Chem. A.,* 2004, **108**, 6474.
[35] (a) P. Hohenberg, W. Kohn, *Phys. Rev. A.,* 1964, **136**, 864. (b) H. Chermette, *Coord. Chem. Rev.,* 1998, **178-180**, 699. (c) A. Dreuw, M. Head-Gordon, *Chem. Rev.,* 2005, **105**, 4009.
[36] A. Vlcek Jr, S. Zalis, *Coord. Chem. Rev.,* 2007, **251**, 258.
[37] W. Kohn, L.J. Sham, *Phys. Rev. A.,* 1965, **140**, 1133.
[38] C.J. Cramer, D.G. Truh, *Phys. Chem. Chem. Phys.,* 2009, **11**, 10757.
[39] (a) G. Pacchioni, F. Frigoli, D. Ricci, J.A. Weil, *Phys. Chem. B: Condens. Matter Mater. Phys.,* 2000, **63**, 0351018. (b) J.L. Gavartin, P.V. Sushko, A.L. Schluger, *Phys. Chem. B: Condens. Matter Mater. Phys.,* 2003, **67**, 035108. (c) J. Paier, M. Marsman, G. Kresse, *J. Chem. Phys.,* 2007, **127**, 024103. (d) P. Hirva, M. Haukka, M. Jakonen, M.A. Moreno, *J. Mol. Model.,* 2008, **14**, 171.
[40] T. Yanai, D.P. Tew, N.C. Handy, *Chem. Phys. Lett.,* 2004, **393**, 51.
[41] J. Heyd, G.E. Scruseria, M. Ernzerhof, *J. Chem. Phys.,* 2003, **118**, 8207.
[42] F. Ding, H. Wang, Q. Win, T.V. Voorhis, S. Chen, J.P. Konopelski, *J. Phys. Chem. A.,* 2010, **114**, 6039.
[43] Q. Win, T.V. Voorhis, *Phys. Rev. A.,* 2005, **72**, 024502.

[44] M.J. Frisch, G.W. Trucks, H.B. Schlegel, G.E. Scuseria, M.A. Robb, J.R. Cheeseman, J.A. Montgomery Jr., T. Vreven, K.N. Kudin, J.C. Burant, J.M. Millam, S.S. Iyengar, J. Tomasi, V. Barone, B. Mennucci, M. Cossi, G. Scalmani, N. Rega, G.A. Petersson, H. Nakatsuji, M. Hada, M. Ehara, K. Toyota, R. Fukuda, J. Hasegawa, M. Ishida, T. Nakajima, Y. Honda, O. Kitao, H. Nakai, M. Klene, X. Li, J.E. Knox, H.P. Hratchian, J.B. Cross, C. Adamo, J. Jaramillo, R. Gomperts, R.E. Stratmann, O. Yazyev, A.J. Austin, R. Cammi, C. Pomelli, J.W. Ochterski, P.Y. Ayala, K. Morokuma, G.A. Voth, P. Salvador, J.J. Dannenberg, V.G. Zakrzewski, S. Dapprich, A.D. Daniels, M.C. Strain, O. Farkas, D.K. Malick, A.D. Rabuck, K. Raghavachari, J.B. Foresman, J.V. Ortiz, Q. Cui, A.G. Baboul, S. Clifford, J. Cioslowski, B.B. Stefanov, G. Liu, A. Liashenko, P. Piskorz, I. Komaromi, R.L. Martin, D.J. Fox, T. Keith, M.A. Al-Laham, C.Y. Peng, A. Nanayakkara, M. Challa- combe, P.M.W. Gill, B. Johnson, W. Chen, M.W. Wong, C. Gonzalez, J.A. Pople, GAUSSIAN 03, Revision C.02, Gaussian Inc., Wallingford, CT, 2004.

[45] (a) M. Renz, K. Theilacker, C. Lambert, M. Kaupp, *J. Am. Chem. Soc.,* 2009, **131**, 16292. (b) C. Lambert, C. Risko, V. Coropceanu, J. Schelter, S. Amthor, N.E. Gruhn, J.C. Durivage, J-L. Bredas, *J. Am. Chem. Soc.,* 2005, **127**, 8508. (c) V. Coropceanu, M. Malagoli, J.M. Andre, J-L. Bredas, *J. Am. Chem. Soc.,* 2002, **124**, 10519.

[46] M.A. Fox, R.L. Roberts, T.E. Baines, B. Le Guennic, J.F. Halet, F. Hartl, D.S. Yufit, D. Albesa-Jove, J.A.K. Howard, P.J. Low, *J. Am. Chem. Soc.,* 2008, **130**, 3566.

Chapter 2: Cycloheptatrienyl Molybdenum Alkynyl Complexes

2.1 Introduction

Metal alkynyl complexes have been a prevalent area of research in organometallic chemistry for nearly 30 years. The initial interest in metal alkynyl complexes began with comparisons of their properties with isoelectronic cyanide complexes.[1] Since the initial investigations metal acetylides have been shown to display a wide range of useful physical properties such as non-linear optical responses,[2] luminescence and photoconductivity,[3] delocalized electronic structures[4] and liquid crystallinity.[5] These properties are due to the linear structure, high stability and d-π-mixing between the metal end cap and the alkynyl ligand. Tuning the metal atom, along with the ancillary ligands and alkynyl substituents, allows these properties to be altered.

2.1.1 Cyclic Polyenes

Cyclic polyenes of various ring sizes have featured prominently as ligands in organometallic chemistry. The smallest cyclic polyene, cyclobutadiene, had eluded chemists for many years. However, through the co-ordination of the cyclobutadiene ring to a metal centre, for example $[Mo(CO)_4]$,[6] the ring system could be studied in greater detail.[7] Metal fragments act to stablise these reactive ring systems by providing, in the case of cyclobutadiene, two metal orbitals of the correct symmetry to interact with the π electrons on the ring.[8] The stability imparted to the ring by the interaction of

the metal d-orbitals and π-orbitals has led to a vast number of cyclic olefins being coordinated to metal fragments.

Unsaturated ring systems have featured heavily in organometallic chemistry. For example cyclooctadiene (COD) is reported to be readily displaced from [RuCl(COD)(η^5-C_5Me_5)], giving access to a whole host of substituted [$RuClL_2$(η^5-C_5Me_5)] complexes (Scheme 1).[9] The larger cyclooctatetraenyl (COT) systems has shown its worth as an important ancillary ligand in organolanthanide chemistry.[10] The use of metal supported cyclic olefins has allowed other highly reactive species to be studied, such as cyclononatetraene, which has been implicated in the rearrangement of *cis*-bicyclo[6.1.0]nona-2,4,6,triene to *cis*-8,9-dihydroindene.[11]

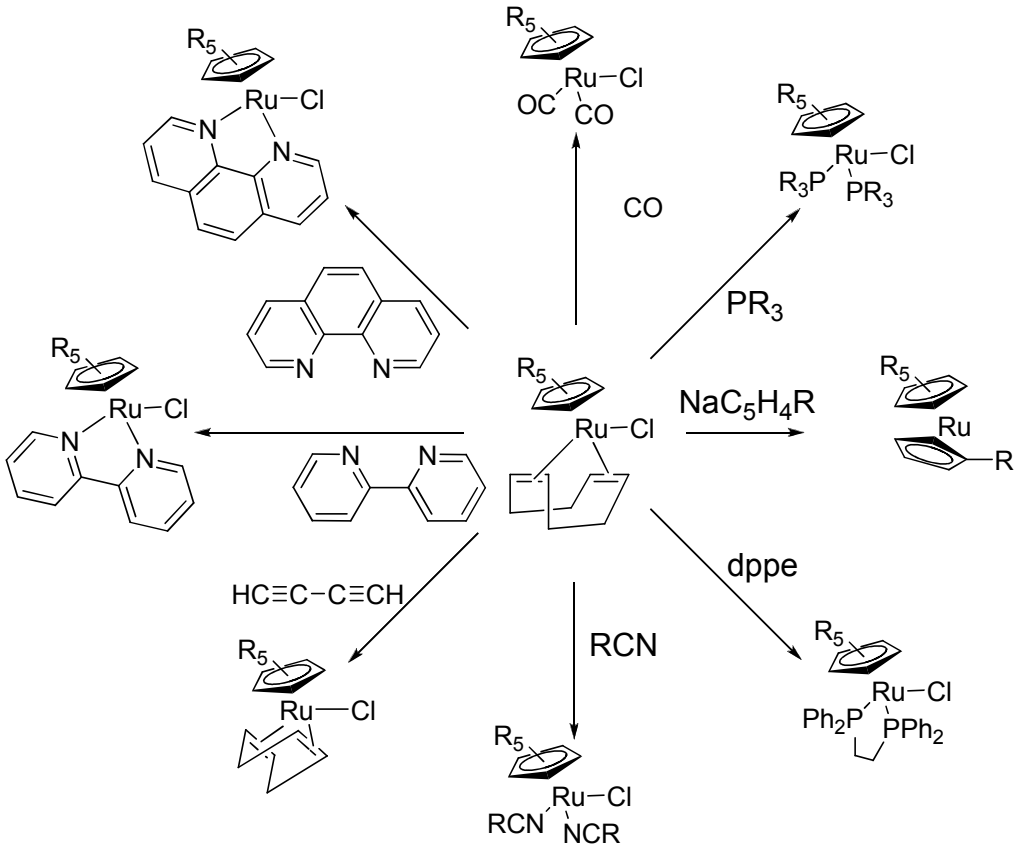

Scheme 1: Transformations of RuCl(COD)(η^5-C_5R_5) (where R = H, Me).

2.1.2 Metallocenes

Despite the practical uses of poly-olefin ligands, the most widely studied complex containing a cyclic polyene is ferrocene, [Fe(η^5-C_5H_5)$_2$], in which the metal atom is sandwiched between the two ring systems. Since its discovery in the early 1950's there have been nearly 12000 papers published[12] and 74800 complexes[13] of derivatives of ferrocene reported. The discovery of ferrocene led to a renaissance in organo-transistion metal chemistry as it established that strong bonds could be easily formed between metal fragments and hydrocarbons. The Fe-ring interaction is strong enough that ferrocene itself is stable at high temperatures, in water and unaffected by strong acids or alkalis. This stability coupled with an improved theoretical understanding of bonding and the wide availability of accurate methods of structure determination, continues to fuel the exploration of modern organometallic chemistry.[14]

Apart from being the constituent of ferrocene, the cyclopentadienyl ring has featured heavily in the literature in the form of half-sandwich complexes, [ML_x(η^5-C_5R_5)]. These half-sandwich complexes are generally quite facile to prepare and can be supported by a large variety of ligands (L). Examples of particular relevance to the work in this thesis include [RuL(dppe)(η^5-C_5Me_5)] and [FeL(dppe)(η^5-C_5Me_5)], where the electronic structure and reactivity of each with a variety of alkynyl[15] and cumulenic[16] substituents have been investigated.

An interesting subsection of cyclopentadienyl containing complexes are the cyclopentadienyl cycloheptatrienyl organometallic sandwich complexes, M(η^5-C_5H_5)(η^7-C_7H_7) which have allowed the detailed study of the bonding of both

cyclopentadienyl and the larger cycloheptatrienyl ring. For a ring system to be aromatic it must fulfill the Hückel's 4n + 2 rule of π electrons.[17] The seven member cycloheptatrienyl ring possesses two sets of degenerate orbitals which can be used to satisfy Hückel's rule with either 6 or 10 π-electrons. This leads to the cyclic olefin having a formal charge of +1 or -3 (Figure 1).

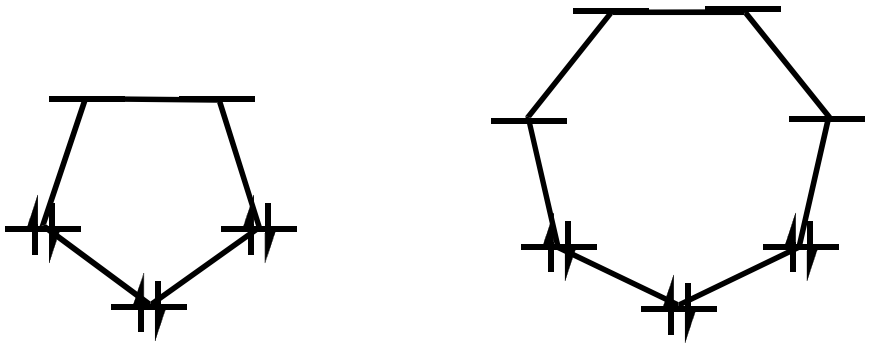

Figure 1: Hückel aromaticity plot of $C_5H_5^-$ and $C_7H_7^+$.

The main thrust of the experimental and theoretical research carried out on these mixed ring complexes has been to address how the two rings bond to the metal centre, which in turn establish the number and nature of ancillary ligands the metal centre could support. $[M(\eta^5\text{-}C_5H_5)(\eta^7\text{-}C_7H_7)]$ has been synthesised with a variety of metal centres, from group four to group eight. In moving across the periodic table from group four to eight, the metal centres increase the number of electrons available for bonding to ancillary groups, the number of electrons available for bonding dictates the character of the bond between the metal and cycloheptatrienyl ring.

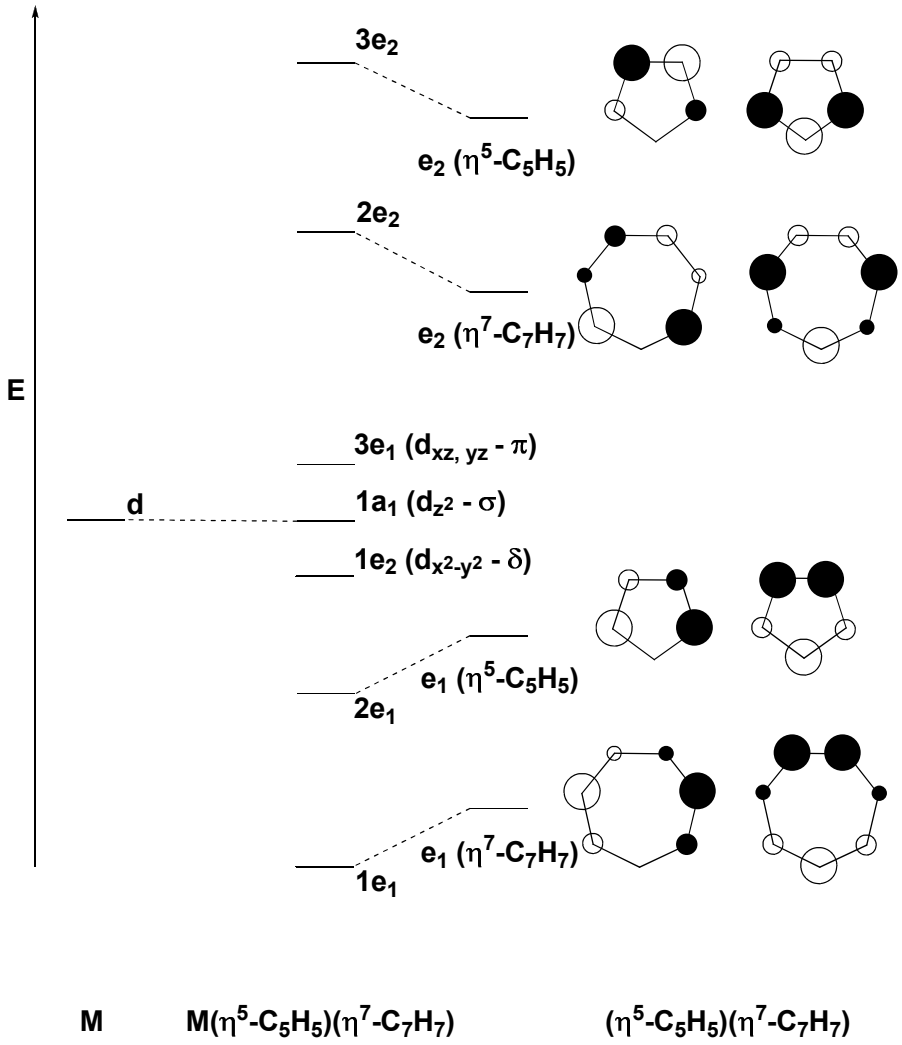

Figure 2: Generic molecular orbital diagram for M(η^5-C$_5$H$_5$)(η^7-C$_7$H$_7$).

The interaction of the metal d-orbitals and the ring system breaks down into predominantly three sets of interactions (Figure 2). The highest energy interaction is a σ type interaction between the d_{z2} orbital with the cycloheptatrienyl ring. For higher group metals, when the d_{z2} orbital is filled, the d_{z2} orbital points towards the mid-point of the ring. This causes the nature of the bonding interaction to be dictated by the relative energy of the metal d-orbitals and the ring π-system.[18] For lower group metals, such as titanium, this σ interaction is non-bonding as the d_{z2} orbital of the metal is empty, therefore the bonding is centered around a δ-interaction with the filled d_{x2-y2} and d_{xy} and due to a good match in symmetry, the bond becomes more cycloheptatrienyl in

character. [19] This leaves the d_{zx} and d_{zy} orbital un-occupied, which are involved in a π-interaction with the cyclopentadienyl ring, all of which are clearly seen from DFT molecular orbital analysis.[20] The character of these orbitals is also dependant on the relative energy of the metal d-orbitals and their energy match with the cycloheptatrienyl ring. The poorer the match, the more metal in character the orbitals become, for example it has been shown that [Cr(η^5-C_5H_5)(η^7-C_7H_7)] has the most metal character δ-interactions out of all the elements from groups four to six.[21]

2.1.3 Half-Sandwich Cycloheptatrienyl Complexes

Apart from its appearance in sandwich organometallic complexes[22] and its coordination with early transition metals,[23] there are relatively few half-sandwich cycloheptatrienyl complexes when compared with the plethora of cyclopentadienyl and arene complexes. The majority of the chemistry of cycloheptatrienyl complexes has been carried out on early transition metals, and group 6 metals. In general the cycloheptatrienyl ring system is derived from η^6 co-ordination of cycloheptatriene to the metal, subsequent hydride abstraction causes the η^7 bonding of the cycloheptatrienyl ring.

In addition to this, the ring (whether it is bound to a metal centre or not) can be subjected to a whole host of lithiation and nucleophilic attacks, allowing the cycloheptatrienyl complex to be coordinated to another organometallic moiety through the ring.[24] Analogous to the cyclopentadienyl ring systems, the steric bulk of the ring can be increased, giving rise to 1,3,6 and hepta-alkylated cycloheptatrienyl and cycloheptatriene rings.[25] It is through this area of chemistry that higher group (eight and above) metals have been co-ordinated to the 7-membered ring either by a pendant

arm on the ring or η^7 to the ring.[26] The identity of the pendant arm can be almost any organic fragment, for example PR_3[19e] and CH_3,[27] or it can be a σ-bonded organometallic moiety such as $[Fe(CO)_2(\eta^5\text{-}C_5H_5)]$[28] or $[Re(CO)_5]$.[29]

The ability of cycloheptatriene to adopt several different hapticities, from η^1 to η^7, and interconvert between these with relative ease is one aspect of its chemistry that has been explored. The η^5 to η^3 interconversion of the cycloheptatrienyl ring (ring slip) is unique as the two bonding regimes can both be isolated and studied,[30] a feature that is reserved for all but a few acyclic pentadienyl ligands.[31] The ring slip can be induced by the reaction of $[Mo(CO)_4(\eta^5\text{-}C_7H_9)]^+$ with CN^tBu in acetonitrile which results in the η^3 bound ring, $[Mo(CO)_4(\eta^3\text{-}C_7H_9)]^+$ (Scheme 3, **A**). A similar ring slip can take place causing the cycloheptatrienyl ring to dramatically interconvert from η^7 to η^3, which can be caused by the facile reaction of $[Mo(CO)_2CN^tBu(\eta^7\text{-}C_7H_7)]^+$ with CN^tBu in acetonitrile at room temperature (Scheme 3, **B**).[32]

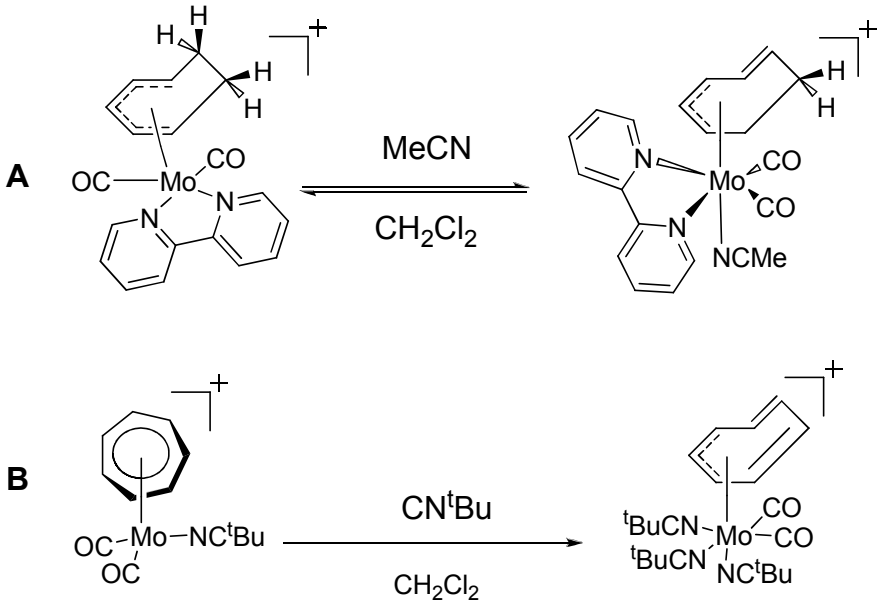

Scheme 2: A; η^5 to η^3 ring slip. B; η^7 to η^3 ring slip.

CN^tBu has been used in both cases as it promotes an associative ligand-substitution process, whereas CNMe binds too weakly and reversibly to the metal centre causing ring slippage. Investigations into the ring slippage of cycloheptatrienyl has been of importance for the understanding of organometallic reaction mechanisms and for potential catalytic applications.

2.1.4 Half-Sandwich Alkynyl Complexes

There has been a vast quantity of research on group 8 cyclopentadienyl alkynyl complexes, $[M(C{\equiv}CX)(L_2)(\eta^5\text{-}C_5R_5)]$ (M = Fe, Ru, Os, $L_2 = PR_3$, $R_2PCH_2CH_2PR_2$, CO, R = H, CH_3).[33] Although the electronic character of the alkynyl ligand can be tuned to alter the electronic character of the complexes, the nature of the metal centre also plays a role in determining the character of the frontier molecular orbitals, hence the intrinsic properties of the complex. An alternative metal /ring combination that is isoelectronic to $[Ru(\eta^5\text{-}C_5Me_5)]$ and $[Fe(\eta^5\text{-}C_5Me_5)]$ is $[Mo(\eta^7\text{-}C_7H_7)]$.[34] The steric requirements of the cycloheptatrienyl ring are similar to pentamethylcyclopentadienyl, cone angle of $C_5Me_5 = 142^o$ and $C_7H_7 = 154^o$, therefore allowing broadly similar ancillary ligands to be coordinated to the molybdenum centre.[35] Although the chemistry associated with the $[Mo(\eta^7\text{-}C_7H_7)]$ fragment has been known for a long time,[36] there has been little work done compared to the $[M(\eta^5\text{-}C_5Me_5)]$ (M = Fe, Ru) systems.

The chemistry of cycloheptatrienyl molybdenum complexes that is known is broadly similar to that of the group 8 cyclopentadienyl complexes, where the metal alkynyl complexes have been accessed by several methods. $[Mo(C{\equiv}CR)(CO)L(\eta^7\text{-}C_7H_7)]$ (L = CO, PMe_3) alkynyl complexes can be prepared by copper (I) /amine mediated

transmetallation reactions or by the reaction of the metal halide, $MoBr(CO)L(\eta^7\text{-}C_7H_7)$, with a lithiated acetylide, $LiC{\equiv}CR$ ($R = {}^tBu$, $SiMe_3$).[37] The more prominently studied electron-rich $[Mo(dppe)(\eta^7\text{-}C_7H_7)]$ auxiliary follows the reactivity of the group 8 cyclopentadienyl counterparts, such as $[Ru(CO)_2(\eta^5\text{-}C_5H_5)]$[38] and $[Fe(CO)_2(\eta^5\text{-}C_5H_5)]$ supported complexes.[39] $[Mo(solvent)(dppe)(\eta^7\text{-}C_7H_7)]^+$ (solvent = MeCN or acetone) reacts with $HC{\equiv}CR$ to give the cationic vinylidene complex, $[Mo\{=C=CR(H)\}(dppe)(\eta^7\text{-}C_7H_7)]^+$, which can be deprotonated to give the metal alkynyl.[40] The vinylidene complex, $[Mo\{=C=CR(H)\}(dppe)(\eta^7\text{-}C_7H_7)]^+$, has a unique orientation with respect to the metal centre. For the analogous group 8 complexes the vinylidene is approximately in the plane of the cyclopentadinyl ring. For the $[Mo(dppe)(\eta^7\text{-}C_7H_7)]$ supported complex, the vinylidene is orthogonal to the plane of the cycloheptatrienyl ring (Figure 3).

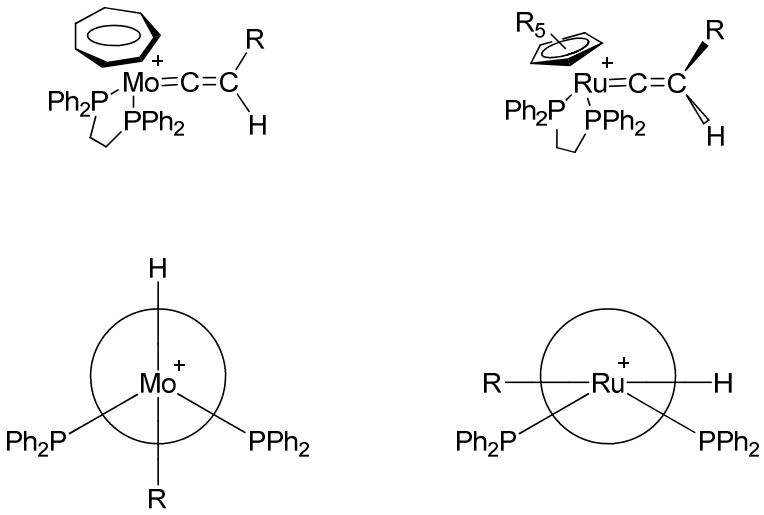

Figure 3: Orientation of $Ru(dppe)(\eta^5\text{-}C_7H_7)$ and $Mo(dppe)(\eta^7\text{-}C_7H_7)$ vinylidene complexes.

This geometric difference is due to the difference in electronic structure brought about by the strong δ-interactions of the cycloheptatrienyl ring and the metal d-orbitals. This causes the vinylidene moiety to adopt the most sterically favorable position due to the

lack of strong dπ-interactions, which dominate the ruthenium based system.[41] The number of molybdenum acetylides [Mo(C≡CR)(dppe)(η^7-C_7H_7)] (R = C_6H_5, ^{t}Bu and ^{n}Bu) synthesised has been limited, but these three complexes have demonstrated that the [Mo(C≡CR)(dppe)(η^7-C_7H_7)] alkynyls are very thermodynamically stable with respect to oxidation. The $E_{1/2}$ value for [Mo(C≡CC_6H_5)(dppe)(η^7-C_7H_7)] (**1**) less positive than the analogous group 8 alkynyl complexes by 0.11 V and 0.56 V [Fe(C≡CC_6H_5)(dppe)(η^5-C_5Me_5)] (**2**),[42] and [Ru(C≡CC_6H_5)(dppe)(η^5-C_5Me_5)] (**3**), [43] respectively. This stability has been exploited and the redox pair, $\mathbf{1}^{n+}$ (n = 0 or 1), was one of the earliest organometallic examples to be structurally characterised.[44] The ability to generate the stable radical cation $\mathbf{1}^+$, has allowed the complex to be investigated by EPR spectroscopy. The spectrum of $\mathbf{1}^+$ is very well resolved, from which the hyperfine values can be easily determined for the electron coupling to the molybdenum centre, the hydrogen nuclei of the cycloheptatrienyl ring and to the phosphorus atoms.

Although the radical cation [Mo(C≡CC_6H_5)(dppe)(η^7-C_7H_7)]$^+$ is stable enough to structurally characterise, it is subject to radical dimerisation at the C_2 position over time to give a bis(vinylidene) product, [{Mo(dppe)(η^7-C_7H_7)}$_2${μ-=C=(C_6H_5)CC(C_6H_5)=C=}]$^{2+}$ ($\mathbf{29}^{2+}$) (Scheme 4).[45]

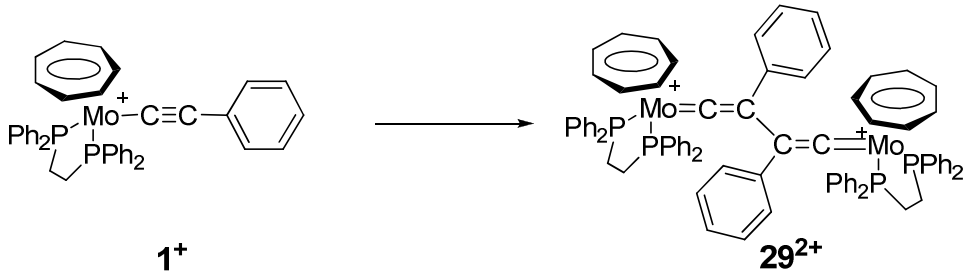

Scheme 3: Dimerisation of [Mo(C≡CC_6H_5)(dppe)(η^7-C_7H_7)]$^+$.

Although this reactivity is not unique to molybdenum alkynyl radicals, the same can be electrochemically induced for [Fe(C≡CH)(dppe)(η^5-C_5Me_5)] (**4**).[46] Dimerisation of acetylide radical cations is a common trait among many half sandwich organometallic systems, for example [Fe(C≡CCH_3)(dppe)(η^5-C_5H_5)]$^+$ (**31**$^+$), will dimerise via the C_2 carbon when reacted with **31** resulting in [{Fe(dppe)(η^5-C_5H_5)}$_2${μ-=CC(CH_3)C(CH_3)C=}]$^{2+}$ (**32**).[47] The generation of the bis-vinylidene intermediate from the radical dimerisation of **4**$^+$ and subsequent deprotonation has been used in the formation of the butadiyndiyl complex [{Fe(dppe)(η^5-C_5Me_5)}$_2$)(μ-C≡CC≡C)] (**53**).[48] The reduction of [Cr(C≡CC_6H_5)$(CO)_3$(η^5-C_5H_5)] (**34**), with potassium results in the loss of CO, carbon-carbon bond formation and rearrangement to produce a carbene based bridge [{$Cr(CO)_2$(η^5-C_5H_5)}$_2${≡CC(C_6H_5)C(C_6H_5)C≡}] (**35**).[49] Other carbonyl containing complexes such as [Tp'$(CO)_2$M≡CCH(C_6H_5)CH(C_6H_5)C≡M$(CO)_2$Tp'] (M = W, Mo and Tp' = trispyrazolylborate), can be formed by the reductive coupling of two molecules of [Tp'$(CO)_2$M=C=CR(H)]$^+$.[50]

2.2 Synthesis

In order to explore the electronic structure of the molybdenum acetylide a new series of aryl acetylide complexes, [Mo(C≡CC_6H_4X-4)(dppe)(η^7-C_7H_7)], have been synthesised with subtituents of varying electron donor and acceptor properties, where X = NH_2 (**6**), OMe (**7**), CH_3 (**8**), CHO (**9**), CO_2Me (**10**). In addition, the previously reported complexes [Mo(C≡CC_6H_5)(dppe)(η^7-C_7H_7)] (**1**) and [Mo(C≡CFc)(dppe)(η^7-C_7H_7)] (**11**),[40e] (where Fc = (C_5H_4)Fe(η^5-C_5H_5) have been re-synthesised using the new methodologies described here. To complement the aryl acetylide complexes, and to

further show the adaptability of the synthetic methodologies, the non-aryl acetylide complexes [Mo(C≡C^{t}Bu)(dppe)(η^7-C_7H_7)] (**12**), [Mo(C≡CCO_2Me)(dppe)(η^7-C_7H_7)] (**13**), [Mo(C≡C$C_{14}H_9$)(dppe)(η^7-C_7H_7)] (**14**), were synthesised. Complexes **1**, **8**, **12** and **13** were synthesised at the University of Manchester by Dr. Emma C. Fitzgerald.

The development of the facile synthesis of MoBr(dppe)(η^7-C_7H_7) (**5**), from $Mo(CO)_6$ has allowed the development of two methodologies for the synthesis of molybdenum acetylides (Scheme 4).[44]

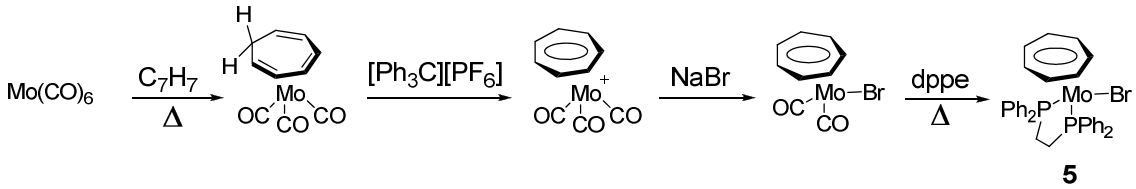

Scheme 4: Synthesis of 5.

The most direct method utilizes the straightforward formation of the vinylidene complex [Mo{=C=CR(H)}(dppe)(η^7-C_7H_7)]Br *in situ* from the reaction of **1** with HC≡CR in refluxing methanol. Subsequent efficient *in situ* deprotonation by either NaOMe solution or KO^{t}Bu gave the acetylide complex in good yield (40-60 %).

The second method involves the reaction between trimethylsilyl protected acetylenes, Me_3SiC≡CR, and KF, which is used to desilylate the acetylene. Previous reports have argued that the desilylmetallation process could proceed via two possible mechanisms (Scheme 5). The first is where the acetylene is first desilylated by the fluorine anion and the vinylidene product deprotonated by methoxide formed *in situ*. The second would involve the formation of a trimethsilyl vinylidene,

$[Mo\{=C=CR(SiMe_3)\}(dppe)(\eta^7\text{-}C_7H_7)]^+$, promoted by the halide abstracting abilities of the $[PF_6]^-$ anion, followed by the disilylation of the vinylidene complex to produce the acetylide product. Nevertheless, although the precise mechanism is not yet known, desilylmetallation reactions are now established as viable routes to metal acetylide complexes.[51]

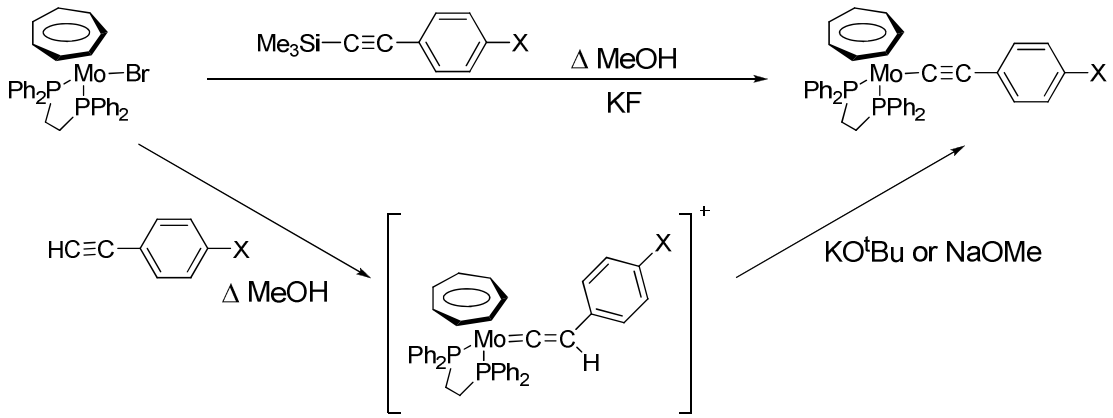

Scheme 5: Routes towards $[Mo(C{\equiv}CC_6H_4X\text{-}4)(dppe)(\eta^7\text{-}C_7H_7)]$.

In the case of the preparation of **7** and **9** from $Me_3SiC{\equiv}CC_6H_4CHO$-4 and $Me_3SiC{\equiv}CC_6H_4OMe$-4 it was not necessary to add $[PF_6]^-$ for the reaction to complete, and the addition of the anion made no difference to the yield, which reflects the lability of the bromide ligand. Using these methodologies the molybdenum acetylides could be isolated in good yields (50-60 %). Depending on the donor /acceptor capacity of the aryl substituent the complexes were isolated as green powders for strong donor substituents and purple /black powders for strongly withdrawing substituents. Compounds **12** and **13**, where no aryl ring is attached to the acetylide moiety, were more yellow to orange in colour, respectively.

Despite cationic molybdenum acetylide complexes being susceptible to dimerisation, it has been shown this is a relatively slow process (24 hours), allowing the isolation of the

cationic complexes. Chemical oxidation using $[Fe(\eta^5\text{-}C_5H_5)_2]PF_6$ and $[Fe(\eta^5\text{-}C_5H_5)_2]BF_4$ in dichloromethane were undertaken for **12** and **14**. The resulting cationic complexes [**12**]BF_4 and [**14**]PF_6 were isolated and their identities confirmed by infrared spectroscopy and elemental analysis.

2.3 Molecular Structures

The molecular structures of **9** (Figure 4), **10** (Figure 5) and **14** (Figure 6) were determined by the X-ray crystallography service at Durham University and the structures of **8**, **12**, **13**, and [**12**]BF_4 at the University of Manchester. A selection of key bond lengths and bond angles are summarised in Table 1. The molecular structure of **1** and [**1**]BF_4 was determined in previous work by Whiteley *et al*, but is included here as a point of comparison.[44]

Table 1: Selected bond length and angles for 1, $[1]^+$, 8, 9, 10, 12, $[12]^+$, 13, 14. Where [Mo] = Mo(dppe)(η^7-C_7H_7)

Complex	**1**	$[\mathbf{1}]^+$	**8**	**9**	**10**	**12**	$[\mathbf{12}]^+$	**13**	**14**
[Mo]C≡CX	C_6H_5	C_6H_5	$C_6H_4CH_3$-4	C_6H_4CHO-4	$C_6H_4CO_2Me$-4	^tBu	^tBu	CO_2Me	$C_{14}H_9$
Bond lengths /Å									
Mo-C_1	2.138(5)	2.067(9)	2.140(5)	2.1094(19)	2.122(7)	2.1382(17)	2.070(11)	2.146(2)	2.164(2)
C_1-C_2	1.205(6)	1.196(11)	1.196(6)	1.212(3)	1.191(10)	1.216(2)	1.201(12)	1.179(3)	1.158(3)
C_2-$C_{(substituent)}$	1.434(7)	1.445(12)	1.441(7)	1.426(3)	1.453(10)	1.485(2)	1.507(14)	1.436(3)	1.449(3)
Mo-P	2.477(1), 2.467(1)	2.538(2), 2.528(3)	2.4677(14), 2.4525(14)	2.4767(5), 2.4772(5)	2.477(2), 2.455(2)	2.4648(4), 2.4520(4)	2.537(3), 2.528(3)	2.4731(6), 2.4686(6)	2.4487(5), 2.4502(5)
Bond Angles /º									
Mo-C_1-C_2	178.5(4)	174.6(8)	174.0(5)	178.54(16)	174.17(6)	175.17(14)	175.1(10)	176.33(18)	175.58(16)
C_1-C_2-$C_{(substituent)}$	177.9(5)	175.0(10)	174.6(6)	176.71(19)	171.0(8)	177.42(18)	178.2(12)	177.6(2)	177.2(2)
P-Mo-P	78.2(1)	78.4(1)	78.39(5)	78.558(18)	78.63(7)	78.312(14)	78.70(10)	78.38(2)	77.92(5)
P-Mo-C_1	83.8(2), 77.3(2)	83.5(3), 75.1(3)	81.59(13), 77.96(13)	84.47(5), 76.73(5)	81.21(2), 77.43(2)	80.24(4), 78.67(4)	80.5(3), 75.0(3)	80.52(5), 79.18(5)	85.08(5), 79.218(16)

There is little structural change in the Mo(dppe)(η^7-C_7H_7) moiety upon changing the para substitutent on the aryl ring, as emphasised in changing the substituent from CH_3 to CO_2Me. The Mo-C_1 bond changes by less than 0.01 Å, and the Mo-P bonds vary by less than 0.01 Å, showing that the aryl substituent has little influence upon the geometry around the metal centre. Upon increasing the size of the aromatic ring on the acetylide as in the anthracene derivative, **14**, similar small changes are seen across the bond lengths and bond angles. Upon removing the aryl substituent and changing it to a non-aryl substituent as in **12** and **13**, the Ru-C_1 and C_1-C_2 bond lengths are still very similar with the largest change occurring, as expected, for the C_2-$C_{substituent}$ of 0.02 Å as a result of changing the hybridization of the $C_{substituent}$ carbon.

The isolation of the redox pair **12** and [**12**]BF_4, as described above, and the known structures of the redox pair **1** and [**1**]BF_4 allows the structural effects of oxidation upon the complex to be more widely investigated. The removal of an electron from the neutral complex causes a contraction of the Mo-C_1 bond by 0.06 Å and an elongation of the Mo-P by 0.07 Å, although there is a comparatively small change (0.01 Å) in the C_1-C_2 bond lengths. These localised structural changes to the complex indicate that the electron must have been removed from a frontier orbital which is predominantly metal centre in character.

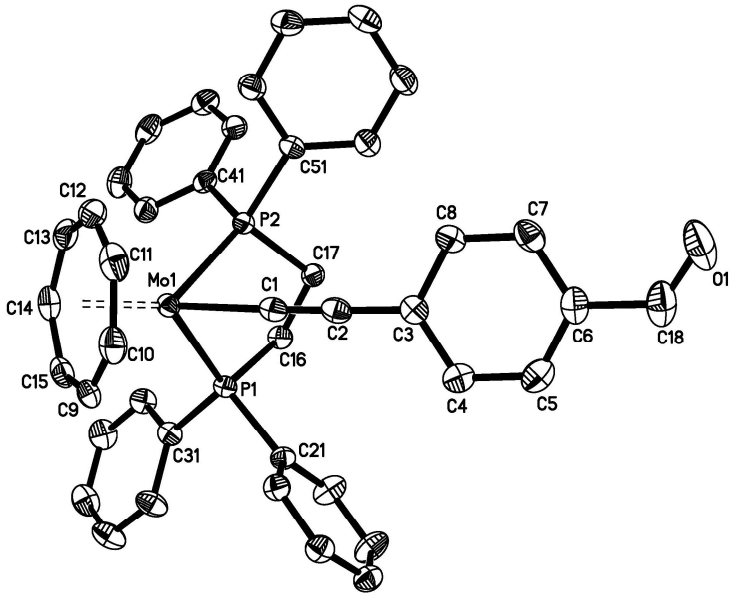

Figure 4: ORTEP plot of 9 showing the labeling scheme. The hydrogen atoms omitted for clarity. The thermal ellipsoids are plotted at 50 % probability.

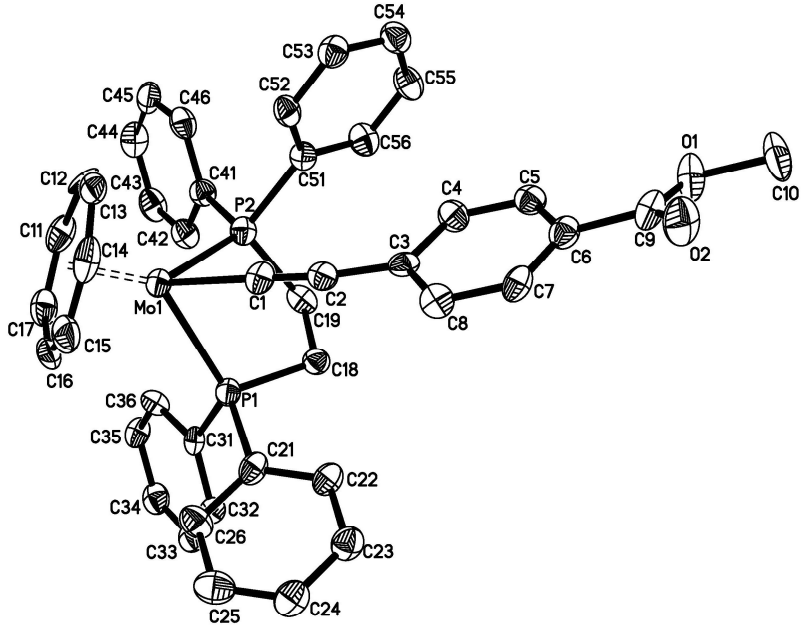

Figure 5: ORTEP plot of 10 showing the labeling scheme. The hydrogen atoms omitted for clarity. The thermal ellipsoids are plotted at 50 % probability.

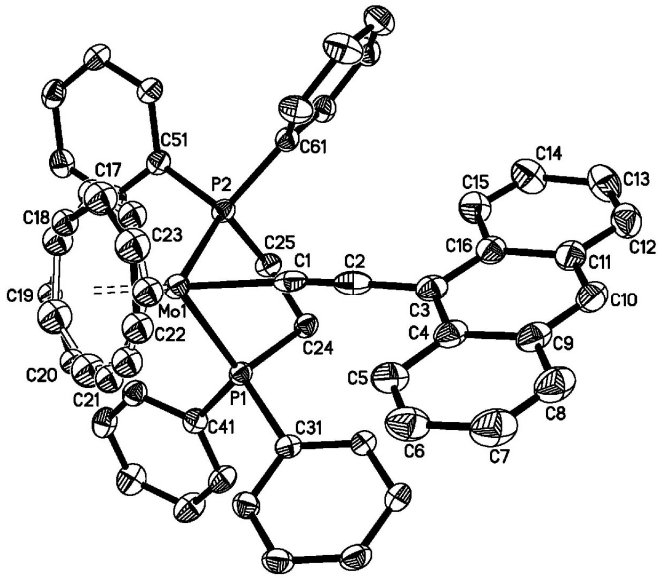

Figure 6: ORTEP plot of 14 showing the labeling scheme. The hydrogen atoms omitted for clarity. The thermal ellipsoids are plotted at 50 % probability (Disorder in the orientation of the C_7H_7 ring).

2.4 Spectroscopic Investigations

All the complexes **6-14** were characterised by a variety of techniques including elemental analysis or high-resolution mass spectrometry, low-resolution mass spectrometry, infrared spectroscopy and ^{1}H, ^{31}P and ^{13}C NMR spectroscopies. Using these spectroscopic techniques the electronic effect of the acetylide substituent on the electronic structure of the neutral complexes could be easily monitored.

Upon changing the electronic character of the aryl *para* substituent, from electron donating to withdrawing, the ν(C≡C) shifts to lower wavenumbers, for example 2053 cm^{-1}, **6**; 2027 cm^{-1}, **10**. This trend is similar to that noted in the analogous ruthenium series, [Ru(C≡CC_6H_4X-4)(dppe)(C_5Me_5)], where X = NH_2 (ν(C≡C) = 2072 cm^{-1}) and where X = NO_2 (ν(C≡C) = 2050 cm^{-1}). The lack of significant influence of the aryl

substituent on the electronic character of the metal fragment is supported by the narrow range of the ^{31}P NMR resonances for **1**, **6-14** which fall between δ 64-66 ppm. $^{13}C\{^{1}H\}$ NMR data show a very distinct range for the C_1 resonances for strongly electron withdrawing substituents δ C_1 is around 160 ppm, and for strongly donating substituents δ C_1 140 ppm (Table 2). For complexes **6** and **7**, the C_1 resonance was not observed. This is most likely due to the low intensity resonance being masked by the much stronger resonance of the dppe carbons.

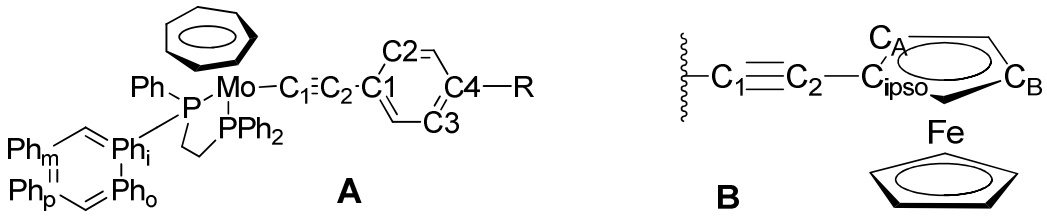

Figure 7: ^{13}C NMR labeling scheme for an aryl acetylide complex (A) and for ferrocene containing complex 11 (B).

Table 2: $^{13}C\{^1H\}$ NMR data, all recorded in CD_2Cl_2, removal of paramagnetic residues from the mixture was carried out by the addition of $[Co(\eta^5\text{-}C_5H_5)_2]$. Labeling scheme in Figure 7.

^{13}C resonance	**12**	**11**	**13**	**6**	**7**	**8**	**1**	**9**	**10**
	Non-aryl acetylide			Aryl acetylide					
C_1	t, 113.1, J_{CP} = 27	t, 132.0, J_{CP} = 27	t, 157.7, J_{CP} = 24	-	-	t, 139.3, J_{CP} = 26	t, 141.4 J_{CP} = 26	t, 160.0, J_{CP} = 26	-
C_2	br, 132.6	br, 116.2	br, 115.0	br, 119.6	br, 120.9	-	br,121.6	t, 132.9, J_{CP} = 8.3	t, 130.9, J_{CP} = 4.8
C_7H_7	s, 86.6	s, 86.8	s, 87.8	s, 87.0	s, 87.0	s, 87.2	s, 86.8	s, 87.3	s, 87.2
CH_2 x 2	m, 26.7	m, 26.6	m, 26.7	m, 26.6	m, 26.5	m, 26.8	m, 26.3	m, 26.5	m, 26.5
C1	-	-	-	s, 121.3	s, 121.8	s, 121.8	s, 122.6	s, 130.8	s, 132.8
C2				s, 130.1	s, 130.0	s, 129.0	s, 129.3	s, 134.2	s, 128.7
C3				s, 114.3	s, 112.9	s, 128.2	s, 128.1	s, 128.7	s, 128.7
C4				s, 142.7	s, 155.9	s, 132.6	s 128.6	s, 124.8	s, 123.5
Ph_i	m, 136.3, 141.7	m, 135.9, 141.2	m, 135.6, 140.2	m, 136.3, 141.2	m, 136.2, 141.1	m, 136.3, 141.3	m, 135.7, 140.8	m, 135.3, 140.6	m, 135.5, 140.6
Ph_o	dd, 131.2, 134.4, J_{CP} = 5.8, 4.8	dd, 134.4, 134.4, J_{CP} = 5, 4.8	dd, 132.2, 133.8, J_{CP} = 5.1, 5.1	dd, 131.8, 134.1, J_{CP} = 4.8 Hz, 5.8	dd, 131.7, 134.0, J_{CP} = 5.3 , 5.8	dd, 131.9, 134.2, J_{CP} = 5.0, 5.0	m, 131.4, 133.8	dd, 131.6, 133.9, J_{CP} = 5.5 , 5.5	dd, 131.6, 133.9, J_{CP} = 5.3 , 5.8
Ph_m	dd, 127.4, 127.9, J_{CP} = 3.7, 4.5	dd, 127.6, 128.0, J_{CP} = 3.9, 4.8	br 128.2, 128.6	dd, 127.9, 128.3, J_{CP} = 4.8 , 3.8	dd, 127.9, 128.3, J_{CP} = 4.8 , 4.3	dd, 128.1, 128.5, J_{CP} = 7.0, 4.0	m, 127.7, 128.0	dd, 128.2, 128.4, J_{CP} = 4.8 , 4.2	dd, 128.1, 128.4, J_{CP} = 4.8 , 4.3
Ph_p	s, 128.3, 129.0	s, 129.4, 128.6	s, 129.6, 129.8	s, 128.9, 129.4	s, 128.9, 129.4	s, 129.1, 129.7	s, 127.1, 128.6	s, 129.1, 129.8	s, 129.1, 129.7
Substituent	s, 28.3, *C*Me$_3$	s, 68.5, C_5H_5	s, 50.9, OCH_3	-	s, 55.2, OMe	s, 21.1, CH_3	-	s, 190.7, C=O	s, 51.7, OCH_3
Substituent	s, 31.4, C(*C*H$_3$)	s, 74.5, C_{ipso} s, 68.1, C_A, s, 65.8, C_B	s, 152.3, C=O			-		s, 167.1, C=O	-

The non-aryl complexes show a greater varience when compared to the aryl acetylides, where by ^{13}C NMR δ C_1 varies from 113.1 ppm for **12** to 157.7 ppm for **13**. A similar trend is seen for δ C_2, although as for the aryl acetylides, the effect is less pronounced. The $\nu(C\equiv C)$ stretch for these complexes reveals the increased electronic effect of the substituent on the electronic structure, where the strongly electron withdrawing methyl propiolate ligand in **13** provides the lowest $\nu(C\equiv C)$ in the series.

2.5 Electrochemistry

In cyclic voltammetry experiments, the complexes **1** and **6-14** resulted in a single one electron reversible waves with comparable peak to peak seperation to the internal ferrocene /decamethylferrocene standard (Table 3).

Table 3: Cyclic voltammetry data recorded in 0.1 M $^{n}Bu_4NPF_6$ /CH_2Cl_2 solutions at a Pt electrode. All values referenced to FcH /FcH^+ = 0.00 V.

Compound	$E_{1/2}$ /V
1 (–30 °C)	-0.72
6	-0.81
7 (–30 °C)	-0.74, +0.60[a]
8 (–30 °C)	-0.72
9	-0.70
10	-0.65
11	-0.79, +0.07
12 (–30 °C)	-0.82
13 (–30 °C)	-0.50
14	-0.69, +0.50

[a] irreversible oxidation process.

The potentials for the aryl acetylides fall within a comparatively small window of 160 mV, which is significantly smaller than the range of values found in the analogous ruthenium series that spans 440 mV. In general, [Mo(C≡CR)(dppe)(η^7-C_7H_7)]

acetylides oxidise at considerably less positive potentials than the analogous ruthenium series. The extension of the aryl ligand system to the anthracene derivative, **14**, causes the oxidation potential to shift by 30 mV in comparison to **1**, due to the increased electron withdrawing effect of the anthracyl group. The non-aryl acetylide complexes **12** and **13** are much more sensitive to the electronic nature of the substituent as the potential falls within a much greater range, 320 mV, which is to that found for the ruthenium aryl acetylide series.

Table 4: Cyclic voltammetry data for a selection of $Fe(C{\equiv}CC_6H_4X)(dppe)(\eta^5\text{-}C_5Me_5)$ and $Ru(C{\equiv}CC_6H_4X)(dppe)(\eta^5\text{-}C_5Me_5)$ aryl acetylides. All values corrected to $FcH/FcH^+ = 0.00$ V couple.

Compound	$E_{1/2}$ /V
$Ru(C{\equiv}CC_6H_4NH_2\text{-}4)(dppe)(\eta^5\text{-}C_5Me_5)$	-0.41
$Ru(C{\equiv}CC_6H_5)(dppe)(\eta^5\text{-}C_5Me_5)$	-0.16
$Ru(C{\equiv}CC_6H_4NO_2\text{-}4)(dppe)(\eta^5\text{-}C_5Me_5)$	-0.06
$Ru(C{\equiv}CC_{14}H_8)(dppe)\ (\eta^5\text{-}C_5Me_5)$	-0.17
$Fe(C{\equiv}CC_6H_4NH_2\text{-}4)(dppe)(\eta^5\text{-}C_5Me_5)$	-0.71
$Fe(C{\equiv}CC_6H_5)(dppe)(\eta^5\text{-}C_5Me_5)$	-0.61
$Fe(C{\equiv}CC_6H_4CH_3\text{-}4)(dppe)(\eta^5\text{-}C_5Me_5)$	-0.64

In addition to the one molybdenum centered oxidation event, complexes **8**, **11** and **14** have second oxidation events on their respective ligands. For complex **8** the oxidation is only partially reversible and takes place on the methoxy substituent of the aryl ring, which is characteristic for complexes containing this ligand.[15b] The nature of the second oxidation event for **11** has already been discussed in a previous publication[52] where it was concluded to take place on the ferrocenyl substituent, this conclusion was reached as the molybdenum centre oxidises much more readily than the iron centre. Complex **14** had a second fully reversible oxidation that is assumed to take place on the anthracene substituent. This is in comparison to the ruthenium analogue that exhibited an irreversible oxidation at higher potentials, showing that the molybdenum anthryl acetylide exhibits a unique stability for this ligand centered oxidation.[15a]

2.6 Infrared Spectroelectrochemistry

Using the electrochemical results as a guide, spectroelectrochemical investigations were undertaken to establish the effect of oxidation on both the geometric and electronic structure of a complex. The use of spectroelectrochemical techniques has allowed the quick and easy generation of the cationic complexes *in situ* rather than having to isolate and purify the cationic complexes as salts. The acetylide bond is an ideal vibrational probe for investigating the interaction of the Mo(dppe)(η^7-C_7H_7) fragment with an *sp*-hybridised carbon chain, as it is very sensitive to the degree of metal /ligand mixing. When the frontier orbitals of the complex arise from effective mixing of the metal d-orbitals and the cylindrical π-orbital system on the acetylide moiety, the ν(C≡C) stretch will be strongly affected by the removal of an electron from the complex. This can be seen in the ruthenium acetylide series whereby removal of an electron from the system causes ν(C≡C) stretch to shift up to -145 cm^{-1}, this shows that the metal is mixing well with the organic ligand indicating that the electron is being removed from a frontier orbital that is mostly ligand in character.

Table 5: Infrared spectroelectrochemical results recorded in 0.1 M $^{n}Bu_4NPF_6$ /CH_2Cl_2.

Compound	ν(C≡C) /cm^{-1}			Δν(C≡C) /cm^{-1}
	n = 0	n = 1	n = 2	
1^{n+}	2045	2032	-	-13
6^{n+}	2055	1996	-	-59
7^{n+}	2055	2011	-	-44
8^{n+}	2050	2017	-	-33
9^{n+}	2047	2033	-	-14
10^{n+}	2030, 1993	2031	-	-1
12^{n+}	2057	2044	-	-13
11^{n+}	2057	2009	-	-48
13^{n+}	2020	-	-	-
14^{n+}	2020	1994	2136	-26

All the complexes **1**, **6-14** exhibited comparatively small shifts for ν(C≡C) on oxidation, the greatest being -59 cm^{-1} for **6**. In some cases the shift in ν(C≡C) is negligible, in others the band for the cation complex is of such low intensity that it could not be distinguished from the spectroscopic noise. This is especially true for complexes **10** and **13**, which have strongly electron withdrawing substituents, that have less intense ν(C≡C) bands in any event due to a smaller dipole being present across the C≡C bond. Complex **10** displays multiple bands for the neutral complex due to Fermi coupling, which is often observed in the iron acetylide complexes [Fe(C≡CR)(dppe)(C_5Me_5)].[34] The small magnitude of change in the ν(C≡C) between the neutral and cation species across the aryl and non-aryl acetylides series, indicates that there is little mixing between the metal d-orbitals and the acetylide π-orbitals in the HOMO of these complexes.

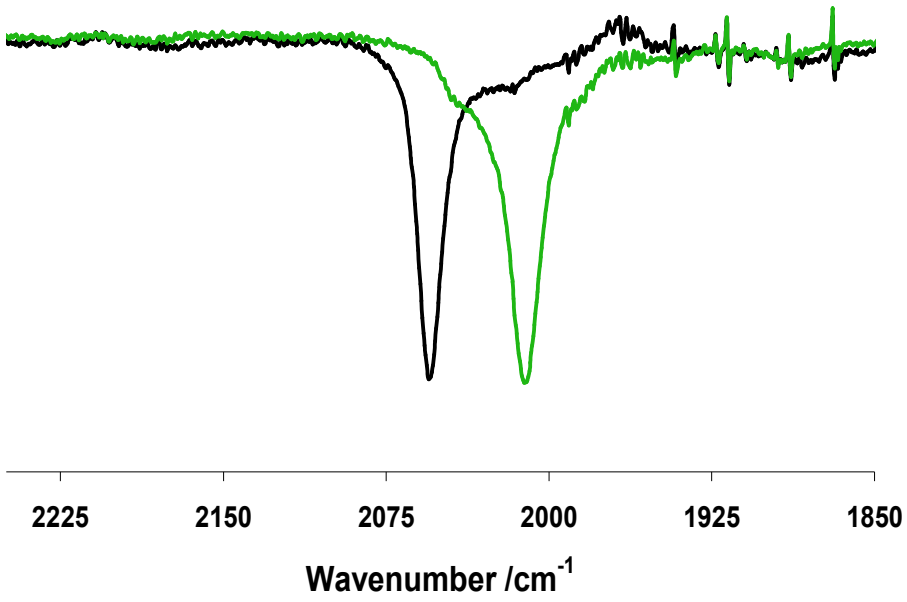

Figure 8: Infrared spectra for 7^{n+}, where n = 0 (Black) and n = 1 (Green) (Recorded in 0.1 M $^{n}Bu_4PF_6$ /CH_2Cl_2).

The second oxidation event for **11** was assessed by this method and was found to be irreversible under the experimental conditions with the original spectrum unrecoverable. On the other hand, the sequence **14** / $\mathbf{14}^{+}$ / $\mathbf{14}^{2+}$ was fully reversible and showed a large positive shift from ν(C≡C) 1994 cm^{-1} to 2136 cm^{-1}, from the monocation to the dication, indicating that the second oxidation is very much centered upon the anthryl group.

2.7 EPR Spectroscopy

EPR measurements were kindly conducted by Dr. E. Fitzgerald and Dr. R. Edge at the Manchester National EPR centre on complexes $\mathbf{1}^+$, $\mathbf{7}^+$, $\mathbf{8}^+$, $\mathbf{10}^+$ and $\mathbf{13}^+$. The well resolved EPR signal for the ^{96}Mo centre allows for the exact mapping of the electron on the complex. The radical cation complexes, $[Mo(C{\equiv}CR)(dppe)(\eta^7\text{-}C_7H_7)]^+$ were generated *in situ* by the titration of [FcH][PF_6] in CH_2Cl_2 at 243 K and fluid spectra taken of the samples. X-band spectra of the complexes were recorded and show that the hyperfine coupling parameters vary very little upon changing the nature of the substituent.

Table 6 X-Band solution spectra in CH_2Cl_2 at 243 K, hyperfine couplings in gauss.

	A_{iso}(Mo)	$a_{iso}(^{31}P)$	$a_{iso}(^{1}H)$	g_{iso}
$\mathbf{1}^+$	31.3[b]	22.6	4.3	1.996
$\mathbf{7}^+$	31.3	22.1	4.2	1.995
$\mathbf{8}^+$	31.3	22.1	4.3	1.995
$\mathbf{10}^+$	31.3	22.8	4.3	1.996
$\mathbf{13}^+$	31.3	23.3	4.5	1.996

Anisotropic values were found for the electron coupling to the protons on the cycloheptatrienyl ring and the phosphorus atoms on the dppe ligand. However, no significant values were evidenced for the coupling of the electron to the alkynyl ligand. In addition to solution spectra, solid-state spectra were recorded for [**1**]PF_6 at W-band which reveals anisotropic *g* values, (g_1 = 1.9992, g_2 = 1.9958, g_3 = 1.9892; $\Delta g = g_1 - g_3 = 0.0100$). The *g* anisotropy values for $\mathbf{1}^+$ are very small in comparison to the values obtained for the frozen solution spectra of $\mathbf{2}^+$ (Δg = 0.489)[15e] and $\mathbf{3}^+$

(Δg = 0.239)[53] small g anisotropy values indicate that the electron is localised on the Mo(dppe)(η^7-C_7H_7) fragment rather than delocalised across the acetylide moiety.

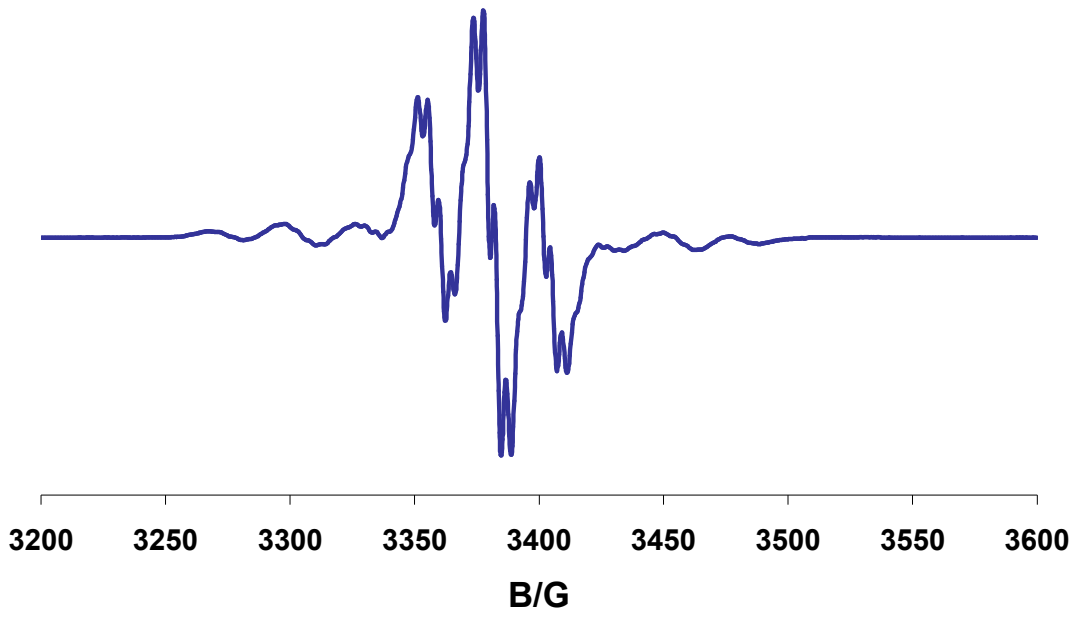

Figure 9: First derivative X-band fluid solution (CH_2Cl_2, 243 K) of 8^+.

2.8 Electronic Structure Calculations

Electronic structure calculations were carried out by Dr. J. W. W. McDouall at the University of Manchester and are included here for completeness and to help explain the metal centered character of the $[Mo(C{\equiv}CR)(dppe)(\eta^7\text{-}C_7H_7)]^{n+}$ complex.

The optimised structures for $[Mo(C{\equiv}CR)(dppe)(\eta^7\text{-}C_7H_7)]^{n+}$, denoted **1H** and $\mathbf{1H^+}$ to distinguish them from the experimental system, were generated using the hybrid-functional B3LYP and the def-SVP basis set obtained from the Turbomole library[54] for the atoms C, H and P. The Mo centre was modeled using the basis set LANL2DZ. The optimised geometries were confirmed to be real by the frequency calculations as no imaginary frequencies were found.

Table 7: Selected calculated bond lengths and angles from 1H and $1H^+$ and a comparison to the experimental data of 1 and 1^+.

Complex	**1H**	**1**	$\mathbf{1H^+}$	$\mathbf{1^+}$
Bond lengths /Å				
$Mo\text{-}C_1$	2.125	2.138(5)	2.073	2.067(9)
$C_1\text{-}C_2$	1.238	1.205(6)	1.239	1.196(11)
$C_2\text{-}C_{(substituent)}$	1.429	1.434(7)	1.427	1.445(12)
Mo-P	2.529 2.527	2.477(1) 2.467(1)	2.596 2.591	2.538(2) 2.528(3)
Bond Angles /º				
$Mo\text{-}C_1\text{-}C_2$	177.6	178.5(4)	176.5	174.6(8)
$C_1\text{-}C_2\text{-}C_{(substituent)}$	179.8	177.9(5)	179.5	175.0(10)
P-Mo-P	78.6	78.2(1)	79.1	78.4(1)
$P\text{-}Mo\text{-}C_1$	84.2 77.7	83.8(2) 77.3(2)	83.1 77.5	83.5(3) 75.1(3)

The key feature of the electronic structure of **1H** is the d_{z2} which dominates the HOMO of the structure. The origin of this interaction is due to the strong δ-interaction between the d_{x2-y2} and d_{xy} and the e_2 level of C_7H_7 ring system. This acts to stablize the d_{x2-y2} and d_{xy} metal orbitals, thus lowering their energy and removing them from the frontier orbitals. This in turn causes the promotion of the d_{z2} orbital to be the dominat orbital of the frontier molecular orbitals. The other two metal d-orbitals, d_{zx} and d_{zy}, are shifted to much lower (HOMO-18 and HOMO-19) energies by a strong π-type interaction with the C_7H_7 ring and contribute to the bonding of the metal centre to the alkynyl ligand, via π and σ interactions. This effect is shown in the orbital contributions for the HOMO, where the acetylide moiety has only 25 % of the electron density with the rest being situated on the metal end cap. The strong π- and δ-type interactions between the lower lying metal d-orbitals and the C_7H_7 ring, as represented by the large amount of electron density situated on the C_7H_7 ring and the molybdenum centre for the occupied frontier orbitals which contain these interactions. This type of bonding character mirrors that seen for the well studied $[M(\eta^5C_5R_5)(\eta^7\text{-}C_7H_7)]$ complexes (M = see introduction for examples).

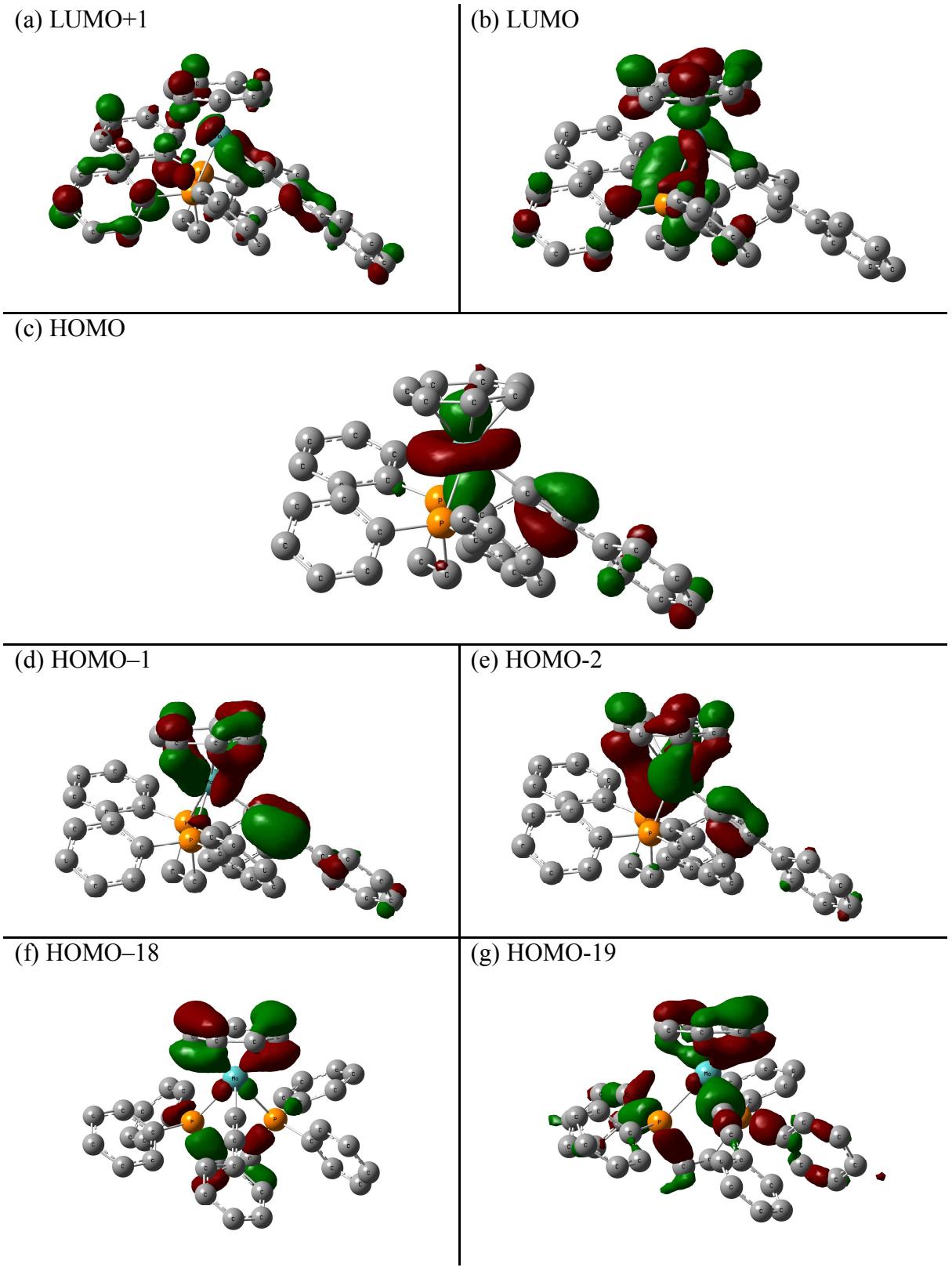

Figure 10: LUMO+1, LUMO, HOMO, HOMO-1, HOMO-2, HOMO-18, and HOMO-19 of 1H at B3LYP /SVP (including PCM solvation in CH_2Cl_2) plotted as an isosurface of 0.04 au.

The strong Mo-C_7H_7 δ-bonding interactions are in contrast to the smaller cyclopentadienyl systems, [Fe(C≡CR)(dppe)($\eta^5C_5Me_5$)] and [Ru(C≡CR)(dppe)(C_5Me_5)], which are unable to form a strong δ interaction with the metal centre. In these systems the interaction of the orthogonal π-system of the alkynyl system dictates the nature of the occupied frontier orbitals. This serves to provide the HOMO with a favorable symmetry, and strong π interaction between the almost degenerate d_{zx} and d_{zy} and the acetylide moiety π-system, hence the HOMO of the complex has a large degree of ligand character.

On oxidation of the ruthenium acetylides, where the metal d-orbitals are of the correct symmetry and energy to interact well with the acetylide moiety, there is a strengthening of the metal carbon bond and a weakening of the C≡C bond. However, due to the symmetry constraints imposed by the d_{z2} orbital for the molybdenum system this effect is not realised. Therefore, the removal of an electron from **1H** to give **1H**$^+$, cases little or no change in the length or strength of the carbon chain, indicative of a HOMO which is largely metal in character.

2.9 UV /vis /NIR Spectroelectrochemistry and TD-DFT Calculations

The UV /vis spectra of complexes **1**, **7**, **8**, **10**, **12**, **13**, and **14**, were recorded and their corresponding radicals generated *in situ* using spectroelectrochemical methods. The processes were fully reversible using the spectroelectrochemical cell and the original spectra were recovered in full after each oxidation. Complexes **1**, **7**, **8**, **10** and **14** all showed a very similar band structure at high energy, and at lower energy (16000 to 19000 cm^{-1}) lower intensity substituent dependent bands were found. These lower energy bands are responsible for the colour changes from green to black, depending on the electronic nature of the aryl substituent. In addition to this, all the complexes exhibited a low intensity broad band around 11000 cm^{-1}, with the exception of **14** which was found at much lower energy (7500 cm^{-1}), tailing off the more intense broad band at 17000 cm^{-1}. The spectra for the non-aryl acetylide complexes followed a similar pattern, however the lower energy transitions were shifted to higher energy (20000 cm^{-1}), hence explaining the yellow /orange colour of the complexes.

Table 8: UV /vis spectroelectrochemical data recorded in 0.1 M $^{n}Bu_4NPF_6$ /CH_2Cl_2 solutions.

Compound	n = 0	n = 1	n = 2
$\mathbf{1}^{n+}$	32700 (21000) 27000 (12200) 18900 (1000)	33300 (15600) 28300 (8400) 18900 (2100) 16900 (4800) 12300 (390)	
$\mathbf{7}^{n+}$	32500 (17600) 27900 (11100) 17000 (650)	28200 (8600) 16000 (5900) 12400 (770)	
$\mathbf{8}^{n+}$	32680 (18300) 27100 (12800) 19200 (800)	28250 (7800) 16600 (5300) 12500 (150)	
$\mathbf{10}^{n+}$	31700 (16300) 22200 (16200) 17300 (2200)	27850 (10500) 24200 (6500) 18600 (2400) 16800 (3500) 11800 (200)	
$\mathbf{12}^{n+}$	33900 (8400)	33900 (7100) 20000 (720)	
$\mathbf{13}^{n+}$	33800 (26800) 28300 (18800) 18700 (890)	30100 (19100) 21600 (8000) 18600 (3200)	
$\mathbf{14}^{n+}$	28900 (10500) 26200 (9800) 22200 (10000)	26200 (9500), 24800 (11900), 23500 (10600) 17300 (2900), 16000 (4600) 7500 (1600)	23400 (7400) 14600 (2300)

To elucidate the nature of these transitions TD-DFT calculations on the first 100 excited states were undertaken on the model complex **1H** and $\mathbf{1H}^{+}$, using the calculated oscillator strengths as a guide, the nature of the electronic transition in the band was assessed. These calculations were kindly completed by Dr. J.J.W. McDouall at the University of Manchester. The TD-DFT generated spectra of **1H** and $\mathbf{1H}^{+}$ agreed well with the experimentally derived spectra for **1** and $\mathbf{1}^{+}$. The calculated spectra for **1H** showed two intense transitions, firstly at 29700 cm^{-1}, which was assigned a $Mo(C_7H_7)$ to phosphine transition, and secondly at 26600 cm^{-1}, which was assigned a molybdenum

to $C{\equiv}CC_6H_5$ transition. The lower lying transition, which is seen in the majority of the aryl acetylides, was assigned to HOMO to LUMO+1 transition and is responsible for the colour of the neutral complexes.

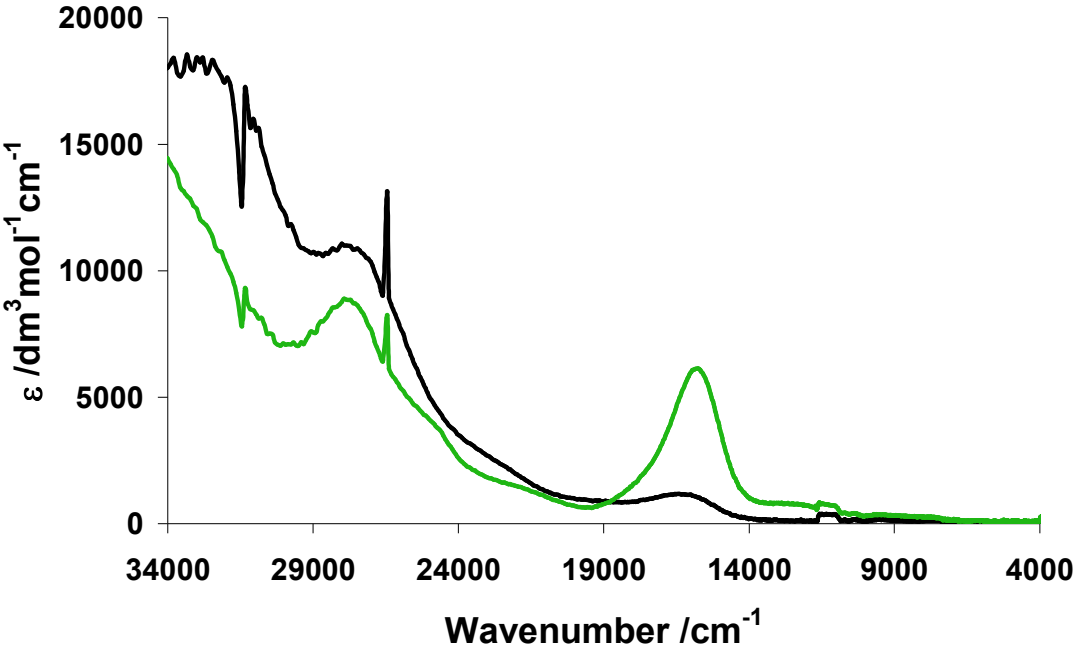

Figure 11: UV /vis spectra for 7^{n+}, where n = 0 (Black) and n = 1 (Green) (Recorded in 0.1 M $^{n}Bu_4PF_6$ /CH_2Cl_2)

Upon oxidation, the calculated $\mathbf{1H}^+$ spectra showed two similar high-energy transitions, as in **1H**, which have the same electronic transition assignment. An intense band is calculated at 16500 cm^{-1}, which is in agreement with the experimental spectra for the aryl acetylide series. This is assigned to a transition from the $C{\equiv}CC_6H_5$ moiety to the [Mo(dppe)(η^7-C_7H_7)] centre, therefore LMCT in character. Although the calculation failed to reproduce the lower energy transitions, lower than 10000cm^{-1}, it is assumed that they are interconfigurational transitions, IC, arising from transitions between the lower lying filled metal d-orbitals to the SOMO on the 17 electron [Mo(dppe)(η^7-C_7H_7)] fragment.

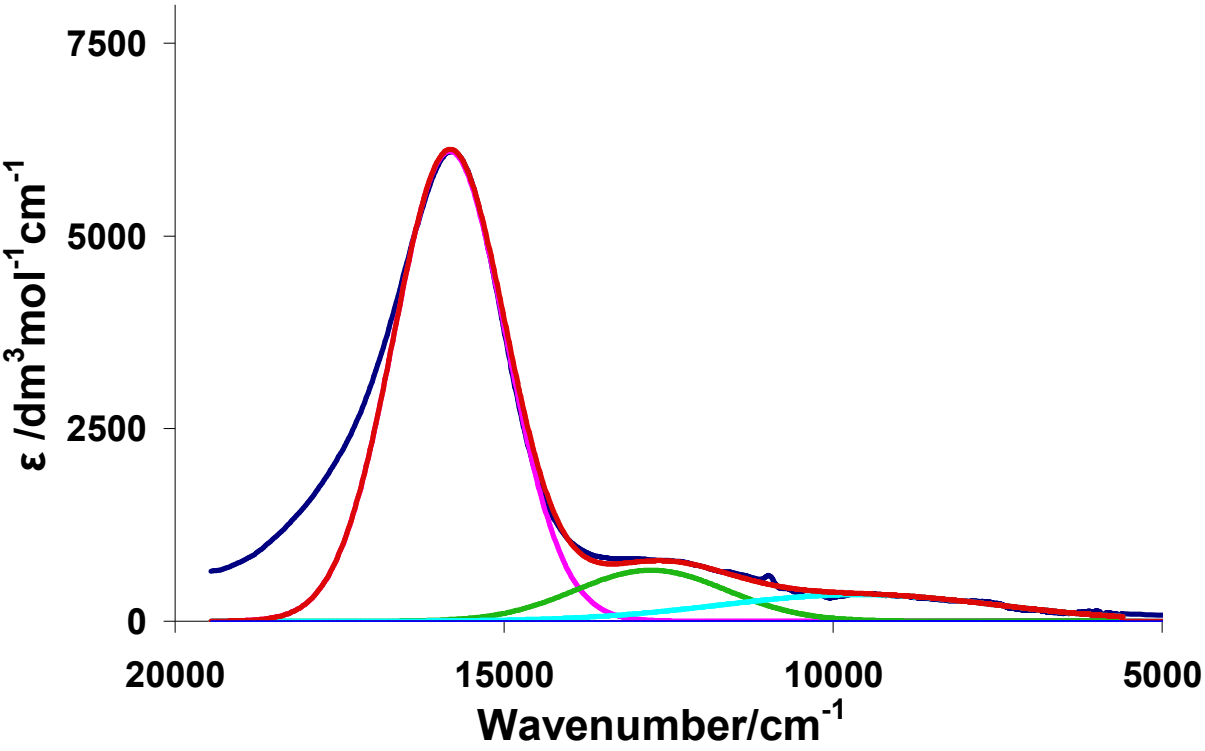

Figure 12: Deconvolution using a Gaussian fitting routine of the NIR band of 7^{+}. Showing the LMCT (Pink), IC (Green), IC (Light blue), experiemntal spectra (Dark blue) and Gaussian summation (Red).

2.10 Conclusion

These investigations into the molybdenum acetylides have established reliable and high yielding routes to the complexes, across a wide range of both aryl, non-aryl and inorganic acetylenes. The electronic structure of the complexes has been examined by the systematic synthesis of a series of molybdenum acetylides and examined using a range of spectroscopic, spectroelectrochemical and computational techniques. The frontier orbitals for the complexes are largely metal centre in character, due to the cycloheptatrienyl ring stabilising symmetry favorable metal d-orbitals by strong δ and π-type interactions. This leaves the metal d_{z2} orbital, which is not of sufficient symmetry to interact with the acetylide moiety, to be the principal atomic orbital of the HOMO. This unique property of the Mo(dppe)(η^7-C_7H_7) fragment and its interaction with the acetylide moiety offer the potential to enhance the stability of highly reactive radicals of extended carbon chain complexes and to facilitate the understanding of the components of ligand and metal centered redox processes.

2.11 Experimental

2.11.1 General Procedures

The preparation, purification and reactions of the complexes described were carried out under dry nitrogen using standard Schlenk techniques. Methanol was best available commercial grade, or dried on an Innovative Technologies SPS-400 system, and deoxygenated thoroughly by sparging with dry nitrogen before use. The alkynes HC≡CFc, $HC{\equiv}CC_6H_4CHO$-4, $HC{\equiv}CC_6H_4OMe$-4 and $HC{\equiv}CC_6H_4CO_2Me$ were prepared by standard methods[55] or purchased from commercial sources (HC≡CPh, $HC{\equiv}CBu^t$, $HC{\equiv}CCO_2Me$, $HC{\equiv}CC_6H_4NH_2$-4, $HC{\equiv}CC_6H_4Me$-4). NMR spectra were recorded from CD_2Cl_2 solutions (unless otherwise stated) containing trace amounts of $CoCp_2$ to prevent accumulation of Mo^I species by aerial oxidation on Varian Inova 300, 400, 500 spectrometers, or Bruker DRX-400 spectrometers at room temperature and referenced against solvent resonances (^1H, ^{13}C) or external H_3PO_4 (^{31}P). Infrared spectra were obtained on Perkin Elmer FT RX1 or Nicolet Avatar spectrometers. Mass spectra were recorded using Thermo Quest Finnigan Trace GC/MS or Thermo Electron Finnigan LTQ FT mass spectrometers. MALDI mass spectra were recorded using a Micromass/Waters TOF Spec 2E instrument. Microanalyses were by the staff of the Microanalytical Services of the School of Chemistry, University of Manchester, and the Department of Chemistry, Durham University. Cyclic voltammograms were recorded (ν = 100 mV s^{-1}) from 0.1 M $^nBu_4NPF_6$ CH_2Cl_2 solutions *ca*. 1 x 10^{-4} M in analyte using a gas-tight single compartment three-electrode cell equipped with a Pt disc working electrode, Pt wire counter electrode and Pt wire pseudo-reference electrode, and data collected on an Autolab PG-STAT 30 potentiostat. The working electrode was polished with alumina paste before each scan. All

redox potentials are reported with reference to an internal standard of the ferrocene / ferrocenium couple (FcH/FcH^+ = 0.46 V) *vs* SCE.[56] Electrochemical measurements at sub-ambient temperatures were performed in the same cell, immersed in a bath of dry-ice acetone. UV/ vis /NIR and IR spectroelectrochemical experiments were performed at room temperature with an air-tight OTTLE cell equipped with Pt minigrid working and counter electrodes, a Ag wire reference electrode and CaF_2[57] windows using either a Nicolet Avatar spectrometer or a Perkin Elmer Lambda 900 spectrophotometer. EPR experiments were conducted on a Bruker BioSPin EMX microspectrometer at X-band (9 GHz); spectra were recorded at 243 K and are the average of 16 scans. Spectral analysis and simulation were carried out using Bruker WinEPR software (Bruker Biospin Ltd.).

2.11.2 Preparations

2.11.2.1 Preparation of [Mo(C≡CPh)(dppe)(η^7-C_7H_7)] (1)

A mixture of **5** (813 mg, 1.15 mmol), HC≡CPh (587 mg, 5.75 mmol) and $KOBu^t$ (387 mg, 3.45 mmol) in methanol (50 cm^3) was heated at reflux for 3 hours. The resulting deep-brown precipitate was collected, washed with hexane and dried *in vacuo*. The solid was dissolved in CH_2Cl_2 (*ca.* 5 cm^3) and loaded onto a hexane/ alumina column and eluted with CH_2Cl_2/hexane/acetone (45:45:10 v:v:v). The major brown band was collected and evaporated to dryness to give a deep-brown solid which was reprecipitated from CH_2Cl_2/hexane; yield: 425 mg (54%). ^{1}H NMR: δ 2.11 (m, 2H, CH_2), 2.49 (m, 2H, CH_2), 4.82 (t, 7H, J_{HP} = 2.1 Hz, C_7H_7), 6.03 (d, 2H, J_{HH} 7.0 Hz, C≡CPh$_o$), 6.74 (m, 1H, C≡CPh$_p$), 6.84 (m, 2H, C≡CPh$_m$), 7.33 – 7.85 (m, 20H, Ph). $^{31}P\{^1H\}$ NMR ($CDCl_3$): δ 64.6 (s, dppe). IR (CH_2Cl_2) ν(C≡C) 2045 cm^{-1}. MALDI-MS (m/z) 687 $[M]^+$, 586 [(M –

C≡CPh)]$^+$. Anal. Calcd. (%) for $C_{41}H_{36}MoP_2$: C, 71.7%; H, 5.3%. Found, C, 71.4%; H, 5.2%.

2.11.2.2 Preparation of [Mo(C≡CBu^t)(dppe)(η^7-C_7H_7)] (12)

This was prepared and purified in an identical fashion to **1**, using HC≡CBu^t (870 mg, 10.60 mmol), **5** (1.50 g, 2.12 mmol) and KOBu^t (0.71 g, 6.36 mmol). The product was obtained as a dark brown solid; yield: 430 mg (30%). ^{1}H NMR: δ 0.40 (s, 9H, Bu^t), 2.20 (m, 2H, CH_2), 2.60 (m, 2H, CH_2), 4.66 (s, 7H, C_7H_7), 7.25 – 7.82 (m, 20H, Ph). ^{31}P{^{1}H} NMR ($CDCl_3$): δ 66.2 (s, dppe). IR (CH_2Cl_2) ν(C≡C) 2057 cm^{-1}. MALDI-MS (m/z) 668 [M]$^+$. Anal. Calcd. (%) for $C_{39}H_{40}MoP_2$: C, 70.3%; H, 6.1%. Found, C, 70.3%; H, 6.0%.

2.11.2.3 Preparation of [Mo(C≡CFc)(dppe)(η^7-C_7H_7)] (11)

A warm (*ca.* 50 °C) solution of **5** (100 mg 0.14 mmol) in methanol (20 cm^3) was treated with HC≡CFc (38 mg, 0.18 mmol) and the resulting mixture heated at reflux point for 90 min. The solution was allowed to cool to room temperature before addition of Na metal (100 mg, 4 mmol). The solution was allowed to stir for 20 min, after which time effervescence had ceased, and the solvent removed *in vacuo*. The solid residue was extracted with CH_2Cl_2 (5 cm^3), the extracts filtered, and the filtrate taken to dryness *in vacuo* to give a dark coloured solid which was washed with Et_2O (3 x 5 cm^3) and hexane (3 x 5 cm^3), or until the washings were colourless, and dried to afford **2c** as a free-flowing brown powder; yield: 10 mg (9%). ^{1}H NMR: δ 2.17 (m, 2H, CH_2), 2.64 (m, 2H, CH_2), 3.29 (t, $J_{HH,}$ = 2 Hz, 2H, Cp$_\beta$), 3.60 (s, 5H, Cp), 3.69 (t, J_{HH} = 2 Hz, 2H, Cp$_\alpha$), 4.71 (br, 7H, C_7H_7), 7.29 – 7.89 (m, 20H, Ph). ^{31}P{^{1}H} NMR: δ 65.6 (s, dppe).

MALDI-MS: (m/z) 796.2 $[M]^+$. Anal. Calcd. (%) for $C_{45}H_{40}FeMoP_2$: C, 68.0%; H, 5.0%. Found, C, 68.4%; H, 5.2%.

2.11.2.4 Preparation of [Mo(C≡CCO$_2$Me)(dppe)(η^7-C$_7$H$_7$)] (13)

This was prepared and purified in an identical fashion to **1**, using methyl propiolate (288 mg, 3.43 mmol) in place of HC≡CPh, **5** (808 mg, 1.14 mmol) and $KOBu^t$ (211 mg, 1.88 mmol). The product was obtained as a purple-red solid; yield: 240 mg (31 %).^{1}H NMR: δ 1.89 (m, 2H, CH_2), 2.35 (m, 2H, CH_2), 3.18 (s, 3H, Me), 4.71 (br, 7H, C_7H_7), 7.19 – 7.67 (m, 20H, Ph). $^{31}P\{^1H\}$ NMR ($CDCl_3$): δ 62.2 (s, dppe). IR (CH_2Cl_2) ν(C≡C) 2020, ν(C=O) 1657 cm^{-1}. MALDI-MS (m/z) 669 $[M]^+$. Anal. Calcd. (%) for $C_{37}H_{34}MoP_2$: C, 66.5%; H, 5.1%. Found, C, 66.2%; H, 5.1%.

2.11.2.5 Preparation of [Mo(C≡CC$_6$H$_4$NH$_2$-4)(dppe)(η^7-C$_7$H$_7$)] (6)

The reaction between **5** (100 mg 0.14 mmol) and HC≡C$C_6H_4NH_2$-4 (27 mg, 0.23 mmol) was carried out in a manner similar to that described for **1**, affording **6** as a deep green solid; yield 40 mg (38%). ^{1}H NMR: δ 2.06, 2.48 (2 x m, 2 x 2H, 2 x CH_2); 3.40 (s, 2H, NH_2), 4.75 (t, J_{PH} = 2.0 Hz, 7H, C_7H_7), 5.87, 6.20 (2 x AB, J_{HH} *ca.* 8 Hz, 2 x 2H, C_6H_4), 7.30-7.81 (m, 20H, Ph). $^{31}P\{^1H\}$ NMR: δ 65.7 (s, dppe). IR (CH_2Cl_2) ν(C≡C) 2053. ES+-MS (m/z) 701.2 $[M]^+$. HR ES+-MS (m/z) For $MoNP_2C_{41}H_{37}$ 703.14552. Found 703.14469.

2.11.2.6 Preparation of [Mo(C≡CC$_6$H$_4$OMe-4)(dppe)(η^7-C$_7$H$_7$)] (7)

A solution of Me$_3$SiC≡CC$_6$H$_4$OMe-4 (29 mg, 0.23 mmol) and KF (26 mg, 0.452 mmol) in methanol (20 cm^3) was treated with **5** (100 mg, 0.14 mmol) and $NaPF_6$ (25 mg, 0.151 mmol). The resulting solution was heated at reflux point for 90 min before the solvent was removed. The residue was washed with hexane (2 x 10 cm^3) and Et_2O (2 x 10 cm^3) or until the washings were clear. The remaining solid was extracted with CH_2Cl_2 (5 cm^3), and cannula filtered into stirred hexane (15 cm^3) to give **7** as a dark british racing green coloured precipitate; yield: 40 mg (37 %). ^{1}H NMR: δ 2.03 (m, 2H, CH_2); 2.50 (m, 2H, CH_2); 3.63 (s, 3H, OMe); 4.78 (br, 7H, C$_7$H$_7$); 5.96, 6.40 (2 x AB, 2 x 2H, J_{HH} *ca*. 9 Hz, C$_6$H$_4$); 7.29 – 7.83 (m, 20 H, Ph). ^{31}P{^{1}H} NMR: δ 64.1 (s, dppe). IR (CH_2Cl_2): ν(C≡C) 2051; ν(Ar) 1604 cm^{-1}. ES+-MS (m/z): 715.9 [M]$^+$. HR ES+-MS (m/z) For $MoOP_2C_{42}H_{38}$; 718.1466. Found; 718.1446

2.11.2.7 Preparation of [Mo(C≡CC$_6$H$_4$CH$_3$-4)(dppe)(η^7-C$_7$H$_7$)] (8)

A mixture of **5** (1.46 g, 2.06 mmol), HC≡CC$_6$H$_4$CH$_3$ (720 mg, 6.20 mmol) and KOBu^t (485 mg, 4.32 mmol) in methanol (50 cm^3) was heated at reflux for 2 h. The reaction mixture was cooled and reduced in volume to *ca.* 20 cm^3. The deep-brown precipitate was collected, washed with hexane and dried *in vacuo*; yield: 1.123 g (78%). ^{1}H NMR: δ1.97 (m, 2H, CH_2), 2.04 (s, 3H, C$_6$H$_4$C*H*$_3$), 2.38 (m, 2H, CH_2), 4.70 (br, 7H, C$_7$H$_7$), 5.81 (d, 2H, J_{HH} 8.0 Hz, C≡CPh$_o$), 6.54 (d, 2H, J_{HH} 8.0 Hz, C≡CPh$_m$), 7.20 – 7.71 (m, 20H, Ph). ^{31}P{^{1}H} NMR ($CDCl_3$): δ 64.6 (s, dppe). IR (CH_2Cl_2) ν(C≡C) 2048 cm^{-1}, MALDI-MS (m/z) 703 [M]$^+$. Anal. Calcd (%) for $C_{42}H_{38}MoP_2$: C, 72.0%; H, 5.5%. Found, C, 72.0%; H, 5.4%.

2.11.2.8 Preparation of [Mo(C≡CC$_6$H$_4$CHO-4)(dppe)(η^7-C$_7$H$_7$)] (9)

The reaction between **5** (100 mg, 0.14 mmol) KF (0.013 g, 0.225 mmol) and Me$_3$SiC≡C(C$_6$H$_4$CHO-4) (0.036 g, 0.180 mmol) in methanol (20 cm^3) was carried out in a manner similar to that described for **7**, affording **9** as a dark purple solid; yield: 73 mg (68 %). ^{1}H NMR: δ 2.13 (m, 2H, CH$_2$), 2.42 (m, 2H, CH$_2$), 4.83 (br, 7H, C$_7$H$_7$), 5.94, 7.31 (2 x AB, J_{HH} = 8.0 Hz, 2 x 2H, C$_6$H$_4$), 7.29 – 7.84 (m, 20H, Ph), 9.65 (s, 1H, C*H*O). ^{31}P{^{1}H} NMR: δ 63.6 (s, dppe). IR (CH$_2$Cl$_2$): ν(C≡C) 2023; ν(C=O) 1680 cm^{-1}. HR ES+-MS (m/z) MoOP$_2$C$_{42}$H$_{36}$; 716.12953. Found; 716.12860. Crystal data: *M* = 0.32 x 0.25 x 0.18 mm^3, space group (P – 1), *V* = 1670.40 (8) Å^3, *Z* = 2, F_{000} = 736,, *T* = 120(2) K, 22417 reflections collected, unique (R_{int} = 0.0584). Final *GooF* = 1.085, *R1* = 0.0344, *wR2* = 0.0882.

2.11.2.9 Preparation of [Mo(C≡CC$_6$H$_4$CO$_2$Me-4)(dppe)(η^7-C$_7$H$_7$)] (10)

The reaction between **5** (500 mg, 0.70 mmol) and HC≡CC$_6$H$_4$CO$_2$Me-4 (300 mg, 1.88 mmol) in methanol (100 cm^3) was carried out in a manner similar to that described for **1**, with deprotonation being effected by addition of Na (250 mg, 10 mmol) affording **10** as a black solid; yield: 280 mg (50%). ^{1}H NMR: δ 2.14, 2.47 (2 x m, 2 x 2H, 2 x CH$_2$); 3.80 (s, 3H, Me); 4.85 (br, 7H, C$_7$H$_7$); 5.37, 7.50 (2 x AB, J_{HH} *ca.* 5 Hz, 2 x 2H, C$_6$H$_4$), 7.35 – 7.85 (m, 20H, Ph). ^{31}P{^{1}H} NMR: δ 64.9 (s, dppe). IR (CH$_2$Cl$_2$) ν(C≡C) 2027, 1991; ν(C=O) 1702. ES(+)-MS (m/z) 744.3 [M]$^+$. HR ES+-MS (m/z) MoO$_2$P$_2$C$_{43}$H$_{38}$; 746.14150. Found; 746.13946. Crystal data: *M* = , 0.20 x 0.12 x 0.01 mm^3, monoclinic, space group *P*2$_1$/*c* (No. 14), *a* = 21.834(2), *b* = 9.4090(10), *c* = 17.5983(19) Å, *β* =

109.75(3)°, V = 3402.7(6) Å^3, Z = 4, D_c = 1.453 g/cm^3, F_{000} = 1536,, T = 120.0(2) K, 21624 reflections collected, unique (R_{int} = 0.1767). Final *GooF* = 1.006, *R1* = 0.1713, *wR2* = 0.1951.

2.11.2.10 Preparation of [Mo(C≡C$C_{14}H_9$)(dppe)(η^7-C_7H_7)] (14)

A solution of $Me_3SiC{\equiv}CC_{14}H_9$ (82 mg, 0.300 mmol) and KF (26 mg, 0.450 mmol) in methanol (20 cm^3) was treated with **5** (200 mg 0.300 mmol). The resulting solution was heated at reflux point for 90 min before the solvent was removed. The residue was washed with hexane (2 x 10 cm^3) and Et_2O (2 x 10 cm^3) or until the washings were clear. The remaining solid was extracted with CH_2Cl_2 (5 cm^3), and cannula filtered into stirred hexane (15 cm^3) to give the product as a green coloured precipitate (200 mg, 85 %). ^{1}H NMR (CD_2Cl_2) δ 2.13 (m, 2H, CH_2), 2.71 (m, 2H, CH_2), 4.96 (t, J_{HH} = 2.0 Hz, 7H, C_7H_7), 6.80 – 8.00 (m, 29H, Ph). ^{31}P NMR (CD_2Cl_2) 64.5 (s, dppe). IR (CH_2Cl_2) ν(C≡C) 2018 cm^{-1}. Found ES+ MS (m/z) : 788.16556 [**M**]$^+$. Needed $MoP_2C_{49}H_{40}$: 788.16538. Crystal data: M = 0.4 x 0.32 x 0.21 mm^3, , space group $P2_{1/n}$ (No. 14), V = 3769.04(13) Å^3, Z = 4, F_{000} = 1624, T = 120(2) K, 49425 reflections collected, unique (R_{int} = 0.0301). Final *GooF* = 1.034, *R1* = 0.0452, *wR2* = 0.0992.

2.11.3 Crystallography

The majority of details of the structure analyses carried out on complexes **8**, **9**. **10**. **12**, [**12**]$^+$, **13**, and **14** are given in the appendices CD. In all cases the X-ray data were collected using graphite monochromated MoK_α (λ = 0.7103Å) radiation. With the exception of **5** and **6**, data collection, cell refinement and data reduction were carried out with Bruker SMART and Bruker SAINT software; SHELXS-97[58] was employed for the computing structure solution and SHELXL-97[59] for the computing structure refinement and an absorption correction was applied with the aid of the SADABS programme.[60] Diffraction data for **5**, **6** and **11** were collected on a Bruker 3-circle diffractometer with a SMART 6K area detector; reflection intensities were integrated using the SAINT V6.45 program and a numerical absorption correction was applied. All structures were solved by direct methods with refinement by full-matrix least squares based on F^2 against all reflections. With the exception of [**9**]$^+$, all non-hydrogen atoms were refined anisotropically and hydrogen atoms were included in calculated positions. In the case of [**9**]$^+$ the asymmetric unit contains four crystallographically independent pairs of ions and 1.5 molecules of CH_2Cl_2 and the crystal diffracted very weakly so the data were cut at 0.95Å resolution. One phenyl ring was contrained to a regular hexagon with restraints also applied to some geometric parameters. The key Mo-C_1 distances (Å) in the 4 independent molecules of [**9**]$^+$ are: 2.070(11), 2.076(11), 2.050(13), 2.067(13).

2.11.4 Computational Details

Electronic structure calculations were carried out at the University of Manchester by Dr. J. J. W McDouall. Calculations carried out on **1H** and the corresponding cation, $\mathbf{1H}^{+}$. Starting from the crystallographic structure of **1H**, full geometry optimisations were performed on **1H** and $\mathbf{1H}^{+}$ using the Def2-SVP basis obtained from the Turbomole library.[61] For H, C and P atoms, this constitutes an all electron split valence plus polarisation basis, while for Mo an effective core potential is applied to account for 28 core electrons (*K*, *L* and *M* shells) with a split valence orbital set including a set of *f* type polarization functions. This basis was also used to obtain IR frequencies and the UV/Vis spectra (via time-dependent density functional theory). For calculations of EPR *g* tensors and hyperfine coupling tensors, the Mo basis was changed to the all electron TZVPP-All-S2 basis, again from the Turbomole library.[64] In the all electron calculations, *s* type functions on all atoms were uncontracted. Convergence of the EPR parameters was checked by the inclusion of additional tight *s* functions (the exponents being obtained in geometric progression) on all atoms. Typically it was found that the inclusion of two additional sets of *s* functions was sufficient, since any further addition produced changes of less than 1 MHz (0.36 G) in the computed hyperfine tensors.

DFT calculations were performed in the generalised gradient approximation (GGA) with the BP86 exchange-correlation functional.[62] For the TD-DFT, *g* tensor and hyperfine tensor calculations, the B3LYP hybrid exchange-correlation functional[63] was used. Hybrid functionals are generally found to give better predictions for UV/Vis spectra and EPR parameters. For the latter, the PBE0 functional[64] was also used since this functional was designed for use in calculations of magnetic properties.

The IR frequencies were calculated from analytic second derivatives using the Gaussian suite of programs.[65] For *g* tensor calculations the gauge including atomic orbitals (GIAO), were employed with a one-electron spin-orbit operator with a scaled charge. The ORCA program[66] was also used for *g* tensor calculation employing a mean field spin-orbit operator. In this work we are only interested in isotropic values of the hyperfine coupling constants. Accordingly, the Fermi contact term of the hyperfine interaction was evaluated and also the spin-orbit contribution. The ORCA code was used for the latter. The spin-spin dipole contribution is a traceless tensor and does not affect the isotropic hyperfine couplings. The influence of relativistic effects on the Mo hyperfine interaction was investigated within the zero-order regular approximation (ZORA),[67] including the picture change transformation necessary for the correct treatment of the FC terms.[68]

2.12 References

[1] J. Jortner, M. Ratner, Molecular Electronics, Blackwell Science, Oxford, 1997.
[2] N.J. Long, *Angew. Chem. Int. Ed.,* 195, **34**, 21.
[3] M. Younus, A. Kohler, S. Cron, N. Chawdhury, M.R.A. Al-Madani, M.S. Kahn, N.J. Long, R.H. Friden, P.R. Raithby, *Angew. Chem.. Int. Ed.,* 1995, **37**, 3036.
[4] P.J. Low, *Dalton. Trans.,* 2005, 2821.
[5] D.W. Bruce in *Inorganic Materials* (Eds.: D.W. Bruce, D. O'Hare), Wiley, Chichester, 1996, 429.
[6] R.G. Amiet, P.C. Reeves, R. Pettit, *J. Chem. Soc., Chem. Commun.,* 1967, 1208.
[7] A. Efraty, *Chem. Rev.,* 1977, **77**, 691.
[8] H.C. Longuet-Higgins, L.E. Orgel, *J. Chem. Soc.,* 1956, 1969.
[9] (a) M.O. Albers, D.J. Robinson, A. Shaver, E. Singleton, *Organometallics,* 1986, **5**, 2199. (b) M.O. Albers, H.E. Oosthuizen, D.J. Robinson, A. Shaver, E. Singleton, *J. Organomet. Chem.,* 1985, **282**, C49. (c) M.O. Albers, D.J. Robinson, E. Singleton, *J. Organomet. Chem.,* 1986, **311**, 207. (d) N. Oshima, H. Suzuki, Y. Moro-Oka, *Chem. Lett.,* 1984, 1161.
[10] (a)W.J. Evans, R.D. Clark, M.A. Ansari, J.W. Ziller, *J. Am. Chem. Soc.,* 1998, **120**, 9555. (b) P. Poremba, F.T. Edelmann, *J. Organomet. Chem.,* 1998, **553**, 393. (c) C. Meermann, K. Ohno, K.W. Tornroos, K. Mashima, R. Anwander, *Eur. J. Inorg. Chem.,* 2009, 76.
[11] G. Deganello, H. Maltz, J. Kozarich, *J. Organomet. Chem.,* 1973, **60**, 323.
[12] Web of science search 16/2/10, search term "ferrocene'.
[13] SciFinder search 16/2/10, search term "ferrocene pictorial structure"
[14] P.L. Pauson, *J. Organomet. Chem.,* 2001, **637-639**, 3.
[15] (a) M.A. Fox, R.L. Roberts, W.M. Khairul, F. Hartl, P.J. Low, *J. Organomet. Chem.,* 2007, **692**, 3277. (b) M.I. Bruce, M. Jevric, C.R. Parker, W. Patalinghug, B.W. Skelton, A.H. White, N.N. Zaitseva, *J. Organomet. Chem.,* 2008, **693**, 2915. (c) S. Abbott, S.G. Davies, P. Werner, *J. Organomet. Chem.,* 1983, **246**, C65. (d) F. Paul, L. Toupet, J-Y. Thepot, K. Costuas, J-F. Halet, C. Lapinte, *Organometallics,* 2005*,* **24**, 5464. (e) R. Denis, L. Toupet, F. Paul, C. Lapinte, *Organometallics,* 2000, **19**, 4240. (f) J. Kiesewetter, G. Poignant, V. Guerchais, *J. Organomet. Chem.,* 2000, **595**, 81.
[16] M.I. Bruce, B.G. Ellis, M. Gaudio, C. Lapinte, F. Paul, B.W. Skelton, M.E. Smith, L. Toupet, A.H. White, *Dalton. Trans.,* 2004, 1601.
[17] E. Huckel, *Z. Phys.,* 1931, **70**, 204; **72**, 310.
[18] J.C. Green, N. Kaltsoyannis, K.H. Sze, M. MacDonald, *J. Am. Chem. Soc.,* 1994, **116**, 1994.
[19] (a) J.E. Anderson, E.T. Maher, L.B. Kool, *Organometallics,* 1991, **10**, 1248. (b) J.C. Green, M.L.H. Green, N. Kaltsoyannis, P. Mountford, P. Scott, *Organometallics,* 1992, **11**, 3353. (c) M. Tamm, *Chem. Commun.,* 2008, 3089. (d) D.W. Clack, K.D. Warren, *Theore. Chim. Acta.* 1977, **46**, 313. (e) C.J. Groenenboom, H.J. de Liefde Meijer, F. Jellinek, *J. Organomet. Chem.,* 1974, **69**, 235.
[20] H. Braunschweig, T. Kupfer, M. Lutz, K. Radacki, *J. Am. Chem. Soc.,* 2007, **129**, 8893.
[21] G. Menconi, N. Kaltsoyannis, *Organometallics,* 2005, **24**, 1189.
[22] S. Buschel, T. Bannenberg, C.G. Hrib, A. Glockner, P.G. Jones, M. Tamm, *J. Organomet. Chem.,* 2009, **694**, 1244.

[23] (a) M.L.H. Green, N.M. Walker, *J.Chem. Soc., Chem. Commun.,* 1989, 850. (b) G.M. Diamond, M.L.H. Green, P. Mountford, N.M. Walker, J.A.K. Howard, *J. Chem. Chem., Dalton. Trans.,* 1992, 417.
[24] M.L.H. Green, D.K.P. Ng, *Chem. Rev.,* 1995, **95**, 439.
[25] (a) M. Tamm, B. Drebel, R. Frohlich, K. Bergander, *Chem. Commun*., 2000, 1731. (b) M. Tamm, T. Bannenberg, R. Frohlich, S. Grimme, M. Gerenkamp, *Dalton, Trans.,* 2004, 482.
[26] T. Meyer-Friedrichsen, H. Wong, M.H. Prosenc, J. Heck, *Eur. J. Inorg. Chem.,* 2003, 936.
[27] C. Jiabi, Y. Jienguo, L. Guixin, X. Weihus, S. Meicheng, Z. Zeying, T. Youqi, *J. Organomet. Chem.,* 1987, **329**, 69.
[28] M. Tamm, A. Grzegorzewski, I. Brudgam, H. Hartl, *Chem. Commun.,* 1997, 2227.
[29] H.-J. Muller, U. Nagel, M. Steimann, K. Polborn, W. Beck, *Chem. Ber.,* 1989, **122**, 1387.
[30] (a) R.L. Beddoes, J.R. Hinchliffe, M.W. Whiteley, *J. Chem. Soc., Dalton. Trans.,* 1993, 501. (b) R.L. Beddoes, J.R. Hinchliffe, A-L.A.B de Souza, M.W. Whiteley, *J. Chem. Soc., Dalton. Trans.,* 1994, 2303.
[31] S-F. Luch, S-H Wang, G-H. Lee, S-M. Peng, S-M. Peng, S-L. Wang, R-S. Lui, *Organometallics,* 1990, **9**, 1862.
[32] (a) J.R. Hinchliffe, A. Ricalton, M.W. Whiteley, *Polyhedron,* 1991, **10**, 267. (b) R. Breeze, M.S. Plant, A. Ricalton, D.J. Sutton, M.W. Whiteley, *J. Organomet. Chem.,* 1988, **356**, 343.
[33] F. Paul, J-Y. Mevellec, C. Lapinte, *Dalton. Trans.,* 2002, 1783.
[34] H. Brunner, J. Klankermayer, M. Zabel, *Organometallics,* 2002, **21**, 5746.
[35] C.E. Davies, I.M. Gardiner, J.C. Green, M.L.H. Green, P.D. Grebenik, V.S.B. Mtetwa, K. Prout, *J. Chem. Soc., Dalton. Trans.,* 1985, 669.
[36] E.F. Ashworth, J.C. Green, M.J.H. Green, J. Knight, R.B.A. Pardy, N.J. Wainwright, *J. Chem. Soc., Dalton. Trans.,* 1977, 1693.
[37] J. Cambridge, A. Choudhary, J. Friend, R. Garg, G. Hill, Z.I. Hussain, S.M. Lovett, M.W. Whiteley, *J. Organomet. Chem.,* 1999, **577**, 249.
[38] (a) M.I. Bruce, B.G.Ellis, M. Gaudio, C. Lapinte, G. Melino, F. Paul, B.W. Skelton, M.E. Smith, L. Toupet, A.H. White, *Dalton. Trans.,* 2004, 1601. (b) C.E. Powell, M.P. Cifuentes, A.M. McDonagh, S.K. Hurst, N.T. Lucas, C.D. Delfs, R. Stranger, M.G. Humphrey, S. Houbrechts, I. Asselberghs, A. Persoons, D.C.R. Hockless, *Inorg. Chim. Acta.* 2003, **352**, 9.
[39] M.I. Bruce, D.A. Harbourne, F. Waugh, F.G.A. Stone, *J. Chem. Soc., Inorg. Phys. Theor.,* 1968, 356.
[40] (a) J.S. Adams, C. Bitcon, J.R. Brown, D. Collison, M. Cunningham, M.W. Whiteley, *J. Chem. Soc., Dalton. Trans.,* 1987, 3049. (b) J.S. Adams, M. Cunningham, M.W. Whiteley, *J. Organomet. Chem.,* 1985, **293**, C13. (c) R.L. Beddoes, C. Bitcon, A. Ricalton, M.W. Whiteley, *J. Organomet. Chem.,* 1989, **367**, C21. (d) C. Bitcon, R. Breeze, P.F. Miller, M.W. Whiteley, *J. Organomet. Chem.,* 1989, **364**, 181. (e) Z.I. Hussain, M.W. Whiteley, E.J.L. McInnes, *J. Organomet. Chem.,* 1997, **543**, 237. (f) R.W. Grime, M.W. Whiteley, *J. Chem. Soc., Dalton. Trans.,* 1994, 1671.
[41] R.W. Grime, M. Helliwell, Z.I. Hussain, H.N. Lancashire, C.R. Mason, J.J.W. McDouall, C.M. Mydlowski, M.W.W. Whiteley, *Organometallics,* 2008, **27**, 857.
[42] R. Denis, L. Toupet, F. Paul, C. Lapinte, *Organometallics,* 2000, **19**, 4240.
[43] M.A. Fox, R.L. Roberts, W.M. Khairul, F. Hartl, P.J. Low, *J. Organomet. Chem.,* 2007, **692**, 3277.

[44] R.L. Beddoes, C. Bitcon, M.W. Whiteley, *J. Organomet. Chem.,* 1991, **402**, 85.
[45] R.L. Beddoes, C. Bitcon, A. Ricalton, M.W. Whiteley, *J. Organomet. Chem.,* 1989, **367**, C21.
[46] N. Le Narvor, C. Lapinte, *J. Chem. Soc., Chem. Commun.,* 1993, 357.
[47] R.S. Iyer, J.P. Selegue, *J. Am. Chem. Soc.,* 1987, **109**, 910.
[48] N. Le Narvor, C. Lapinte, *J. Chem. Soc., Chem. Commun.,* 1993, 357.
[49] N.A. Ustynyuk, V.N. Vinogradova, V.G. Andrianov, Y.T. Struchkov, *J.Organomet. Chem.,* 1984, **268**, 73.
[50] B.E. Woodworth, P.S. White, J.L. Templeton, *J. Am. Chem. Soc.,* 1997, **119**, 828.
[51] M.I. Bruce, B.C. Hall, B.D. Kelly, P.J. Low, B.W. Skelton, A.H. White, *Dalton, Trans.,* 1999, 3719.
[52] Z.I. Hussain, M.W. Whiteley, E.J.L. McInnes, *J. Organomet. Chem.,* 1997, **543**, 237.
[53] F. Paul, B.G. Ellis, M.I. Bruce, L. Toupet, T. Roisnl, K. Costuas, J.-F. Halet, C. Lapinte, *Organometallics,* 2006, **25**, 649.
[54] (a) D. Andrae, U. Haeussermann, M. Dolg, H. Stoll, H. Preuss, *Theor. Cheim. Acta.* 1990, **77**, 123. (b) F. Weigend, R. Ahlrichs, *Phys. Chem. Chem. Phys,* 2005, **7**, 3297. http://bases.turbo-forum.com/TURBOMO-LE_BASISSET_LIBRARY/tbl.html.
[55] O. Lavastre, L. Ollivier, P.H. Dixneuf, S. Sinbandhit, *Tetrahedron*, 1995, **52**, 5495.
[56] N.G. Connelly, W.E. Geiger, *Chem. Rev.,* 1996, **96**, 877.
[57] (a) M. Krejeik, M. Danek, F. Hartl, *J. Electroanal. Chem.,* 1991, **317**, 179. (b) Spectroelectrochemistry; W. Kaim, A. Klein, Eds.; Royal Society of Chemistry: Cambridge, 2008.
[58] Sheldrick, G. M. SHELXS-97, Program for Crystal Structure Solution; Universität Göttingen, Germany, 1997.
[59] Sheldrick, G. M. SHELXL-97, Program for Crystal Structure Refinement; Universität Göttingen: Germany, 1997.
[60] Sheldrick, G. M. SADABS, an Empirical Absorption Corrections Program; Universität Göttingen: Germany, 1997.
[61] K. Eichkorn, F. Weigend, O. Treutler, R. Ahlrichs, *Theor. Chem. Acc.,* 1997, **97**, 119.
[62] (a) A. D. Becke, *Phys. Rev. A.,* 1988, **38**, 3098. (b) J.P. Perdew, *Phys. Rev. B.,* 1986, **33**, 8822.
[63] A.D. Becke, *Chem. Phys.,* 1993, **98**, 5648.
[64] C. Adamo, V.J. Barone, *Chem. Phys.,* 1999, **110**, 6158.
[65] M.J. Frisch, G.W. Trucks, H.B. Schlegel, G.E. Scuseria, M.A. Robb, J.R. Cheeseman, J.A. Montgomery Jr., T. Vreven, K.N. Kudin, J.C. Burant, J.M. Millam, S.S. Iyengar, J. Tomasi, V. Barone, B. Mennucci, M. Cossi, G. Scalmani, N. Rega, G.A. Petersson, H. Nakatsuji, M. Hada, M. Ehara, K. Toyota, R. Fukuda, J. Hasegawa, M. Ishida, T. Nakajima, Y. Honda, O. Kitao, H. Nakai, M. Klene, X. Li, J.E. Knox, H.P. Hratchian, J.B. Cross, C. Adamo, J. Jaramillo, R. Gomperts, R.E. Stratmann, O. Yazyev, A.J. Austin, R. Cammi, C. Pomelli, J.W. Ochterski, P.Y. Ayala, K. Morokuma, G.A. Voth, P. Salvador, J.J. Dannenberg, V.G. Zakrzewski, S. Dapprich, A.D. Daniels, M.C. Strain, O. Farkas, D.K. Malick, A.D. Rabuck, K. Raghavachari, J.B. Foresman, J.V. Ortiz, Q. Cui, A.G. Baboul, S. Clifford, J. Cioslowski, B.B. Stefanov, G. Liu, A. Liashenko, P. Piskorz, I. Komaromi, R.L. Martin, D.J. Fox, T. Keith, M.A. Al-Laham, C.Y. Peng, A. Nanayakkara, M. Challa- combe, P.M.W. Gill, B. Johnson, W. Chen, M.W. Wong, C. Gonzalez, J.A. Pople, GAUSSIAN 03, Revision C.02, Gaussian Inc., Wallingford, CT, 2004.
[66] F. Neese, ORCA, An Ab Initio, Density Functional, and Semi- empirical Program Package, version 2.6, Rev. 35; Univ. Bonn: Bonn, 2008.

[67] E. van Lenthe, E.J. Baerends, J.G. Snijders, *J. Chem. Phys.,* 1993, **99**, 4597.
[68] E. van Lenthe, A. van der Avoird, P.E.S. Wormer, *J. Chem. Phys.,* 1998, **108**, 4783.

Chapter 3: Molybdenum complexes bearing diynyl and triynyl ligands

3.1 Introduction

The chemistry of transition metal ynyl complexes has its origins in the development of synthetic routes to metal complexes carrying acetylide or alkynyl (C≡CR) ligands, and in the exploration of the derivative chemistry of these prototypical systems.[1,2] However, longer chain one dimensional polyynyl ligands have more recently been objects of great interest owing to their unusual electronic, magnetic and optical properties,[3] especially when they are incorporated into multi-metallic systems with potential use in molecular-scale electronic devices.[4] Synthetic work has preceded the physical studies, and key to the development of these systems has been identifying convenient synthetic routes to both monometallic polyynyl and bimetallic polyyndiyl complexes. In such studies, monometallic complexes featuring terminal polyynyl ligands, have proven particularly useful as reagents in the preparation of homo and heterometallic polyyndiyl systems through further metallation and cross-coupling reactions of the terminal C≡CH functional group.[5]

The length of the polyynyl chain, which can be directly added to a metal end cap to give polyynyl complexes $L_xM\{(C{\equiv}C)_yR\}$, is limited only by the organic precursors which are available. Terminal acetylene derivatives HC≡CR are readily available, and together with the diverse synthetic strategies that have been developed for the construction of the

M-*C*≡C bond accounts for the vast array of metal acetylides which have been synthesised. However, in seeking to build complexes featuring longer polyynyl chains, the number of reagents which directly add a $(C{\equiv}C)_nR$ ligand to the metal fragment decreases rapidly as the chain length increases. A great deal of research has been carried out on extended *sp*-hybridised chains and whilst such work has demonstrated that chain lengths in excess of 16 carbons can be synthesised, work has not been carried out regarding the coordination of such chains directly to a metal end cap.[6] Consequently, much of the synthetic chemistry that affords higher polyynyl complexes is based around the extension of shorter $L_xM\{(C{\equiv}C)_yH\}$ through cross-coupling protocols.[7, 5b]

The most common members of the polyynyl series $L_xM\{(C{\equiv}C)_yR\}$, where $y > 1$, are 1,3-butadiynyl derivatives, ($y = 2$). The choice of methodology for the preparation of butadiynyl complexes is highly dependant on the metal fragment and the nature of the R substituent on the chain, to accommodate this, numerous synthetic strategies have been developed.

A number of butadiynyl complexes are available directly from the reaction of a terminal butadiyne HC≡CC≡CR, including HC≡CC≡CH, with a metal halide in the presence of an amine base (typically $NHEt_2$) and catalytic amounts of CuI.[8] This route is particularly effective for group 10 metal complexes, and electron poor metal centres, such as $[W(CO)_3(\eta^5\text{-}C_5R_5)]$ (R = H, Me) (Scheme 1, **A**). However, the method is unsuccessful when an electron rich metal end cap, for example $[Ru(L)_2(\eta^5\text{-}C_5R_5)]$ (R = H, Me and L = PPh_3, dppe) is used.[9] A drawback in using this method is the generation and handling of the rather sensitive terminal butadiynes,[10] especially the potentially

explosive HC≡CC≡CH reagent. An alternative to using diacetylene is HC≡CC≡CSiMe$_3$ which can be readily synthesised from Me$_3$SiC≡CC≡CSiMe$_3$ and MeLi /LiBr.[6e] Using similar coupling conditions to HC≡CC≡CH (the presence of the metal halide, CuI and NHEt$_2$) metal diynyl complexes supported by electron rich metal fragments can be readily synthesised (Scheme 1, **B**).[11]

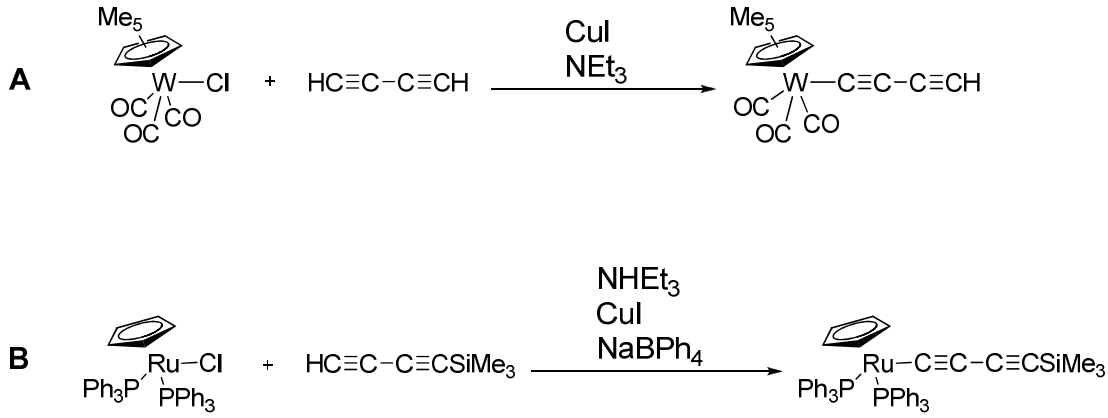

Scheme 1: Formation of metal diynes using CuI /NEt$_3$ coupling methodologies.

Ligand substitution reactions between a metal substrate, featuring a suitable leaving group or vacant coordination site, and a lithiated butadiynyl reagent (typically LiC≡CC≡CH) have found success in synthesizing diynyl complexes. The compound [Ru(C≡CC≡CSiMe$_3$)(PPh$_3$)$_2$(η^5-C$_5$H$_5$)] (**15**), can be readily obtained from the reaction of [Ru(thf)(PPh$_3$)$_3$(η^5-C$_5$H$_5$)] with LiC≡CC≡CSiMe$_3$.[6e] In addition, the preparation of [Fe(C≡CC≡CSiMe$_3$)(CO$_2$)(η^5-C$_5$H$_5$)] (**16**), can also be achieved from the reaction of lithiated diacetylene (LiC≡CC≡CSiMe$_3$) and [FeCl(CO)$_2$(η^5-C$_5$H$_5$)] (Scheme 2).[12]

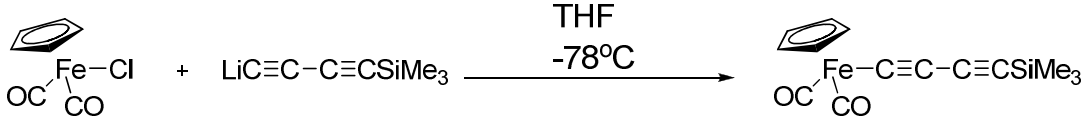

Scheme 2: Synthesis of metal diynes using lithiated reagents.

The polyyne chain can be added using organostannane reagents $R_3Sn(C{\equiv}C)_nX$ (n = 0 or 1) in the presence of a palladium catalyst under mild Stille-like coupling conditions. A successful outcome has been achieved in the coupling of polyynes, which are two and four carbons in length, to $[Fe(CO)_2(\eta^5\text{-}C_5H_5)]$ (Scheme 3).[13] Despite this, the method has not been employed in recent times due to the difficulty in safely handling organo-tin reagents and the development of other mild coupling methodologies.

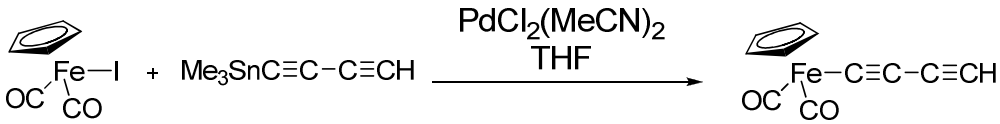

Scheme 3: Synthesis of metal diynes using Stille reagents.

The use of fluoride anion to promote the reaction between $Me_3SiC{\equiv}CC{\equiv}CC_6H_5$ and $[RuCl(PPh_3)_2(\eta^5C_5H_5)]$ (**17**) (Scheme 4, **A**)[9, 14] and also $Me_3SiC{\equiv}CC{\equiv}CSiMe_3$ between $[ReCl(CO)_3(^tBu_2bipy)]$ (Scheme 4, **B**), successfully prepare butadiynyl complexes.[15]

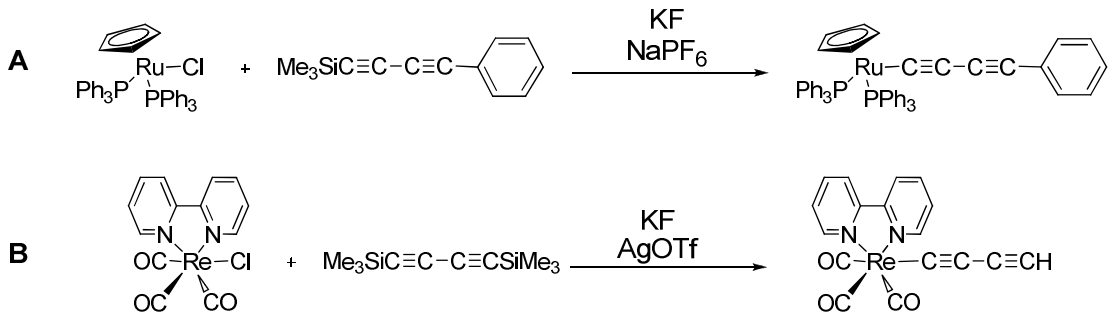

Scheme 4: Synthesis of metal diynes using fluoride anion de-silylation methodologies.

Whilst reactions of terminal butadiynes with metal centres can often lead to highly reactive butatrienylidene systems[12, 16] through careful modification of the reaction conditions or metal substrate it is possible to direct the formation of M-C≡CC≡CR

systems.[17] The metal moiety, $[Re(NO)(PPh_3)(\eta^5\text{-}C_5Me_5)]$ can be used to form butadiynyl complexes via a unique pathway in comparison to the common group 6 and 8 metal end caps. The reaction of $[Re(ClC_6H_5)(NO)(PPh_3)(\eta^5\text{-}C_5Me_5)]$ (**18**), with $HC{\equiv}CC{\equiv}SiMe_3$ affords the η^2 bound $[Re\{\mu\text{-}HC{\equiv}C(C{\equiv}CSiMe_3)\}(NO)(PPh_3)(\eta^5\text{-}C_5Me_5)]^+$. The subsequent reaction of $[Re\{\mu\text{-}HC{\equiv}C(C{\equiv}CSiMe_3)\}(NO)(PPh_3)(\eta^5\text{-}C_5Me_5)]^+$ with KO^tBu results in the σ-bound diynyl chain complex $[Re(C{\equiv}CC{\equiv}CSiMe_3)(NO)(PPh_3)(\eta^5\text{-}C_5Me_5)]$ (**19**) (Scheme 5).[5c]

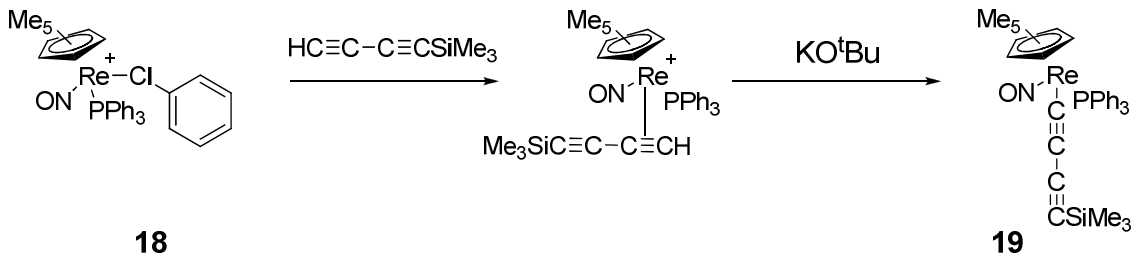

Scheme 5: Synthesis of rhenium diynes.

Both diynyl and triynyl complexes can be extended to form longer polyyne chains by the sequential addition of bromine-substituted alkynes using Cadiot-Chodkiewicz coupling protocols (Scheme 6). This methodology relies on the formation of a copper terminated polyyne chain *in situ* followed by treatment with a bromo-alkyne, either two or four carbons in length, in $NHEt_2$ at low temperature (-20°C). Using this coupling methodology, mono-metallic polyynes of 10 carbon atoms in length have been synthesised where $[Re(NO)(PR_3)(\eta^5\text{-}C_5Me_5)]$ is the supporting metal moiety.[18] An alternative coupling strategy, using $[Pt(PR_3)_2Ar]$ as the supporting metal fragment, employs the coupling of excess trimethylsilyl protected alkynes ($H(C{\equiv}C)_nSiMe_3$) in the presence of Cu /TMEDA and O_2 in acetone. This route has produced monometallic complexes supporting chains of up to 16 carbons in length.[19]

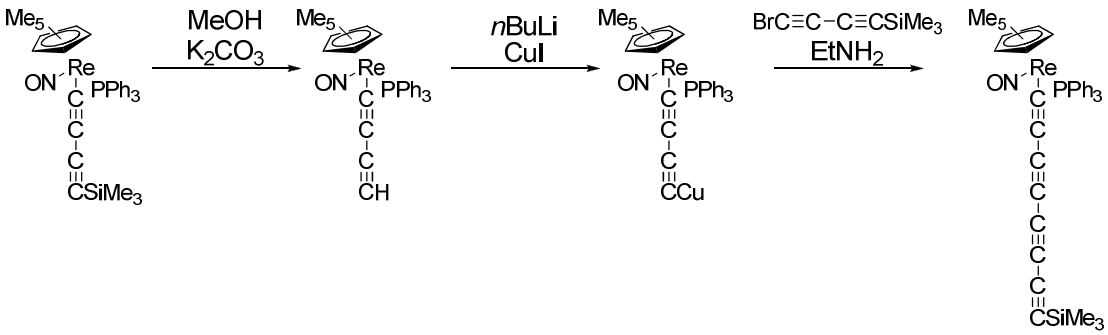

Scheme 6: Cadiot-Chodkiewicz coupling methodology.

These very long chain complexes have mainly been used in the synthesis of bimetallic complexes, where the bridge has been used to model carbyne, an interesting hypothetical linear allotrope of carbon.[6b] In addition, the long chain platinum complexes, $[Pt(C{\equiv}C)_n\{P(p\text{-tol})_3\}_2(C_6F_5)]$, have been shown to readily undergo copper(I)-promoted "click" 3+2 cycloadditions with organic azides.[20] Carbon-carbon triple bonds are susceptible to coordination with a variety of metal clusters, including $[Co_2(CO)_4(dppm)]$ and $[Ru_3(CO)_{12}]$. This has led to the synthesis of a large number of monometallic polyyne complexes with cluster moieties, which has allowed a unique insight into structural, physical and electronic properties of the multi-metallic systems.[21]

3.2 Synthesis

The synthesis of [Mo(C≡CC≡CH)(dppe)(η^7-C_7H_7)] (**20**), and relevant intermediates have already been investigated and reported,[22] however, a summary of the method is included here for completeness. Synthetic work towards the development of a viable route to [Mo(C≡CC≡CC≡CH)(dppe)(η^7-C_7H_7)] (**21**), was carried out by Hannah N. Lancashire at the University of Manchester and is reproduced here with permission to compliment the synthetic work of **21**.

Despite the success of [MoBr(dppe)(η^7-C_7H_7)] (**5**) as an entry point to acetylide complexes [Mo(C≡CR)(dppe)(η^7-C_7H_7)], similar routes were unsuccessful in the synthesis of extended polyynyl systems. However, [MoBr(bipy)(η^7-C_7H_7)] (**22**), which could be readily synthesised from the reaction of [$Mo(CO)_3$(η^7-C_7H_7)]PF_6 with 2,2-biypridine,[23] proved to be a more viable precursor. The reaction of **22** with LiC≡CC≡C$SiMe_3$, formed from the reaction of Me_3SiC≡CC≡C$SiMe_3$ with MeLi/LiBr complex, afforded [Mo(C≡CC≡C$SiMe_3$)(bipy)(η^7-C_7H_7)] (**23**). The thermal substitution of the 2,2-biypridine ligand with dppe produced [Mo(C≡CC≡C$SiMe_3$)(dppe)(η^7-C_7H_7)] (**24**), and subsequent desilyation with $^nBu_4NF$ in THF gave the target complex **20** (Scheme 7).

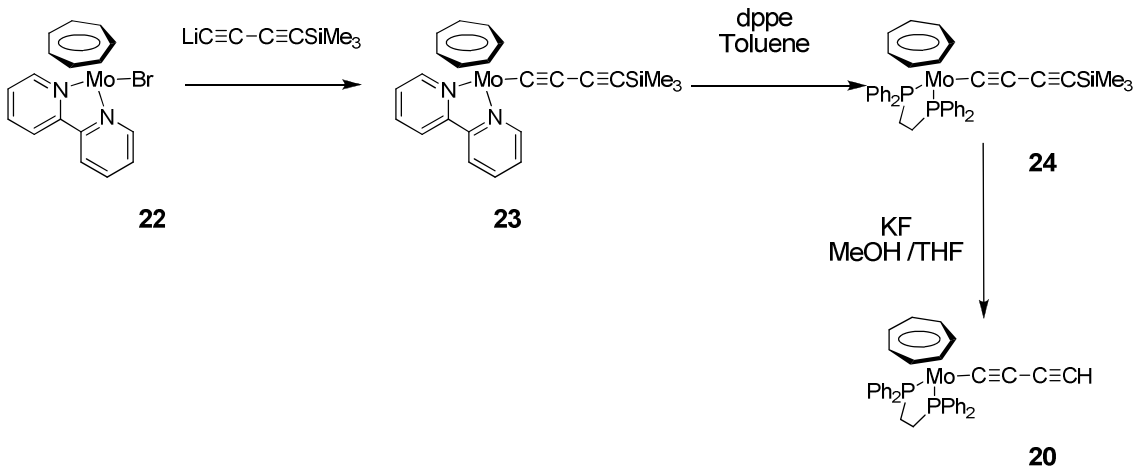

Scheme 7: Synthesis of 21 from 22.

The triynyl complexes were synthesised using an analogous method, whereby the reaction of $LiC{\equiv}CC{\equiv}CC{\equiv}CCSiMe_3$ with **22**, under carefully controlled conditions, to afford $[Mo(C{\equiv}CC{\equiv}CC{\equiv}CSiMe_3)(bipy)(\eta^7\text{-}C_7H_7)]$ (**25**), as a deep purple powder. Subsequent substitution of 2,2-biypridine with dppe and further purification using a Celite column yielded $[Mo(C{\equiv}CC{\equiv}CC{\equiv}CSiMe_3)(dppe)(\eta^7\text{-}C_7H_7)]$ (**26**), as a deep green powder. Attempts to desilylate **26** to give **21** were unsuccessful, which resulted in the decomposition of **26**, such results can be contrasted with rhenium and ruthenium systems (for example $[Re(C{\equiv}CC{\equiv}CSiMe_3)(NO)(PPh_3)(\eta^5\text{-}C_5Me_5)]$ and $[Ru(C{\equiv}CC{\equiv}CSiMe_3)(dppe)(\eta^5\text{-}C_5Me_5)]$)where desilylation with K_2CO_3 or $^nBu_4NF$ have proved successful.[24]

The radical cations of **20**, **23** and **24** were readily synthesised from the addition of one equivalent of $[FcH]PF_6$ to yield $[\mathbf{20}]PF_6$, $[\mathbf{23}]PF_6$ and $[\mathbf{24}]PF_6$. It must be noted that the observation of these radical, cationic diynyl complexes is unique to the $Mo(L)_2(\eta^7\text{-}C_7H_7)$ series, which has allowed a detailed experimental analysis of these unprecedented polyynyl radicals.[25] The biypridine substituted radical complex $[\mathbf{23}]PF_6$ was relatively stable and persistent in solution. In contrast, the dppe substituted complexes $[\mathbf{20}]PF_6$

and [**24**]PF_6 rapidly dimerise (in comparison to the molybdenum acetylides) through C-C bond forming reactions at the C_2 position to give the corresponding bis-vinylidene complexes [{Mo(dppe)(η^7-C_7H_7)}$_2${μ-C=C(C_2H)C(C_2H)=C}][PF_6]$_2$, [**27**][PF_6]$_2$, and [{Mo(dppe)(η^7-C_7H_7)}$_2${μ-C=C(C_2SiMe$_3$)C(C_2SiMe$_3$)=C}][PF_6]$_2$, [**28**][PF_6]$_2$ (Scheme 8).

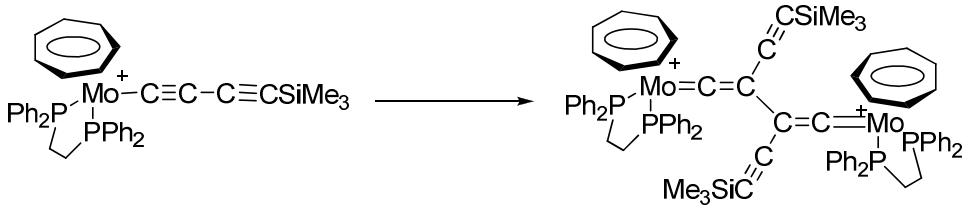

24 **28**

Scheme 8: Dimerisation of molybdenum diyne.

The same analogous reactivity has been reported for the **1**$^+$ radical which dimerises through C_2 to give [{Mo(dppe)(η^7-C_7H_7)}$_2${μ-=CC(C_6H_5)C(C_6H_5)C=}][PF_6]$_2$, [**29**][PF_6]$_2$.[26] It is suggested that one factor in this dimerisation reaction is the steric hindrance of the C_2 position brought about by the substituent R, [Mo(C≡CR)(dppe)(η^7-C_7H_7)]$^+$. Thus the radical cation [Mo(C≡C^{t}Bu)(dppe)(η^7-C_7H_7)]$^+$ (**12**$^+$) does not dimerise, instead in the presence of a source of H^+, forms the vinylidene complex, [Mo{=C=C^{t}Bu(H)}(dppe)(η^7-C_7H_7)]$^+$ (**30**$^+$).

3.3 Spectroscopic Investigations

All the complexes were characterized by elemental analysis, ^{1}H, $^{31}P\{^{1}H\}$, ^{13}C NMR spectroscopy and high resolution mass spectroscopy. All the complexes display typical ^{13}C resonances for both diynyl and triynyl chains. It is interesting to note the systematic decreases in the frequency of the ^{13}C resonance as the assigned carbon atom is further away from the [Mo(dppe)(η^{7}-C_7H_7)] moiety. For **20**, **23**, and **24** the carbon resonances decrease to the lowest value on the terminal carbon atom. This is a common trait amongst diynyl complexes.[27] The exact value of the chemical shift of the terminal carbon shift is dependant upon both the nature of the metal centre and the identity of the substituent at the end of the chain. For example, there is a difference of 17.2 ppm in the C_4 resonance of **24** (R = $SiMe_3$) and **20** (R = H). The difference is mirrored in the related complexes, [Re(C≡CC≡CR)(NO)(PPh_3)(η^{5}-C_5Me_5)] (R = H, $SiMe_3$) is 15.4 ppm.

On increasing the chain length of the polyynyl ligand to six carbons, there is no longer a linear decrease in the chemical shift of the carbon centres from C_1 to C_6. Instead, the last carbon C≡C set of the chain are found at lower field than the two carbons at the centre of the chain. This phenomenon has been noted in all linear carbon chains which are greater than four carbons in length, and can be explained by making a comparison with data collected for the free acetylenic complexes, such as ^{t}BuC≡CC≡CC≡CC≡C^{t}Bu. ^{13}C NMR data for this complex shows that the centre carbon resonances are grouped around a single value of 54 ppm, this value is taken as the limiting value associated with an infinite polymeric carbyne structure.[28] This limiting value alters slightly for the

shorter chain metal supported complexes, as the centre of the chain is not solely carbyne in character due to the influence of the metal centre. Depending on the metal moiety that is employed this limiting value changes, for complex **25** it is 57 ppm, whereas for the analogous ruthenium and rhenium systems the value is 67 ppm and 81 ppm, respectively. In support of these assignments, 2-D NMR experiments have been performed on complexes containing the $Re(NO)(PPh_3)(\eta^5\text{-}C_5Me_5)$ fragment, however, the amount of material needed to perform this experiment on the complexes described in this Chapter, in addition to the stability of the neutral complexes in solution made this experiment impractical. As a compromise, NMR predictions based on the calculated geometries (**20H**, **21H**, **36H**, **37H** and **38H**) have been made to assist in the assignment of the ^{13}C NMR spectrum for **26**, the results of which are discussed later (Section 3.6.1).

Table 1: Selected experimental ^{13}C NMR (Bracketed values refer to the J_{CP} coupling values in Hz) and calculated ^{13}C NMR spectra. In CD_2Cl_2 solution unless stated otherwise. Calculated ^{13}C shifts for 20H, 21H and 36H referenced to $(200 - \delta_{(calculated)})$. 37H and 38H referenced to $(211 - \delta_{(calculated)})$.

L = bipy	C_1	C_2	C_3	C_4	C_5	C_6	$SiMe_3$
37H	148.1	112.3	82.4	77.1	-	-	-
23	142.1	95.1	91.6	76.7	-	-	-0.4
38H	156.0	113.4	75.37	76.71	83.5	79.3	-
25	-	-	-	-	-	-	-
L = dppe							
36H	130.5	110.7	-	-	-	-	-
20H	138.8	112.1	71.6	64.9	-	-	-
20	138.7, t, (25.1)	103.6	72.7, t, (3.8)	59.5	-	-	
24	142.8, t, (25.0)	105.1, t, (2)	93.0, t, (4)	75.7	-	-	0.6
21H	147.8	112.5	64.4	65.1	72.5	68.5	-
26	151.9, t, (25.2)	105.1	66.2, t, (5.0)	57.0	91.4	83.5	0.0

Infrared spectroscopy of the trimethylsilyl substituted complexes **23** and **24** show a common three band structure, with two bands around 2150 and 2050 cm^{-1} and one weak band around 1980 cm^{-1}, all three corresponding to the diynyl moiety. When the trimethylsilyl group is replaced by a terminal hydrogen the infrared structure reduces to two single bands. This difference is a common effect amongst metal diynyl complexes,[12] the origins of this effect have been investigated here using DFT methods.

Table 2: Solution (CH_2Cl_2) infrared results.

Complex	IR ν(C≡C) cm^{-1}
23	2151 (m), 2111 (m), 1991 (w)
24	2153 (w), 2105 (sh), 2090 (m), 2063 (sh), 1976 (w)
20	3301 (m) ≡CH, 2098 (m), 1956 (w)
25	2131 (s), 2106 (m), 1967 (s)
26	2121 (m), 2092 (m), 1949 (s)

3.4 Electrochemistry

All the monometallic complexes **20**, **23**, **24**, **25** and **26** exhibit a diffusion controlled, chemically reversible, one electron oxidation process under the conditions stated in Table 3, with the separation between the cathodic and anodic peak potentials comparable to that determined for the internal ferrocene standard. As was concluded for the related acetylide complexes, when compared to the analogous iron and ruthenium complexes, the polyynyl complexes derived from [Mo(dppe)(η^7-C_7H_7)] are considerably easier (in the thermodynamic sense) to oxidise.

Table 3: All potentials recorded at ambient temperature, at a Pt dot working electrode in 0.1 M $^{n}Bu_4NPF_6$ /CH_2Cl_2. Re-referenced to FcH /FcH^+ = 0.00 V

Complex	$E_{1/2}$ /V
20	-0.58
23	-0.66
24	-0.58
25	-0.64
26	-0.53

In comparison to the acetylide complexes [Mo(C≡CC_6H_5)(dppe)(η^7-C_7H_7)], **1**, increasing the chain length to C_4, **24**, gives a 0.14 V positive shift in potential. Increasing the chain length by another two carbons causes the potential to increase by a further 0.05 V (**26**). A smaller increase of 0.02 V is seen for **23** and **25** indicating that the extension of the carbon chain has a consistent, but limited, effect on the redox properties of these molybdenum polyynyl complexes. In relationship to the acetylide complexes studied in Chapter two, increasing the chain length has a similar effect to adding an electron withdrawing group to the C_2 chain, for example **10** ($E_{1/2}$ = -0.65 V) and **1** ($E_{1/2}$ = -0.72 V). This observation is consistent with previous computational work that has suggested a greater degree of polarisation along the metal-carbon chain for complexes with longer polyynyl ligands.[29] In replacing the bipyridine ligand with the dppe ligand there is a consistent increase in oxidation potential of 0.11 V, showing that the dppe complexes are harder to oxidise than their bipyridine counterparts.

In contrast to the acetylide complexes, where the identity of the substituent causes a modest shift in the potential when the substituent is changed from trimethylsilyl to hydrogen, **24** to **20**, no change is seen in the potentials. This feature can be found in other extended chain systems where the character of the frontier orbitals is mainly metal centered, for example [Fe(C≡CC≡CR)(dppe)(η^5-C_5Me_5)] (R = H, $SiMe_3$).[19] However, as the frontier orbitals become more ligand centered, larger variations in $E_{1/2}$ are seen as

the substituent is changed, as demonstrated with [Ru(C≡CC≡CR)(dppe)(η^5-C_5Me_5)], R = H ($E_{1/2}$ = 0.52 V), R = $SiMe_3$ ($E_{1/2}$ = 0.58 V).[12]

3.5 Infrared Spectroelectrochemistry

Although it is possible to isolate the stable 17 electron radical complexes, for ease of data collection and to reduce the amount of dimerised products formed, the radicals were generated *in situ* by spectroelectrochemical methods (Table 4). The gradual conversion of species allows the easy identification of low intensity bands, which can often be difficult to distinguish from background effects and solvent overtones in the case of static spectra.

Table 4: Infrared spectroelectrochemical results recorded in 0.1 M ^{n}Bu$_4$NPF$_6$ /CH_2Cl_2.

Complex	ν(C≡C) /cm^{-1} n = 0	ν(C≡C) /cm^{-1} n = 1	Δν(C≡C) /cm^{-1} for the lowest band.	Δν(C≡C) /cm^{-1} for the middle band.	Δν(C≡C) /cm^{-1} for the highest band.
20^{n+}	2103, 2011 br	2103, 1953 br	-58	-	0
23^{n+}	2158, 2117, 1998	2152, 2112, 1989	-9	+5	-7
24^{n+}	2154, 2106, 2092, 1976	1971	-5	0	0
25^{n+}	2133, 2107, 1968	2146	-	-	-7
26^{n+}	2122, 2093, 1950	2137, 2105 br, 1948 sh, 1933	-17	+13	+15

The neutral 18 electron complexes [Mo(C≡CC≡C$SiMe_3$)(L_2)(η^7-C_7H_7)], where L = biypridine (Figure 1) or dppe (Figure 2) all display a similar three band pattern between 2200 and 1900 cm^{-1}. Upon oxidation, the lowest energy band decreases in intensity

producing a small positive shift in wavenumber, the higher energy bands (2150 – 2000 cm^{-1}) reduce again in intensity and lower in energy, approximately 10 cm^{-1} in energy. Although complexes **23** and **24** both show a three band structure, **24** exhibits a more complex band pattern with at least one shoulder on each of the higher energy bands. Replacing the trimethylsilyl substituent in **24** with terminal hydrogen (**20**), the spectrum simplifies to two bands, and upon oxidation the higher energy band disappears to the baseline and the lower energy band shifts by 4 cm^{-1}. However, the stability of the radical cation decreases once the $SiMe_3$ group is removed, resulting in the presence of the bis-vinylidene β-dimerisation product in the spectra if the radical cation is observed for prolonged periods of time.

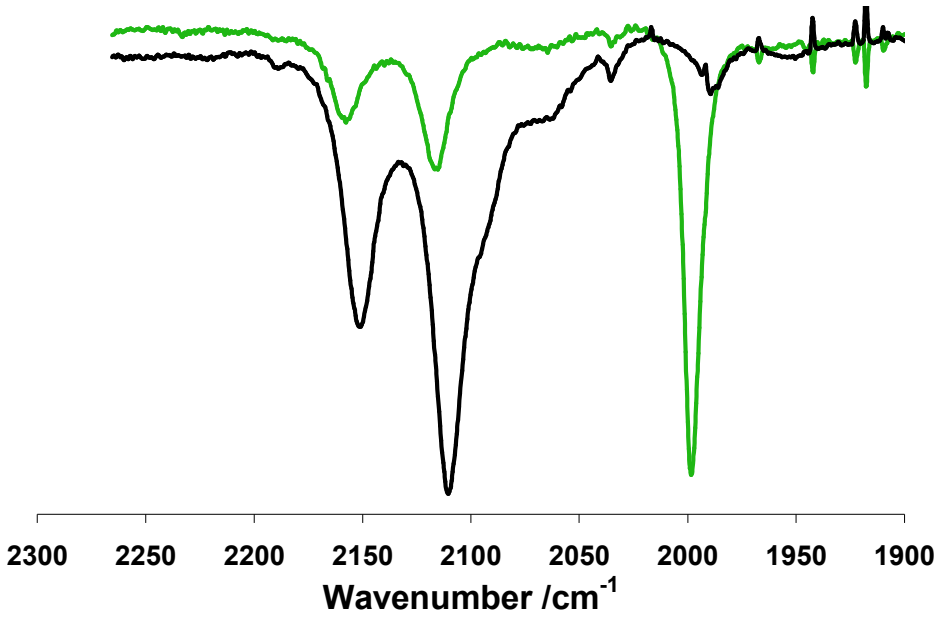

Figure 1: Infrared spectra for 23^{n+}, where n = 0 (Black), n = 1 (Green) (Recorded in0.1 M $^{n}Bu_4NPF_6$ /CH_2Cl_2).

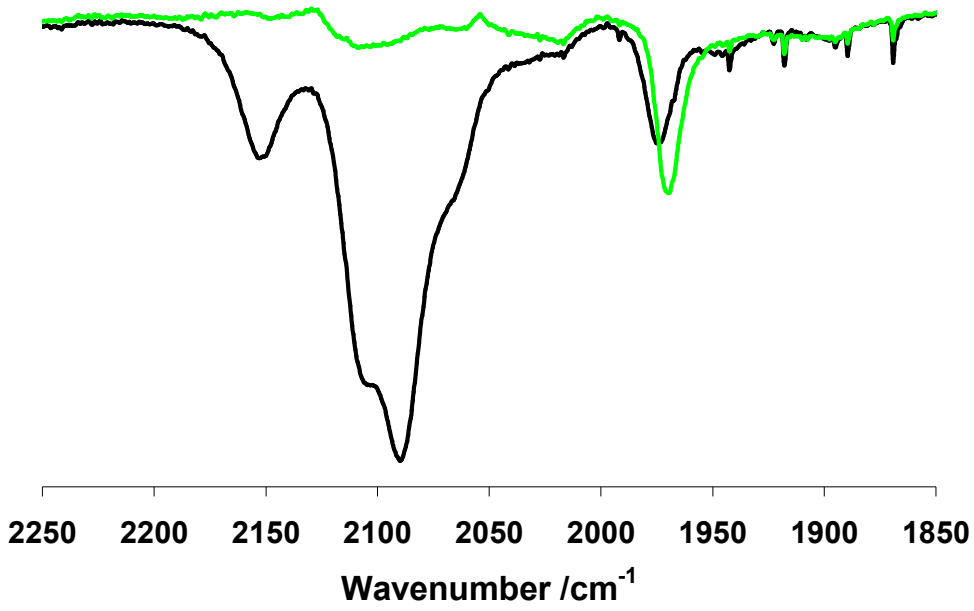

Figure 2: Infrared spectra for 24^{n+}, where n = 0 (Black), n = 1 (Green) (Recorded in0.1 M $^{n}Bu_4NPF_6$ /CH_2Cl_2).

The triynyl complexes give a three band pattern regardless of the identity of the end group. Upon oxidation of both **25** and **26** the bands only shift by *ca.* 10 cm^{-1}. However, **25** has a much simpler spectrum than **26**. The latter displays a complex band structure with multiple shoulders on the ν(C≡C) stretches. Particular note must be taken of the disappearance of two of the three bands in complex **26**, this points to towards the minimization of the dipole moment across the chain, which is indicative of an electron being removed from an orbital that is more ligand in character.

3.6 Electronic Structure Calculations

A computational investigation was conducted to further explore and assist in understanding the effects of extending the linear carbon chain on the electronic structure of the complexes. Moreover, the computational analysis may explain why [**23**]$^{+}$ does not dimerise, but [**24**]$^{+}$ dimerises to give [**28**]$^{2+}$. Initial attempts to model the polyynyl series using a simplified dHpe supporting ligand, [Mo{(C≡C)$_n$C≡CH}(dHpe)(η^7-C_7H_7)], yielded a model with poor structural and spectroscopic agreement with the experimental results. The study was therefore performed using the full ligand structures, [Mo{(C≡C)$_n$C≡CH}(dppe)(η^7-C_7H_7)] (where n = 0 (**20H**), 1 (**36H**), 2 (**21H**)), and [Mo{(C≡C)$_n$C≡CH}(bipy)(η^7-C_7H_7)] (where n = 1 (**37H**), 2 (**38H**)). This investigation allows the examination of the effect of chain extension from two to six carbons and comparison with experimental results was used to refine the computational model. In addition to the hydrogen terminated chains, the trimethylsilyl terminated complexes [Mo(C≡CC≡CSiMe$_3$)(bipy)(η^7-C_7H_7)] (**23Si**), and [Mo(C≡CC≡CC≡CSiMe$_3$)(bipy)(η^7-C_7H_7)] (**25Si**), were also modelled to ascertain the nature of the three band structure which is unique to the trimethylsilyl substituted diynyl chains, **23** and **24**.

3.6.1 Neutral Species Calculations

The general orbital features of **20H**, **21H** and **36H**,dppe supported complexes remain largely unchanged by the nature of the (poly)ynyl ligand and closely resemble the characteristics found in molybdenum acetylides (Chapter 2). The HOMO is separated from the HOMO-1 by approximatly 0.5 eV, and is dominated by the d_{z2} orbital of the

molybdenum centre. The metal character of the HOMO decreases as the chain length is increased. This is accompanied by a reduction in the relative energy of the HOMO across the series, thus supporting the electrochemical observation, where by the oxidation becomes more difficult, as the chain length is increased. Alongside this, as the chain increases in length there is an increase in the percentage contribution of the chain to the HOMO from 17 % for **36H** to 38 % for **21H**.

The energies of the metal d-orbitals with a δ interaction with the cycloheptatrienyl ring, d_{xy} and d_{x2-y2}, remain relatively constant across the series, with the contribution from the chain increasing sequentially (for d_{xy} 24 % (**36H**), 41 % (**20H**) and 51 % (**21H**)) as the chain length is increased. As observed for the molybdenum acetylides and for many other cycloheptatrienyl capped metal moieties, the d_{zx} and d_{zy} are stabilized by a π-interaction with the cycloheptatrienyl ring by 3.3 eV compared to the d-orbials which have a δ-interaction with the ring. The LUMO consists of contributions predominantly from the [Mo(dppe)(η^7-C_7H_7)] fragment (**36H** 99 % to, **20H** 95 % and **21H** 95 %) and result from the anti-bonding combination from the δ-interaction between the d_{xy} metal orbital and the cycloheptatrienyl ring. As the chain length increases the HOMO-LUMO gap decreases slightly (≈ 0.07 eV per 2 carbons added onto the chain) but remains ≈ 3 eV across the series, **36H** to **21H** (Table 5).

Table 5: Percentage contributions for calculated geometries 36H, 21H and 36H at B3LYP /6-31g* /LANL2DZ.

	Orbital /metal d-orbital	Energy /eV	Mo %	dppe %	C_7H_7 %	C_1 %	C_2 %	C_3 %	C_4 %	C_5 %	C_6 %
36H	LUMO	-0.73	11	66	22	0	1	-	-	-	-
	HOMO /d_{z2}	-3.69	72	5	6	3	14	-	-	-	-
	HOMO-1 /d_{xy}	-4.53	28	7	40	6	18	-	-	-	-
	HOMO-2 /d_{x2-y2}	-4.97	46	8	40	3	3	-	-	-	-
	HOMO-16/d_{zy}	-8.25	12	13	75	0	0	-	-	-	-
	HOMO-17 /d_{zx}	-8.38	17	9	57	14	2	-	-	-	-
36H	LUMO	-0.86	15	56	24	1	2	2	0	-	-
	HOMO /d_{z2}	-4.05	62	4	6	4	13	10	1	-	-
	HOMO-1 /d_{xy}	-4.54	20	6	33	10	16	13	2	-	-
	HOMO-2 /d_{x2-y2}	-5.08	47	8	36	4	3	2	1	-	-
	HOMO-18 /d_{zy}	-8.40	11	17	71	0	0	0	0	-	-
	HOMO-19 /d_{zx}	-8.62	12	37	32	14	4	0	1	-	-
21H	LUMO	-1.09	18	29	26	5	5	3	6	1	6
	HOMO /d_{z2}	-4.16	56	4	5	4	13	1	10	1	7
	HOMO-1 /d_{xy}	-4.58	15	6	28	10	14	4	12	1	10
	HOMO-2 /d_{x2-y2}	-5.21	46	7	30	5	3	2	3	1	3
	HOMO-18 /d_{zy}	-8.54	11	18	71	0	0	0	0	0	0
	HOMO-20 /d_{zx}	-8.80	11	23	20	14	6	7	9	6	3

The analogous bipyridine systems (**37H** and **38H**) exhibit similar trends to the dppe systems. The complexes become harder to oxidise (compared to ferrocene) as a result of the HOMO becoming more stabilised due to an increased contribution from the (poly)ynyl fragment. The d_{xy} and d_{x2-y2} orbitals involved in the δ interaction with the cyclohepatrienyl ring, are separated by similar energies as found in the dppe series, and are removed from the HOMO by a comparable energy, 0.4 eV. However, **37H** and **38H** models predict a larger stabilization of the d_{zy} and d_{zx} orbitals by 1 eV when compared to **20H** and **21H** (Table 6). An analysis of the orbital contributions reveal that these π-interaction molecular orbitals have an increased contribution from the bipyridine ligand, over 70 %, whereas the dppe complexes have a 70 % contribution form the cycloheptatrienyl ring. This reversal of roles between the bipyridine ligand and the cycloheptatrienyl ring is due to a more favorable symmetry match between the bipyridine ring to the metal d-orbitals. A consequence of this is the reversal of energies of the d_{zx} and d_{zy} orbitals, compared to the dppe complexes. The increased ability of the bipyridine ligand to stabilise metal d-orbitals through π-type interactions is also exemplified with a reduction in the HOMO-LUMO energy, which is 1 eV less than the dppe analogues.

Table 6: Percentage contributions for the calculated geometries 37H and 38H at B3LYP /6-31g* /LANL2DZ.

	Orbital /metal d-orbital	Energy /eV	Mo %	bipy %	C_7H_7 %	C_1 %	C_2 %	C_3 %	C_4 %	C_5 %	C_6 %
37H	LUMO	-2.00	12	83	4	0	0	0	0	-	-
	HOMO /d_{z2}	-4.15	50	18	4	5	13	1	10	-	-
	HOMO-1 /d_{xy}	-4.63	16	3	33	13	16	3	15	-	-
	HOMO-2 /d_{x2-y2}	-5.02	47	2	36	6	4	1	4	-	-
	HOMO-14 /d_{zx}	-9.16	10	72	16	2	0	0	0	-	-
	HOMO-15 /d_{yz}	-9.21	12	65	23	0	0	0	0	-	-
38H	LUMO	-2.12	11	84	4	0	0	0	0	0	0
	HOMO /d_{z2}	-4.25	46	16	4	5	12	2	9	1	6
	HOMO-1 /d_{xy}	-4.68	13	2	28	12	14	5	13	1	11
	HOMO-2 /d_{x2-y2}	-5.11	47	2	31	6	3	3	4	1	4
	HOMO-16 /d_{zx}	-9.28	11	71	15	2	0	0	0	0	0
	HOMO-17 /d_{yz}	-9.33	12	65	23	0	0	0	0	0	0

The calculations on **23Si** and **25Si** did not reproduce the multiple ν(C≡C) stretching modes seen in the experimental spectra. The origin of these multiple bands is therefore a consequence of non-fundamental stretching modes, the nature of which could be attributable overtones or Fermi resonance, although the present results preclude an accurate assignment of this.

The NMR predictions performed on the optimised geometries with (**20H**, **21H**, **36H**, **37H** and **38H**) have been tabulated (table 1). The general trends exhibited in the experimental measurements are mirrored by the calculated spectra, whereby the terminal carbon atoms for six carbon analogues (**26**) are predicted to be at lower field than the central carbon pair. This correlates well with the 2-D NMR experiments performed on the rhenium systems.[28]

3.7 EPR Spectroscopy

As previously shown through synthetic and electrochemical investigations, the 17 electron species derived from the one-electron oxidation of complexes **23**, **24**, **25**, and **26** are relatively thermodynamically and kinetically stable, which has allowed Dr. E. Fitzgerald at the National EPR Centre, Manchester, to undertake a thorough X-band EPR investigation. As is typical with the [Mo(dppe)(η^7-C_7H_7)] supported complexes, a well resolved EPR signal is observed which allows an accurate description of the location of the unpaired electron in the complex to be established. The complexes [**20**]$^+$, [**23**]$^+$, [**24**]$^+$ (Figure 3) and [**25**]$^+$ were generated by *in situ* oxidation with

$[Fe(\eta^5\text{-}C_5H_5)_2][PF_6]$, followed by cooling to 243 K, which is the optimum temperature to accurately determine the hyperfine coupling constants (Table 7).

Table 7: X-band EPR fluid solution (CH_2Cl_2, 253 K) for $\mathbf{20}^+$, $\mathbf{23}^+$, $\mathbf{24}^+$, $\mathbf{25}^+$, $\mathbf{26}^+$.

	a_{iso}(Mo)	$a_{iso}(^{31}P)$	$a_{iso}(^{14}N)$	$a_{iso}(^{1}H)$	g_{iso}
$\mathbf{20}^+$	32	23.0	-	4.3 (C_7H_7), 1.9 (C_4H)	1.996
$\mathbf{23}^+$	38	-	2.1	4.6 (C_7H_7)	1.975
$\mathbf{24}^+$	32	22.8	-	4.3 (C_7H_7)	1.996
$\mathbf{25}^+$	38	-	-	-	1.974
$\mathbf{26}^+$	31	22.6	-	4.1 (C_7H_7)	1.995

The leaching of the spin density on the longer chains is apparent from the, albeit small, decrease in the hyperfine values of the $^{95/97}$Mo, ^{14}N and ^{31}P atoms. Comparison between $\mathbf{24}^+$ and $\mathbf{26}^+$ shows that the hyperfine values decrease by 1 G producing a value that is very close to those obtained for $[Mo(C{\equiv}CC_6H_5)(dppe)(\eta^7\text{-}C_7H_7)]^+$ ($\mathbf{1}^+$), the same is seen for the biypridine supported complexes. The hyperfine values for ^{14}N could not be determined for **25** due to the small size of the value being beyond the resolution of the apparatus. However, based upon the hyperfine values for $^{95/97}$Mo the effect of the chain on the spin distribution across the complex is likely to be minimal. The EPR results for $[\mathbf{20}]^+$ are of particular interest as the spectrum displays a very small coupling to the terminus H atom on the C_4 chain of 1.9 G. This is in contrast to **1** where there is no coupling to the para position on the aryl ring.

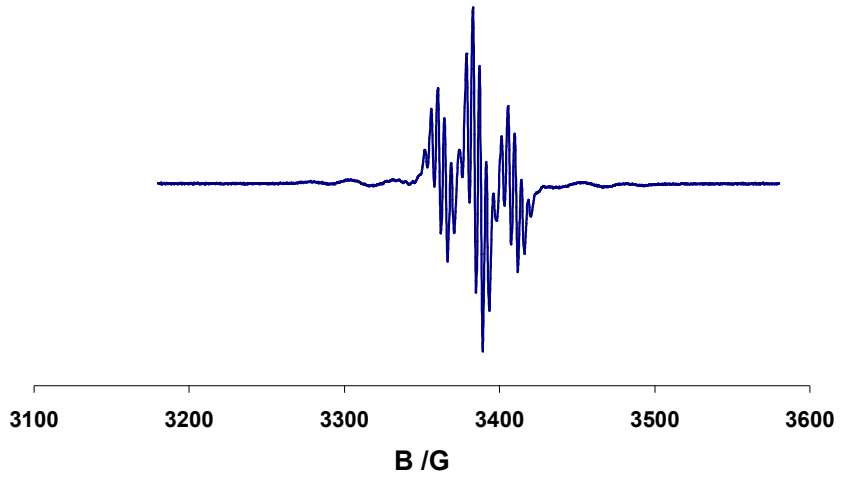

Figure 3: First derivative X-band EPR fluid solution (CH_2Cl_2, 243 K) of 24^+.

3.7.1 Cationic Species Calculations

The cationic optimised geometries **20H**$^+$, **21H**$^+$, **36H**$^+$, **37H**$^+$, **38H**$^+$, accurately model the decrease in the Mo-C_1 bond lengths and the small increase of the Mo-P and Mo-N bond lengths compared to neutral species. They are a result of the decreased back-donation from the electron deficient metal centre. Across the series, the carbon-carbon bonds of the polyynyl chain experience the smallest change upon oxidation, (Table 8) which is consistent with the crystallographically determined structures of **23** and **[23]PF$_6$**.[26] Previous theoretical studies on [Ru{(C≡C)$_n$C≡CR}(PH$_3$)$_2$(η^5-C$_5$H$_5$)] have shown a larger effect, whereby the carbon-carbon bond lengths change by *ca* 0.3 Å, therefore a more cumulenic chain is formed upon oxidation. The effect is less distinct in the [Mo(dppe)(η^7-C$_7$H$_7$)] supported complexes, with a smaller change of 0.05 Å, indicating that the molecular orbital from which the electron was removed is more metal in character than in the ruthenium model. The changes in the longer chain systems, **38H**$^+$ and **21H**$^+$, are of a similar magnitude.

Table 8: Selected crystallographic and calculated geometries.

Complex	**36H (36H$^+$)**	**20H (20H$^+$)**	**20**	**21H (21H$^+$)**	**26[b]**	**37H (37H$^+$)**	**23[a]**	**23$^+$ [c]**	**38H (38H$^+$)**	**25Si**
Mo-C_1	2.142 (2.086)	2.118 (2.063)	2.114(3)	2.105 (2.050)	2.099(3)	2.112 (2.059)	2.135(2)	2.134(22)	2.105 (2.049)	2.117(7)
C_1-C_2	1.230 (1.229)	1.240 (1.241)	1.223(4)	1.245 (1.248)	1.237(4)	1.236 (1.239)	1.207(3)	-	1.241 (1.245)	1.221(10)
C_2-C_3	-	1.364 (1.358)	1.369(4)	1.350 (1.344)	1.356(5)	1.365 (1.359)	1.382(3)	-	1.352 (1.345)	1.365(10)
C_3-C_4	-	1.219 (1.218)	1.198(4)	1.231 (1.232)	1.220(5)	1.218 (1.217)	1.214(3)	-	1.230 (1.231)	1.202(10)
C_4-C_5	-	-	-	1.357 (1.353)	1.370(5)	-	-	-	1.358 (1.353)	1.367(11)
C_5-C_6	-	-	-	1.218 (1.217)	1.212(5)	-	-	-	1.218 (1.217)	1.166(12)
Mo-N	-	-	-	-	-	2.178, 2.180 (2.238, 2.238)	2.1341(18) 2.1417(18)	-	2.182, 2.182 (2.236, 2.236)	2.154(6) 2.137(5)
Mo-P	2.519, 2.524 (2.587, 2.586)	2.517, 2.525 (2.580, 2.583)	2.4726(7) 2.4578(6)	2.521, 2.528 (2.580, 2.581)	2.4641(10) 2.4686(10)	-	-	-	-	-

[a]reference 26.
[b]reference to HNL thesis unpublished work
[c]reference 39

As the chain length increases the contribution of the polyynyl chain to the α- and β-HOSO's increases by approximately 10 % per addition of a C≡C unit. The β-LUSO closely resembles the HOMO of the neutral complex independent of the supporting ligand. Whereas the α-LUSO of the bipyridine complexes are predominantly bipyridine in character and the dppe complexes are cycloheptatrienyl in character. The similarity between the neutral and oxidised structures, both electronically and structurally, account for the very small Δν(C≡C) seen both theoretically and experimentally thus supporting the assignment of a largely metal based HOMO.

Plots of the Mulliken spin density of the cations show that the spin is essentially delocalized over the entire chain, with decreasing amounts of both α and β spin on the carbons furthest from the molybdenum centre. An analysis of the molecular orbital plots shows that increasing the chain length also increases the contribution of the chain to the HOMO. The summation of the spins on each atom of the chain (Σ(Chain)) demonstrates a gradual increase of the spin on the chain with an increase in chain length, irrespective of the supporting ligand (Table 9).

Model compound **20H**$^{+}$ shows the largest percentage of spin density, 0.854, on the polyyne chain irrespective of the length of the chain or the supporting moeities. The increase of spin density on the chain supports the experimentally observed EPR measurements of **20**$^{+}$, which shows the coupling of the electron to the terminal hydrogen atom of the chain, and demonstrates how the increased spin density on the chain has allowed the hyperfine coupling values to be resolved by EPR.

Table 9: Calculated Mulliken spin density of $20H^+$, $21H^+$, $37H^+$, 38^+, $36H^+$ at B3LYP /6-31g* and LANL2DZ.

	$36H^+$	**$20H^+$**	**$21H^+$**	**$37H^+$**	**$38H^+$**
Mo	1.166	0.988	1.015	1.023	0.999
C_1	-0.128	-0.172	-0.124	-0.135	-0.120
C_2	0.288	0.314	0.221	0.247	0.219
C_3	-	-0.134	-0.088	-0.095	-0.089
C_4	-	0.234	0.135	0.166	0.143
C_5	-	-	-0.034	-	-0.036
C_6	-	-	0.047	-	0.051
Σ(Chain)	0.416	0.854	0.649	0.643	0.658
C_7H_7	-0.256	-0.223	-0.192	-0.251	-0.240
Dppe	-0.030, -0.032	-0.024, -0.024	-0.020, -0.023	-	-
bipy	-	-	-	-0.019 -0.019	-0.023 -0.023

The difference in reactivity between the **23^+** and **24^+** can also be rationalised using spin density arguments, whereby **24^+** dimerises readily to form **28^{2+}** but, **23^+** is a stable species which is able to be studied by crystallographic techniques. The dimerisation of **24^+** takes place at the C_2 position, comparison of the spin density for **23^+** and **24^+** for this atom shows that C_2 for **24^+** has 0.067 more spin than its counterpart. Therefore, the Mo(dppe)(η^7-C_7H_7) fragment promotes the reactivity by stabilisation of the charge at this position. The effect is not seen for the six carbon chain compound (**26^+**) as the spin along the chain is more evenly distributed along its length, which as seen for **23^+**, does not promote radical dimerisation behaviour.

3.8 UV /vis /NIR Spectroelectrochemistry and TD-DFT Calculations

Using spectroelectrochemical techniques the neutral and cationic species of **21**$^{n+}$, **23**$^{n+}$, **24**$^{n+}$, **25**$^{n+}$ and **26**$^{n+}$ (n = 0 or 1) were rapidly generated and analyzed by UV /vis /NIR spectroscopy. To assist in the assignments of the electronic transitions, TD-DFT calculations were conducted using the model geometries described earlier and using the same functional /basis set combination (B3LYP LANL2DZ /3-21g*).

The UV /vis spectra of the neutral, 18 electron complexes **24** and **26** closely resemble that of **1** with common transitions occurring at 35000 cm^{-1} and 27000 cm^{-1} resulting from transitions from the molybdenum centre to the dppe fragment (Figure 4). As the chain lengthens less intense transitions appear which arise from allowed transitions between the molybdenum centre and the cycloheptatrienyl ring.

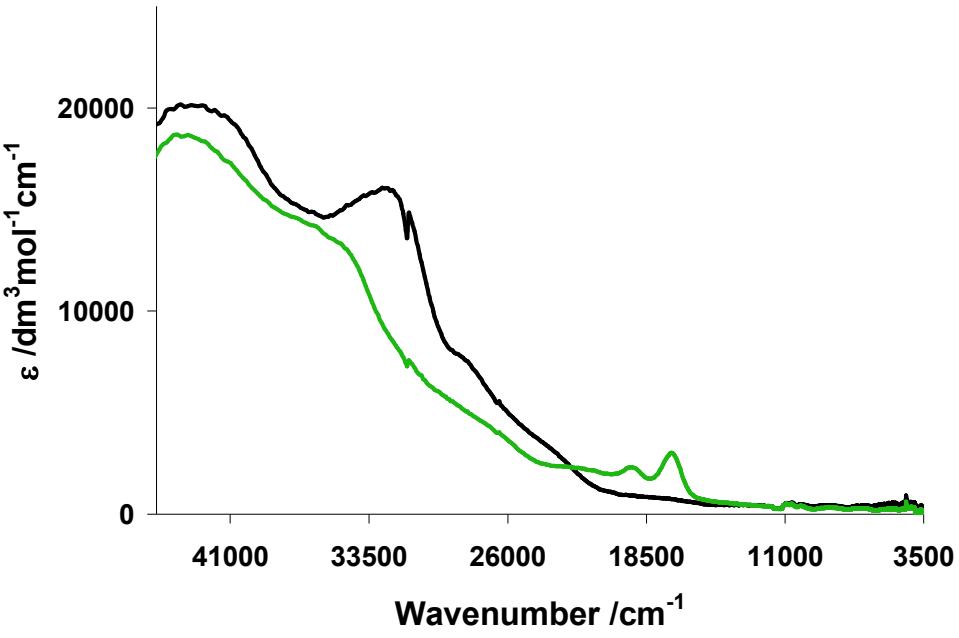

Figure 4: UV /vis /NIR spectra of 24^{n+}, where n = 0 (Black) and n = 1 (Green). Recorded in 0.1 M $^{n}Bu_4NPF_6$ /CH_2Cl_2.

Upon oxidation of the dppe supported complexes, as in the acetylide series, the 17 electron species exhibit strong bands at 16000 cm^{-1}, with low intensity bands trailing off at low energies. These intense bands around 16000 cm^{-1} are calculated to be LMCT type transitions between the chain and the [Mo(dppe)(η^7-C_7H_7)] fragment. As the chain increases in length, the energy and intensity of this transition decreases. The low intensity transitions at low energy are shown to be interconfigurational transitions, and are at near identical energies for all the models **36H$^+$**, **20H$^+$**, and **21H$^+$** (Table 10 – 12).

Table 10: TD-DFT assignments for 36H^{n+} (n = 0, 1).

36H^n$^+$	Calculated Transition /cm^{-1} (intensity)	Character of Transition
n = 0	34000 (0.0389)	MoC_7H_7→dppe*
	25700 (0.0191)	MoC_7H_7→dppe*
	18000 (0.0048)	MoC_7H_7→dppe*
n = +1	36200 (0.0344)	MoC_7H_7→dppe*
	26400 (0.0169)	C≡CH→MoC_7H_7
	20100 (0.02)	Dppe→Mo*
	10600 (0.0002)	C≡CH and C_7H_7→Mo*
	7700 (0)	C≡CH and C_7H_7→Mo*

Table 11: Experimental UV /vis /NIR results 24^{n+} (n = 0, 1) and TD-DFT assignments for 20H^{n+} (n = 0, 1).

	24^{n+}	**20H^{n+}**	
	Experimental Transition /cm^{-1} (ε /$dm^3mol^{-1}cm^{-1}$)	Calculated Transition /cm^{-1} (intensity)	Character of Transition
n = 0	43670 (20170)	37500 (0.0875)	Mo →dppe
	32700 (16000)	34400 (0.0578)	Mo(C≡CC≡C)(C_7H_7)→dppe
	Sh 28000 (7600)	24700 (0.0461)	Mo(C≡CC≡C)(C_7H_7)→dppe
n = +1	35200 (13400)	32900 (0.0696)	dppe→MoC_7H_7*
	19500 (17700)	25100 (0.0687)	C≡CC≡CH→MoC_7H_7*
	17300 (2800)	20000 (0.0003)	C≡CC≡CH→MoC_7H_7*
	Sh 15100 (800)	17300 (0.0037)	C≡CC≡CH→MoC_7H_7*
	-	16800 (0.0469)	Dppe/C≡CC≡CH→MoC_7H_7*
		10300 (0.0022)	C≡CC≡CH→MoC_7H_7*
		6800 (0.0001)	C≡CC≡CH→MoC_7H_7*

Table 12: Experimental UV /vis /NIR results and TD-DFT assignments for 21^{n+} and $21H^{n+}$ (n = 0, 1).

+	21^{n+}	$21H^{n+}$	
	Experimental Transition /cm^{-1} (ε /$dm^3mol^{-1}cm^{-1}$)	Calculated Transition /cm^{-1} (intensity)	Character of Transition
n = 0	37450 (23800)	36400 (0.1405)	MoC_6 →dppe*
	31150 (14400)	32750 (0.187)	MoC_6 →dppe*
	26300 (10400)	23800 (0.0433)	Mo →dppe*
	Sh 15900 (3200)	17700 (0.0016)	Mo →C_7H_7*
		16600 (0.0023)	MoC_6 →dppe* /C_7H_7*
n = +1	43700 (20600)	30700 (0.1581)	MoC_6 →dppe*
	37300 (14200)	23950 (0.1167)	C_6 →MoC_7H_7*
	vbr 7300 (1700)	14600 (0.0734)	C_6 →Mo*
		10300 (0.0098)	C_6 →Mo*
		6050 (0.0001)	C_6 →Mo*

An analysis of the bipyridyl supported complexes reveals a set of characteristic spectral features for the neutral 18 electron complexes **23** and **25**, which can be traced to the starting material **22** (Figure 5). Each spectrum has four distinct transitions, which vary with intensity depending on the length of the chain or the π-donor ability (as for the parent **22**) but are all based around transitions to a bipyridine excited state. The highest energy transitions (35000 cm^{-1}) are predominantly bipy → bipy* in character. These transitions near 22000 cm^{-1} become more chain → bipy* in character. The characteristic transition at 18000 cm^{-1} is observed in all [Mo(η^7-C_7H_7)] complexes and is of Mo → C_7H_7* in character. The lowest energy transitions, 13000 and 11000 cm^{-1}, which vary the most with the identity of the chain, are MoC_n → bipy* in character. The decrease in intensity of these low energy bands as the chain length increases, is brought about due to the larger ligand character of the frontier orbitals removing electron density from the metal centre and hence the weight of the transition.

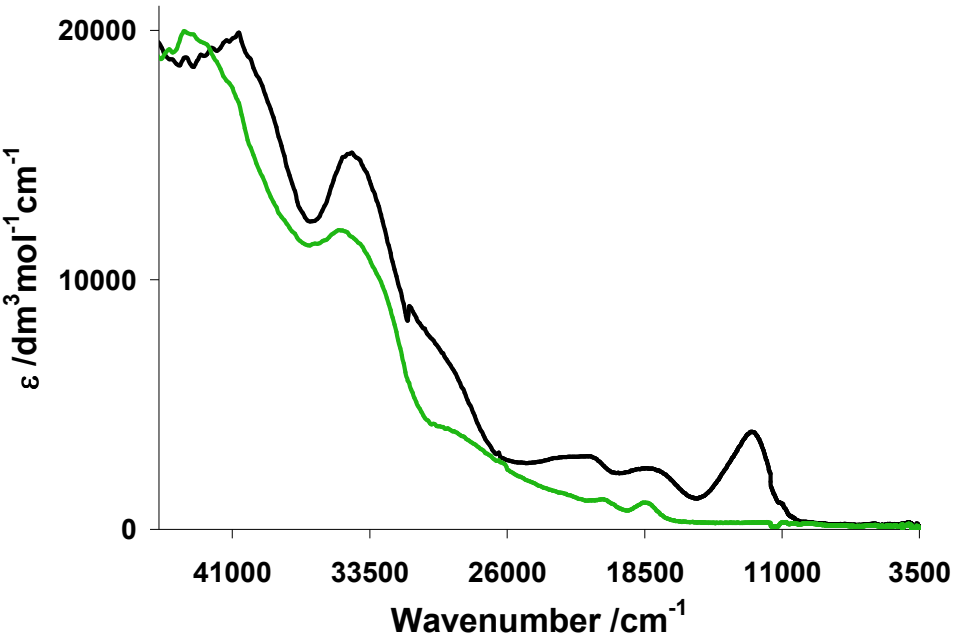

Figure 5: UV /vis /NIR spectra of 23^{n+}, where n = 0 (Black) and n = 1 (Green). Recorded in 0.1 M $^{n}Bu_4NPF_6$ /CH_2Cl_2.

Oxidation causes the loss of both Mo → bipy* character transitions, but the higher energy transitions of a similar character to the neutral complexes are retained. The spectrum of the oxidised species closely resembles that of $\mathbf{24}^+$ and $\mathbf{26}^+$, with moderately intense bands forming at 21000 cm^{-1} and 18000 cm^{-1} (albeit blue shifted by 1000 cm^{-1} in comparison to the dppe complexes). These bands are not present in the bromide analogue, $\mathbf{22}^+$, indicating that they are a result of transitions involving the alkynyl chain, and are LMCT in character, an observation which is supported by the TD-DFT computations (Table 13 – 15).

Table 13: Experimental UV /vis /NIR results for 22^{n+} (n = 0, 1).

	22^{n+}
	Experimental Transition /cm^{-1} (ε /$dm^3mol^{-1}cm^{-1}$)
n = 0	33300 (35400) 22900 (10700) 18100 (10700) 12700 (16300)
n = +1	32900 (30300) 24200 (5600)

Table 14: Experimental UV /vis /NIR results 23^{n+} (n = 0, 1) and TD-DFT assignments for $37H^{n+}$ (n = 0, 1).

	23^{n+}	$37H^{n+}$	
	Experimental Transition /cm^{-1} (ε /$dm^3mol^{-1}cm^{-1}$)	Calculated Transition /cm^{-1} (intensity)	Character of Transition
n = 0	40700 (20000)	44500 (0.1455)	C_7H_7→bipy*
	34700 (15000)	36900 (0.3321)	bipy→bipy*
	21500 (2900)	24500 (0.091)	C≡CC≡CH→bipy*
	18000 (2400)	21900 (0.0291)	Mo→C_7H_7*
	12900 (3800)	19200 (0.0236)	Mo→bipy*
	11000 (1000)	13800 (0.0635)	Mo→bipy*
n = +1	43300 (19800)	38500 (0.083)	Mo→bipy*
	35200 (12000)	36200 (0.0924)	MoC≡CC≡CH→bipy*
	28800 (3900)	25900 (0.0606)	MoC≡CC≡CH→bipy*
	20900 (1200)	24000 (0.0345)	C≡CC≡CH→Mo*
	18700 (1000)	15600 (0.0509)	C≡CC≡CH→Mo*
		8800 (0.0048)	C≡CC≡CH→Mo*

Table 15: Experimental UV /vis /NIR results 25^{n+} (n = 0, 1) and TD-DFT assignments for $38H^{n+}$ (n = 0, 1).

	25^{n+}	$38H^{n+}$	
	Experimental Transition /cm^{-1} (ε /$dm^3mol^{-1}cm^{-1}$)	Calculated Transition /cm^{-1} (intensity)	Character of Transition
n = 0	41500 (16500)	37000 (0.3031)	$C_7H_7 \rightarrow C_6$*
	34300 (16500)	32600 (0.3838)	Mo $\rightarrow C_7H_7$*
	27000 (4900)	23600 (0.0831)	$MoC_6 \rightarrow$bipy*
	12900 (2000)	13700 (0.0642)	$MoC_6 \rightarrow$bipy*
n = +1	40500 (15700)	37400 (0.207)	$MoC_6 \rightarrow$bipy*
	33700 (10300)	27200 (0.0858)	$MoC_6 \rightarrow$bipy*
	27900 (4600)	22800 (0.0805)	$MoC_6 \rightarrow$bipy*
	19000 (1600)	13600 (0.0806)	$MoC_7H_7 \rightarrow C_6$*
	16900 (1400)	8600 (0.0148)	$MoC_7H_7 \rightarrow C_6$*
		6400 (0.0001)	$MoC_7H_7 \rightarrow C_6$*

3.9 Conclusion

The study shows that the lengthening of the *sp*-hybridised chain $[Mo((C\equiv C)_nC\equiv CR)(dppe)(\eta^7\text{-}C_7H_7)]$ from n= 0, 1 and 2, has a modest effect on the electronic structure. The combination of careful spectroscopy and computational techniques have described the subtle effects of both changing the supporting ligand from dppe to biypridine, and increasing the chain length. Increasing the chain length, causes the HOMO to become more ligand in character. However, EPR measurements have highlighted that the electron still resides close to the metal centre, this is in a marked contrast to the previously studied ruthenium and rhenium systems.[21b] The bipyridyl supported complexes are better able to stabilise positive charge on the metal centre, as bipyridine is a better π-donor than dppe, this has allowed the isolation of the first radical cation diynyl complex, $\mathbf{23}^+$.[25] When dppe is the ancillary ligand, more of the electron density is situated on the chain of the neutral species, thus causing the

radical cations $\mathbf{20}^{+}$ and $\mathbf{24}^{+}$ to be prone to radical dimerisation at the C_2 position on the chain.

3.10 General Procedures

3.10.1 Spectroscopic Details

Refer to Chapter two.

3.10.2 Computational Details

All calculations were carried out using the Gaussian 03 package.[30] The model geometries $\mathbf{20H^{n+}}$, $\mathbf{21H^{n+}}$, $\mathbf{36H^{n+}}$, $\mathbf{37H^{n+}}$, $\mathbf{38H^{n+}}$, **23Si** and **25Si** (n = 0 or 1) discussed here were optimised using B3LYP,[31] with no symmetry constraints. A mixed basis set was used containing the pseudo-potential LANL2DZ[32] for the Mo atom and 6-31g*[33] basis set for all the other atoms. Frequency calculations were carried out these optimised geometries at the corresponding levels and shown to have no imaginary frequencies. Molecular orbital and TD-DFT computations were carried out on these optimised geometries at the appropriate level of theory and the orbital contributions were generated with the aid of the GaussSum.[34]

3.11 References

[1] R. Nast, *Coord. Chem. Rev.,* 1982, **47**, 89.
[2] N.J. Long, C.K. Williams, *Angew. Chem. Int. Ed.,* 2003, **42**, 2596.
[3] (a) F. Paul, C. Lapinte, *Coord. Chem. Rev.,* 1998, **178-180**, 431. (b) N.J. Long, *Angew. Chem. Int. Ed.,* 1995, **34**, 21. (c) H. Lang, *Angew. Chem. Int. Ed.,* 1994, **33**, 547. (d) U.H.F. Bunz, *Angew. Chem. Int. Ed.,* 1996, **35**, 969. (e) C. Lapinte, *J. Organomet. Chem.,* 2008, **693**, 793. (f) C.E. Powell, M.G. Humphrey, *Coord. Chem. Rev.,* 2004, **248**, 725. (g) M.P. Cifuentes, M.G. Humphrey, *J. Organomet. Chem.,* 2004, **689**, 3968. (h) G.T. Dalton, M.P. Cifuentes, L.A. Watson, S. Petrie, R. Stranger, M. Samoc, M.G. Humphrey, *Inorg. Chem.,* 2009, **48**, 6534. (i) M.I. Bruce, P.J. Low, *Adv. Organomet. Chem.,* 2004, **50**, 179. (j) V.W-W. Yam, *Acc. Chem. Res.,* 2002, **35**, 555.
[4] (a) R. Baer, D. Neuhauser, *Chem. Phys. Lett.,* 2003, **374**, 459. (b) N.J. Tao, *Nature,* 2006, **1**, 173. (c) P.J. Low, *Dalton. Trans.,* 2005, 2821. (d) S.S. Datta, D.R. Strachan, A.T.C. Johnson, *Phys. Rev. B.,* 2009, **79**, 205404.
[5] S. Rigaut, J. Perruchon, L. Le Pichon, D. Touchard, P.H. Dixneuf, *J. Organomet. Chem.,* 2003, **670**, 37. (b) M.I. Bruce, M. Ke, P.J. Low, *Chem. Commun.,* 1996, 2405. (c) B. Bartik, R. Dembinski, T. Bartik, A.M. Arif, J.A. Gladysz, *New. J. Chem.,* 1997, **21**, 739.
[6] (a) K. Azyat, E. Jahnke, T. Rankin, R.R. Tykwinski, *Chem. Commun.,* 2009, 433. (b) S. Eisler, N. Chahal, R. McDonald, R.R. Tykwinski, *Chem. Eur. J.,* 2003, **9**, 2542. (c) A.D. Slepkov, F.A. Hegmann, S. Eisler, E. Elliott, R.R. Tykwinski, *J. Chem. Phys.,* 2004, **120**, 6807. (d) J. Hlavaty, L. Kavan, J. Kubista, *Carbon,* 2002, **40**, 345. (e) E. Kloster-Jensen, *Angew. Chem. Int. Ed.,* 1972, **11**, 438. (f) R. Eastmond, T.R. Johnson, D.R.M. Walton, *Tetrahedron,* 1972, **28**, 4601.
[7] R. Dembinski, T. Bartik, B. Bartik, M. Jaeger, J.A. Gladysz, *J. Am. Chem. Soc.,* 2000, **122**, 810.
[8] (a) R.L. Roberts, H. Puschmann, J.A.K. Howard, J.H. Yamamoto, A.J. Carty, P.J. Low, *Dalton. Trans.,* 2003, 1099. (b) D.L. Lichtenberger, S.K. Renshaw, A. Wong, C.D. Tagge, *Organometallics,* 1993, **12**, 3522. (c) M.I. Bruce, M. Ke, P.J. Low, B.W. Skelton, A.H. White, *Organometallics,* 1998, **17**, 3539. (d) K. Sonogashira, T. Yatake, Y. Tohda, S. Takahashi, N. Hagihara, *J. Chem. Soc., Chem. Commun.,* 1977, 291.
[9] M.I. Bruce, B.C. Hall, B.D. Kelly, P.J. Low, B.W. Skelton, A.H. White, *Dalton, Trans.,* 1999, 3719.
[10] M.I. Bruce, P. Hinterding, P.J. Low, B.W. Skelton, A.H. White, *J. Chem. Soc., Dalton. Trans.,* 1998, 467.
[11] M.I. Bruce, B.G. Ellis, M. Gaudio, C. Lapinte, G. Melino, F. Paul, B.W. Skelton, M.E. Smith, L. Toupet, A.H. White, *Dalton. Trans.,* 2004, 1601.
[12] (a) F. Coat, C. Lapinte, *Organometallics,* 1996, **15**, 477. (b) A. Wong, P.C.W. Kang, C.D. Tagge, D.R. Leon, *Organometallics,* 1990, **9**, 1992.
[13] (a) C.L. Sterzo, *J. Chem. Soc., Dalton. Trans.,* 1992, 1989. (b) G.H. Young, R.R. Willis, A. Wojcicki, M. Callogaris, P. Faleschini, *Organometallics,* 1992, **11**, 154.
[14] D.J. Armitt, M.I. Bruce, B.W. Skelton, A.H. White, *J. Organomet. Chem.,* 2008, **693**, 3571.

[15] (a) V.W-W. Yam, S. H-F. Chong, C-C. Ko, K-K. Cheung, *Organometallics.* 2000, **19**, 5092. (b) V.W-W. Yam, S.H-F. Chong, K-K. Cheung, *Chem, Commun.,* 1998, 2121.
[16] (a) S. Hartmann, R.F. Winter, B.M. Brunner, B. Sarkar, A. Knodler, I. Hartenbach, *Eur. J. Inorg. Chem.,* 2003, 876. (b) R.F. Winter, F.M. Hornung, *Organometallics,* 1999, **18**, 4005. (c) R.F. Winter, *Chem. Commun.,* 1998, 2209. (d) R.F. Winter, F.M. Hornung, *Organoemtallics,* 1997, **16**, 4248.
[17] F. Coat, M-A. Guillevic, L. Toupet, F. Paul, C. Lapinte, *Organometallics,* 1997, **16**, 5988.
[18] T. Bartik, B. Bartik, M. Brady, R. Dembinski, J.A. Gladysz, *Angew. Chem. Int. Ed.,* 1996, **35**, 414.
[19] (a) Q. Zheng, J.A. Gladysz, *J. Am. Chem. Soc.,* 2005, **127**, 10508. (b) T.B. Peters, J.C. Bohling, A.M. Arif, J.A. Gladysz, *Organometallics,* 1999, **18**, 3261.
[20] S. Gauthier, N. Weisbach, N. Bhuvanesh, J.A. Gladysz, *Organometallics,* 2009, **28**, 5597. (c) W. Mohr, T.B. Peters, J.C. Bohling, F. Hampel, A.M. Arif, J.A. Gladysz, *C.R. Chemie.,* 2002, **5**, 111.
[21] (a) M.I. Bruce, P.A. Humphrey, M. Jevric, B.W. Skelton, A.H. White, *J. Organomet. Chem.,* 2007, **692**, 2564. (b) O.F. Koentjoro, P.J. Low, R. Rousseau, C. Nervi, D.S. Yufit, J.A.K. Howard, K.A. Udashin, *Organometallics,* 2005, **24**, 1284, (c) M.I. Bruce, N.N. Zaitseva, B.W. Skelton, *J. Organomet. Chem.,* 2006, **691**, 759. (d) M.I. Bruce, B.C. Hall, B.W. Skelton, M.E. Smith, A.H. White, *Dalton. Trans.,* 2002, 995. (e) M.I. Bruce, K. Costuas, J-F. Halet, B.C. Hall, P.J. Low, B.K. Nicholson, B.W. Skelton, A.H. White, *Dalton. Trans.,* 2002, 383.
[22] H.N. Lancashire, R. Ahmed, T.L. Hague, M. Helliwell, G.A. Hopgood, L. Sharp, M.W. Whiteley, *J. Organomet. Chem.,* 2006, **691**, 3617.
[23] S.P.M Disley, R.W. Grime, E.J.L. McInnes, D.M. Spencer, N. Swainston, M.W. Whiteley, *J. Organomet. Chem.,* 1998, **566**, 151.
[24] R. Dembinski, T. Lis, S. Szafert, C.L. Mayne, T. Bartik, J.A. Gladysz, *J. Organomet. Chem.,* 1999, **578**, 229.
[25] N.J. Brown, D. Collison, R. Edge, E.C. Fitzgerald, P.J. Low, M. Helliwell, Y.T. Ta, M.W. Whiteley, *Chem. Commun.,* 2010, **46**, 2253.
[26] R.L. Beddoes, C. Bitcon, A. Ricalton, M.W. Whiteley, *J. Organomet. Chem.,* 1989, **367**, C21.
[27] A. Wong, P.C.W. Kang, C.D. Tagge, D.R. Leon, *Organometallics.* 1990, **9**, 1992.
[28] R.J. Lagow, J.J. Kampa, H-C. Wei, S.L. Battle, J.W. Genge, D.A. Laude, C.J. Harper, R. Bau, R.C. Stevens, J.F. Haw, E. Munson, *Science.* 1995, **267**, 362.
[29] O.F. Koentjoro, R. Rousseau, P.J. Low, *Organometallics,* 2001, **20**, 4502.
[30] M.J. Frisch, G.W. Trucks, H.B. Schlegel, G.E. Scuseria, M.A. Robb, J.R. Cheeseman, J.A. Montgomery Jr., T. Vreven, K.N. Kudin, J.C. Burant, J.M. Millam, S.S. Iyengar, J. Tomasi, V. Barone, B. Mennucci, M. Cossi, G. Scalmani, N. Rega, G.A. Petersson, H. Nakatsuji, M. Hada, M. Ehara, K. Toyota, R. Fukuda, J. Hasegawa, M. Ishida, T. Nakajima, Y. Honda, O. Kitao, H. Nakai, M. Klene, X. Li, J.E. Knox, H.P. Hratchian, J.B. Cross, C. Adamo, J. Jaramillo, R. Gomperts, R.E. Stratmann, O. Yazyev, A.J. Austin, R. Cammi, C. Pomelli, J.W. Ochterski, P.Y. Ayala, K. Morokuma, G.A. Voth, P. Salvador, J.J. Dannenberg, V.G. Zakrzewski, S. Dapprich, A.D. Daniels, M.C. Strain, O. Farkas, D.K. Malick, A.D. Rabuck, K. Raghavachari, J.B. Foresman, J.V. Ortiz, Q. Cui, A.G. Baboul, S. Clifford, J. Cioslowski, B.B. Stefanov, G. Liu, A. Liashenko, P. Piskorz, I. Komaromi, R.L. Martin, D.J. Fox, T. Keith, M.A. Al-Laham, C.Y. Peng, A.

Nanayakkara, M. Challa- combe, P.M.W. Gill, B. Johnson, W. Chen, M.W. Wong, C. Gonzalez, J.A. Pople, GAUSSIAN 03, Revision C.02, Gaussian Inc., Wallingford, CT, 2004.
[31] (a) A.D. Becke, *J. Chem. Phys.,* 1993, **98**, 648. (b) C. Lee, W. Yang, R.G. Parr, *Phys. Rev. B.,* 1988, **37**, 785. (c) A.D. Becke, *Phys. Rev. A.,* 1988, **38**, 3098. (d) J.P. Perdew, *Phys. Rev. B.,* 1986, **33**, 8822.
[32] (a) P.J. Hay, W.R. Wadt, *J. Chem. Phys.,* 1985, **82**, 270. (b) W.R. Wadt, P.J. Hay, *J. Chem. Phys.,* 1985, **82**, 284. (c) P.J. Hay, W.R. Wadt, *J. Chem. Phys.,* 1985, **82**, 299.
[33] (a) G.A. Petersson, M.A. Al-Laham, *J. Chem. Phys.,* 1991, **94**, 6081. (b) G.A. Petersson, A. Bennett, T.G. Tensfeldt, M.A. Al-Laham, W.A. Shirley, J. Mantzaris, *J. Chem. Phys.,* 1988, **89**, 2193.
[34] N.M. O'Boyle, A.L. Tenderholt, K.M. Langner, *J. Computational. Chem.,* 2007, **5**, 839.

Chapter 4: Cycloheptatrienyl Molybdenum Complexes of *C,C'*-Bis(ethynyl)carboranes

4.1 Introduction

π-Conjugated organic bridges feature predominantly in mixed valence complexes, [{L_nM^n}(μ-Bridge){$M^{n+1}L_n$}]. Within this vast body of work carbon rich bridges, C≡CXC≡C (where X is a π-conjugated spacer) have been used extensively to construct a myriad of model complexes from which chemists can study mixed valence charge transfer.[1]

Many of the spacer moieties (X) studied have consisted of hydrocarbon fragments, for example benzene rings and variations of that theme.[2] However, there are examples of heteroaromatic spacers, such as thiophene[3] and pyridine,[4] which have been used in conjunction with polyynyl chains. An unusual spacer moiety is the icosahedral 1,12-dicarba-*closo*-dodecaborane, *para*-carborane, which is a highly symmetric, chemically and thermally robust moiety that possesses a three-dimensional aromatic system (Figure 1).[5]

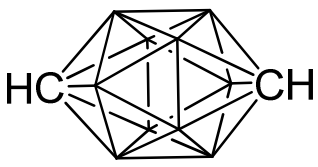

Figure 1: *Para*-carborane. (Note un-labeled vertexes are BH units)

The chemical robustness of *para*-carborane and its unusually delocalised electronic structure has led the *para*-carborane moiety to feature in a wide-ranging sphere of

chemistry, from the formation of structurally interesting motifs, such as "nanocars"[6] and carborarods,[7] to non-linear optic applications[8] and liquid crystals.[9] The high boron content and well established synthetic chemistry of the carborane cage has also led to applications of *para*-carborane and other carboranes in boron neutron capture therapy for the targeted treatment of malignant cells.[10]

Key to the development of organometallic complexes containing the *para*-carborane moiety has been the synthesis of RC≡C($C_2B_{10}H_{10}$)C≡CR, where R = H (**49**), $SiMe_3$ (**48**),[11] which allow the easy coordination of organometallic moeities using conventional M-C≡C forming methodologies. Using a combination of **49**, ethynyl pyridine *para*-carborane, {NC_5H_4C≡C}$_2$(1, 12-$C_2B_{10}H_{10}$), **39**, and platinum cores, $Pt(PEt_3)_2$, a range of self assembling highly soluble, molecular polygons, from triangles to hexagons, can be formed.[12] In addition to polygons, alkynyl gold rigid rods can be formed from the facile reaction of **49** with various gold precursors, for example [$AuCl(SMe_2)$], $AuClPPh_3$ and PPN[$Au(acac)_2$], mirroring similar systems containing 1,4-diethynyl benzene links.[13]

One important aspect in the study of mixed valence complexes derived from *para*-carborane and related systems, are the antipodal carbon sites which are able to transmit electronic effects through the cage structure. Despite these attractive qualities, only a few mixed valence complexes based on carborane bridges have been synthesised. Complexes containing *para*-carborane and [$Fe(CO)_2(\eta^5$-$C_5H_5)$] metal fragment have been synthesised, in which the metal atom is either directly bonded to the carborane cage (**40**) or connected by an ethynyl bridge (**41**), have been examined by electrochemical methods (Figure 2).

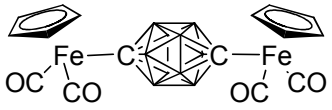

40

41

Figure 2: $Fe(CO)_2(\eta^5\text{-}C_5H_5)$ containing *para*-carborane complexes, 40 and 41.

When the metal is directly bonded to the carborane cage the cyclic voltammogram contains two irreversible waves, however, when metal ethynyl groups are coordinated to the cage, only a single irreversible wave was observed.[14] The presence of a second irreversible wave following the first irreversible wave is not indicative of "electronic communication", but may indicate the formation of an electroactive species after the initial oxidation, which is likely due to the known instability of these $[Fe(CO)_2(\eta^5\text{-}C_5H_5)]$ complexes, i.e. an ECE process. Low temperature electrochemical and spectroelectrochemical experiments would be needed to clearly ascertain if there is any electronic communication between the iron dicarbonyl centres through the carborane cage.

A more thorough examination of electronic communication properties through the *para*-carborane cage has been carried out by M.A. Fox *et al* using a variety of substituted aryl derivatives,[15] cobalt clusters (**43**)[16] and the well known $[Ru(dppe)(\eta^5\text{-}C_5Me_5)]$ metal fragment (**42**) (Figure 3).[17] An analysis of **42** and **43** have been undertaken using a full range of spectroscopic and computational methods. In summary, the *para*-carborane cage does indeed allow electronic communication between the $[Co_2(CO)_4(dppm)]$ or $[Ru(dppe)(\eta^5\text{-}C_5Me_5)]$ fragments, however, the mechanism differs somewhat from its

benzene counterparts (see Chapter six). Despite the presence of a three dimensional delocalised aromatic structure through which "electronic communication" could conceivably take place through, as is common on polyynyl and benzene bridges, electronic interactions between the metal centres take place via a purely σ-based bridge entity, owing to the mis-match between the energies of the cage and the ethynyl π-system. The *para*-carborane cage may therefore be considered electronically analogous to bicyclo[1.1.1]pentane, and severely attenuates the degree of electronic interaction between two electrophores through the carborane cage.[18]

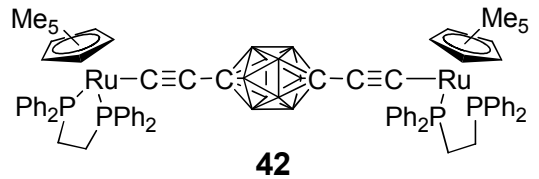

42

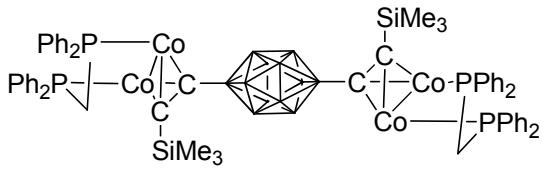

43

Figure 3: Metallo-substituted *para*-carborane complexes, 42 and 43.

4.2 Synthesis

To fully understand the electronic structure of a bimetallic complex, [{Mo(dppe)(η^7-C_7H_7)}$_2${μ-C≡C($C_2B_{10}H_{10}$)C≡C}] (**45**), it is of fundamental importance to elucidate the electronic structure of the mono-metallic complex, [Mo(C≡C$CC_2B_{10}H_{11}$)(dppe)(η^7-C_7H_7)] (**44**) and the redox product **44**$^+$. Comparative studies of **45**$^{n+}$ and **44**$^{n+}$ then permit the metal-bridge interactions to be identified and distinguished from genuine metal-metal interactions. The methodologies developed in Chapter two for [Mo(C≡CR)(dppe)(η^7-C_7H_7)] were employed to generate **44**. [19] Due to the ease of handling and storage $Me_3SiC{\equiv}CC_2B_{10}H_{11}$ (**46**), was used as the alkyne precursor, rather than the highly volatile $HC{\equiv}CC_2B_{10}H_{11}$ (**47**). Compound **46** was kindly donated by Dr. M.A. Fox for use in this project, however, **46** can be readily synthesised by the reaction of a lithiated *para*-carborane with $BrC{\equiv}CSiMe_3$ in the presence of Cu^I.[15] The reaction of **46** with [MoBr(dppe)(η^7-C_7H_7)] in the presence of KF afforded **44** in moderate yield (65 %) as a light brown powder (Scheme 1).

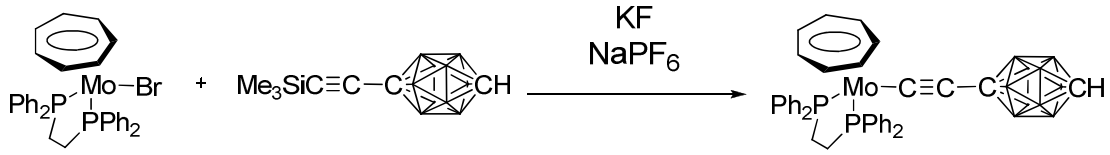

5 **46** **44**

Scheme 1: Synthesis of 44.

To access the bimetallic system, **45**, the bis-trimethylsilylethynyl carborane, $Me_3SiC{\equiv}C(C_2B_{10}H_{10})C{\equiv}CSiMe_3$ (**48**), was prepared. However, unlike the monometallic system, metallation of **48** in the presence of KF was not successful.

Therefore, compound **48** was deprotected using KOH /MeOH to produce HC≡C($C_2B_{10}H_{10}$)C≡CH (**49**), which was then allowed to react with **5** in the presence of KO^{t}Bu. Unlike the analogous Ru(dppe)(η^5-C_5Me_5) capped carborane complex where both metallic moieties could be added in one step with **48**, the optimised synthesis of the molybdenum system invovles a two step reaction with **49**. The first step creates a mixture of mono and di-substituted products, this mixture precipitating from refluxing methanol. To drive the reaction towards completion, the precipitate is added to a fresh reaction vessel charged with more **5** and additional base. Under these conditions, the mixture of solids was fully converted to **45** (Scheme 2).

The reaction conditions can be altered to produce the mono-substituted bis-ethynyl carborane complex, [Mo{C≡C($C_2B_{10}H_{10}$)C≡CH}(dppe)(η^7-C_7H_7)] (**50**), by allowing the first step of the reaction to be heated for 24 hours. After filtration of the precipitate, which removes the less soluble bimetallic component, slow evaporation of the methanol solution yielded **50** as a light brown crystalline solid.

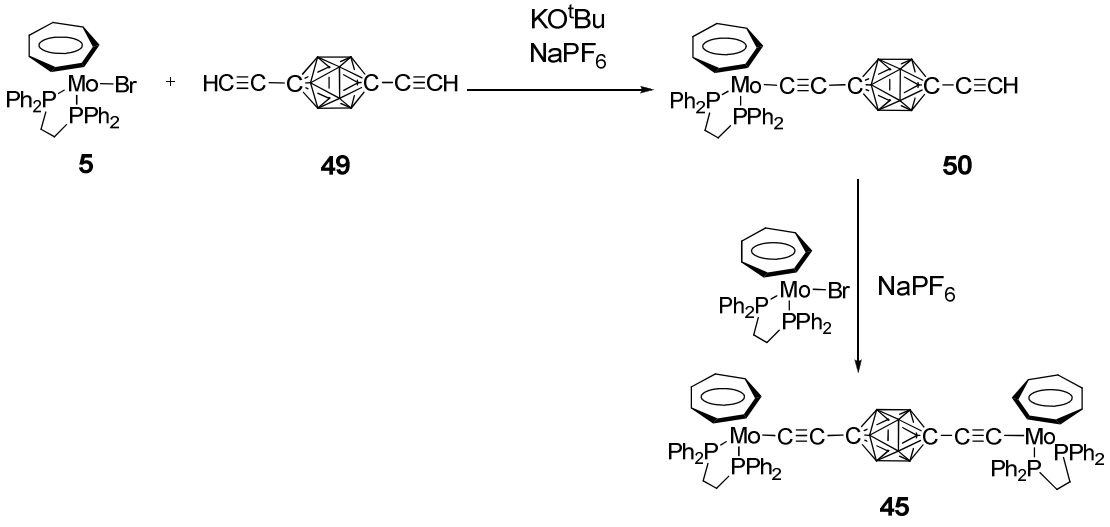

Scheme 2: Synthesis of 45 and 50.

As shown in Chapters two and three polyynyl [Mo(dppe)(η^7-C_7H_7)] capped complexes form very stable cationic complexes after one electron oxidation. As such **45** was reacted with one equivalent of [Fe(η^5-C_5H_5)$_2$]PF_6 to produce the mixed valence complex [**45**]PF_6. The pale brown solid, [**45**]PF_6, was then used for the detailed analysis of the charge transfer interaction taking place between the molybdenum centres across the ethynyl carborane bridge.

4.3 Spectroscopic Investigations

Each of the complexes **44**, **45** and **50** was characterised by ^{1}H, ^{31}P, ^{13}C and ^{11}B NMR spectroscopy, infrared spectroscopy and high resolution mass spectrometry. Comparison of **44** to the other [Mo(C≡CR)(dppe)(η^7-C_7H_7)] complexes reveals similar spectroscopic trends to those of the *para*-substituted phenyl acetylides described in Chapter two. The ^{31}P NMR resonances fall within the same range as the phenyl acetylides (63 - 66 ppm), as does the ^{1}H resonance of the cycloheptatrienyl ring (4.56 - 4.62 ppm). The ^{13}C NMR resonances for C_2 lie in the same region as the strongly electron withdrawing phenyl acetylides, R = C_6H_4CHO (**9**) (132.9 ppm) and R = $C_6H_4CO_2Me$ (**10**) (130.9 ppm) although not as low as [Mo(C≡CCO_2Me)(dppe)(η^7-C_7H_7)] (**13**), 115.0 ppm, indicating the electron withdrawing nature of the carborane is acting through the σ-system rather than through a π bond mechanism. The C_1 resonance is not observed for **44**. The lack of intensity of the C_1 carbon even with long ^{13}C NMR acquisition times and pulse delays, seems to be a general trend for strongly electron withdrawing π-systems, for example [Mo(C≡C$C_6H_4CO_2$Me-4)(dppe)(η^7-C_7H_7)] (**10**).

The ^{11}B NMR data collected for **44** is similar to [Ru(C≡C$C_2B_{10}H_{11}$)(dppe)(η^5-C_5Me_5)] (**51**)[17] where the boron atoms closest to the metal centre are shifted to higher field (-16.5 ppm) compared to the free ligand **47** (-15.1 ppm). The sensitivity of the boron cage to the local chemical environment, and the use of ^{11}B NMR to monitor these changes, is a well studied phenomenon.[20]

The ^{13}C resonance for the cage<u>C</u>H of the free ligand **47** is in a similar position to **51**, (54.8 and 53.4 pp respectively), in comparison to the free ligand **46**, the ^{13}C NMR resonance is 6 ppm lower (**46** = 60.3 ppm), indicating that the metal moiety is having some influence over the antipodal carbon atom cage<u>C</u>H. Comparison between the analogous molybdenum phenyl acetylide complex (**1**) and ruthenium complex (**3**) does not show this behaviour. In comparison to the free ligand, HC≡CC_6H_5, the *para* carbon (which is equivalent cage<u>C</u>H on the carborane cage) does not change upon coordination with the molybdenum fragment (**7** = 128.6 ppm, HC≡CC_6H_5 = 128.7 ppm), whereas coordination to the [Ru(dppe)(η^5-C_5Me_5)] moiety (**3**) the *para* carbon resonance is lowered to 122.4 ppm. Therefore, the degree of mixing between the alkynyl and metal moieties is influential for the resonance of the *para* carbon on the phenyl ring, but makes no difference for the cage<u>C</u>H of the carborane. This indicates that the carborane cage is an efficient conduit for σ-communication but poor π-communication (as the magnitude in the change of the cage<u>C</u>H resonance is unaffected by the identity of the metal moiety), and vice-versa for the phenyl ring.

The ^{11}B NMR of **50** contains the familiar resonance at -11.6 ppm that corresponds to the half of the carborane which is *not* coordinated to the [Mo(dppe)(η^7-C_7H_7)] substituent.

However, the resonance corresponding to the half of the carborane cage which *is* coordinated to the [Mo(dppe)(η^7-C_7H_7)] cap is shifted to lower field, in comparison to **44**, by 3 ppm (-13.3 ppm). This reflects a small change in the electronic character of the carborane cage when two conjugated π-systems, the ethynyl groups, are bonded through the carbon atoms (Table 1).

Table 1: ^{11}B NMR values.

Complex	$\underline{B}_5H_5C$-R /ppm	Mo-C≡CC$\underline{B}_5H_5$ /ppm
44	-11.6	-16.5
50	-11.8	-13.3
45	-	-13.9
	$\underline{B}_5H_5C$-R /ppm	Ru-C≡CC$\underline{B}_5H_5$ /ppm
51	-11.1	-16.3
42	-	-12.2

Solution infrared spectroscopy gives two characteristic bands for all three complexes, **44**, **45**, and **50**, at 2064 cm^{-1}, ν(C≡C), and 2612 cm^{-1} ν(BH), regardless of the nature of the complex. A second ν(C≡C) stretch, corresponding to the un-coordinated C≡CH moiety, was not observed for **50**, however, a stretch (at 3200 cm^{-1}), corresponding to ν(CH), was observed in addition with the correct molecular ion in MALDI mass spectrometery, thus confirming the presence of the C≡CH group and the identity of **50**.

4.4 Electrochemistry

All the complexes **44**, **45** and **50** exhibit one (**44**, **50**) or two (**45**) diffusion controlled, chemically reversible, one electron oxidation process under the conditions stated in Table 2, with the separation between the cathodic and anodic peak potentials comparable to that determined for the internal ferrocene standard. As found for the related aryl acetylide complexes, the [Mo(dppe)(η^7-C_7H_7)] moiety is considerably easier (in the thermodynamic sense) to oxidize than the analogous ruthenium complexes.[17]

Table 2: Cyclic voltametry results all carried out using 0.1 M ^{n}Bu$_4$NPF$_6$ /CH$_2$Cl$_2$ solutions at Pt electrode. All values referenced to FcH /FcH$^+$ = 0. [a] carried out in 0.1 M ^{n}Bu$_4$NB(C$_6$F$_5$)$_4$ /CH$_2$Cl$_2$ solutions.

Compound	$^1E_{1/2}$ /V	$^2E_{1/2}$ /V	ΔE^o /mV
44	-0.68	-	-
50	-0.64	-	-
45	-0.63	-0.71	80
45[a]	-0.69	-0.77	80

The oxidation potentials of **44** and **50** are comparable to [Mo(C≡C$C_6H_4CO_2$Me-4)(dppe)(η^7-C_7H_7)] (**10**) ($E_{1/2}$ = -0.65 V) although [Mo(C≡CCO_2Me)(dppe)(η^7-C_7H_7)] (**13**) is still 0.14 V harder to oxidize than **44** and **50**.[19]

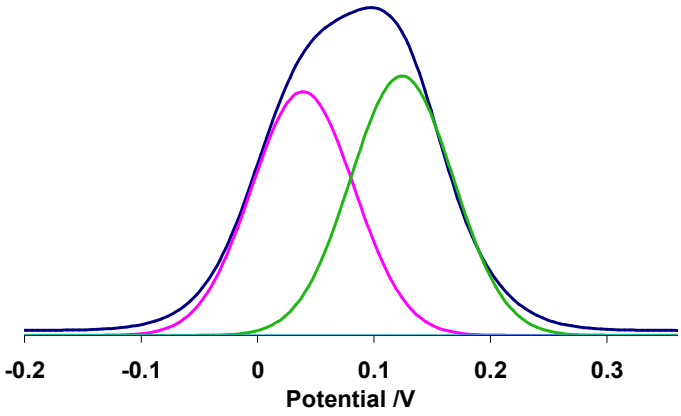

Figure 4: Deconvoluted differential pulse trace of 20, $^{1}E_{1/2}$ (Pink) and $^{2}E_{1/2}$ (Green), actual trace (Dark blue). (Recorded in 0.1 M $^{n}Bu_4NPF_6$ /CH_2Cl_2 at RT)

The bimetallic complex, **45**, exhibits two oxidation potentials, when recorded in $^{n}Bu_4NPF_6$ /CH_2Cl_2, exhibiting a ΔE^o = 80 mV, which could only be resolved using differential potential cyclic voltammetry, and by deconvoluting the curve using a Gaussian fitting routine (Figure 4). Similar ΔE^o values (ΔE^o = 90 mV (0.1 M $^{n}Bu_4NBF_4$ /CH_2Cl_2) and ΔE^o = 80 mV (0.1 M $^{n}Bu_4NB(C_6F_5)_4$ /CH_2Cl_2)) are found for **42**. For any complex containing multiple redox processes, the value of ΔE^o is dependant upon the stability of the cation /anion pair.[21] Therefore, changing the anion can affect the value of ΔE^o, and the sensitivity of ΔE^o to the identity of the anion can be useful in resolving the two closely separated oxidation events, as seen for **45**.[22] In order to fully assess the stability of $\mathbf{45}^+$ and its dependence on the identity of the supporting anion, electrochemical measurements were also undertaken using $^{n}Bu_4NB(C_6F_5)_4$ /CH_2Cl_2. The presence of a large weakly coordinating may help to destabilise the dication by reducing the favourable ion-pairing interactions, therefore giving a larger ΔE^o value. The ΔE^o measurements of $\mathbf{45}^+$ in solutions where the anion is $[PF_6]^-$ and $[B(C_6F_5)_4]^-$ differ by only 5 mV, indicating that the anion has a limited association with $\mathbf{45}^+$, implying ion-pairing interactions are of limited significance in stabilising $\mathbf{45}^+$. From ΔE^o the

comproportion constant (K_c) can be calculated revealing very low value for **45** ($K_c = 29$) where the anion is $[PF_6]^-$.

$$K_c = \exp\left(\frac{\Delta E^o F}{RT}\right)$$

In comparison to the ruthenium carboranyl analogue ($K_c = 35$) showing that both the mixed valence species $\mathbf{45}^+$ and $\mathbf{50}^+$ are more susceptible to disproportionation. For similar all-carbon bridged systems very much larger K_c values are obtained, [{Ru(dppe)(η^5-C_5Me_5)}$_2$(μ-C≡CC≡C)] (**52**) (K_c = 9.7 x 10^{10}),[23] [{Fe(dppe)(η^5-C_5Me_5)}$_2$(μ-C≡CC≡C)] (**53**) (K_c = 1.6 x 10^{12}),[24] [{Os(dppe)(η^5-C_5Me_5)}$_2$(μ-C≡CC≡C)] (**54**) (K_c = 2.1 x 10^{10})[25] and [{Re(NO)(PPh_3)}$_2$(μ-C≡CC≡C)] (**55**) (K_c = 1.1 x 10^9).[26]

4.5 Molecular Structures

Through careful recrystallisation, crystals of **44** (Figure 5) and **45** (Figure 6) were suitable for X-ray diffraction studies. Only poor quality crystals of **50** could be produced, the data collected support the identity of **50**, the low precision of the structure prevents a detailed discussion of the latter.

Table 3: Bond lengths and bond angles for complexes 13, 42, 44, 45 and 51.

Bond Length /Å	**13 (Mo)**	**44 (Mo)**	**42 (Ru)**	**45 (MoMo)**	**51 (RuRu)**
Mo_1-C_1	2.146(2)	2.135(2)	1.991(4)	2.130(2)	2.004(2)
C_1-C_2	1.179(3)	1.214(3)	1.205(4)	1.206(3)	1.212(2)
C_2-C_3	1.436(3)	1.446(3)	1.454(5)	1.449(3)	1.437(2)
Mo_1-P_1 /Mo_1-P_2	2.4731(6), 2.4686(6)	2.4540(6), 2.4612(6)	2.2509(10), 2.2638(11)	2.4622(7), 2.4723(6)	2.2463(4), 2.2656(4)
Bond Angle /^{o}					
Mo_{1A}-C_{1A}-C_{2A}	176.33(18)	176.0(2)	172.4(3)	176.7(2)	176.6(2)
C_{1A}-C_{2A}-C_{3A}	177.6(2)	174.6(2)	171.8(4)	172.9(2)	176.0(2)
P_{1A}-Mo_{1A}-P_{2A}	78.38(2)	79.24(2)	83.52(4)	79.73(2)	81.16(2)

The Mo-C_1 bond for **44** is shorter than **13**, but is very similar to the molybdenum aryl acetylide. In addition, the Mo-P bond lengths of **13** and **45** are very similar, indicating that the electron density at the metal centre is relatively un-affected by the coordination of the ethynyl carborane moiety. Coordinating the metal moieties [Mo(dppe)(η^7-C_7H_7)] and [Ru(dppe)(η^5-C_5Me_5)] to the ethynyl carborane does not cause very large changes in the C_1-C_2 or C_2-C_3 bond lengths, which shows that the carborane moiety does not mix well with the metal fragment, supporting the ^{13}C NMR observations discussed earlier.

The structure of **45** is symmetrical about the carborane cage, where each half resembles the structure of **44**. As shown for the mono-metallic complexes the bond lengths of the carborane bridge remain almost identical regardless of the identity of the metal fragment or the number of them.

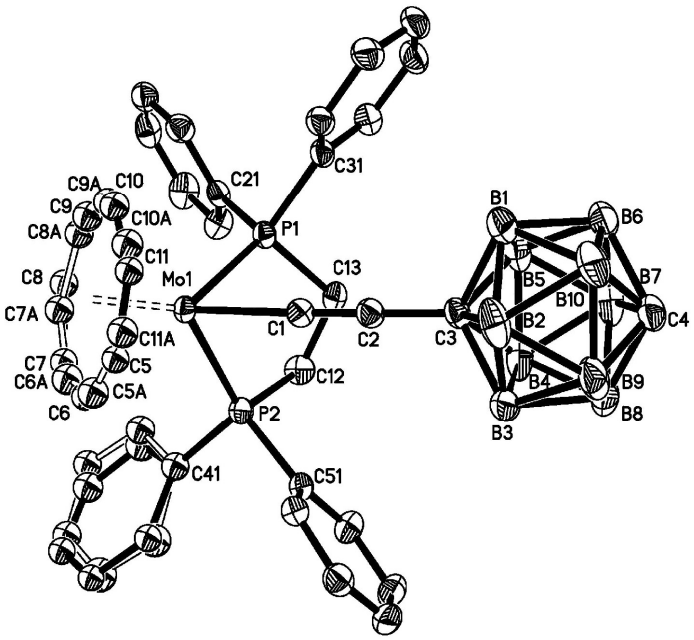

Figure 5: ORTEP plot of 44 showing the labeling scheme. The hydrogen atoms omitted for clarity. The thermal ellipsoids are plotted at 50 % probability (Disorder in the orientation of the C_7H_7 ring).

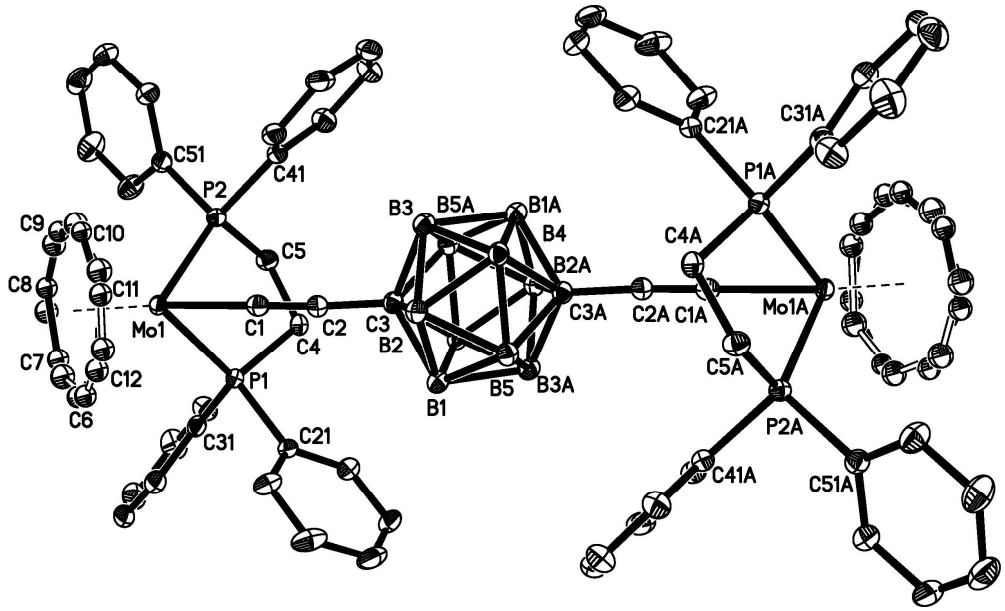

Figure 6: ORTEP plot of 45 showing the labeling scheme. The hydrogen atoms omitted for clarity. The thermal ellipsoids are plotted at 50 % probability(Disorder in the orientation of the C_7H_7 ring)

4.6 Infrared Spectroelectrochemistry

Although complexes based on the [Mo(dppe)(η^7-C_7H_7)] moiety can be easily chemically oxidised, for the ease of collecting data, the oxidised forms of the mono, and especially the bi-metallic species, **44**, **45** and **50** were generated *in situ* by spectroelectrochemical techniques (Table 4). The key feature of the alkynyl carborane system is the presence of two vibrational probes, ν(BH) and ν(C≡C), which can be used to monitor the structural and electronic changes upon the bridge during the oxidation of the complex. To confirm the oxidised species is an electrochemically generated complex, and not the product of a chemical reaction, each experiment was conducted in a cycle of oxidation and reduction with recovery of the original spectrum demonstrating the chemical reversibility of the redox chemistry.

Infrared spectroelectrochemical experiments performed on the mono-nuclear **44** demonstrate that upon oxidation there is a small shift of +3 cm^{-1} for the ν(BH) stretch. This is accompanied by the reduction in intensity of the ν(C≡C) stretch to such an extent that it could not be distinguished from the base line. The reduction in intensity of the ν(C≡C) of $\mathbf{44}^{+}$ is a common feature for strongly electron withdrawing [Mo(C≡CR)(dppe)(η^7-C_7H_7)] complexes such as the mono-nuclear complex $\mathbf{13}^{+}$ (Chapter two). Similar behaviour is noted for the oxidation of the ethynyl substituted mono-nuclear complex, from **50** to $\mathbf{50}^{+}$, however, the ν(C≡C) of $\mathbf{50}^{+}$ still retains some intensity upon oxidation, exhibiting a small shift of -3 cm^{-1}. Oxidation of **50** causes no change in ν(BH), which is indicative of the oxidation taking place without significant involvement of the carborane cage. However, unlike $\mathbf{44}^{+}$, $\mathbf{50}^{+}$ was not as stable under the spectroelectrochemical conditions, resulting in a small amount of an unknown decomposition product being formed upon oxidation, characterised by the presence of bands at 2447 and 2555 cm^{-1}.

Table 4: Infrared spectroelectrochemical results, all performed in 0.1M $^{n}Bu_4NPF_6$ /CH_2Cl_2 solutions using modified OTTLE cells.

	$\mathbf{44}^{n+}$		$\mathbf{50}^{n+}$		$\mathbf{45}^{n+}$	
	ν(C≡C)	ν(BH)	ν(C≡C)	ν(BH)	ν(C≡C)	ν(BH)
n = 0	2067	2611	2064	2606	2065	2608
n = +1	-	2613	2061	2606	2065	2609
n = +2		-			2065	2609

To give insight into how molybdenum alkynyl carboranes react to oxidation, infrared spectroelectrochemical studies were conducted on **45**. Upon successive oxidation of **45**, to $\mathbf{45}^{+}$ and $\mathbf{45}^{2+}$, the infrared spectrum remains essentially the same, with a small variation in the intensity of the ν(C≡C) for $\mathbf{45}^{+}$, and a shift of +1 cm^{-1} for the ν(BH) band. From the electrochemical measurements the calculated K_c value is very small

(K_c = 29) therefore isolating **45**$^+$ on the spectroelectrochemical apparatus is fraught with difficulty owing to disproportionation issues. As the ν(C≡C) and ν(BH) stretches changed very little upon oxidation, the identity of **45**$^+$ was confirmed by the presence of a broad, low intensity electronic transition at 3500 cm^{-1}, that was not present in the spectra of **45** or **45**$^{2+}$ (Figure 7). This absorption feature is identified as the tail of the charge transfer band and is a common feature in mixed valence complexes of this type. The analogous ruthenium carborane system, **42**, exhibits more significant changes to the infrared spectra upon progressing from **42** to **42**$^+$ to **42**$^{2+}$. The monocation, **2**$^+$, has two distinct stretches for ν(C≡C) stretch and a comparable modest shift of +7 cm^{-1} for ν(BH). The appearance of two individual bands for ν(C≡C) is expected for [Ru(dppe)(η^5-C_5Me_5)] containing complexes owing to the localised mixed valence nature of this complex, and increased mixing between the ruthenium d-orbitals and the ethynyl π-system which leads to more significant ethynyl character in the redox active orbital.

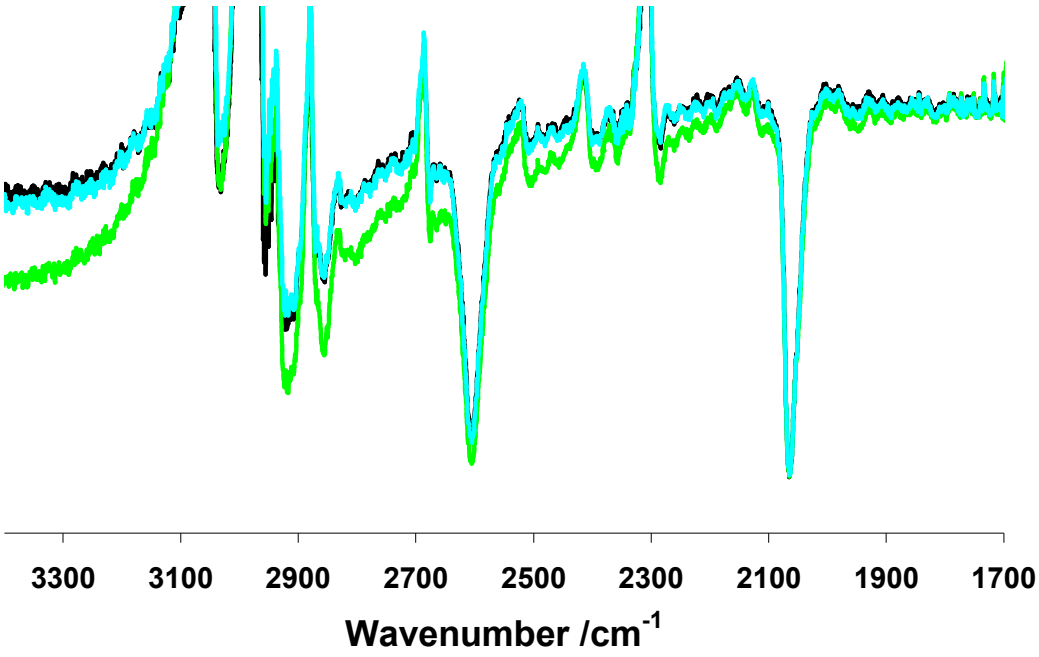

Figure 7: Infrared spectra for 45^{n+}, where n = 0 (Black), n = 1 (Green), n = 2 (Blue) (Recorded in 0.1 M ^{n}Bu$_4$NPF$_6$ /CH$_2$Cl$_2$)

The ν(C≡C) vibration gains intensity in $\mathbf{45}^{+}$ as it is coupled with the charge transfer transition. The coupling of vibronic motions with electronic transitions is a fundamental aspect of PKS theory for charge transfer.[27] For $\mathbf{45}^{2+}$ although there is no charge transfer transition, the gain in intensity of the ν(C≡C) can be rationalised by the ν(C≡C) vibronic motion being coupled to an MLCT-type transition that takes place along a similar vector.

4.7 Electronic Structure Calculations

To rationalise the electronic structure of **44** and **45**, DFT calculations were performed on model complexes of the systems, $[Mo(C{\equiv}CC_2B_{10}H_{11})(dHpe)(\eta^7\text{-}C_7H_7)]^{n+}$ (**44H**), and $[\{Mo(dHpe)(\eta^7\text{-}C_7H_7)\}_2(\mu\text{-}C{\equiv}C(C_2B_{10}H_{10})C{\equiv}C)]^{n+}$ (**45H**), with dHpe ($PH_2CH_2CH_2PH_2$) being used as a model for the full dppe ligand for computational efficiency. The model geometries, calculated with various functionals and basis sets, were tested against the experimental structural and infrared data. As for the ruthenium example,[17] the functional MPW1K proved to be effective in generating a localised electronic structure for $\mathbf{45H}^{+}$. The geometries of **44H** and **45H** were calculated using both the frozen core potential basis set LANL2DZ and the split-valence basis set 3-21G*, but the two basis sets produced no significant difference. Therefore, the less computationally intensive LANL2DZ basis set was used for both **44H** and **45H**.

4.7.1 Neutral Species Calculations

As the model chemistry, MPW1K /LANL2DZ, used produced the localised geometry for **45H**$^{+}$ the same functional was used to calculate the model geometry for **44H**$^{n+}$ (n = 0, 1). A comparison with the molecular structure determined for **44** shows the model geometry to be in good agreement, with most of the bond lengths only 0.02 Å longer than the experimental values (Table 5). The calculated infrared spectra for **44H** and **44H**$^{+}$ gave two bands corresponding to ν(C≡C) and ν(BH), although, the frequencies are somewhat higher than the experimental values for **44** and **44**$^{+}$.

Table 5: Calculated bond lengths and angles for model geometries 44H and 44H^{+}.

Bond length / Å	**44H**	**44H^{+}**
Mo_1-C_1	2.10419	2.05691
C_1-C_2	1.23423	1.23172
C_2-C_3	1.43176	1.43393
Mo_1-P_1 /Mo_1-P_2	2.49333, 2.4888	2.54400, 2.53694
Bond Angle /^{o}		
Mo_{1A}-C_{1A}-C_{2A}	178.107	178.723
C_{1A}-C_{2A}-C_{3A}	178.936	178.131
P_{1A}-Mo_{1A}-P_{2A}	79.278	79.264

A similar analysis of the d-orbital separation, as described for the diynyl and triynyl complexes (Chapter three) provides an insight into the effects of the nature of the acetylide moiety on the electronic structure of the complex. Once again the presence of the cycloheptatrienyl ring dictates the overall order of the metal d-orbitals and the type of interaction which they make with the other ancillary ligands. As a point of comparison, the model geometry **1H**, was prepared and calculations were performed at the same level of theory as for **44H**. Although the ordering of the d-orbitals remains constant, in terms of δ and π-interactions, the relative energies of these orbitals alter

slightly between **44H** and **1H**. As a result, the energy of the HOMO in **44H** is raised 0.09 eV in comparison to **1H**. This is in agreement with the similarly small shift in $E_{1/2}$ value of 0.04 V, from **1** to **44**. The molecular orbitals which involve the d_{xy} and d_{x2-y2}, also show this dependence on the electronic character of the alkynyl moiety. Following coordination of the molybdenum fragment to the electron withdrawing ethynyl carborane there is a contraction in the energy difference between the d_{xy} and d_{x2-y2} orbitals in comparison to the ethynyl phenylene moiety. Extension of the ynyl chain, which has a similar electronic effect as increasing the electron withdrawing nature of the moiety, also causes a contraction of the energy difference between these molecular orbitals (Chapter three). The metal d-orbitals involved in π-interactions with the ring and the LUMO, remain relatively unaffected by the identity of the alkynyl /ynyl moiety attached to the [Mo(dppe)(η^7-C_7H_7)] fragment.

The application of the MPW1K LANL2DZ functional and basis set conditions to **45H** gave a model geometry that contained no imaginary frequencies and produced similarly contracted bond lengths as compared to the experimental X-ray structure. A closer inspection of the model geometries of **45H** and **44H**, reveals that **45H** is a mirror of **44H**, centered on the carborane cage (Table 6). Although the uncorrected calculated frequencies are not true to the experimental values, the picture generated from the calculation fits the experimental spectra, i.e. there are two bands of large intensities corresponding to the symmetric ν(C≡C) and ν(BH) stretches, and one band of near zero intensity for the asymmetric stretch of ν(C≡C). Analysis of the d-orbital energies in bimetallic complexes is inherently fraught with problems as there are now two metal centres on which to base the Cartesian axis. Nevertheless, the problem is simplified as there are sets of almost degenerate d-orbitals interactions, each mirroring the interaction

on the opposite metal centre separated by the carborane cage. For this reason the d-orbital analysis was performed on one metal centre only. The HOMO of **1A** is calculated to have a very similar energy to **44H**, which is reflected experimentally by the similar $E_{1/2}$ value for the first oxidation of **45**. As a consequence of **45H** mirroring **44H**, the other δ- and π-interactions are all of similar energies. This similarity in electronic structure, helps explain the similarities between the molecular structure and the spectroscopic properties of **44** and **45**.

Table 6: Calculated bond lengths and angles for $45H^{n+}$, n = 0, 1 and 2.

Bond Length /Å	**45H**	**$45H^+$**		**$45H^{2+}$**
		$Mo_1C_1{\equiv}C_2$	Mo_2-$C_6{\equiv}C_5$	
Mo_1-C_1	2.105	2.05	2.101	2.016
C_1-C_2	1.234	1.233	1.236	1.244
C_2-C_3	1.432	1.432	1.427	1.419
Mo_1-P_1 /Mo_1-P_2	2.493, 2.488	2.543, 2.539	2.491, 2.489	2.518, 2.518
Bond Angle /°				
Mo_{1A}-C_{1A}-C_{2A}	178.726	178.136	179.632	179.894
C_{1A}-C_{2A}-C_{3A}	179.176	179.297	176.490	178.493
P_{1A}-Mo_{1A}-P_{2A}	79.275	79.231	79.257	79.571

A comparison with the calculations performed on the ruthenium complex (**45H**) reveals a significant difference between the contributions of the bridge to the HOMO. For the Ru(dppe)(η^5-C_5Me_5) example, 47 % of the electron density is on the bridge, particularly on the C≡C moeity, whereas for **45H** it is only 21 %. The difference between the two complexes can be accounted for by the promotion of the d_{z2} metal d-orbital to the HOMO in **45H**, and the poor symmetry match between the d_{z2} orbital and the bridge π-system. Thus in the case of **45**, the majority of the molecular orbital resides on the metal (79 %), and does not feature the significant ligand contribution observed for ynyl complexes based upon the Ru(dppe)(η^5-C_5Me_5) moiety.

4.8 EPR Spectroscopy

The ability to readily generate stable 17 electron complexes that produce well resolved X-band EPR spectra is a key feature of the [Mo(dppe)(η^7-C_7H_7)] end cap. The complex **44**$^+$ were generated *in situ*, from the parent complex **44** by chemical oxidation using [Fe(η^5-C_5H_5)$_2$]PF_6 (Table 7). Their EPR spectra were kindly collected by H.N. Lancashire and Dr. R. Edge at the University of Manchester. As shown by the electrochemical experiments, **45** has a small K_c value and therefore **45**$^+$ is more likely to disproportionate into **45** and **45**$^{2+}$ species. Owing to the sensitivity of EPR spectroscopy to the presence of un-paired electrons, and difficulties in accurately adding small amount of oxidising agent to the EPR sample, **45**$^+$ was isolated as a light brown slightly air sensitive solid, [**45**]PF_6, by careful addition of [Fe(η^5-C_5Me_5)$_2$]PF_6 to **45** under strict anaerobic conditions. The sample obtained was a mixture of **45**, **45**$^+$ and **45**$^{2+}$ with the proportions determined by the comproportionation equilibrium. The complex **45**$^{2+}$ was generated electrochemically and the generation of the species confirmed by a steady equilibrium current reading.

Table 7: X-band solution spectra (CH_2Cl_2 at 243 K) hyperfine couplings in gauss.

Complex	a_{iso}(Mo)	a_{iso}(^{31}P)	a_{iso}(^{1}H)	g_{iso}
1$^+$	31.3	22.6	4.3	1.996
44$^+$	32.0	23.4	4.6	1.993
45$^+$	32.0	23.4	4.6	1.992
45^{2+}	32.0	23.4	4.6	1.996

The EPR spectrum of $\mathbf{44}^+$ is typical of [Mo(C≡CR)(dppe)(η^7-C_7H_7)], in addition, there is no evidence of the electron coupling to the carborane cage CH, similar to $\mathbf{1}^+$ where there is no coupling to the proton in the *para* position of the aryl ring.

On the formation of $\mathbf{45}^+$ the EPR spectra was identical to that of $\mathbf{44}^+$, signifying that the oxidation is taking place exclusively on one of the metal centres (Figure 8). This behaviour can only occur when the bridging ligand does not allow the extensive delocalisation of charge through the π-system. The physical separation of the two electrophores is exemplified in the EPR spectrum of $\mathbf{45}^{2+}$ (Figure 9), which has very similar parameters as $\mathbf{44}^+$ and $\mathbf{45}^+$, showing that the oxidation is taking place on two identical, yet isolated, [Mo(dppe)(η^7-C_7H_7)] fragments. This also explains why the two oxidation potentials for **45** are so close, as each of the metal centres is in a near identical environment, hence a similar energy is needed to remove the electron. This type of behaviour for the dicationic species leads to a singlet biradical being formed, i.e. two non-interacting radical species which are physically separated from one another.

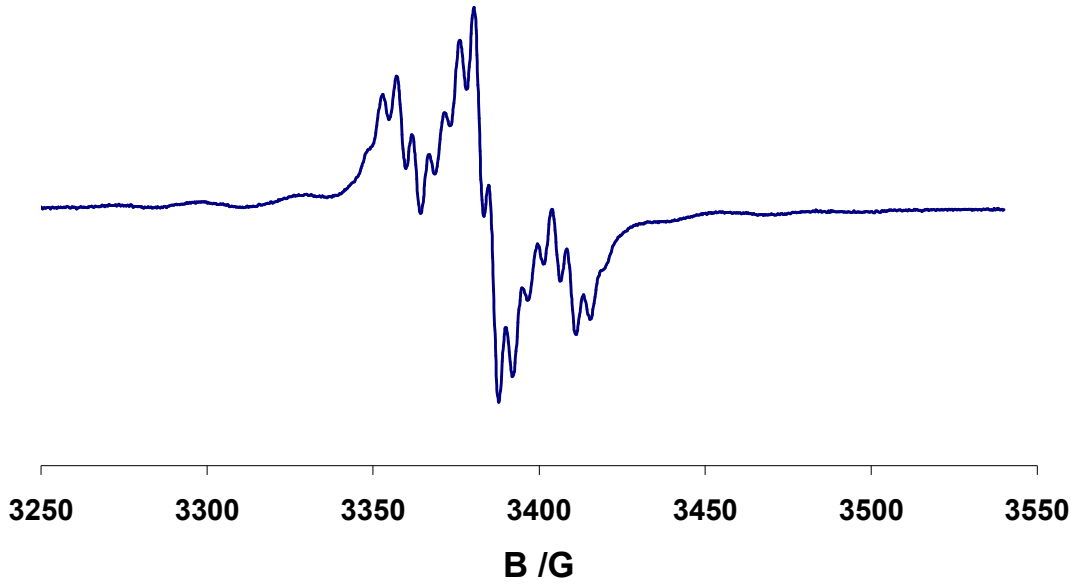

Figure 8: First derivative X-band EPR fluid solution (CH_2Cl_2, 243 K) of [45]PF_6 .

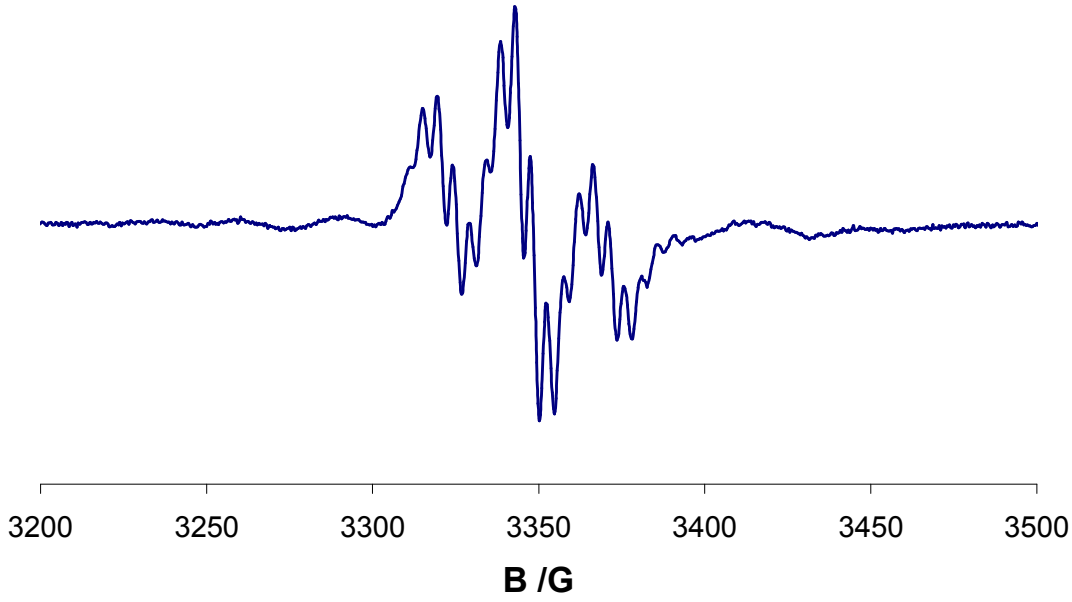

Figure 9: First derivative X-band EPR fluid solution (CH_2Cl_2, 243 K) of [45][PF_6]$_2$.

4.8.1 Cationic Species Calculations

Calculation of the geometry **44H**$^+$ reveals a contraction of the Mo-C_1 bond and an elongation of the Mo-P bond lengths relative to **44H**, all of which are consistent to the removal of an electron from the metal centre. As expected from the EPR measurements, the removal of an electron to generate the 17 electron species only affects the atoms which are directly bonded to the molybdenum centre. The bonds associated with the alkynyl subsituent, C_1-C_2 and C_2-C_3, remain un-disturbed by the presence of the unpaired electron, and as such resemble those found for **44H**. As apparent from the calculation on **44H**, the accurate predictions of the energy of the ν(C≡C) stretches is rarely attained. Nevertheless, the calculation shows two closely separated infrared stretches, 14 cm^{-1}, for the symmetric and asymmetric stretching modes of the bridge. The calculations also correlate well with the observed small shift for ν(BH) stretch, an averaged value has been taken as the calculation gives each individual stretch a specific frequency, whereas experimentally these stretches are unresolved in solution at room temperature.

An analysis of the spin density has proven useful in previous work (Chapters two and three) as a way of explaining the features of the EPR spectrum. Yet again, the results show that the spin density is almost entirely localised at the molybdenum centre (Table 8, Figure 10 and Figure 11). This is a feature that has been prevalent in all [Mo(dppe)(η^7-C_7H_7)] supported polyyne systems, with very little distribution of the spin on the short C_2 alkynyl chain due to symmetry considerations.

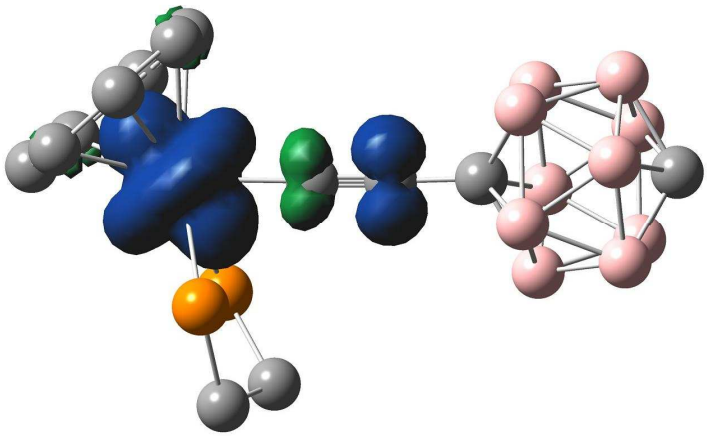

Figure 10: Spin density plot of $44H^+$. (Hydrogen atoms omitted for clarity)

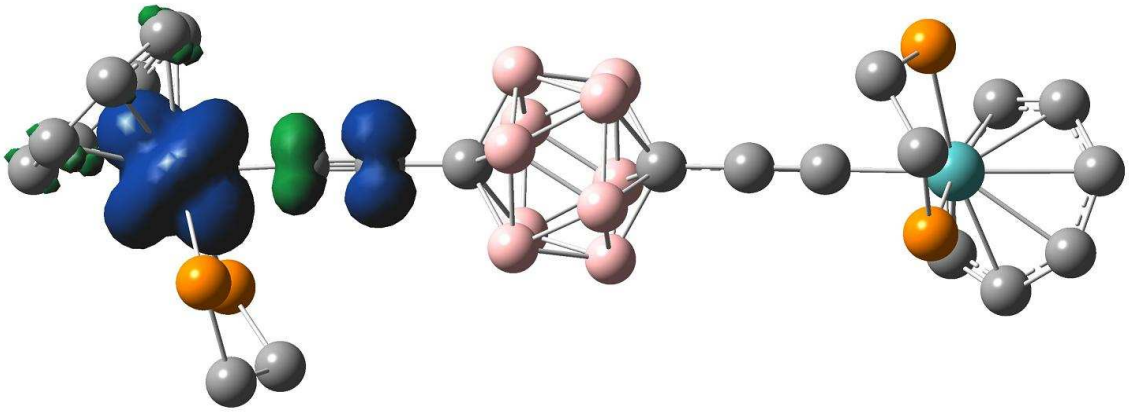

Figure 11: Spin density plot of $45H^+$. (Hydrogen atoms omitted for clarity)

Table 8: Mulliken spin density for $44H^+$ and $45H^+$; Mo_1 and Mo_2 refer to each Mo(dppe)(η^7-C_7H_7) fragment.

Atom	**$44H^+$**	**$45H^+$** /Mo_1	**$45H^+$** /Mo_2
Mo	1.282526	1.264462	-0.000809
C_1	-0.201401	-0.204665	0.006298
C_2	0.303804	0.319152	-0.002189
P_1	-0.042557	-0.041616	0.00243
P_2	-0.043174	-0.042112	0.00244

As demonstrated by the similarities of the EPR spectrum for the hyperfine coupling constants to Mo in **44**$^+$ and **45**$^+$, the spin density calculated for **45H**$^+$ is identical to that calculated for **44H**$^+$. Thus, the spin density calculations support the conclusion that the

oxidation is taking place solely on one molybdenum centre and the charge is not propagated through the bridge. This conclusion is further supported by the calculated geometry of **45H**$^{+}$, whereby one half of the model has the geometry of **44H**, and the other half resembles the geometry of **44H**$^{+}$.

4.8.2 Dication Species Calculations

Both the triplet and singlet states for the dication, **45H**$^{2+}$, were calculated and highlighted that the singlet state has the lowest energy by 0.07963 a.u. The calculated geometry of **45H**$^{2+}$ is symmetrical about the carborane cage. Both Mo-C_1 bonds are slightly contracted in comparison to **44H**$^{+}$ (0.0453 Å) and both Mo-P bond lengths are contracted by 0.021 Å. Although the calculated frequency for ν(C≡C) does not quite follow the same trend as the experimental results, where there is no change in the ν(C≡C) energy, the calculation still predicts a modest intensity for the stretching frequency as per experimental results. However, as witnessed in the calculations of the previous models, the frequencies for these carboranes are not in complete agreement with the experimental results.

An analysis of the molecular orbitals in **45H**$^{2+}$ show that they are distributed evenly across the complex with the HOMO consisting of metal d_{z2} orbitals, which causes 75 % of the molecular orbital to be distributed evenly over the two molybdenum centres (Figure 12). The identical nature of the two [Mo(dppe)(η^7-C_7H_7)]$^{+}$ substituents explains the very similar nature of the EPR spectra for **45**$^{2+}$ and **45**$^{+}$. The calculated LUMO electronic structure has nearly the same distribution of the electron density of the complex, but is the anti-bonding conformer. This retention of the electronic

structure on each [Mo(dppe)(η^7-C_7H_7)] end cap is indicative of the second oxidation process taking place on an electronically isolated, strongly metal centered oxidation.

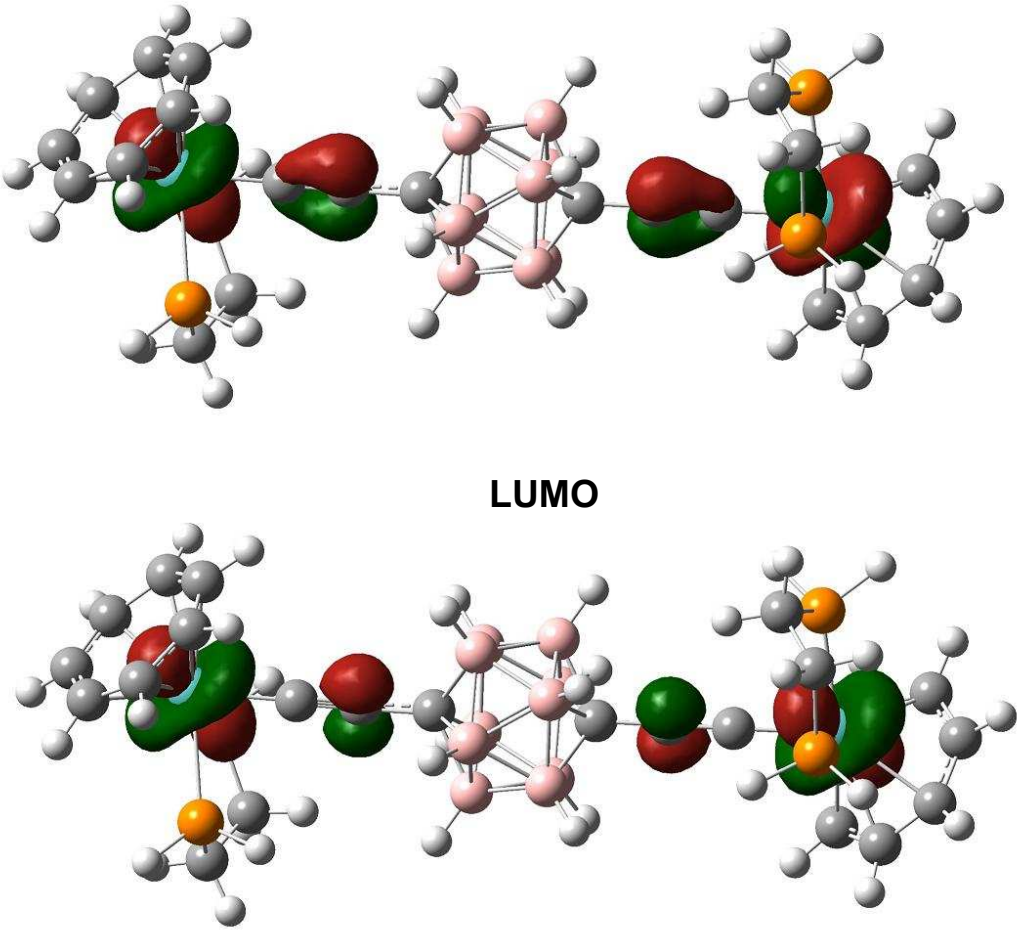

Figure 12: Molecular orbital plots of the HOMO and LUMO for $45H^{2+}$ (plotted as an isosurface of 0.04 au).

4.9 UV /vis Spectroelectrochemistry and TD-DFT

The species $\mathbf{44}^{n+}$ and $\mathbf{45}^{n+}$ were studied *in situ* using UV /vis spectroelectrochemical methods (50000 – 10000 cm^{-1}). In addition, to help assign the electronic spectra, TD-DFT calculations were undertaken on the model geometries $\mathbf{44H}^{n+}$ (n = 0, 1) and $\mathbf{45H}^{n+}$ (n = 0, 1, 2).

The electronic spectrum of **44** /$\mathbf{44}^{+}$, is similar to the previously studied molybdenum acetylides, with higher energy bands corresponding to transitions associated with in the [Mo(dppe)(η^7-C_7H_7)] fragment (Table 9). The primary difference between aryl acetylides and the carborane acetylides is the much higher energy of the LMCT type transitions for the monocation, $\mathbf{44}^{+}$. Similar LMCT energies are obtained for the non-aryl acetylides complexes studied, for example [Mo(C≡C^{t}Bu)(dppe)(η^7-C_7H_7)] (**12**) (20000 cm^{-1}). Whereas aryl acetylides have LMCT transitions between the aryl alkynyl moiety and the molybdenum centre, at 17000 cm^{-1}, $\mathbf{44}^{+}$ has a LMCT type transition, at 20800 cm^{-1}, and consists only of the transition between a C≡C moiety to the molybdenum centre. The non-involvement of the carborane cage in LMCT type transitions is a common feature for this type of *para*-carborane complex.[17]

Table 9: UV /vis results for 44^{n+}, n = 0 and 1, and TD-DFT assignments.

	$\mathbf{44}^{n+}$	$\mathbf{44H}^{n+}$	
n	Transition /cm^{-1} (ε /M^{-1} cm^{-3})	Transition /cm^{-1} (intensity)	Character of transition
0	34100 (21200)	35300 (0.1018)	C_7H_7→ ModHpe
	Sh 28100 (6600)	28500 (0.0161)	Mo → C_7H_7
	24400 (4200)	20100 (0.0004)	Mo → C_7H_7
1	32900 (8500)	32750 (0.0228)	C≡C → dHpe
	24300 (3100)	28900 (0.0416)	C≡C → C_7H_7
		24950 (0.0627)	C≡C → Mo
	20800 (2300)	18800 (0.0016)	C_7H_7 → Mo

The bimetallic complex $\mathbf{45}^{n+}$ exhibits a similar spectra as $\mathbf{44}^{n+}$, and $\mathbf{45}^{+}$ gives a spectrum which is a supposition of both **45** and $\mathbf{44}^{+}$ (Table 10, Figure 13). For the oxidised species, $\mathbf{45}^{+}$ and $\mathbf{45}^{2+}$, the lowest energy transitions are both LMCT in character, however, compared to $\mathbf{44}^{+}$ the transitions involves molecular orbitals which have a much larger contribution from the carborane cage.

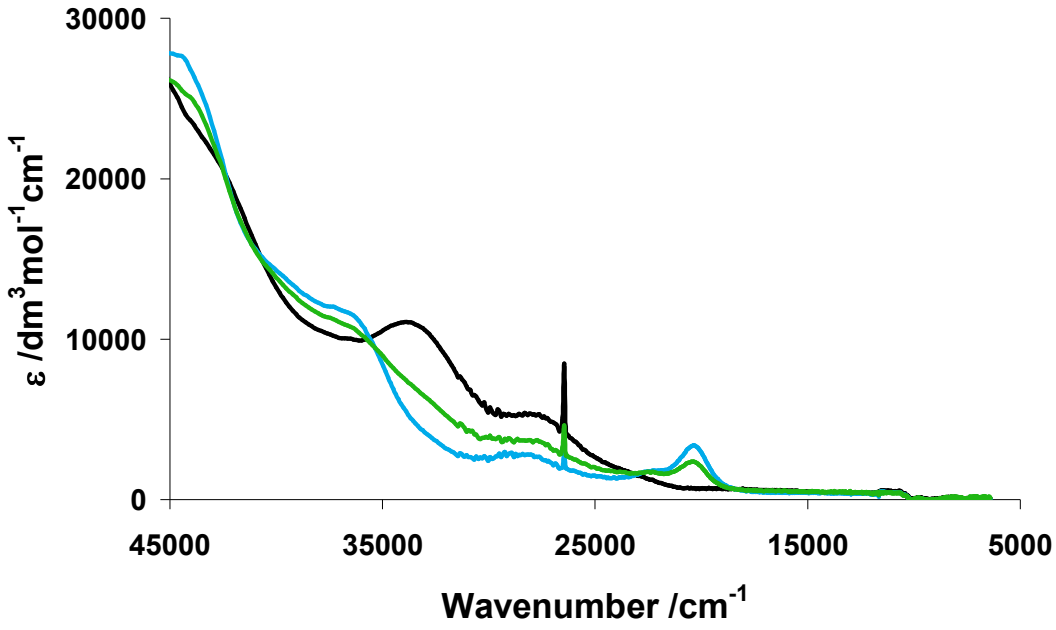

Figure 13: UV /vis spectroelectrochemical result for 45^{n+}, where n = 0 (Black), n = 1 (Green), n = 2 (Light blue) (Recorded in 0.1 M $^{n}Bu_4NPF_6$ /CH_2Cl_2).

Table 10: UV /vis results for 45^{n+}, n = 0, 1 and 2, and TD-DFT assignments.

n	**45^{n+}**	**$45H^{n+}$**	
	Transition /cm^{-1} (ε /M^{-1} cm^{-3})	Transition /cm^{-1} (intensity)	Character of transition
0	33800 (11000)	38300 (0.3911)	Mo(1) → Mo(2)C≡CCb
		35100 (0.3657)	C_7H_7 → ModHpe
	27800 (5300)	28400 (0.0439)	Mo → C_7H_7
		20900 (0.0009)	Mo → C≡CCb
1	38000 (11200)	38200 (0.2023)	Mo → C≡C
	33800 (10400)	34600 (0.2052)	Mo(1)C_7H_7→ Mo(2)C≡CCb
	27850 (5000)	23750 (0.0846)	MoC_7H_7 → ModHpe
	20600 (800)	20700 (0.0217)	C≡CCb → Mo
2	36600 (11600)	39400 (0.6339)	Mo → C_7H_7
	28900 (2900)	28400 (0.1366)	Mo → C_7H_7
	22500 (1800)	23450 (0.7699)	C≡C → Mo
	20500 (3300)		

4.10 Resonance Raman Spectroscopy

The appearance of a single IR ν(C≡C) band for **45**$^{+}$ promoted further investigation by resonance Raman spectroscopy as it was predicted from calculations that there should be two sets of ν(C≡C) stretching modes, due to the localised geometry of the mixed valence complex. The Raman spectrum of **45**$^{+}$ was collected using two different laser energies, 532.21 nm and 632.817 nm, this allows the complex to be excited on-resonance, with the LMCT-type transition at 20600 cm^{-1}, and off-resonance therefore, allowing the resonance enhancement features to be distinguished.

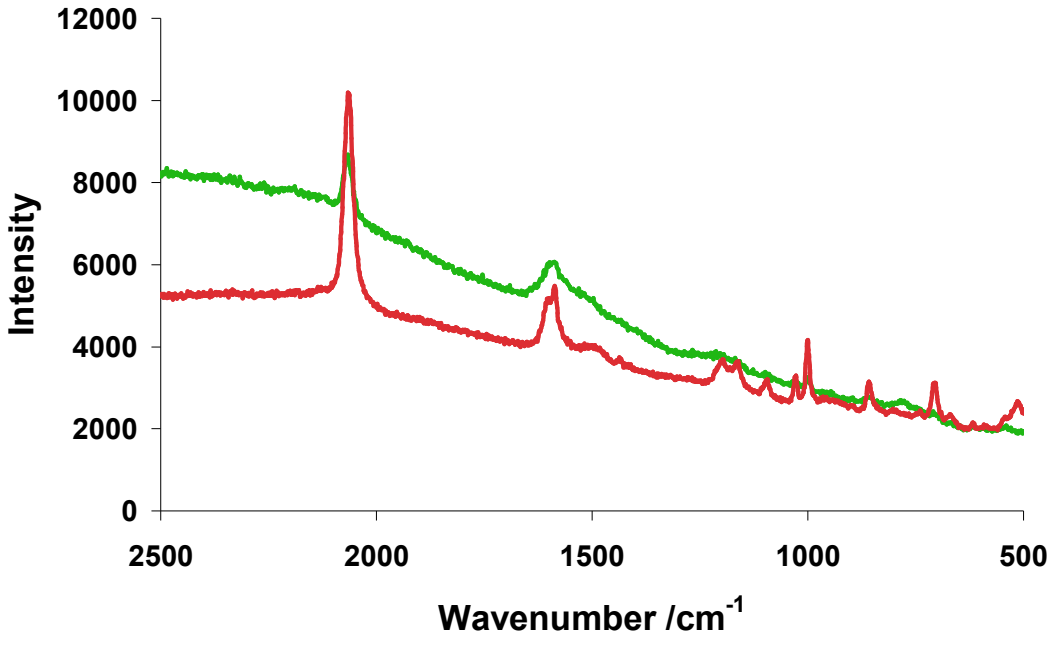

Figure 14: Raman spectrum of [45]PF_6 recorded at 532.21 nm (Green) and 632.817 nm (Red).

Table 11: Raman data for [45]PF_6.

Laser Energy /nm	ν(C≡C) /cm^{-1} (Intensity from baseline)
532.21	2067 (1040)
632.817	2067 (4810)

The off-resonance Raman spectra (632.817 nm) gives rise to a single ν(C≡C) at the same frequency as observed in the infrared spectrum of **45**$^+$. Upon changing the laser to 532.21 nm (to be on-resonance with the LMCT-type transition) the background fluorescence increases and the relative intensity of the ν(C≡C) decreases (Table 11, Figure 14).

Compound **45**$^+$ is not symmetrical, a consequence of the oxidation taking place largely on a [Mo(dppe)(η^7-C_7H_7)] fragment, therefore, the rule of mutual exclusion does not apply and the symmetric and asymmetric stretches will both have intensity in the Raman and infrared spectra. From the calculation of the infrared spectrum for **45**$^+$, the symmetric and asymmetric bands are very close in energy, 39 cm^{-1}. The experimental band envelope could therefore contain both symmetric and asymmetric modes of the ν(C≡C) moieties. This would account for the apparent coincidence between the observed Raman and infrared energies for ν(C≡C) in **45**$^+$. This type of coincidence is not un-heard of, for example, the incorporation of a phenylene moiety into an acetylenic chain produces differences of 5-10 cm^{-1} between the observed Raman and infrared spectra.[28]

4.11 NIR Spectroscopy

Complex $\mathbf{45}^{n+}$ was also studied using NIR spectroelectrochemical techniques (10000 – 2000 cm^{-1}). The *in situ* generation of both **45** and $\mathbf{45}^{2+}$, and also **44** and $\mathbf{44}^{+}$, revealed no bands in this region that could be distinguished from the base line. However, $\mathbf{45}^{+}$ gave a single, unique, broad band, spanning over 7000 cm^{-1}. The synthesis of the mixed valence complex [**45**]PF_6, has allowed the thorough investigation of this broad band, which as shown in previous studies,[17] contains a wealth of information about the electronic states involved in the charge transfer process between the two electrophores, [Mo(dppe)(η^7-C_7H_7)].

The NIR spectrum of [**45**]PF_6 was collected in several different solvents, CH_2Cl_2, MeCN, and acetone so as to characterize the effect of solvent on the charge transfer process. Upon increasing the dielectric of the solvent from CH_2Cl_2 to acetone and MeCN, the overall shape of the band becomes broader by 3000 cm^{-1}. Unfortunately, due to the poor solubility of [**45**]PF_6 in acetonitrile and acetone precise extinction coefficients could not be calculated for all the NIR spectra. However, at very low concentrations $\mathbf{45}^{+}$ was soluble in CH_2Cl_2 thus allowing the determination of extinction coefficients in this solvent. To gain an accurate extinction coefficient, the thermodynamic stability of $\mathbf{45}^{+}$ must be considered due to the small value of K_c, which means that a certain percentage of the sample at equilibrium will consist not as $\mathbf{45}^{+}$, but as **45** or $\mathbf{45}^{2+}$.

It has been shown in many other bimetallic and polymetallic complexes that the NIR band does not only contain transitions solely concerning the charge transfer process, but

also transitions corresponding to interconfigurational transitions, or d-d transitions. The observation of the NIR band composing of a number of different transitions is a consequence of the electronic asymmetry in the ligand field; a low electronic symmetry.[29] As a result of this asymmetric ligand field, interconfigurational transitions, which are normally Laporte forbidden and are a result of transitions from Kramers Doublets to the semi-occupied HOSO on the 17 electron [Mo(dppe)(η^7-C_7H_7)] fragment, gain intensity. In addition, the number of intervalence transitions increases to three, this occurs due to the differences in the energies and symmetries of the filled orbitals on the 18 electron Mo(dppe)(η^7-C_7H_7) end cap (Figure 15).

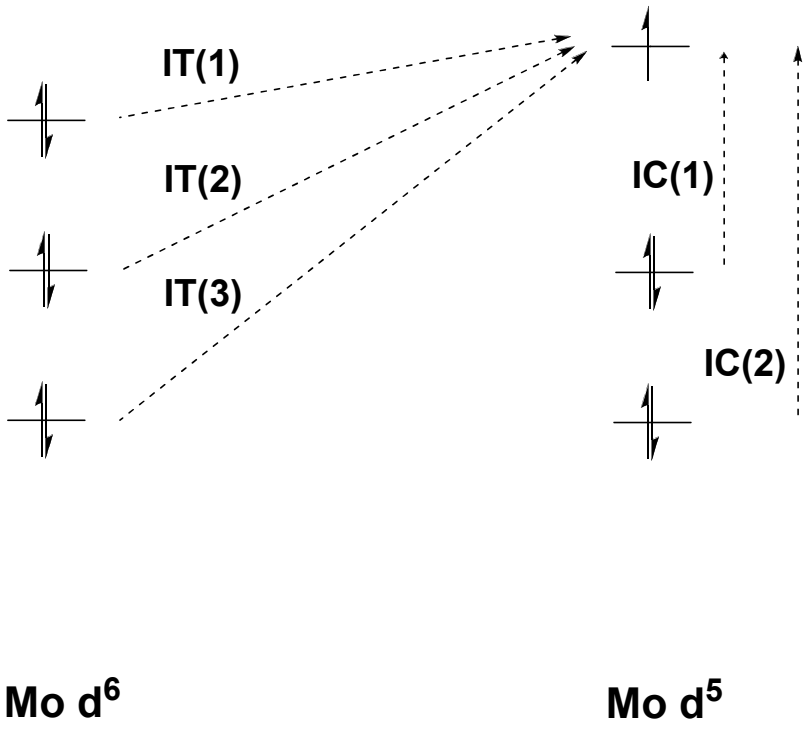

Figure 15: Possible transitions in the NIR region for transition metal complexes.

The deconvolution of the NIR band, using the summation of Gaussian curves, exposes the true nature of the band by producing five distinct Gaussian shaped bands, three of which are moderately intense (ca. 5300, 7300 and 12450 cm^{-1}) and two which are much

less intense (ca. 3000 and 8800 cm^{-1}) (when [**45**]PF_6 is recorded in CH_2Cl_2). Upon increasing the dielectric of the solvent medium, the bands assigned band two, three and five show the strongest solvatochromic behavior. The two weaker bands (bands one and four) are the least affected by changes in the solvent medium, but do gain intensity relative to the other bands as the dielectric constant of the solvent medium is increased (Table 12-15, Figure 16-18).

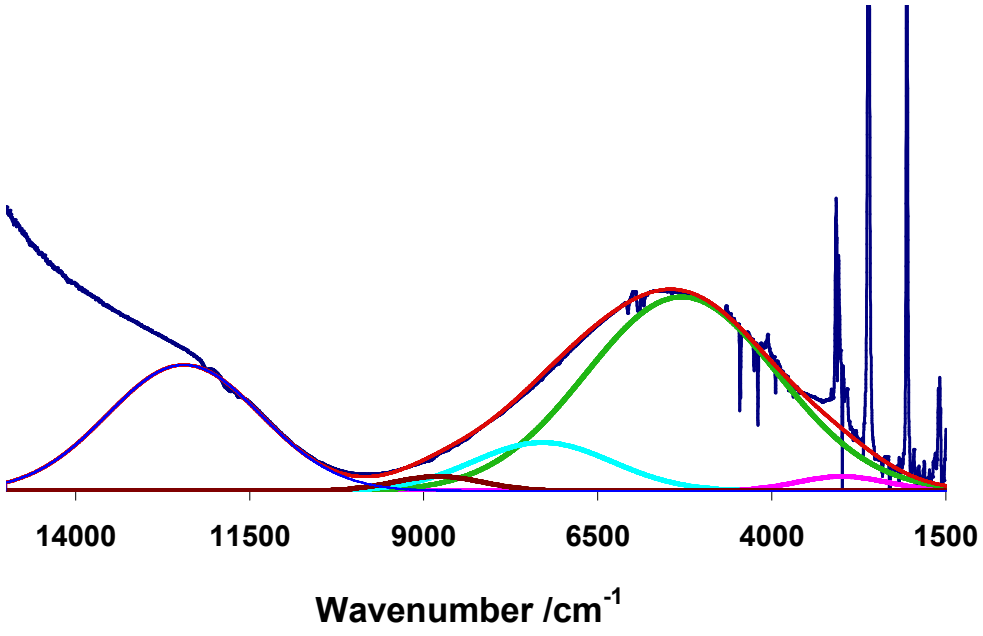

Figure 16: Gaussian deconvolution of the NIR band for [45]PF_6 recorded in CH_2Cl_2 .

Table 12: Deconvoluted band data for [45]PF_6 in CH_2Cl_2.

CH_2Cl_2	IC (1)	IT (1)	IT (2)	IC (2)	IT (3)
ν /cm^{-1}	3000	5300	7300	8800	12450
$\Delta\nu_{1/2}$ /cm^{-1}	1500	3200	2300	1500	2600
ε /$dm^3mol^{-1}cm^{-1}$	8.1	108	27	8.1	70
Corrected ε /$dm^3mol^{-1}cm^{-1}$	20	260	65	20	170

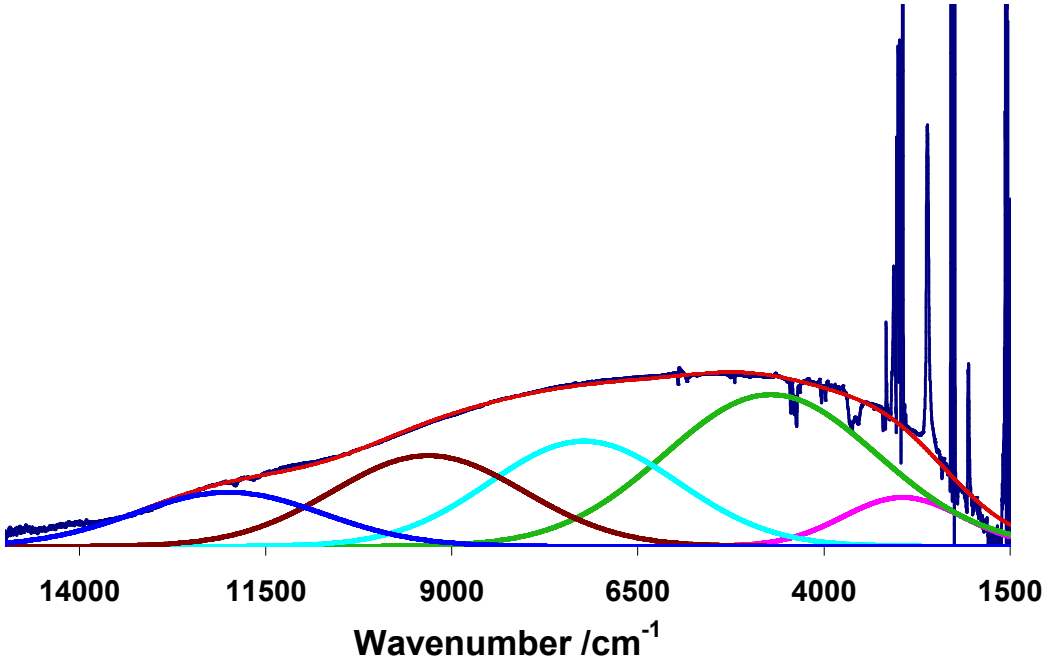

Figure 17: Gaussian deconvolution of the NIR band for [45]PF_6 recorded in MeCN .

Table 13: Deconvoluted band data for [45]PF_6 in MeCN.

MeCN	IC (1)	IT (1)	IT (2)	IC (2)	IT (3)
ν /cm^{-1}	3000	4700	7200	9300	12000
$\Delta\nu_{1/2}$ /cm^{-1}	1600	2900	2500	2600	2500
Intensity	0.009	0.028	0.019	0.017	0.010

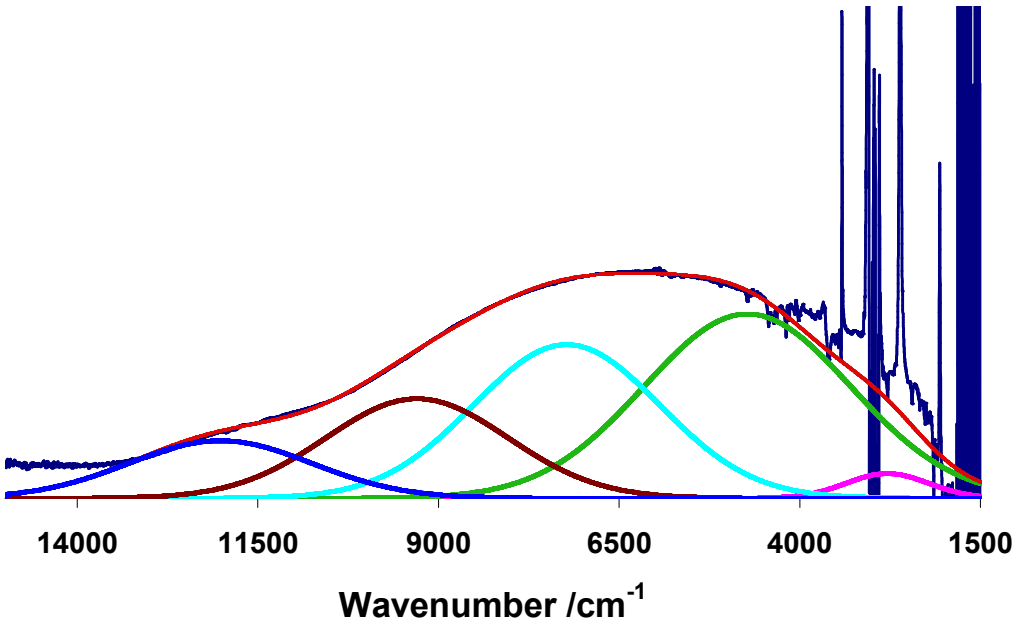

Figure 18: Gaussian deconvolution of the NIR band for [45]PF_6 recorded in acetone.

Table 14: Deconvoluted band data for [45]PF_6 in acetone.

Acetone	IC (1)	IT (1)	IT (2)	IC (2)	IT (3)
ν /cm^{-1}	2800	4700	7200	9300	12000
$\Delta\nu_{1/2}$ /cm^{-1}	1300	3400	3100	2900	3200
Intensity	0.005	0.037	0.031	0.0202	0.011

The solvatochromic behaviour of bands two, three and five identify these transitions as intervalence transitions, as described by Meyer (Figure 15), and bands one and four as the interconfigurational transitions. The apparent gain in intensities of the IC transitions is misleading, rather the IT transitions are losing intensity as the solvent medium changed. This is a consequence of the weak intensity of the band the IT transitions are of a similar intensity to the IC transitions.

The relationship between the three IVCT bands and the two interconfigurational bands is shown schematically in Figure 15. In an ideal system, the energy difference between IT(1) and IT(2) should equal IC(1), and the difference between IT(1) and IT(3) should equal IC(2) (Figure 19).

$$\lambda_{IT(2)} = \lambda_{IT(1)} + IC_{(1)}$$

$$\lambda_{IT(3)} = \lambda_{IT(1)} + IC_{(2)}$$

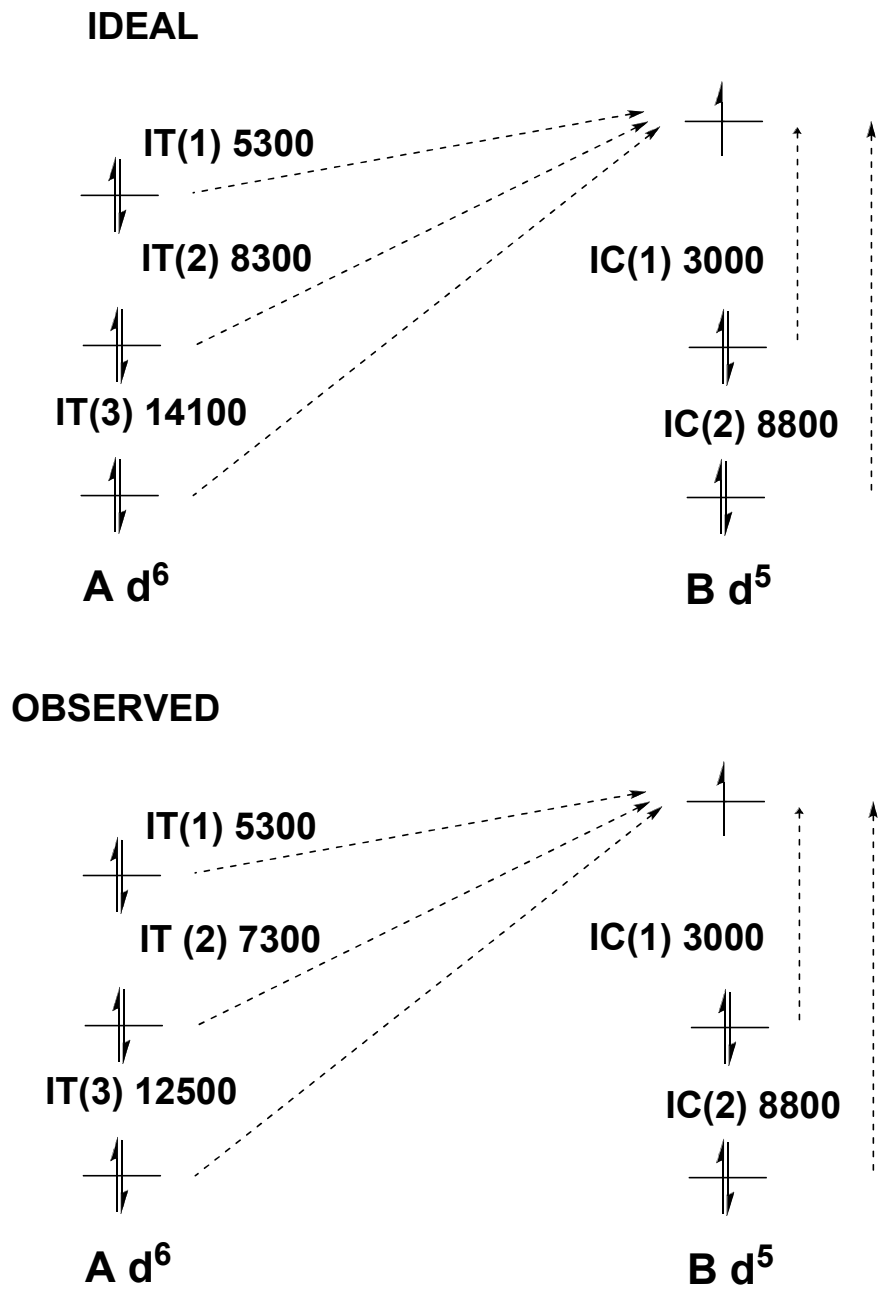

Figure 19: IT transition energy predictions and observed band energies observed for [45]PF_6 recorded in CH_2Cl_2.

From Figure 19 it can be concluded that the band assignments are correct and [**45**]PF_6 behaves as a near-ideal mixed valence system.

To support these assignments TD-DFT calculations on **45H**$^{+}$ were undertaken, as it has been shown that the use TD-DFT calculations can aid the allocation of the nature of the bands.[17] Analysis of the TD-DFT calculated spectrum of **45H**$^{+}$ reveals five transitions of low energy, less than 11000 cm^{-1}, which, upon careful analysis of the nature of each of the transitions, can be used to form a Meyer-type diagram of the transitions expected in the NIR region (Figure 20).

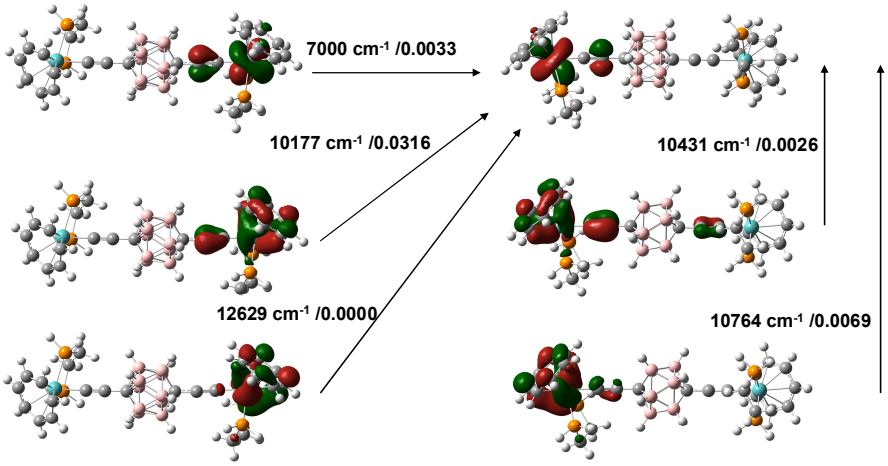

Figure 20: TD-DFT assignments for the first 5 electronic transitions (Molecular orbitals plotted as isosurfaces at 0.04 au) (Values displayed as calculated energy /oscillation strength).

Although the general picture correlates well with the spectroscopic results, the TD-DFT calculation fails in predicting the absolute energies of the transitions and their relative order. Despite this, the calculation models reproduce the relative energies of the IT transitions, where the energy differences between the calculated IT bands correlate well with the observed IC transitions (IT(1)/(2) = 3177 cm^{-1} and IT(1)/(3) = 5829 cm^{-1}), giving similar results to that shown in Figure 19.

From the plots of the molecular orbitals it is clear that the carborane cage does not allow any mixing between the two Mo(dppe)(η^7-C_7H_7) moieties via a high lying π-conjugated system, this acts to remove the bridge, at least electronically, from taking part in the charge transfer process. In addition, the lack of any hyperfine coupling from the carborane cage protons to the electron in the EPR spectrum of **45**$^+$ and the lack of movement of ν(BH) upon oxidation of **45**, further indicate that the carborane cage, $C_2B_{10}H_{10}$, is merely a spectator in this process, acting as an electronically inert linker between the two electrophores. The absence of the bridge taking part in the electronic transitions allows the simple Marcus-Hush two state model to accurately describe the characteristics of the charge transfer process.[30] The solvatochromic behaviour of the NIR band and the TD-DFT calculations indicate that **45**$^+$ has an electronically localised ground state.

The thorough identification of a localised electronic ground state coupled with the assumption that all the vibrational motions which are coupled to the charge transfer are harmonic and that **45**$^+$ is essentially symmetrical, which is entirely plausible for **45**$^+$, allows classical equations describing the charge transfer process to be used.[31] The predicted band widths ($\Delta\nu_{1/2}$) of **45**$^+$ in the different solvent media (Table 15) have been calculated. The lowest energy band, IT(1), is taken as being the principle intervalence charge transfer, IVCT, agrees with Hush's relationships derived for weakly coupled mixed valence systems based on a point charge (two state) model.

$$\Delta\nu_{1/2} = \sqrt{2310\nu_{\max}}$$

Table 15: Calculated and observed band widths for IT(1) recorded in various solvents.

Solvent	Observed IT(1) $\Delta\nu_{1/2}$ /cm^{-1}	Calculated IT(1) $\Delta\nu_{1/2}$ /cm^{-1}
CH_2Cl_2	3200	3500
MeCN	2900	3300
Acetone	3400	3300

This good agreement allows Hush analysis to be correctly used for this system, and physically meaningful estimates of the properties associated with the charge transfer process to be determined.

The low thermodynamic stability of **45**$^+$ with respect to disproportionation requires the concentration of the monocation to be re-calculated, so as to account for the neutral and di-cation components in the solution. At the equilibrium

$$[A] + [A^{2+}] \Leftrightarrow 2[A^+]$$

therefore,

$$K_c = \frac{[A^+]^2}{[A] + [A^{2+}]}$$

Assuming that the concentration of [A] is equal to that of [A^{2+}] (assumed [A_{org}], the original concentration), allows the unknown concentration of [A^{+}] to be calculated

$$K_c = \frac{x^2}{([A_{org}] - x)^2} \qquad \text{(where } [A^+] = x)$$

Solving the resulting quadratic equation gives [A^{+}] in CH_2Cl_2 as 0.0071 moldm^{-3}, and therefore the corrected extinction coefficient for the lowest energy IT band to be 260 dm^{3}mol^{-1}cm^{-1} (Table 12). Using this information an accurate value for the H_{ab} can be calculated for IT(1) using the standard Hush euqation

$$H_{ab} = \frac{\sqrt{(4.2x10^{-4})\varepsilon.\Delta\nu_{1/2}.\nu_{\max}}}{d}$$

From previous experimental and computational results, it has been established the oxidation takes via an almost exclusively metal centered orbital. Therefore using the distance between the two metal centres is a sensible method to estimate the electron transfer distance. Both crystallographic and computationally determined Mo-Mo distances, (12.678 Å and 12.622 Å respectively) have been used to establish H_{ab}, providing the same value (H_{ab} = 108). This value provides a potential energy plot of the electronic ground state as two well separated, deep wells.

As we have assumed the system to be operating on near classical terms the rate constant of charge transfer, k_{ET}, can be determined. The ΔG^o can be determined from the electrochemical results (ΔG^o = 1219 cm^{-1}).

$$\Delta G^o = \frac{(\lambda - 2H_{ab})^2}{4\lambda}$$

$$k_{ET} = \nu_n \exp - \left(\frac{\Delta G^*}{RT}\right)$$

Using this value and where the nuclear vibration frequency (ν_n) is 10^{12} s^{-1}, the upper limit for k_{ET} is calculated as 2.8 x 10^{-9} s^{-1}, which helps explain the nature of the EPR and infrared spectrum for **45**$^+$. The calculated upper k_{ET} value is slower than the X-band EPR timescale (ca. 10^{-9} s) therefore the spectrum only shows the electron residing on one [Mo(dppe)(η^7-C_7H_7)] centre, i.e. it is localised on this timescale. It is also slower on the infrared timescale (10^{-12} s) and therefore localised electronic behaviour should be observed by the presence of two ν(C≡C), or in the case of **45**$^+$, a broader ν(C≡C) stretch.

For **42**$^+$ the correlation between experimental and theoretical determined band widths is poor in comparison, $\Delta\nu_{1/2}$ (theoretical) = 3410 cm^{-1} and $\Delta\nu_{1/2}$ (experimental) = 5040 cm^{-1}.[15] This is most likely due to the [Ru(dppe)(η^5-C_5Me_5)] centre mixing heavily with the diethynyl carborane bridge. The mixing of the bridge with the metal moiety, adds ambiguity to the electronic origin of the charge transfer process, therefore requiring a more complex theoretical model to interpret the process. This mixing of the metal end caps with the bridging ligand is a common feature among many mixed valence organometallic complexes, therefore care must be taken when interpreting the charge transfer process using the classical two state model, unless the assignment of the exact location of the electron can be established.

4.12 Conclusion

The synthetic routes developed in Chapters two and three have been extended towards the synthesis of the novel carborane containing complexes, **44**, **45** and **50**. Of which **44** and **45** have been modelled computationally and studied rigorously via spectroelectrochemical techniques to thoroughly understand their respective electronic structures. The good stability of [**45**]PF_6 and the use of TD-DFT methods to unravel the NIR region of the spectrum, has allowed an in-depth study of the mixed valence complex, and has demonstrated that $\mathbf{44}^+$ has a very localised electronic structure. A combination of the lack of mixing of the [Mo(dppe)(η^7-C_7H_7)] end cap with the chain and known electronic neutrality of the ethynyl carborane bridge, has allowed the charge transfer properties of $\mathbf{45}^+$ to be meticulously explored using a classical interpretation of charge transfer.

4.13 Preparations

4.13.1 General Procedures

General experimental procedures have been described in Chapter two. The ethynylcarboranes $Me_3SiC{\equiv}C(C_2B_{10}H_{11})$ (**46**) $Me_3SiC{\equiv}C(C_2B_{10}H_{10})C{\equiv}CSiMe_3$ (**48**) $HC{\equiv}C(C_2B_{10}H_{10})C{\equiv}CH$ (**49**) were prepared by standard methods.[11a,11b] All Infrared spectra were recorded at 1 cm^{-1} and obtained on a Nicolet Avatar spectrometers.

4.13.1.1 Preparation of $[Mo(C{\equiv}CC_2B_{10}H_{11})(dppe)(\eta^7\text{-}C_7H_7)]$, 44.

A solution of **5** (100 mg, 0.150 mmol), KF (13 mg, 0.225 mmol), and **46** (35 mg, 0.152 mmol) in methanol (20 cm^3) was heated at reflux for two days, where a light brown solid precipitated from the solution. The solution was removed by decantation and the brown solid was dried under vacuum. (80 mg, 65 %). ^1H $\{^{11}B\}$ NMR (CD_2Cl_2) δ: 1.80 (s, 10H, BH), 2.17 (m, 2H, CH_2), 2.25 (s, 1H, $B_{10}H_{10}\underline{C}\mathit{H}$), 2.35 (m, 2H, CH_2), 4.61 (s, 7H, C_7H_7), 7.17 – 7.68 (m, 20H, Ph). ^{31}P NMR (CD_2Cl_2) δ: 66.1 (s, dppe). ^{11}B NMR (CD_2Cl_2) δ: -11.6 (s, $C\underline{\mathit{B}}_5H_5B_5H_5CH$), -16.5 (s, $CB_5H_5\underline{\mathit{B}}_5H_5CH$). ^{13}C NMR (CD_2Cl_2) δ: 27.0 (m, CH_2), 54.8 (s, $CB_{10}H_{10}\underline{C}H$), 87.2 (s, C_7H_7), 115.3 (s, $\underline{C}B_{10}H_{10}CH$), 128.2 (m, Ph_m), 128.8 (s, Ph_p), 128.8 (t, J_{CP} = 19 Hz, C_1), 129.5 (s, Ph_p), 131.4 (dd, $\boldsymbol{J}_{CP}$ = 4.8 Hz, Ph_o), 132.9 (t, $\boldsymbol{J}_{CP}$ = 9.5 Hz, C_2), 134.1 (dd, $\boldsymbol{J}_{CP}$ = 6.2 Hz, Ph_o), 135.7 (m, Ph_i), 141.4 (m, Ph_i). IR (CH_2Cl_2) ν(C≡C) 2065 cm^{-1}; ν(B-H) 2608 cm^{-1}. Accurate mass, ES(+)-MS (*m/z*) 755.28725 Calculated for $[\{Mo(C{\equiv}CC_2B_{10}H_{11})(dppe)(\eta^7\text{-}C_7H_7)\} + 2H]$ 755.2985. Crystal data: M = 0.2 x 0.14 x 0.14 mm^3, , space group $P2_{1/n}$ (No. 0), V = 3670.22(13)

Å^3, Z = 4, F_{000} = 1544, T = 120(2) K, 46711 reflections collected, unique (R_{int} = 0.0555). Final *GooF* = 1.039, *R1* = 0.0567, *wR2* = 0.1060.

4.13.1.2 Preparation of [Mo{C≡C($C_2B_{10}H_{10}$)C≡CH}(dppe)(η^7-C_7H_7)], 50.

A solution of **5** (100 mg, 0.150 mmol), KO^{t}Bu (50 mg, 0.446 mmol), $NaPF_6$ (34 mg, 0.202 mmol) and **49** (29 mg, 0.150 mmol) in methanol (20 cm^3) was heated at reflux for 24 hours. The brown precipitate, a mixture of mono- and di-metallated carborane, was separated by filtration and the brown methanol solution was allowed to slowly evaporate, forming the light brown crystalline product. (24 mg, 21 %). ^{1}H {^{11}B} NMR (CD_2Cl_2) δ: 1.79 (s, 10H, BH), 2.20 (m, 2H, CH_2), 2.33 (m, 2H, CH_2), 3.44 (s, 1H, C≡CH), 4.62 (s, 7H, C_7H_7), 7.19-7.69 (m, 20H, Ph). ^{31}P NMR (CD_2Cl_2) δ: 66.3 (s, dppe). ^{11}B NMR (CD_2Cl_2) δ: -11.8 (s, C$\underline{B}_5H_5B_5H_5$CH), -13.3 (s, $CB_5H_5\underline{B}_5H_5$CH). ^{13}C NMR ($CD_2Cl_2$) δ: 27.0 (m, CH_2), 58.3 (s, $CB_{10}H_{10}\underline{C}$H), 66.6 (s, C≡$\underline{C}$H), 80.7 (s, $\underline{C}$≡CH), 87.3 (s, C_7H_7), 115.2 (s, $\underline{C}B_{10}H_{10}$C≡CH), 128.2 (m, Ph_m), 128.8 (s, Ph_p), 129.6 (s, Ph_p), 131.4 (dd, $\boldsymbol{J}_{CP}$ = 5 Hz, Ph_o), 134.1 (dd, $\boldsymbol{J}_{CP}$ = 6 Hz, Ph_o), 135.5 (m, Ph_i), 141.4 (m, Ph_i). IR (CH_2Cl_2) ν(C≡C) 2064 cm^{-1}, ν(B-H) 2612 cm^{-1}, ν(CH) 3298 cm^{-1}.

4.13.1.3 Preparation of [{Mo(dppe)(η^7-C_7H_7)}$_2${μ-C≡C($C_2B_{10}H_{10}$)C≡C}], 45.

A solution of **5** (100 mg 0.150 mmol), **49** (29 mg, 0.150 mmol), $NaPF_6$ (20 mg, 0.117 mmol) and KO^{t}Bu (35 mg, 0.312 mmol) in methanol (20 cm^3) was heated at reflux for 4 hours. The brown precipitate formed, a mixture of mono and di-metallated carborane, was separated by filtration. Due to the inherent difficulties in separating molybdenum cycloheptarienyl complexes this crude material is used in the subsequent step. A solution of the crude monometallic material (85 mg, 0.109 mmol), **5** (80 mg, 0.120 mmol), KO^{t}Bu (24 mg, 0.218 mmol) and $NaPF_6$ (37 mg, 0.218 mmol) in methanol (20 cm^3) was heated at reflux for 6 hours. Upon cooling of the solution a brown precipitate forms which is isolated by filtration and dried under vacuum. (89 mg, 81 %). ^{1}H {^{11}B} NMR (CD_2Cl_2) δ: 1.43 (s, 10H, BH), 2.08-2.14 (m, 2H, CH_2), 2.27-2.33 (m, 2H, CH_2), 4.56 (t, J_{HH} = 2 Hz, 7H, C_7H_7), 7.14-7.62 (m, 40H, Ph). ^{31}P NMR (CD_2Cl_2) δ: 65.8 (s, dppe). ^{11}B NMR (CD_2Cl_2) δ: -13.9 (s, BH). ^{13}C NMR (CD_2Cl_2) δ: 27.0 (s, CH_2), 87.4 (s, $C_{7\eta}{}^{7}$-C7H7)), 115.7 (s, $\underline{C}B_{10}H_{10}$), 127.1 (t, $\boldsymbol{J}_{CP}$ = 26 Hz, C_a), 128.2 (m, Ph_m), 128.8 (s, Ph_p), 129.5 (s, Ph_p), 131.6 (dd, $\boldsymbol{J}_{CP}$ = 5 Hz, Ph_o), 134.2 (dd, $\boldsymbol{J}_{CP}$ = 6 Hz, Ph_o), 136.1 (m, Ph_i), 141.6 (m, Ph_i) (Note neither the C_1 or C_2 resonances were observed). IR (CH_2Cl_2) ν(C≡C) 2064 cm^{-1}, ν(BH) 2603 cm^{-1}. Accurate mass, ES(+)-MS (*m/z*) 1361.37563 Calculated for [{Mo(dppe)(η^7-C_7H_7)}$_2${μ-C≡C($C_2B_{10}H_{10}$)C≡C}]$^+$ 1361.37189. Crystal data: M = 0.26 x 0.18 x 0.05 mm^3, space group $P2_{1/n}$ (No. 0), V = 3910.9(3) Å^3, Z = 2, F_{000} = 1732, T = 120(2) K, 54095 reflections collected, unique (R_{int} = 0.0506). Final *GooF* = 1.037, *R1* = 0.0550, *wR2* = 0.0944.

4.13.1.4 Preparation of [{Mo(dppe)(η^7-C_7H_7)}$_2$(μ-C≡C($C_2B_{10}H_{10}$)C≡C)]PF_6, [45]PF_6

A solution of **1** (137 mg, 0.101 mmol) and [Fe(η^5-C_5H_5)$_2$][PF_6] (33 mg, 0.101 mmol) in CH_2Cl_2 (15 cm^3) was stirred at room temperature for 30 minutes, after which the brown solution was reduced to 5 cm^3, and Et_2O (25 cm^3) added. The resulting light brown precipitate was collected on a sintered glass funnel and dried under vacuum, (119 mg, 78 %). IR /NIR (CH_2Cl_2): ν(C≡C) 2065 cm^{-1}, ν(B-H) 2609 cm^{-1}, plus a broad band at 6000 cm^{-1}. Anal. Calcd. (%) for [**45**]PF_6. 2.0. CH_2Cl_2: C; 53.03 %, H; 4.57. Collected: C; 52.97, H; 4.10.

4.13.2 Computational Details

All calculations were carried out using the Gaussian 03 package.[32] The model geometries **44H^{n+}** and **45H^{n+}** (n = 0, 1 or 2) discussed here were optimised using MPW1K[33], with no symmetry constraints. The pseudo-potential LANL2DZ[34] was used for all atoms. Frequency calculations were carried out these optimised geometries at the corresponding levels and shown to have no imaginary frequencies (apart from **44H$^+$**). Molecular orbital and TD-DFT computations were carried out on these optimised geometries at the same level of theory and the orbital contributions were generated with the aid of the GaussSum.[35]

4.13.3 Crystallography

See Chapter two for details.

4.14 References

[1] (a) M.I. Bruce, P.J. Low, *Adv. Organomet. Chem.,* 2001, **48**, 71. (b) M.I. Bruce, P.J. Low, *Adv. Organomet. Chem.,* 2004, **50**, 17 (and references within). (c) P.J. Low, R.L. Roberts, R.L. Cordiner, F. Hartl, *J. Solid. State. Electrochem.,* 2005, **9**, 717.

[2] (a) F. Bertini, L. Calucci, F. Cicogna, B. Gaddi, G. Ingrosso, M. Marcaccio, F. Marchetti, D. Paolucci, F. Paolucci, C. Pinzino, *J. Organomet. Chem.,* 2006, **691**, 2987. (b) N. Vila, Y-W. Zhong, J.C. Henderson, H.D. Abruna, *Inorg. Chem.,* 2010, **49**, 796. (c) S.I. Ghazala, F. Paul. L. Toupet, T. Roisnel, P. Hapiot, C. Lapinte, *J. Am. Chem. Soc.,* 2006, **128**, 2463. (d) O. Lavastre, J. Plass, P. Bachmann, S. Gusemi, C. Moinet, P.H. Dixneuf, *Organometallics,* 1997, **16**, 184. (e) D. Beljonne, P.R. Raithby, R.H. Friend, J.L. Bredas, *Synth. Met.,* 1996, **81**, 179. (f) S.K. Hurst, M.P. Cifuentes, A.M. McDonagh, M.G. Humphrey, M. Samoc, B. Luther-Davies, I. Asselberghs, A. Persoons, *J. Organomet. Chem.,* 2002, **642**, 259. (g) F. Paul, A. Bondon, G. de Costa, F. Malvolti, S. Sinbandhit, O. Cador, K. Costuas, L. Toupet, M.L. Boillot, *Inorg. Chem.,* 2009, **48**, 10608.

[3] (a) S. Roue, C. Lapinte, *J. Organomet. Chem.,* 2005, **690**, 594. (b) S. Roue, S. Le Stang, L. Toupet, C. Lapinte, *C. R. Chimie.,* 2003, **6**, 353.

[4] (a) S. Le Stang, D. Lenz, F. Paul, C. Lapinte, *J. Organomet. Chem.,* 1999, **572**, 189. (b) V. Mishra, F. Lloret, R. Mukherjee, *Eur. J. Inorg. Chem.,* 2007, **15**, 2161.

[5] J. Aihara, *J. Am. Chem. Soc.,* 1978, **100**, 3339.

[6] S. Khatua, J.M. Guerrero, K. Claytor, G. Vives, A.B. Kolomeisky, J.M. Tour, S. Link, *Nano,* 2009, **3**, 351.

[7] A. Herzog, S.S. Jalisatgi, C.B. Knobler, T.J. Wedge, M.F. Hawthorne, *Chem. Eur. J.,* 2005, **11**, 7155.

[8] (a) J. Abe, N. Nemoto, Y. Nagase, Y. Shirai, T. Iyoda, *Inorg. Chem.,* 1998, **37**, 172. (b) D.G. Allis, J.T. Spencer, *Inorg. Chem.,* 2001, **40**, 3373.

[9] (a)P. Kaszynski, S. Pakhomov, K.F. Tesh, V.G. Young Jr., *Inorg. Chem.,* 2001, **40**, 6622. (b) A.G. Douglass, K. Czuprynski, M. Mierzwa, P. Kaszynski, *J. Mater. Chem.,* 1998, **8**, 2391.

[10] E.L. Kreimann, M. Miura, M.E. Itoiz, E. Heber, R.N. Garavaglia, D. Batistoni, R.J. Rebagliati, M.J. Roberti, P.L. Micca, J.A. Coderre, A.E. Schwint, *Archives of Oral Biology,* 2003, **48**, 223.

[11] (a) M.A. Fox, T.E. Baines, D. Albesa-Jove, J.A.K. Howard, P.J. Low, *J. Organomet. Chem.,* 2006, **691**, 3889. (b) A.S. Batsanov, M.A. Fox, J.A.K. Howard, J.A.H. MacBride, K. Wade, *J. Organomet. Chem.,* 2000, **610**, 20. (c) M.A. Fox, A.M. Cameron, P.J. Low, M.A.J. Paterson, A.S. Batsanov, A.E. Goeta, D.W.H. Rankin, H.E. Robertson, J.T. Schirlin, *Dalton. Trans.,* 2006, 3544.

[12] H. Jude, H. Disteldorf, S. Fischer, T. Wedge, A.M. Hawkridge, A.M. Arif, M.F. Hawthorne, D.C. Muddiman, P.J. Stang, *J. Am. Chem. Soc.,* 2005, **127**, 12131.

[13] J. Vicente, M-T. Chicote, M.M. Alvarez-Falcon, M.A. Fox, D. Bautista, *Organometallics,* 2003, **22**, 4792.

[14] (a) T.J. Wedge, A. Herzog, R. Huertas, M.W. Lee, C.B. Knobler, M.F. Hathorne, *Organometallics,* 2004, **23**, 482. (b) T.W. Bitner, T.J. Wedge, M.F. Hawthorne, J.I. Zink, *Inorg. Chem.,* 2001, **40**, 5428.

[15] M.A. Fox, J.A.H. MacBride, R.J. Peace, K. Wade, *Dalton. Trans.,* 1998, 401.

[16] (a) M.A. Fox, A.J. Paterson, C. Nervi, F. Galeotti, H. Puschmann, J.A.K. Howard, P.J. Low, *Chem. Commun.,* 2001, 1610. (b) B. Le Guennic, K. Costuas, J-F. Halet, C.

Nervi, M.A.J. Paterson, M.A. Fox, R.L. Roberts, D. Albesa-Jove, H. Puschmann, J.A.K. Howard, P.J. Low, *C.R. Chimie,* 2005, **8**, 1883.
[17] M.A. Fox, R.L. Roberts, T.E. Baines, B. Le Guennic, J-F. Halet, F. Hartl, D.S. Yufit, D. Albesa-Jove, J.A.K. Howard, P.J. Low, *J. Am. Chem. Soc.,* 2008, **130**, 3566.
[18] R. Gleiter, K-H Pfeifer, G. Szeimies, U. Bunz, *Angew. Chem. Int. Ed.,* 1990, **29**, 413.
[19] N.J. Brown, D. Collison, R. Edge, E.C. Fitzgerald, M. Helliwell, J.A.K. Howard, H.N. Lancashire, P.J. Low, J.J.W. McDouall, J. Raferty, C.A. Smith, D.S. Yufit, M.W. Whiteley, *Organometallics,* 2010, **29**, 1261.
[20] S. Hermanek, *Chem. Rev.,* 1992, **92**, 325.
[21] F. Barriere, N. Camire, W.E. Geiger, U.T. Mueller-Westerhoff, R. Sanders, *J. Am. Chem. Soc.,* 2002, **124**, 7262.
[22] E.A. Fellow, F.R. Keene, *J. Phys. Chem. B.,* 2007, **111**, 6667.
[23] M.I. Bruce, P.J. Low, K. Costuas, J-F. Halet, S.P. Best, G.A. Heath, *J. Am. Chem. Soc.,* 2000, **122**, 1949.
[24] N. Le Narvor, L. Toupet, C. Lapinte, *J. Am. Chem. Soc.,* 1995, **117**, 7129.
[25] M.I. Bruce, K. Costuas, T. Davin, J-F. Halet, K.A. Kramarczuk, P.J. Low, B.K. Nicholson, G.J. Perkins, R.L. Roberts, B.W. Skelton, M.E. Smith, A.H. White, *Dalton. Trans.,* 2007, 5387.
[26] M. Brady, W. Weng, Y. Zhou, J.W. Seyler, A.J. Amoroso, A.M. Arif, M. Bohme, G. Frenking, J.A. Gladysz, *J. Am. Chem. Soc.,* 1997, **119**, 775.
[27] S.B Piepho, E.R. Krausz, P.N. Schatz, *J. Am. Chem. Soc.,* 1978, **100**, 2996.
[28] R.D. Markwell, I.S. Butler, A.K. Kakkar, M.S. Khan, Z.H. Al-Zakwani, J. Lewis, *Organometallics,* 1996, **15**, 2331.
[29] K.D. Demadis, C.M. Hartshorn, T.J. Meyer, *Chem. Rev.,* 2001, **101**, 2655.
[30] B.S. Brunschwig, C. Creutz, N. Sutin, *Coord. Chem. Rev.,* 1998, **177**, 61.
[31] C. Creutz, *Prog. Inorg. Chem.,* 1983, **30**, 1.
[32] M.J. Frisch, G.W. Trucks, H.B. Schlegel, G.E. Scuseria, M.A. Robb, J.R. Cheeseman, J.A. Montgomery Jr., T. Vreven, K.N. Kudin, J.C. Burant, J.M. Millam, S.S. Iyengar, J. Tomasi, V. Barone, B. Mennucci, M. Cossi, G. Scalmani, N. Rega, G.A. Petersson, H. Nakatsuji, M. Hada, M. Ehara, K. Toyota, R. Fukuda, J. Hasegawa, M. Ishida, T. Nakajima, Y. Honda, O. Kitao, H. Nakai, M. Klene, X. Li, J.E. Knox, H.P. Hratchian, J.B. Cross, C. Adamo, J. Jaramillo, R. Gomperts, R.E. Stratmann, O. Yazyev, A.J. Austin, R. Cammi, C. Pomelli, J.W. Ochterski, P.Y. Ayala, K. Morokuma, G.A. Voth, P. Salvador, J.J. Dannenberg, V.G. Zakrzewski, S. Dapprich, A.D. Daniels, M.C. Strain, O. Farkas, D.K. Malick, A.D. Rabuck, K. Raghavachari, J.B. Foresman, J.V. Ortiz, Q. Cui, A.G. Baboul, S. Clifford, J. Cioslowski, B.B. Stefanov, G. Liu, A. Liashenko, P. Piskorz, I. Komaromi, R.L. Martin, D.J. Fox, T. Keith, M.A. Al-Laham, C.Y. Peng, A. Nanayakkara, M. Challa- combe, P.M.W. Gill, B. Johnson, W. Chen, M.W. Wong, C. Gonzalez, J.A. Pople, GAUSSIAN 03, Revision C.02, Gaussian Inc., Wallingford, CT, 2004.
[33] (a) B.J. Lynch, P.L. Fast, M. Harris, D.G. Truhlar, *J. Phys. Chem. A.,* 2000, **104**, 4811. (b) B.J. Lynch, Y. Zhao, D.G. Truhlar, *J. Phys. Chem. A.,* 2003, **107**, 1384. (c) G.A. Petersson, M.A. Al-Laham, *J. Chem. Phys.,* 1991, **94**, 6081. (d) G.A. Petersson, A. Bennett, T.G. Tensfeldt, M.A. Al-Laham, W.A. Shirley, J. Mantzaris, *J. Chem. Phys.,* 1988, **89**, 2193.
[34] (a) P.J. Hay, W.R. Wadt, *J. Chem. Phys.,* 1985, **82**, 270. (b) W.R. Wadt, P.J. Hay, *J. Chem. Phys.,* 1985, **82**, 284. (c) P.J. Hay, W.R. Wadt, *J. Chem. Phys.,* 1985, **82**, 299.

[35] N.M. O'Boyle, A.L. Tenderholt, K.M. Langner, *J. Computational. Chem.,* 2007, **5**, 839.

Chapter 5: Synthesis, Spectroscopy and Electronic Structure of $[\{Mo(dppe)(\eta^7\text{-}C_7H_7)\}_2(\mu\text{-}C{\equiv}CC{\equiv}C)]^{n+}$ (n = 0, 1, 2)

5.1 Introduction

Chains of *sp*-hybridised carbon represent the most basic and fundamental bridges available to organometallic chemists in their studies of $\{L_xM^n\}(\mu\text{-bridge})\{M^{n+1}L_x\}$ mixed valence complexes.[1] The most accessible and well studied of these *sp*-hybridised chains of carbon is the simple four carbon chain, $[C{\equiv}CC{\equiv}C]^{2-}$. By linking two metal fragments via a four carbon chain, multiple redox states can be accessed, with the chain adopting various bonding modes from acetylenic to cummulenic and carbyne bonding (Figure 1).[2] The bridge and metal fragments work in synergy with one another; the metal moieties stabilise the bonding of the bridge, and the bridge helps stabilise the higher oxidation state of the metal moiety.

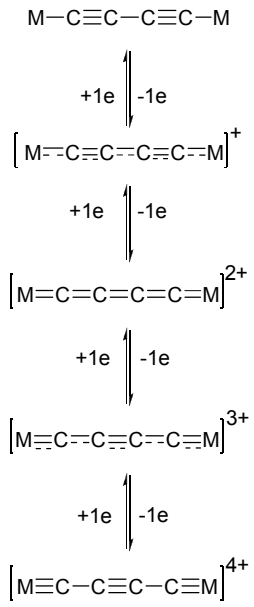

Figure 1: Resonance forms of a generic MC≡CC≡CM compound in different oxidation states.

The vast number of complexes ($[\{L_nM\}_2(\mu\text{-}C{\equiv}CC{\equiv}C)]^{n+}$) containing the four carbon bridge that are known, have been prepared from a similarly vast number of synthetic methodologies. The simplest of these involves the direct coupling of two metal fragments to a four carbon synthon. The Cu(I) catalysed coupling of diacetylene ($HC{\equiv}CC{\equiv}CH$) to $[MoI(CO)_3(\eta^5\text{-}C_5H_5)]$ and $[WCl(CO)_3(\eta^5\text{-}C_5R_5)]$ (R = H, Me)[3] have been used to prepare both diynyl and diyndiyl complexes. Direct coupling of $[Pt(OH)(CH_3)(COD)]$ to diacetylene can be achieved with the loss of water at room temperature.[4] Protected four carbon synthons can be coupled to metal fragments using conventional methods. For example, tin reagents, $Me_3SnC{\equiv}CC{\equiv}CSnMe_3$, in combination with Stille coupling regimes, have been used with $[MnX(dmpe)_2(C_6H_4Me)]$,[5] $[RhL_2\{{=}C{=}CR(H)\}]$[6] and $[PtX_2(PBu_3)_2]$[7] moieties. In addition, the use of fluoride anion desilyation with $Me_3SiC{\equiv}CC{\equiv}CSiMe_3$ has seen success in synthesizing butadiylnyl complexes containing $[RuClL_2(\eta^5\text{-}C_5H_5)]$[8] (Scheme 1), $[FeCl(dppe)(\eta^5\text{-}C_5Me_5)]$[9] and $[RhCl(CO)(P^iPr_3)_2]$ metal fragments.[10]

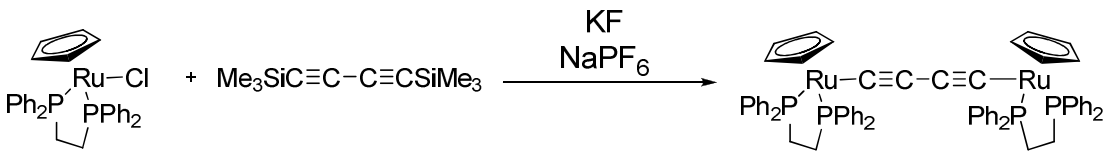

Scheme 1: Synthesis of MC≡CC≡CM compound using a diacetylene synthon.

Alternatively, butadiyndiyl bridged complexes can be made from organometallic synthons. The Glaser-type coupling of $[Re(C{\equiv}CH)(^t\text{Bu-bipy})(CO)_3]$[11] or $[Re(C{\equiv}CH)(NO)(PPh_3)(\eta^5\text{-}C_5Me_5)]$,[12] readily produces the four carbon bridged complexes. Equally, the *in situ* deprotonation of $[Fe(C{\equiv}CC{\equiv}H)(CO)_2(\eta^5\text{-}C_5H_5)]$ with KO^tBu and its reaction with $[FeCl(dppe)(\eta^5\text{-}C_5Me_5)]$ yields the bimetallic complex

[{Fe(CO)$_2$(η^5-C$_5$H$_5$)}(μ-C≡CC≡C){Fe(dppe)(η^5-C$_5$Me$_5$)}].[13] Similarly the lithiated reagent, [Fe(C≡CC≡CLi)(CO)$_2$(η^5-C$_5$H$_5$)], reacts with metal halide complexes to form the corresponding bimetallic complexes,[14] this is the method of choice for many electron-rich complexes. For example those containing [Fe(dppe)(η^5-C$_5$Me$_5$)],[15] [Ru(dppe)(η^5-C$_5$Me$_5$)],[16] [Os(dppe)(η^5-C$_5$Me$_5$)][17] and [Mn(C≡CH)(dmpe)$_2$][18] moieties is by the generation of a radical cation, [M(C≡CH)L$_5$]$^{+\cdot}$, and homo-coupling at C$_2$ with itself or coupling with an equivalent of the neutral acetylide, followed by the deprotonation of the bisvinylidene product. This method generally produces the bimetallic complex in good yield (Scheme 2).

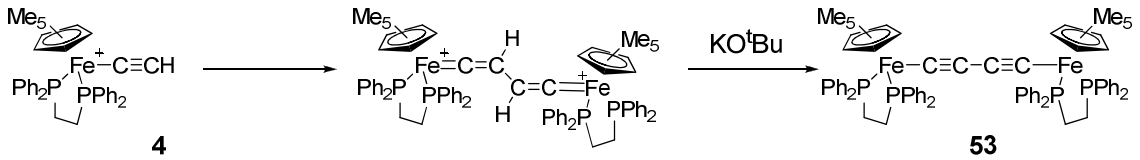

Scheme 2: Synthesis of 53 using radical coupling methodology.

A number of theoretical investigations have been carried out on butadiyndiyl fragments, which have focused on Group eight and rhenium metal moieties, in an attempt to rationalize their electronic structures.[19] In all examples, the four carbon chain provides a π-conjugated conduit between metals at the C$_1$ and C$_4$ positions. The extent to which the electronic structure is delocalised over the chain, and the bonding formalisms which the chain adopts, is dependant upon the identity of the metal fragment. The mixing between the metal d-orbitals and the bridge π-system is dependant upon their relative energies and symmetry considerations of the metal moieties.[20]

For example, ruthenium and iron complexes, [{M(dppe)(η^5-C$_5$Me$_5$)}(μ-C≡CC≡C)] (M = Fe (**53**), Ru (**52**)), whilst from the same group exhibit different character HOMOs,

with the iron having more metal character and the ruthenium possessing more bridge character.[21] Depending on the basis set used for the calculation, **53** has between 38 % (STO-3G) and 44 % (LANL2DZ) contribution from the Fe centre to the HOMO, whereas **52** has a much less metal character HOMO with only 27 % (STO-3G) contribution from the metal centre.[22] Lowering the energy of the metal d-orbitals also causes the frontier orbitals to exhibit significant ligand character, as shown in the rhenium example, [{Re(NO)(PPh_3)(η^5-C_5Me_5)}(μ-C≡CC≡C)] (**55**), where the rhenium character of the HOMO is 24 %.[21] The difference in character between the first and second row transition metals is due to the increasingly diffuse metal d-orbitals, which are able to mix more readily with the diynyl bridge thus, increasing the ligand character of the HOMO.

5.2 Synthesis

The synthesis of $\mathbf{57}^{n+}$ (n = 0, 1 or 2) was carried out by Dr. E.C. Fitzgerald at the University of Manchester, where the cationic derivatives have been isolated as the $[PF_6]^-$ salt, and is included here for completeness. Although, as described in the introduction, there are many routes to coupling two metal fragments to the butadiyndiyl bridge, only radical-radical coupling of molybdenum acetylides through the C_2 carbon proved viable for the [Mo(dppe)(η^7-C_7H_7)] metal fragment. The acetylide [Mo(C≡CH)(dppe)(η^7-C_7H_7)] (**56**), was first synthesised via the reaction of **5** with $HC{\equiv}CSiMe_3$ in the presence of a large excess of KO^{t}Bu. The generation of the radical cation (**56**$^+$) was achieved by the addition of [Fe(η^5-C_5H_5)$_2$][PF_6] to **56** at -78^{o}C, followed by the rapid formation of the bis-vinylidene product, [{Mo(dppe)(η^7-C_7H_7)}$_2${μ-(=C=CH-HC=C=}][PF_6]$_2$ ([**29**][PF_6]$_2$). The formation of bis-vinylidene complexes, such as **29**$^{2+}$, is common for [Mo(dppe)(η^7-C_7H_7)] alkynyl radical cations for reasons which have been explained in Chapters two and three. Subsequent deprotonation of **29**$^{2+}$ with KO^{t}Bu produces the desired butadiyndiyl bridged product as the mixed valence cation, [{Mo(dppe)(η^7-C_7H_7)}$_2$(μ-C≡CC≡C)]PF_6 ([**57**]PF_6) (Scheme 3).

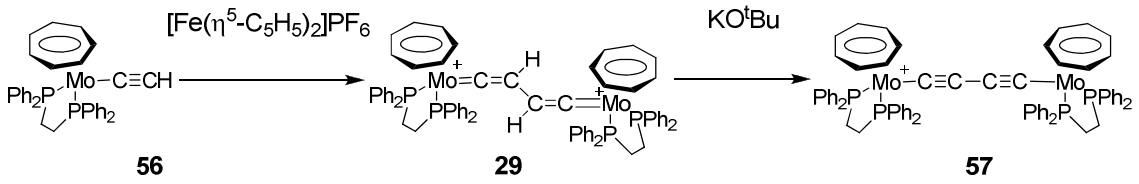

Scheme 3: Synthesis of 57.

The formation of **57** as the monocation from the deprotonation of [**29**][PF_6]$_2$, in contrast to the isolation of **52**[16] and **53**[15] via similar positions, is expected due to the low formal oxidation potentials of **57** (see below). The stability of the [Mo(dppe)(η^7-C_7H_7)] containing complexes with respect to oxidation has permitted the isolation of [**57**][PF_6]$_2$ as a slightly air sensitive emerald green solid, through the reaction of [**57**]PF_6 with [Fe(η^5-C_5H_5)$_2$][PF_6]. The isolation of **57** as the neutral species is possible by the reaction of [**57**]PF_6 with [Co(η^5-C_5H_5)$_2$], however, only limited amounts of material of sufficient purity was obtained.

5.3 Electrochemistry

Complex **57** exhibits four one-electron, diffusion controlled, chemically reversible, oxidation process under the conditions stated in Table 1, with the separation between the cathodic and anodic peak potentials comparable to that determined for the internal ferrocene standard.

Table 1: Cyclic voltammetry results recorded in 0.1 M ^{n}Bu$_4$NPF$_6$ /CH_2Cl_2 solutions at a Pt electrode, 298 K. All values referenced to FcH /FcH$^+$ = 0.00 V. [a] see reference 16.

Complex	$^1E_{1/2}$ /V	$^2E_{1/2}$ /V	$^3E_{1/2}$ /V	$^4E_{1/2}$ /V	ΔE_{12} /mV	K_c (ΔE_{12})
52[a]	-0.89	-0.24	0.58	1.05	650	1.5 x 10^{11}
53[a]	-1.135	-0.415	0.49	-	720	2.4 x 10^{12}
54	-1.08	-0.47	0.36	0.80	610	3.1 x 10^{10}
56	-0.71	-	-	-	-	-
57	-0.94	-0.51	+0.47	+0.54	434	2.5 x 10^7

An initial comparison of the bimetallic complex **57** with **56** and the phenyl molybdenum acetylide, **1**,[23] shows **57** is over 200 mV easier to oxidize than its monometallic counterparts. The monometallic precursor, [Mo(C≡CC≡CH)(dppe)(η^7-C_7H_7)] (**20**)[24] is 360 mV more difficult than to oxidise **57**. The ease at which the first

oxidation event occurs is a common trait amongst all butadiyndiyl bridged complexes (Table 1) and is due to the mixing of the bridge with the metal fragments.

The ΔE^o value between $^1E_{1/2}$ and $^2E_{1/2}$ is small in comparison to Group eight diyndiyl complexes, for example **57** (430 mV) and Group eight complexes (720 – 610 mV). This leads to a K_c value of $\mathbf{57}^+$ which is several orders of magnitude smaller than the iron, ruthenium and osmium analogues. This demonstrates that the mixed valence species, $\mathbf{57}^+$, is less thermodynamically stable than the Group eight examples. In comparison to other butadiyndiyl bridged organometallic complexes, $[\{MnI(dmpe)_2\}_2(\mu\text{-}C{\equiv}CC{\equiv}C)]^+$ **(58)** (K_c = 5.4 x 10^{10}),[25] $[\{Ru(PPh_3)_2(\eta^5\text{-}C_5H_5)\}_2(\mu\text{-}C{\equiv}CC{\equiv}C)]$ (**59**) (K_c = 1.5 x 10^{11}), $[\{Ru(PMe_3)_2(\eta\text{-}C_5H_5)\}_2(\mu\text{-}C{\equiv}CC{\equiv}C)]^+$ (**60**) (K_c = 2.1 x 10^{10})[22] and $[\{Re(NO)(PPh_3)\}_2(\mu\text{-}C{\equiv}CC{\equiv}C)]^+$ (**55**) (K_c = 1.1 x 10^9)[26] further illustrates the reduced thermodynamic stability of $\mathbf{57}^+$. However, in comparison to the carborane complex [**45**]PF_6 (K_c = 29), it is six orders of magnitudes larger.

Like the Group eight analogues, **57** exhibits two further oxidation events at higher potentials (corresponding to $\mathbf{57}^{3+}$ and $\mathbf{57}^{4+}$), which are separated by 70 mV, which is a small value in comparison to **52** (470 mV). This small value indicates that the electronic structure of these highly oxidised species is significantly different to one another. However, the ambiguity of cyclic voltammetry data does not provide electronic structure information and no further specific detail can be inferred from the result.

5.4 Infrared Spectroelectrochemistry

Although $\mathbf{57}^{+}$and $\mathbf{57}^{2+}$ have been obtained as chemically isolated samples, infrared spectroelectrochemical experiments were still carried out, in order to characterize **57** and the highly oxidised species $\mathbf{57}^{3+}$ and $\mathbf{57}^{4+}$, which could not be obtained through chemical oxidation techniques. However, attempts to generate the tri- and tetra-cationic species in the spectroelectrochemical cell were unsuccessful, with electrolysis accompanied by rapid decomposition (Table 2).

Table 2: Infrared spectroelectrochemical data, recorded in 0.1 M $^{n}Bu_4NPF_6$ /CH_2Cl_2 solutions using a modified OTTLE cell. [a] reference 16. [b] reference 15 . [c] reference 17 .

Complex	ν(C≡C) /cm^{-1}		
	n = 0	n = +1	n = +2
$\mathbf{52}^{n+}$ [a]	sh 1977, 1963	1860	1770
$\mathbf{53}^{n+}$ [b]	1955, 1880	1973, 1880	2160, 1950
$\mathbf{54}^{n+}$ [c]	sh 1975, 1965	1860	1781
$\mathbf{57}^{n+}$	-	1930, 1868	w 1727

Complex **57** behaves quite differently to the ruthenium and osmium butadiyndiyl complexes upon oxidation. The neutral species **57** is infrared silent, indicating that there is no dipole moment across the butadiyndiyl bridge. Upon oxidation to the dication species, $\mathbf{57}^{2+}$, a single low energy, low intenisty band around 1700 cm^{-1} is observed, which points towards a cummulenic structure, similar to that of $\mathbf{52}^{2+}$ and $\mathbf{54}^{2+}$. However, the low intensity of ν(C≡C) for $\mathbf{57}^{2+}$ indicates that there is a small dipole across the bridge structure. The absence of infrared data for **57** prompted resonance Raman spectroscopy investigation to help shed light upon their structural and electronic configuration.

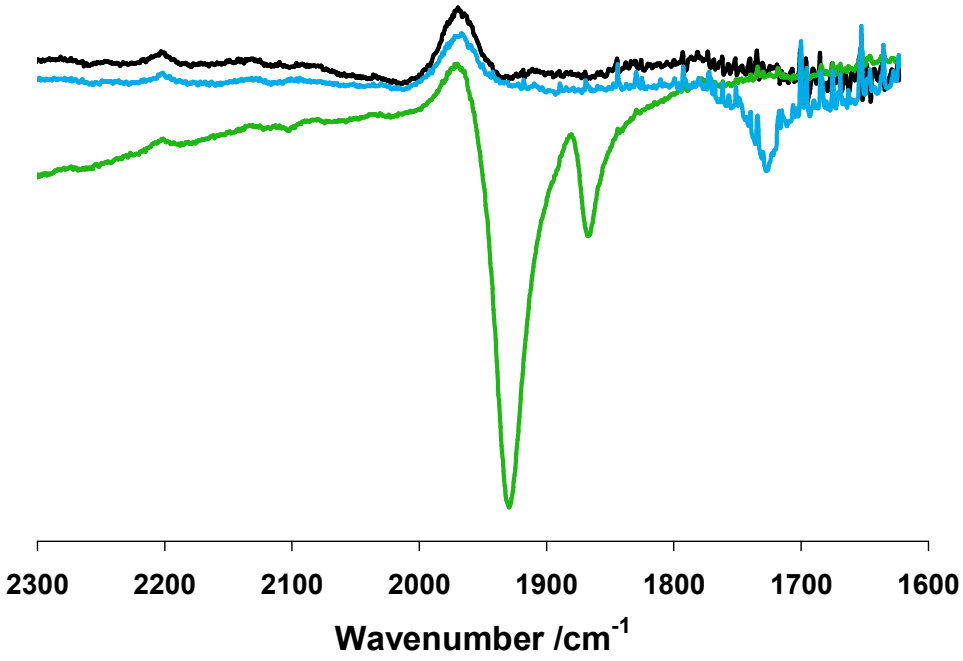

Figure 2: Infrared spectra for 57^{n+}, where n = 0 (Black), n = 1 (Green), n = 2 (Light blue) (Recorded in 0.1 M $^{n}Bu_4NPF_6$ /CH_2Cl_2).

The infrared spectrum of [**57**]PF_6 exhibits two strong ν(C≡C) stretches of different intensities with evidence of a tail from a relatively large, intense and broad electronic transition in the NIR region (Figure 2). The origin and nature of this NIR transition will be discussed in detail later in this Chapter. The presence of two ν(C≡C) bands for the monocation is evidence of a valence trapped electronic structure on the infrared timescale, which is also a feature seen for the iron anaolgue **53**$^+$, indicating that the electron transfer rate is slower than the infrared timescale. This is in contrast to **52**$^+$ and **54**$^+$ which both give a single intense ν(C≡C) band which is synonymous with an electronic structure that is delocalised on the infrared timescale. The difference in intensity of the ν(C≡C) bands of [**57**]PF_6 arises as a consequence of the coupling of the symmetric ν(C≡C) vibronic motion of the bridge with the charge transfer process.[27]

5.5 EPR Spectroscopy

Previous investigations using Mo(dppe)(η^7-C_7H_7) as the supporting metal fragment have shown EPR spectroscopy to be useful in the characterisation of the oxidised species. The EPR spectra of $\mathbf{57}^+$ and $\mathbf{57}^{2+}$ as $[PF_6]^-$ salts were kindly collected by Dr. E.C. Fitzgerald and are included here to aid the discussion of the properties of **57** (Table 3).

Earlier studies have used variable temperature EPR measurements to determine the electron transfer rate. This is done by measuring the activation barrier associated with thermal electron transfer and consequently the rate of electron transfer, however, this is only a viable concept for truly localised electronic structures which conform to a two-state approximation.[28] However, in these studies due to the mixing of the bridge with the metal fragment (evidence by the shift in ν(C≡C) bands upon oxidation) a two state approximation is not viable and therefore, the timescale of EPR spectroscopy is used as a guide to the rate of electron transfer.

X-Band EPR spectroscopy of the monometallic polyyne complexes supported by [Mo(dppe)(η^7-C_7H_7)] produces well resolved spectra which can be interpreted as the electron residing almost exclusively on the metal fragment. EPR measurements of [**57**][PF_6]$_2$ produced a well resolved spectrum resembling that of single [Mo(dppe)(η^7-C_7H_7)]$^{+\cdot}$ moieties and was similar to the spectrum obtained for $\mathbf{45}^{2+}$. These observations indicate that the electrons in [**57**]$^{2+}$ are localised on Mo(dppe)(η^7-C_7H_7) moieties with very little interaction between them, thus forming a diradical species.

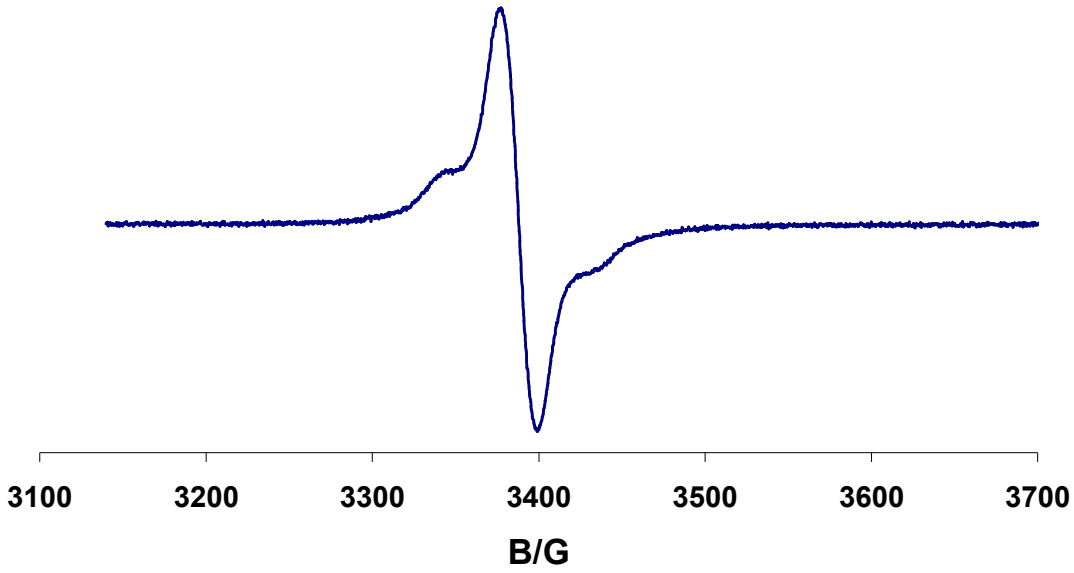

Figure 3: First derivative X-band EPR fluid solution (CH_2Cl_2, 243 K) of [57]PF_6.

Table 3: X-band EPR results recorded in CH_2Cl_2 at 243 K.

Complex	a_{iso} Mo /G	a_{iso} ^{31}P /G	a_{iso} ^{1}H(C_7H_7) /G	g_{iso} /G
[**57**$^{+}$]PF_6	16 (estimated)	-	-	-
[**57**$^{2+}$][PF_6]$_2$	32	23	4.3	1.996
1^{+}	31.3	22.6	4.3	1.996

Conversely, [**57**]PF_6 does not produce a well resolved spectrum (Figure 3). Unsuccessful attempts were made to resolve the spectrum by using variable temperature techniques and by changing the frequency of the EPR measurement. The presence of an unresolved spectrum and the lack of determinable hyperfines for the coupling to ^{31}P and ^{1}H atoms for the mixed valence complex (**57**$^{+}$), indicates that this is a system where the electron transfer rate is on a par with the timescale of the spectroscopic technique. Thus, the spectra represents a coalescence of the electron transfer rate with the spectroscopic technique. By combining the results from X- and S-band spectra an estimate of the a_{iso} Mo is determined to be 16 G. Which is one half of the value of the

typical value, indicating the electron is spread between the two metal fragments. Thus [**57**]PF_6 has delocalised electronic structure on this timescale. This result gives an estimate of the electron transfer rate comparable to that of EPR spectroscopy (10^{-8} – 10^{-9} s) which is much faster than the carborane **45**$^+$.

5.6 Electronic Structure Calculations

As has been shown in previous Chapters computational modeling can give a greater insight into the electronic structure of these molybdenum complexes and the mixing between the metal and ynyl-based ligand. The spectroscopic measurements of **[57**]PF_6 point towards a localised electronic structure for the monocation, and the functional and basis set was varied in order to replicate this localised electronic structure of **57**$^+$. Despite the testing of over 25 combinations including the coulomb attenuated CAM-B3LYP functional, heavily biased Hartree-Fock hybrid functionals and Hartree-Fock computations, a localised electronic structure could not be satisfactorily modelled. The functional and basis set used to model **57** and **57**$^{2+}$ were chosen so as to compliment that found in the literature and also provide cost effective computational effort, therefore the combination of the common hybrid functional B3LYP and the frozen core basis set LANL2DZ was chosen. To reduce the computation time, the dppe ligands were reduced to dHpe and the geometries of [{Mo(dHpe)(η^7-C_7H_7)}$_2$(μ-C≡CC≡C)] (**57H**), and [{Mo(dHpe)(η^7-C_7H_7)}$_2$(μ-C≡CC≡C)]$^{2+}$ (**57H**$^{2+}$), were calculated. Since a satisfactory electronic model could not be generated for **57H**$^+$, the computed results from this species are not discussed here. All geometries were allowed to optimise with no symmetry restrictions and confirmed to be minimum energy conformations by the lack of imaginary frequencies.

5.6.1 Neutral Species Calculations

The optimised geometry of **57H** correlates well with the expected valence description with an alternating pattern of single and triple bonds across the length of the four carbon chain and very similar bond parameters at each molybdenum centre (Table 5).

Table 4: Calculated infrared and Raman frequencies for 57H.

	Infrared ν(C≡C) /cm^{-1}	Intensity	Raman ν(C≡C) /cm^{-1}	Activity
57H	2104	0.44	2104	80350
	1970	1.16	1970	7.2

The infrared and Raman spectra give two ν(C≡C) bands, which can be described in terms of symmetric (2104 cm^{-1}) and asymmetric (1970 cm^{-1}) stretching modes (Table 4). The low calculated intensity of the infrared stretches is consistent with the apparent experimental infrared silence observed for **57**. The observation of a single intense Raman band is consistent with experimental observations (Figure 6, Table 8), corresponding to the symmetric stretching mode of the bridge.

Table 5: Selected calculated bond lengths for 57H and 57H^{2+}.

Bond /Å	**57H**	**57H^{2+}**
Mo (1)-C_1	2.089	1.945
C_1-C_2	1.260	1.298
C_2-C_3	1.373	1.314
C_3-C_4	1.260	1.298
C_4-Mo (2)	2.087	1.945
Mo (1)-P	2.544, 2.544	2.580, 2.579
Mo (2)-P	2.546, 2.533	2.580, 2.579

Although the HOMO of **57H** is dominated by the metal d_{z2} orbital, the contribution of the molybdenum centers is significantly reduced (40 %) in comparison to [Mo(C≡CC≡CH)(dppe)(η^7-C_7H_7)] (**20H**) (62 %) and [{Mo(dHpe)(η^7-

$C_7H_7)\}_2\{C{\equiv}C(C_2B_{10}H_{10})C{\equiv}C\}]$ (**45H**) (67 %). The decrease in metal contribution is indicative of the bridge and metal fragments mixing more efficiently. The increased mixing of the butadiyndiyl bridge with the Mo(dppe)(η^7-C_7H_7) fragment causes the destabilization of the HOMO relative to the HOMO-1 in comparison to the carborane example (1.07 eV for **57**, 0.46 eV for **45**).

Despite this increased mixing between the Mo(dppe)(η^7-C_7H_7) moiety and the butadiyndiyl bridge, the lower lying occupied orbitals have relatively similar contributions to the monometallic derivatives (such as **1A** and **20H**), owing to the dominance of the cycloheptatrienyl ring δ-interaction which governs the mixing of the metal d-orbitals. The LUMO and LUMO+1 molecular orbitals represent the anti-bonding combinations involving the δ-interactions between the molybdenum centre and cycloheptarienyl ring.

5.6.2 Dication Species Calculations

When the geometries of both the singlet state of $\mathbf{57}^{2+}$ was calculated, consistent with the EPR spectroscopy. The calculated geometry predicts the bridge to adopt a more cumulenic structure than in **57H**, with a significant reduction in the Mo-C_1 bond length (0.144 Å) and an elongation of the Mo-P bond lengths (0.040 Å). The calculated infrared spectrum correctly predicts the experimental spectrum with a modestly intense low energy ν(C≡C) (for the asymmetric stretching mode) and a ν(C≡C) band of near zero intensity at higher energy (Table 6).

Table 6: Calculated infrared and Raman frequencies for $57H^{2+}$.

	Infrared ν(C≡C) /cm^{-1}	Intensity	Raman ν(C≡C) /cm^{-1}	Activity
$57H^{2+}$	1978	0.99	1978	1600
	1788	494	1788	7.2

The removal of two electrons from **57H** to form the singlet dication, **$57H^{2+}$**, depopulates the HOMO (d_{z2} orbital). Hence the LUMO of **$57H^{2+}$** resembles the HOMO in **57H** (Figure 4). The HOMO of **$57H^{2+}$** then consists of the d_{xy} metal orbitals and is mixed with the butadiyndiyl bridging moeity. The strong δ-interaction between the molybdenum centre and the ring system dominates the HOMO (68 %). This high contribution to the HOMO from the [Mo(dppe)(η^7-C_7H_7)] fragment represents the limited coupling of the metal moiety from the conjugated bridge [Mo(dHpe)(η-C_7H_7)] 68 %, C_4 32 %).

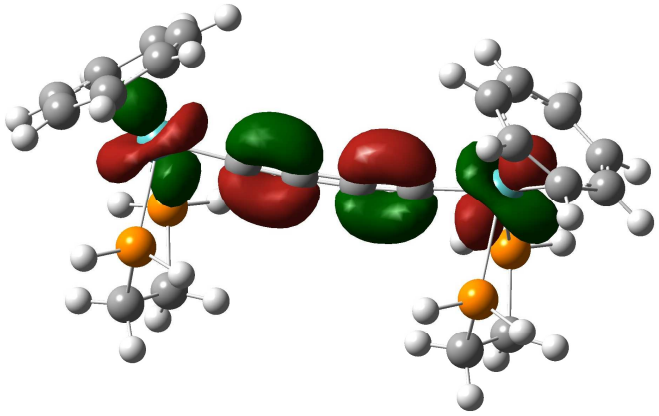

LUMO

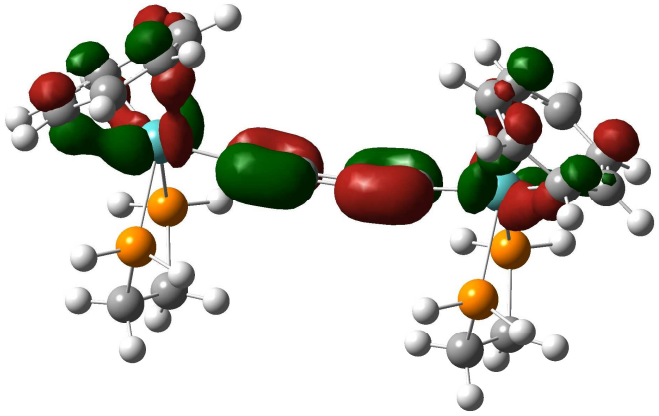

HOMO

Figure 4: Molecular orbital plots of $57H^{2+}$, plotted as isosurfaces at 0.04 au.

5.7 UV /vis Spectroelectrochemistry and TD-DFT

The availability of accurate computational models for **57** and $\mathbf{57}^{2+}$, coupled with the ability to rapidly collect electronic spectra of each oxidation state *in situ*, has allowed the electronic spectra of $\mathbf{57}^{n+}$ (n = 0, 1, or 2) to be obtained and assigned.

The electronic spectrum collected of **57** is similar to spectra from monometallic alkynyl complexes supported by a [Mo(dppe)(η^7-C_7H_7)] moiety. There is an intense transition at around 27000 cm^{-1}, assigned to a molybdenum to ring transition, and lower energy bands are masked by the transition at 27000 cm^{-1}, corresponding to the ethynyl Mo-C≡C moiety to C_7H_7 transitions (Table 7, figure 5).

Table 7: UV /vis experimental data for 57^{n+}, n = 0, 1 and 2, recorded in 0.1 M $^{n}Bu_4PF_6$ /CH_2Cl_2 solutions and transition assignments from TD-DFT calculations.

57^{n+}	Experimental Transition /cm^{-1} (ε /$dm^3mol^{-1}cm^{-1}$)	Calculated Transition /cm^{-1} (intensity)	Character of Transition
n = 0	15700 (2000)	16600 (0.0081)	$MoCC \rightarrow C_7H_7$*
	23600 (17100)	22600 (0.6321)	$MoCC \rightarrow C_7H_7$*
	27500 (14200)	26600 (0.1005)	$Mo \rightarrow C_7H_7$*
n = 1	16400 (7100)	-	-
	18600 (8300)	-	-
	22500 (10800)	-	-
	27000 (13800)	-	-
	33400 (27000)	-	-
n = 2	11200 (2500)	11900 (0.0004)	$MoC_7H_7 \rightarrow CCCC$*
	13000 (4500)	13200 (0.0002)	$MoC_7H_7 \rightarrow CCCC$*
	15300 (11400)	15400 (0.0107)	$MoC_7H_7 \rightarrow CCCC$*
	20500 (20600)	21200 (1.4662)	$MoC_7H_7 \rightarrow CCCC$*
	23500 (1300)	23400 (0.0842)	$Mo \rightarrow C_7H_7$*
	33700 (24000)	30500 (0.3986)	$Mo \rightarrow C_7H_7$*

Upon oxidation to $\mathbf{57}^+$ the higher energy bands, above 21000 cm^{-1}, generally lose intensity and are red-shifted. These bands can be assumed to be of a similar character to the analogous bands seen in the monometallic derivatives. Two transitions appear at 18500 and 16600 cm^{-1}, which in comparison to monometallic derivatives and to $\mathbf{45}^+$ (for which accurate DFT and TD-DFT model were calculated) shows these to be LMCT in character ($C{\equiv}CC{\equiv}C \rightarrow Mo(C_7H_7)$). The nature and origin of the lower energy bands which extend from 10000 cm^{-1} through the NIR region and tail into the infrared will be

discussed later in this Chapter, but the band is sufficiently broad that it is observed in the infrared spectrum overlapping with the ν(C≡C) stretches.

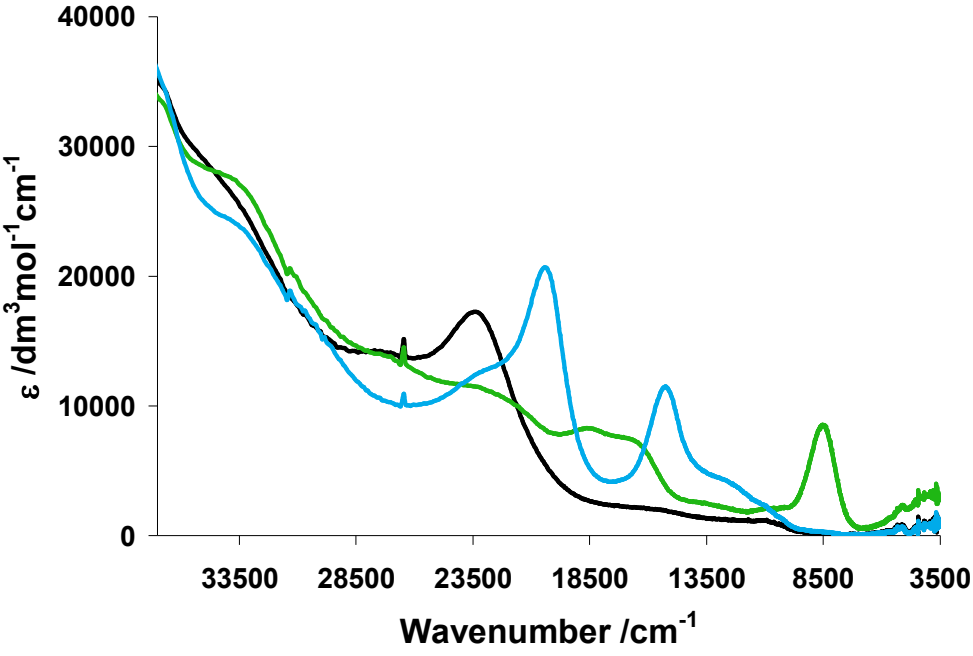

Figure 5: UV /vis spectroelectrochemical result for 57^{n+}, where n = 0 (Black), n = 1 (Green), n = 2 (Light Blue) (Recorded in 0.1 M $^{n}Bu_4NPF_6$ /CH_2Cl_2).

The UV /vis spectrum of the dication species $\mathbf{57}^{2+}$ has a transition at 20500 cm^{-1} which is predicted from TD-DFT calculations to be MLCT in character (Mo → C≡CC≡C). It is worth noting that a similar band is seen for the carborane derivative, thus supporting this assignment. Another intense band at 15300 cm^{-1}, and the accompanying shoulders, also assigned to be predominantly MLCT in character. This second MLCT band envelope can be explained by the difference in energy between each of the occupied d-orbitals on the molybdenum centre. The higher energy band at 20500 cm^{-1} is from the HOMO-1 → LUMO transition. The second MLCT transition (15300 cm^{-1}) is from the HOMO → LUMO, where the calculated energy difference between the HOMO and HOMO-1 is 6200 cm^{-1}, a reasonable approximation of the energy difference between

the two MLCT transitions seen in $\mathbf{57}^{2+}$ (20500 cm^{-1} and 15300 cm^{-1}), even if Koopman's Theorem is not strictly correct. The similarity between the spectrum of $\mathbf{57}^{2+}$ and $\mathbf{20}^{+}$ confirms the decoupling of the Mo(dppe)(η^7-C_7H_7) centres from the bridging moiety and the high bridge character of the LUMO of $\mathbf{57}^{2+}$.

5.8 Resonance Raman Spectroscopy

With information about the electronic spectra and the energy of the absorption bands, Raman spectroscopy can be used, and more particularly, resonance Raman spectroscopy. Raman studies on acetylenic complexes are well known, however, studies on organometallic polyyne complexes are rare, but not unheard of, despite the effectiveness of the spectroscopic technique in linking the electronic and physical structure of a complex. [29] A previous study conducted was concerned with the systematic extension of the polyynediyl chain from four to twenty carbons in length with [Re(PPh_3)(NO)(η^5-C_5Me_5)] termini (although the Raman data was only explained in terms of the number of ν(C≡C) modes associated with the length of the chain of the neutral complexes).[30] Another study analysed the neutral structures of a number of acetylenic polymers containing platinum. Owing to the D_{2h} or C_{2h} symmetry of the complexes, D_{2h} or C_{2h}, the complexes contained a centre of symmetry, therefore using the mutual exclusion rule the symmetric and asymmetric stretching modes of ν(C≡C) could be either infrared or Raman active, but not both. In practice, the ν(C≡C) modes were intense in the Raman and weak in the infrared spectra, due to the small dipole across the bond. In this study, the combination of Raman and infrared studies show that in spite of the increased conjugation produced by longer chains, the acetylenic bridge still retains an alternating triple and single bond structure.[31] Studies of a series of

oxidation states are limited to two examples, one of which is $[\{Mn(C{\equiv}CC_6H_5)(dmpe)_2\}_2(\mu\text{-}C{\equiv}CC{\equiv}C)]^{n+}$ (**61**$^{n+}$) (n = 0, 1, 2)[32] and the rhenium containing complex **55**$^{n+}$ (n = 0, 1, 2).[26] The D_{2h} symmetry of **61** causes the Raman active symmetric stretching modes of ν(C≡C) to be intense, giving rise to single bands for **61** (1824 cm^{-1}), **61**$^{+}$ (1745 cm^{-1}) and **61**$^{2+}$ (2010 cm^{-1}) (where all spectra were collected using a 514 nm laser). The large variation in energy of the symmetric mode indicates significant variation in the electronic structure of the bridge upon oxidation of the complex.

The ability to isolate chemically pure samples of **57**, [**57**]PF_6 and [**57**][PF_6]$_2$ has allowed the recording of the resonance Raman spectra in the solid state using a variety of laser energies. When excited with 532.21 nm laser frequency, which falls within the 18600 cm^{-1} LMCT band envelope in [**57**]PF_6, all three compounds gave spectra which were not obscured by background fluorescence of the complex (Figure 6, table 8). It must be noted that when a 632.817 nm laser is used, which excites various MLCT bands in all of the complexes, significant background fluorescence is observed. This is common for organometallic complexes and has been attributed to the nature of the supporting metal moieties.[32]

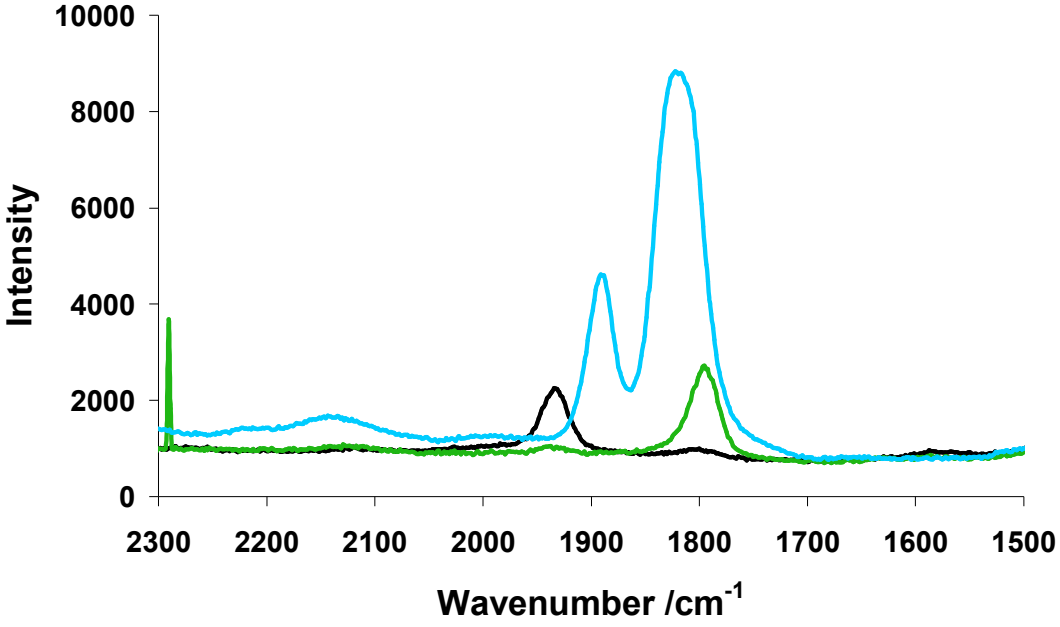

Figure 6: Raman spectra of 57^{n+}, where n = 0 (Black), n = 1 (Green), n = 2 (Light Blue) (Recorded as fine powder, using 532.21 nm laser).

Table 8: Raman and infrared data for 30^{n+} (n = 0, 1 or 2). (where w and vw represent weak and very-weak band descriptions)

57^{n+}	Raman ν(C≡C) /cm^{-1}	Infrared ν(C≡C) /cm^{-1}
n = 0	1939	-
n =1	1800, vw 1940	w 1868, 1930
n = 2	1826, 1894	w 1727

Similar symmetry arguments can be applied to **57** as for **61** (D_{2h} symmetry) therefore the Raman spectrum only contains the symmetric stretching mode ν(C≡C). From the UV /vis studies shown earlier, $\mathbf{57}^{n+}$ has a number of electronic transitions, the band envelopes of which are near or encompass the energies of the laser used to collect the Raman spectra. As such the intensities of the ν(C≡C) stretching modes may be subject to a degree of resonance enhancement if the electronic transition is coupled to one of the modes. In contrast to the manganese complex **61** (ν(C≡CC≡C) = 1824 cm^{-1}), the higher energy of ν(C≡C) for **57** (ν(C≡CC≡C) = 1939 cm^{-1}) indicates that the butadiyndiyl bridge in the Mo example **57** is more acetylenic in character.

The 35 electron complex $\mathbf{57}^{+}$ produces two infrared bands of differing intensities (s 1930, w 1868 cm^{-1}). The Raman spectrum of $\mathbf{57}^{+}$ also contains two bands (w 1940 cm^{-1}, s 1800 cm^{-1}), however, the relative intensities of the bands are not the same. For both IR and Raman spectra, the presence of two bands is rationalized by the asymmetry imposed on the complex due to the oxidation taking place locally on one of the Mo(dppe)(η^7-C_7H_7) moieties, therefore lifting the symmetry of the complex, and thus removing the mutual exclusivity rule. The different intensities of the observed ν(C≡C) bands in the infrared and Raman spectra allow the assignment of the higher wavenumber stretches to be associated with the 18 electron [Mo(dppe)(η^7-C_7H_7)] moiety, which in the Raman spectra correspond to the weakly allowed symmetric stretch mode of ν(C≡C) and strong asymmetric stretch in the infrared spectra. The vibrations observed at lower wavenumber, therefore, are associated with a more cumulenic structure due to the C≡C moiety being bonded to a 17 electron Mo(dppe)(η^7-C_7H_7) fragment. This is in contrast to $\mathbf{61}^{+}$ which displays a single ν(C≡C) Raman stretching mode, indicating that a more delocalised structure as the symmetry of the complex is retained.

EPR and infrared studies suggest there is a symmetrical structure for $\mathbf{57}^{2+}$, where the unpaired electrons are situated largely on the [Mo(dppe)(η^7-C_7H_7)] moieties. The Raman spectra of $\mathbf{57}^{2+}$ collected using 532.21 nm excitation gives two ν(C≡C) stretching modes. However, the calculated Raman spectrum only predicts a single intense ν(C≡C) band at high energy (Table 6) corresponding to symmetric bond vibrations.

The presence of two ν(C≡C) bands originates from the nature of resonance Raman in which particular vibrational modes gain intensity through resonance enhancement arising from coupling of vibrational motion to electronic transitions. The UV /vis region for $\mathbf{57}^{2+}$ has many closely separated electronic transitions. To confirm the assignment of the two ν(C≡C) bands to different resonant processes in the molecule, the energy of the excitation laser was varied so that different electronic transitions were excited, consequently changing the relative intensities of the two bands, denoted **A** and **B** for purposes of the following discussion (Figure 7, table 9).

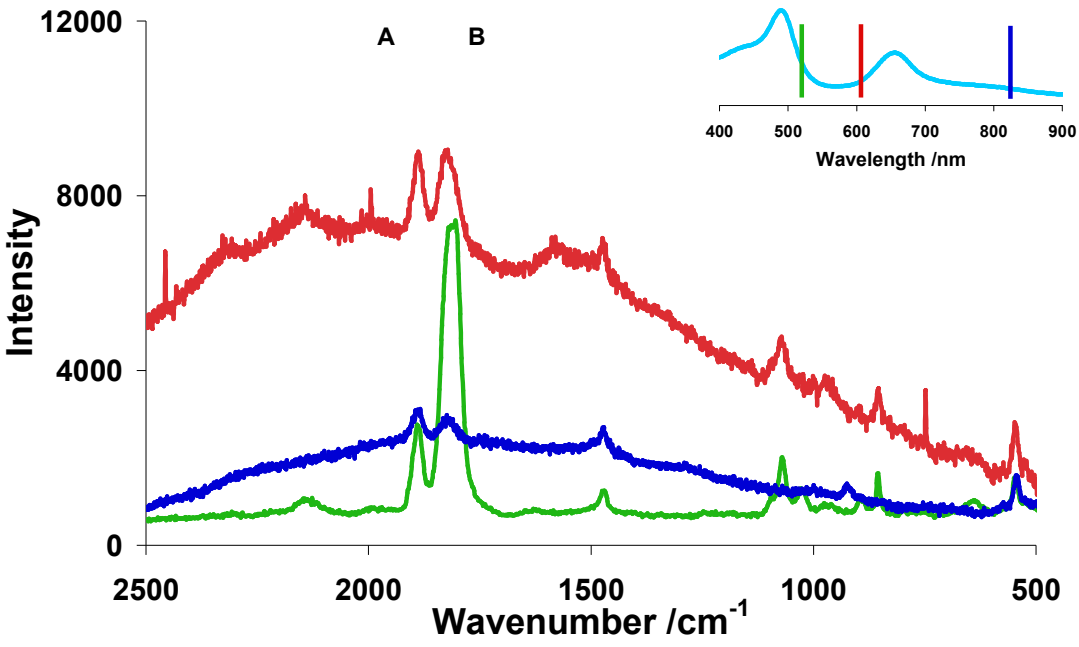

Figure 7: Raman spectrum of 57^{2+} as a fine powder at 532.21 nm (Green), 632.817 nm (Red) and 785.1 nm (Blue). Inset spectra: 57^{2+} UV /vis spectra, line colour corresponds to the laser wavelength 532.21 nm (Green), 632.817 nm (Red) and 785.1 nm (Blue).

Table 9: Raman data for 57^{2+} at different wavelength lasers. Relative intensities are calculated from peak height from baseline.

Laser Energy /nm	**A** ν(C≡C) /cm^{-1}	**B** ν(C≡C) /cm^{-1}	Relative intensity **A**:**B**
532.21	1889	1820	3.4:1.0
632.817	1890	1820	1.0:1.0
785.1	1891	1821	1.0:1.6

The electronic spectrum of $\mathbf{57}^{2+}$ features two intense electronic transitions between 530 and 790 nm which correspond to two MLCT-type transitions between the molybdenum centre and the butadiynyl chain. By changing the energy of the laser to come on- and off-resonance with these transitions the relative intensities of bands **A** and **B** change. **A** gains intensity as the energy of the laser is decreased, therefore it is more strongly coupled with the electronic transition at 20500 cm^{-1}, the converse is true for band **B**, showing that it is coupled to the electronic transition at 15300 cm^{-1}. DFT calculations carried on $\mathbf{57H}^{2+}$ predict that there should only be a single intense, symmetric stretching mode of the bridging moiety. The marked change in the intensity of the band **B** upon changing the frequency of the laser, indicates that this band belongs to the bridge. Band **A**, is therefore anomalous, however, as the band does come in and out of resonance with the laser, it is proposed that this ν(C≡C) stretching mode is associated with $\mathbf{57}^{2+}$, perhaps resulting from the presence of rotamers present in the sample in the solid state. This is further supported by the presence of a weak band at ca. 1600 cm^{-1} which also comes on and off resonance with band **A**. Similar behaviour is observed for the related ruthenium complex, **59**, where different rotamers, with different infrared ν(C≡C) signatures, can be isolated by differential crystallisation of the sample.[33]

5.9 NIR Spectroscopy

The NIR spectra of **57** and $\mathbf{57}^{2+}$ are devoid of any spectral features, however, for $\mathbf{57}^{+}$ there is a broad band near 4000 cm^{-1} and an intense transition, near 8500 cm^{-1}. The identity of the more intense band (at 8500 cm^{-1}) has been established as LMCT in character, and the broad band has been associated with charge transfer transitions (IVCT or IT transition). The availability of [**57**]PF_6 as an isolable solid has allowed the NIR spectrum to be recorded in a range of solvents with different dielectric constants (CH_2Cl_2, MeCN and acetone) which provides an insight into the nature of the electronic ground state. However, due to the limited solubility of $\mathbf{57}^{+}$ in acetone and MeCN the extinction coefficients were only calculated for spectrum recorded in CH_2Cl_2. Upon increasing the dielectric constant of the solvent the band envelope of the entire region becomes much broader, similar to the carborane complex $\mathbf{45}^{+}$, giving weight to the assignment of a localised electronic structure. The broad band is not a single Gaussian, and as such, the band was deconvoluted using the same Gaussian fitting routine as described in Chapter four, to aid the fitting of the band. The solvent overtones have been removed for clarity (Table 10-12, figure 8-10).

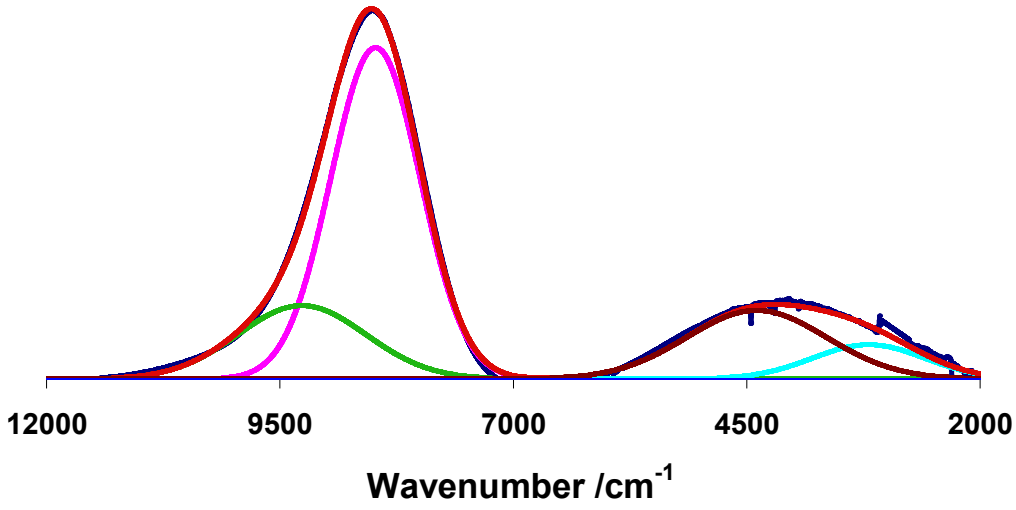

Figure 8: NIR spectrum of [57]PF_6 CH_2Cl_2.

Table 10: Deconvoluted band data for [57]PF_6 in CH_2Cl_2.

CH_2Cl_2	IT (1)	IT (2)	LMCT	IT (3)
ν /cm^{-1}	3200	4400	8500	9300
$\Delta\nu_{1/2}$ /cm^{-1}	600	750	450	690
ε /$dm^3mo^{-1}cm^{-1}$	870	1700	8700	1700

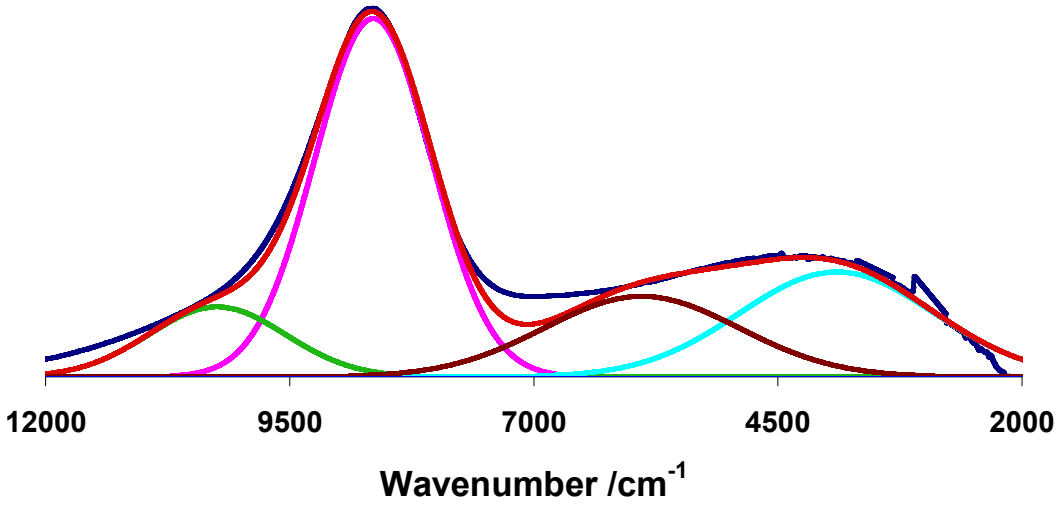

Figure 9: NIR spectrum of [57]PF_6 MeCN.

Table 11: Deconvoluted band data for [57]PF_6 in MeCN.

MeCN	IT (1)	IT (2)	LMCT	IT (3)
ν /cm^{-1}	3500	5300	8800	10100
$\Delta\nu_{1/2}$ /cm^{-1}	800	1000	550	700
A	0.04	0.04	0.17	0.04

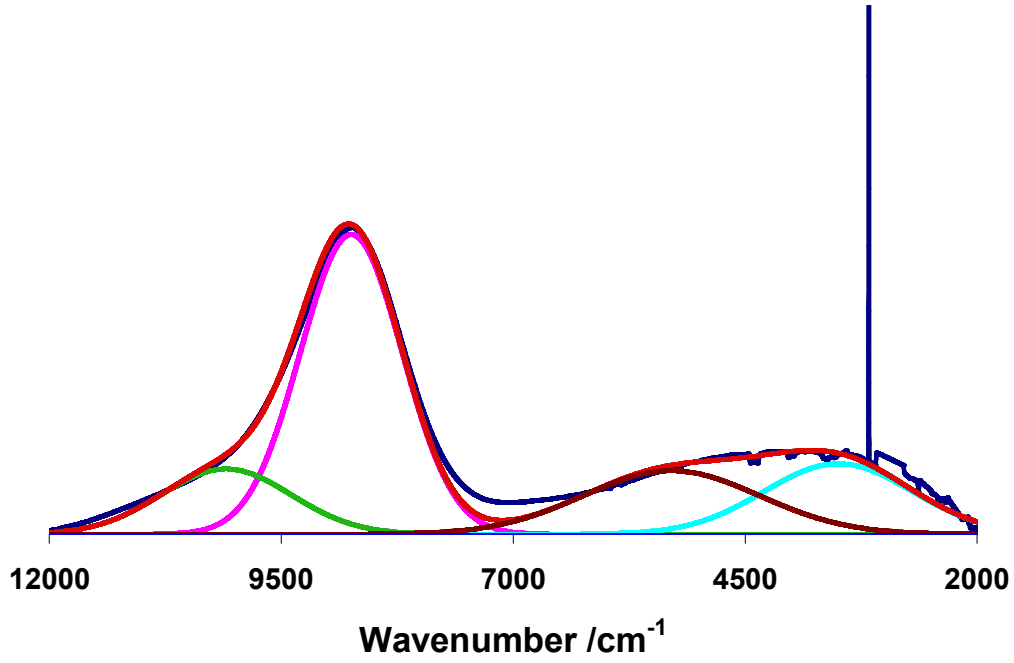

Figure 10: NIR spectrum of [57]PF_6 in acetone.

Table 12: Deconvoluted band data for [57]PF_6 in acetone.

Acetone	IT (1)	IT (2)	LMCT	IT (3)
ν /cm^{-1}	3900	5900	8700	10300
$\Delta\nu_{1/2}$ /cm^{-1}	1000	1000	600	700
A	0.06	0.05	0.21	0.04

In all solvent media the band envelope between 2000 and 12000 cm^{-1} deconvolutes to form four distinct Gaussian bands, where the positions of all the bands vary as a result from changes in the solvent medium. The most intense LMCT band is relatively insensitive to changes of the solvent (varying by less than 300 cm^{-1}). In comparison, the lowest energy band (3500 cm^{-1}) changes up to 700 cm^{-1}, and the other two low intensity bands (5300 and 10000 cm^{-1}) vary by *ca.* 1500 cm^{-1}.

As depicted in Chapter four (Figure 15), the assumption of a two state model can give rise to five transitions, three derived from intervalence transitions and two from interconfigurational transition from the 17 electron [Mo(dppe)(η^7-C_7H_7)] centre. The proximity of the bridge orbitals to the frontier orbital region leads to the possibility of an extra LMCT transition (Figure 11). The mixing of the bridge and the metal electrophore would render a two state approximation of the charge transfer process, and hence Hush's equations describing it, inadequate.

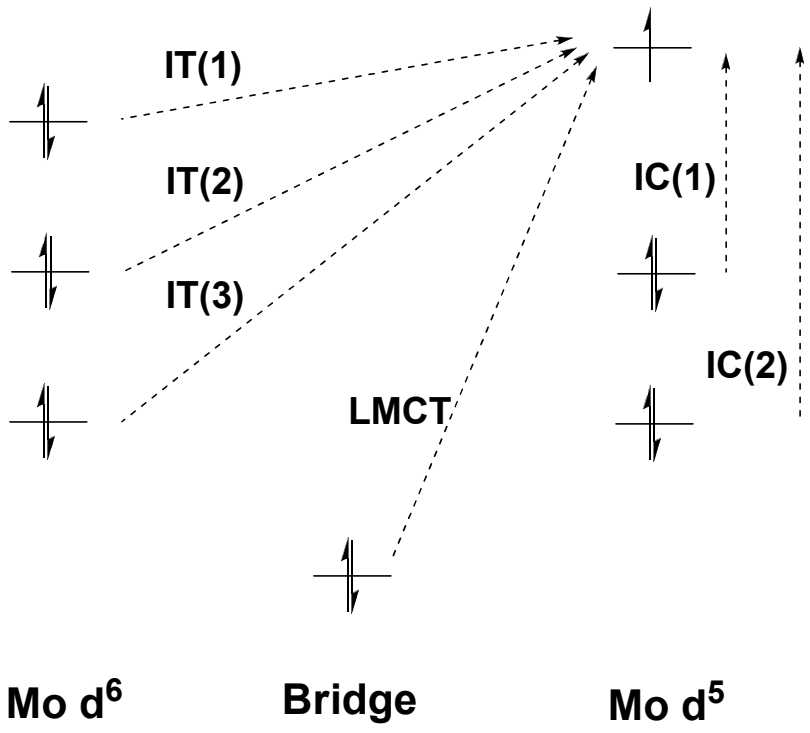

Figure 11: Predicted NIR transitions for transition metal containing complexes.

Using this model, the three lower intensity bands can be described as the three intervalence charge transfer (IVCT or IT) bands. The single intense band, is assigned as an LMCT-type transition. No interconfigurational (IC) bands are seen which are most likely being masked by the other significantly more intense bands. The observation of three solvatochromic IT bands is a well resolved feature for **57**$^+$.

In conventional analyses of the NIR spectra of butadiyndiynl radical complexes, a two state model has been assumed, therefore Hush analysis has been performed. Consequentially, the NIR region has been treated as one single IVCT band, or deconvoluted into two or three bands whereby the lowest energy band is generally the only band analysed. The presence of three IT bands has been observed in heavy metal systems, *cis, cis*-$[\{OsCl(bipy)_2\}_2(\mu\text{-pz})]^{3+}$, where large spin-orbit coupling causes a separation of the IT band energies.[34] Given the lower spin orbit coupling of the light molybdenum system, it would seem that the separation of the IT bands in $\mathbf{57}^+$ is caused by asymmetric ligand field at the metal centre.

Unlike the carborane complex $\mathbf{47}^+$ the IT bands do not agree with the Hush predicted bands widths, being significantly narrower than predicted (for example IT (1); predicted $\Delta\nu_{1/2} = 2700\ cm^{-1}$, actual $\Delta\nu_{1/2} = 650\ cm^{-1}$). Ordinarily, using the two-state model for electron transfer, $\mathbf{57}^+$ would be considered valence averaged. However, the solvatochromism of all the IT bands, the symmetric band shape of the lowest energy band envelope and the spectroscopy (infrared, Raman and EPR) point towards a significantly localised electronic weakly-coupled mixed valence system. This is in direct contrast to almost every other system studied to date, which exhibit significantly delocalised or valence averaged structures.

5.10 Conclusion

By changing the bridging moiety from bis-ethynyl carborane to 1,3-butadiyndiyl the terminal [Mo(dppe)(η^7-C_7H_7)] moieties have become more heavily mixed with the bridge. This is apparent from electrochemical, spectroelectrochemical and computational studies. The increased mixing between the bridge and molybdenum fragment causes the rate of electron transfer for $\mathbf{57}^+$ to increase in comparison to the carborane complex $\mathbf{45}^+$, by several orders of magnitude. Despite this increased mixing, upon oxidation the electron is still removed from a molecular orbital of high [Mo(dppe)(η^7-C_7H_7)] character. The formation of a biradical for $\mathbf{57}^{2+}$, is typical for the homo-bimetallic molybdenum complexes and is seen for the carboranyl derivative $\mathbf{45}^{2+}$ as well. The electronic asymmetry of $\mathbf{57}^+$ forms a localised electronic structure and the splitting of the intervalence charge transfer bands. The increased localisation in comparison to the analgous group eight complexes result in a much slower rate of electron transfer. In addition, it raises pertinent questions about the use of a two state model when the metal and bridge moieties are heavily mixed.

5.11 General Procedures

General experimental procedures have been described in Chapter two.

5.11.2 Computational Details

All calculations were carried out using the Gaussian 03 package.[35] The model geometry **57H^{n+}** (n = 0 or 2) discussed here were optimised using B3LYP[36] and MPW1K[37], with no symmetry constraints. The pseudo-potential LANL2DZ[38] was used for all the atoms. Frequency calculations were carried out these optimised geometries at the corresponding levels and shown to have no imaginary frequencies. Molecular orbital and TD-DFT computations were carried out on these optimised geometries at the appropriate level of theory and the orbital contributions were generated with the aid of the GaussSum.[39]

5.12 References

[1] (a) G.A. Koutsantonis, J.P. Selegue, *J. Am. Chem. Soc.,* 1991, **113**, 2316. (b) M.I. Bruce, K. Costuas, B.G. Ellis, J-F. Halet, P.J. Low, B. Moubaraki, K.S. Murray, N. Ouddai, G.J. Perkins, B.W. Skelton, A.H. White, *Organometallics,* 2007, **26**, 3735.
[2] P. Belanzoni, N. Re, A. Sgamellotti, C. Floriani, *J. Chem. Soc., Dalton. Trans.,* 1998, 1825.
[3] (a) M.I. Bruce, M. Ke, P.J. Low, B.W. Skelton, A.H. White, *Organometallics,* 1998, **17**, 3539. (b) R.L. Roberts, H. Puschmann, J.A.K. Howard, J.H. Yamamoto, A.J. Carty, P.J. Low, *Dalton. Trans.,* 2003, 1099.
[4] A. Klein, K-W. Klinkhammer, T. Scheiring, *J. Organomet. Chem.,* 1999, **592**, 128.
[5] S. Kheradmandan, K. Hienze, H.W. Schmalle, H. Berka, *Angew. Chem. Int. Ed.,* 1999, **38**, 2270.
[6] (a) J. Gil-Rubio, M. Laubender, H. Werner, *Organometallics,* 1998, **17**, 1202. (b) J. Gil-Rubio, M. Laubender, H. Werner, *Organometallics,* 2000, **19**, 1365.
[7] J. Lewis, M.S. Khan, A.K. Kakkar, B.F.G. Johnson, T.B. Marder, H.B. Fyfe, F. Wittmann, R.H. Friend, A.E. Dray, *J. Organomet. Chem.,* 1992, **425**, 165.
[8] (a) M.I. Bruce, P.J. Low, K. Costuas, J-F. Halet, S.P. Best, G.A. Heath, *J. Am. Chem. Soc.,* 2000, **122**, 1949. (b) M.I. Bruce, B.C. Hall, B.D. Kelly, P.J. Low, B.W. Skelton, A.H. White, *Dalto. Trans.,* 1999, 3719.
[9] F. Coat, P. Thominot, C. Lapinte, *J. Organomet. Chem.,* 2001, **629**, 39.
[10] O. Gevert, J. Wolf, H. Werner, *Organometallics,* 1996, **15**, 2806.
[11] V. W-W. Yam, V. C-Y. Lau, K-K. Cheung, *Organometallics,* 1996, **15**, 1740.
[12] Y.Zhou, J.W. Seyler, W. Weng, A.M. Arif, J.A. Gladysz, *J. Am. Chem. Soc.,* 1993, **115**, 8509.
[13] F. Coat, M-A. Guillevic, L. Toupet, F. Paul, C. Lapinte, *Organometallics*, 1997, **16**, 5988.
[14] A. Wong, P.C.W. Kang, C.D. Tagge, D.R. Leon, *Organometallics,* 1990, **9**, 1992.
[15] N. Le Narvor, L. Toupet, C. Lapinte, *J. Am. Chem. Soc.,* 1995, **117**, 7129.
[16] M.I. Bruce, B.G. Ellis, P.J. Low, B.W. Skelton, A.H. White, *Organometallics,* 2003, **22**, 3184.
[17] M.I. Bruce, K. Costuas, T. Davin, J-F. Halet, K.A. Kramarczuk, P.J. Low, B.K. Nicholson, G.J. Perkins, R.L. Roberts, B.W. Skelton, M.E. Smith, A.H. White, *Dalton. Trans.,* 2007, 5387.
[18] F.J. Fernandez, O. Blacque, M. Alfonso, H. Berke, *Chem. Commun.,* 2001, 1266.
[19] G. Fraper, M. Kertesz, *Inorg. Chem.,* 1993, **32**, 732.
[20] P. Belanzoni, N. Re, M. Rosi, A. Sgamellotti, C. Floriani, *Organometallics,* 1996, **15**, 4264.
[21] H. Jiao, K. Costuas, J.A. Gladysz, J-F. Halet, M. Guillemot, L. Toupet, F. Paul, C. Lapinte, *J. Am. Chem. Soc.,* 2003, **125**, 9511.
[22] M.I. Bruce, P.J. Low, K. Costuas, J-F. Halet, S.P. Best, G.A. Heath, *J. Am. Chem. Soc.,* 2000, **122**, 1949.
[23] N.J. Brown, D. Collison, R. Edge, E.C. Fitzgerald, M. Helliwell, J.A.K. Howard, H.N. Lancashire, P.J. Low, J.J.W. McDouall, J. Raferty, C.A. Smith, D.S. Yufit, M.W. Whiteley, *Organometallics,* 2010, **29**, 1261.
[24] H.N. Lancashire, R. Ahmed, T.L. Hague, M. Helliwell, G.A. Hopgood, L. Sharp, M.W. Whiteley, *J. Organomet. Chem.,* 2006, **691**, 3617.

[25] S. Kheradmandan, K. Heinze, H.W. Schmalle, H. Berke, *Angew. Chem. Int. Ed.,* 1999, **38**, 2270.
[26] M. Brady, W. Weng, Y. Zhou, J.W. Seyler, A.J. Amoroso, A.M. Arif, M. Bohme, G. Frenking, J.A. Gladysz, *J. Am. Chem. Soc.,* 1997, **119**, 775.
[27] S.B. Piepho, E.R. Krausz, P.N. Schatz, *J. Am. Chem. Soc.,* 1978, **100**, 2996.
[28] K. Lancaster, S.A. Odom, S.C. Jones, S. Thayumanavan, S.R. Marder, J-L. Bredas, V. Coropceanu, S. Barlow, *J. Am. Chem. Soc.,* 209, **131**, 1717.
[29] (a) Y. Sun, N.J. Taylor, A.J. Carty, *Organometallics,* 1992, **11**, 4293. (b) K. M-C. Wong, C-K. Hui, K-L. Yu, V.W-W. Yam, *Coord. Chem. Rev.,* 2002, **229**, 123. (c) U. Ruschewitz, P. Muller, W. Kockelmann, *Z. Anorg. Allg. Chem.,* 2001, **627**, 513. (d) S. Hemmersbach, B. Zibrowius, W. Kockelmann, U. Ruschewitz, *Chem. Eur. J.,* 2001, **7**, 1952.
[30] R. Dembinski, T. Bartik, M. Jaeger, J.A. Gladysz, *J. Am. Chem. Soc.,* 2000, **122**, 810.
[31] R.D. Markwell, I. S. Butler, A.K. Kakkar, M.S. Kahn, Z.H. Al-zakwani, J. Lewis, *Organometallics,* 1996, **15**, 2331.
[32] K. Venkatesan, T. Fox, H.W. Schmalle, H. Berke, *Organometallics,* 2005, **24**, 2834.
[33] M.I. Bruce, P. Hinterding, E.R.T. Tielink, B.W. Skelton, A.H. White, *J. Organomet. Chem.,* 1993, **450**, 209.
[34] M.J. Powers, T.J. Meyer, *J. Am. Chem. Soc.,* 1980, **102**, 1289.
[35] M.J. Frisch, G.W. Trucks, H.B. Schlegel, G.E. Scuseria, M.A. Robb, J.R. Cheeseman, J.A. Montgomery Jr., T. Vreven, K.N. Kudin, J.C. Burant, J.M. Millam, S.S. Iyengar, J. Tomasi, V. Barone, B. Mennucci, M. Cossi, G. Scalmani, N. Rega, G.A. Petersson, H. Nakatsuji, M. Hada, M. Ehara, K. Toyota, R. Fukuda, J. Hasegawa, M. Ishida, T. Nakajima, Y. Honda, O. Kitao, H. Nakai, M. Klene, X. Li, J.E. Knox, H.P. Hratchian, J.B. Cross, C. Adamo, J. Jaramillo, R. Gomperts, R.E. Stratmann, O. Yazyev, A.J. Austin, R. Cammi, C. Pomelli, J.W. Ochterski, P.Y. Ayala, K. Morokuma, G.A. Voth, P. Salvador, J.J. Dannenberg, V.G. Zakrzewski, S. Dapprich, A.D. Daniels, M.C. Strain, O. Farkas, D.K. Malick, A.D. Rabuck, K. Raghavachari, J.B. Foresman, J.V. Ortiz, Q. Cui, A.G. Baboul, S. Clifford, J. Cioslowski, B.B. Stefanov, G. Liu, A. Liashenko, P. Piskorz, I. Komaromi, R.L. Martin, D.J. Fox, T. Keith, M.A. Al-Laham, C.Y. Peng, A. Nanayakkara, M. Challa- combe, P.M.W. Gill, B. Johnson, W. Chen, M.W. Wong, C. Gonzalez, J.A. Pople, GAUSSIAN 03, Revision C.02, Gaussian Inc., Wallingford, CT, 2004.
[36] (a) A.D. Becke, *J. Chem. Phys.,* 1993, **98**, 648. (b) C. Lee, W. Yang, R.G. Parr, *Phys. Rev. B.,* 1988, **37**, 785. (c) A.D. Becke, *Phys. Rev. A.,* 1988, **38**, 3098. (d) J.P. Perdew, *Phys. Rev. B.,* 1986, **33**, 8822.
[37] (a) B.J. Lynch, P.L. Fast, M. Harris, D.G. Truhlar, *J. Phys. Chem. A.,* 2000, **104**, 4811. (b) B.J. Lynch, Y. Zhao, D.G. Truhlar, *J. Phys. Chem. A.,* 2003, **107**, 1384. (c) G.A. Petersson, M.A. Al-Laham, *J. Chem. Phys.,* 1991, **94**, 6081. (d) G.A. Petersson, A. Bennett, T.G. Tensfeldt, M.A. Al-Laham, W.A. Shirley, J. Mantzaris, *J. Chem. Phys.,* 1988, **89**, 2193.
[38] (a) P.J. Hay, W.R. Wadt, *J. Chem. Phys.,* 1985, **82**, 270. (b) W.R. Wadt, P.J. Hay, *J. Chem. Phys.,* 1985, **82**, 284. (c) P.J. Hay, W.R. Wadt, *J. Chem. Phys.,* 1985, **82**, 299.
[39] N.M. O'Boyle, A.L. Tenderholt, K.M. Langner, *J. Computational. Chem.,* 2007, **5**, 839.

Chapter 6: Synthesis, Spectroscopy and Electronic Structure of $[\{Mo(dppe)(\eta^7\text{-}C_7H_7)\}_2\{\mu\text{-}C{\equiv}C(C_6H_4)C{\equiv}C\}]^{n+}$ (n = 0, +1, +2)

6.1 Introduction

A running theme throughout this thesis has been the coordination of unsaturated carbon groups to organometallic centres. Complexes bridged by simple unsaturated polyyne and polyyndiyl chains are well known and have been important in disseminating electron transfer process in organometallic mixed valence complexes. However, in order to assess the role of the bridge in a charge transfer process between two metal centres, a tunable bridge would be ideal. Unsaturated carbon bridges containing a benzene core are ideally suited to this, owing to the vast number of synthetic methodologies which allow the easy modification of the aromatic centre.[1] Substituted diethynylbenzene based ligands, where the addition of substituents at the ortho and meta positions of the ring can tune the electronic properties of the bridging ligand, are commonly used in organometallic chemistry (Figure 1).

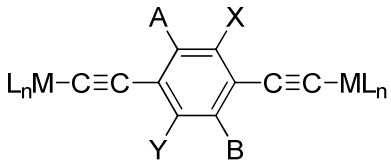

Figure 1: Substituted diethynylbenzene bridged organometallics (where A, B, X, Y are tunable substituents).

Diethynyl bridges containing other aromatic cores such as thiophene,[2] pyridine[3] and fluorenes derivatives,[4] have also been used in the construction of mixed valence complexes, which have served to alter the electronic properties of the bridge. It is also

interesting that the ethynylbenzene core is also an important building block in the syntheses of π-conjugated organometallic dendrimer systems.[5] Dendrimers themselves have potential applications in molecular recognition, catalysis and photoactive devices (Figure 2).[6]

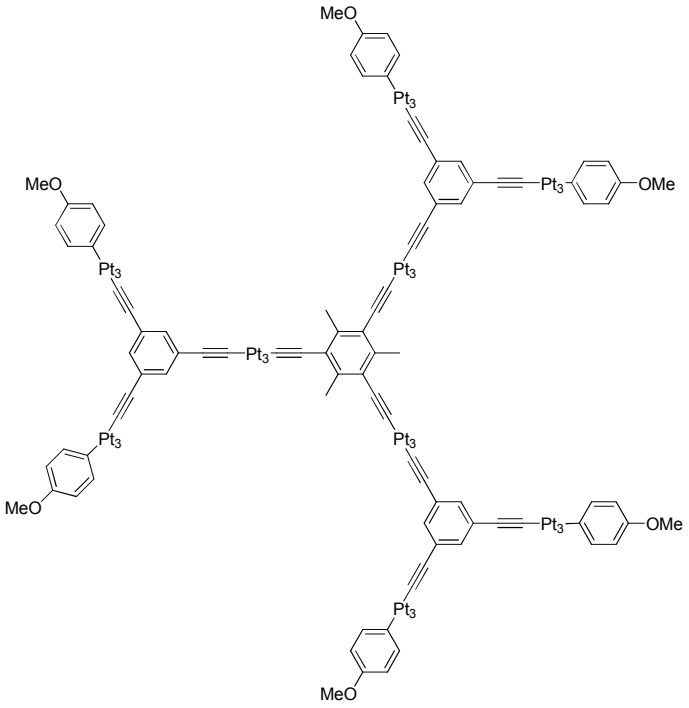

Figure 2: Organometallic dendrimer (Pt_3 = $Pt(PEt_3)_2$).

The synthesis of diethynylbenzene bridged compounds is relatively facile, with many of the routes employed for synthesising the monometallic arylacetylide also finding application for the metallation of each ethynyl moiety in di- and tri-ethynyl benzenes. Unlike the synthesis of linear polyyne bridge precursors, such as HC≡CC≡CH, diethynylbenzene, HC≡C(C_6H_4)C≡CH and derivatives, are generally quite stable and not explosive. In addition, the aryl group can be modified with substituents before it is coordinated to the metal centre, therefore simplifying the synthetic strategies towards these complexes.

Tin derivatives, such as $R_3SnC{\equiv}CArC{\equiv}CSnR_3$, can be readily synthesised by the reaction of the diethynylarylene precursor, $HC{\equiv}CArC{\equiv}CH$, with R_3SnCl and lithium diisopropylamide (LDA). The generation of the stanyl derivative *in situ* and the direct addition of $[FeI(CO)_2(\eta^5\text{-}C_5H_5)]$ gives access to a range of complexes, such as $[\{Fe(CO)_2(\eta^5\text{-}C_5H_5)\}_2(\mu\text{-}C{\equiv}CArC{\equiv}C)]$ (Ar = C_6H_4, $C_6H_2(OC_8H_{17})_2$, SC_4H_2). Subsequent photolysis, in the presence of two equivalents of dppe can produce a series of redox active $Fe(dppe)(\eta^5\text{-}C_5H_5)$ supported complexes.[7] Polymeric chains containing both metal /diethynylaryl repeating units are readily synthesised from the reaction with group 10 metal fragments, $[MCl_2(PR_3)_2]$, (M = Ni, Pd, Pt), in the presence of CuI and amine solvent.[8] Similarly, polymeric chains can be formed through the reaction of diethynylbenzene with $[Rh(PR_3)_4]BPh_4$ or $[Rh(PR_3)_4Me]$ with MeLi.[9] Polymerisation of bis(diethynylbezene) complexes, for example $[(Fe(\eta^5\text{-}C_5H_5)\{C_5H_4C{\equiv}C(C_6H_4)C{\equiv}CH\}_2]$ and $[Ru(dppe)_2)\{C{\equiv}C(C_6H_4)C{\equiv}CH\}]$, is also readily achieved by using group 10 metal fragments as linking moieties (Figure 3).[10]

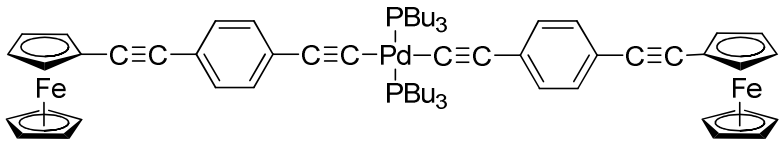

Figure 3: Diethynylbenzene dimer using a $Pd(PBu_3)_2$ bridging moiety.

These polymetallic polymers have been seen to act as redox active molecular wires and have been examined using CP-AFM and cross-wire junction experiments which produce modest charge conductance.[11]

Of more relevance to this discussion is the synthesis of molecular bimetallic species. The coordination of the redox active ferrocene moiety to diethynyl benzene can be

achieved by the reaction of [Fe(η^5-C_5H_5)(η^5-C_5H_4I)] and HC≡CArC≡CH in the presence of a palladium (0) catalyst, CuI and amine.[12] Bimetallic platinum complexes can be synthesised using [PtCl(C_6H_5)(PR_3)$_2$] and copper mediated coupling protocols. This results in complexes exhibiting singlet and triplet photoluminescence, the energies of which decrease as the electronegativity of the bridging moiety is increased.[13]

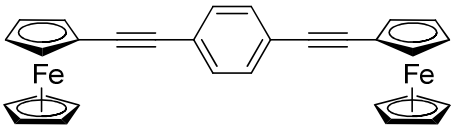

Figure 4: Example of diethynyl-bridged ferrocene complex.

As for the monometallic acetylides and polyyne complexes, diethynylbenzene bridged complexes containing the metal fragments [Fe(dppe)(η^5-C_5Me_5)] (**62**), [Ru(dppe)(η^5-C_5Me_5)] (**63**), and [Ru(dppe)$_2$R] (R = Cl, (**64**), or C≡CC_6H_5, (**65**)) are the corner-stone metal containing moieties for this area of chemistry.

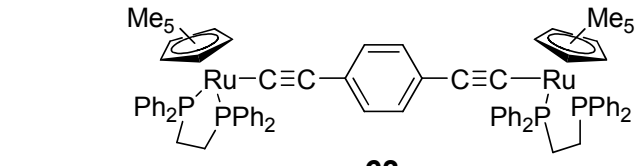

63

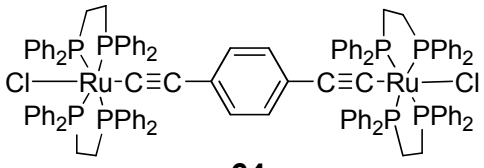

64

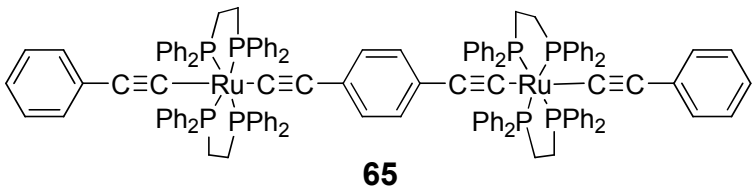

65

Figure 5: Examples of diethynylbenzene bridged organometallic complexes

Bimetallic complexes containing the [M(dppe)(η^5-C_5Me_5)] (M = Ru, Fe) are readily synthesised via the sequential formation of a bis-vinylidene intermediate (which can be isolated if needed) and *in situ* deprotonation (Scheme 1).[14] Bisphosphine complexes based on, *trans*-[MCl(dppe)$_2$] (M = Os, Ru) fragments, can be synthesised by the reaction of *cis*-$MCl_2(dppe)_2$ (in CH_2Cl_2 or THF) in the presence of NH_4PF_6 and the diethynylaryl.[3b,15] Heterobimetallic complexes can be made much more readily than the analogous polyyne systems; monometallic precursors are first isolated, M(C≡CArC≡CH), and similar protocols as described above are used to add the next metal fragment.[16]

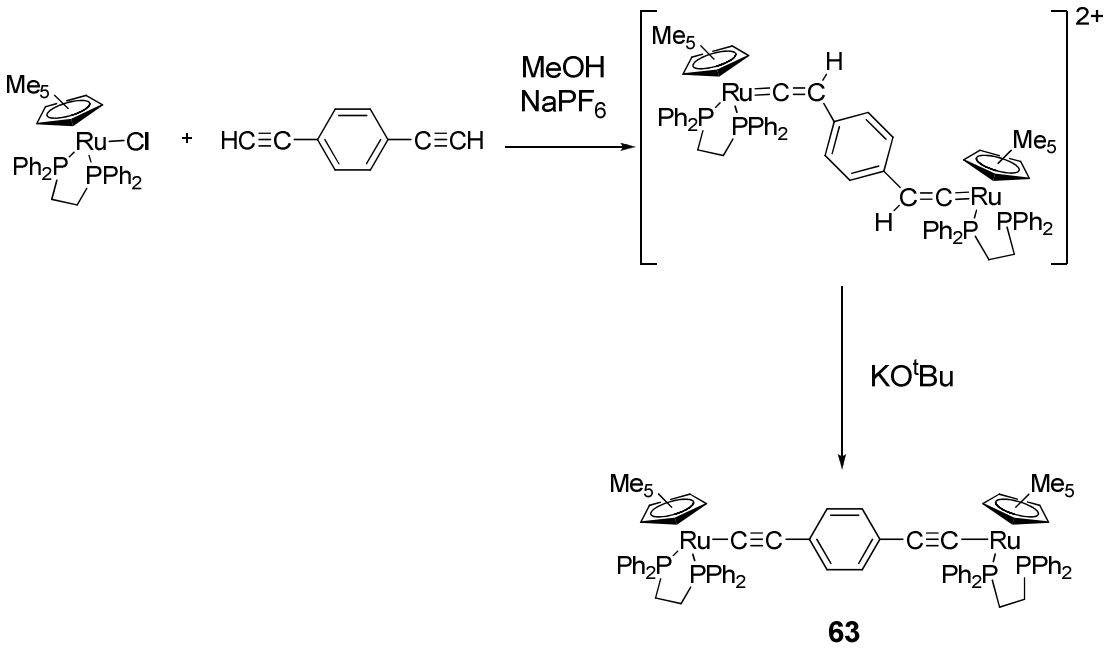

Scheme 1: Coupling methodology for the synthesis of complex 63.

In addition to simple substitutions of a benzene core (C_6H_4) the π-orbital energy of the diethynyl aromatic core can be increased by incorporating a naphthalene or anthracene fragments. These diethynyl bridges can be coordinated to metal fragments using similar coupling strategies as described above.[17] The presence of a largely aromatic core

allows the coordination of arenophiles, such as the 12 electron $[Ru(\eta^5\text{-}C_5Me_5)]^+$ moiety, which serves to alter the electronic characteristics of the bridge, in this case to increase the antiferromagnetic exchange between the two iron centres (Figure 6).[18]

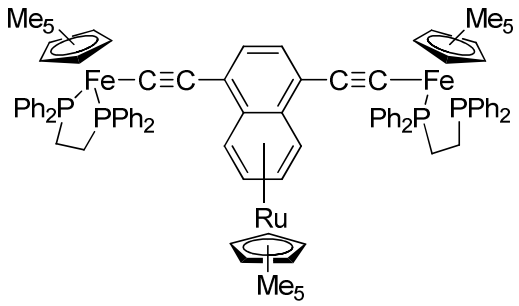

Figure 6: Diethynyl-naphthalene bridged complex with the arenophile $Ru(\eta^5\text{-}C_5Me_5)$ coordinated to the naphthalene moeity.

For mixed valence compounds where intramolecular electron transfer may take place, the 1,4-diethynylbenzene bridge generally promotes a delocalised electronic structure. DFT calculations on model iron systems, $[\{Fe(dHpe)(\eta^5\text{-}C_5H_5)\}_2\{\mu\text{-}C{\equiv}C(C_6H_4)C{\equiv}C\}]$, show that in comparison to the butadiyndiyl bridged analogue, the HOMO is more bridge centred.[17] In homometallic bimetallic systems, this increased bridge character causes a complex NIR band for the mixed valence species. The bands are often truncated at lower energies, very intense, and exhibit little or no solvatochromic behaviour, indicating a delocalised ground state electronic structure.[3b,19] Deconvolution of the band in this region reveal multiple transitions, the assignment of which depend on how the various charge transfer theories are applied.

Replacement of the phenylene ring with anthracene, $[\{Fe(dppe)(\eta^5\text{-}C_5Me_5)\}_2\{\mu\text{-}C{\equiv}C(C_{14}H_8)C{\equiv}C\}]PF_6$ (**62A**),[17] causes no significant change in the NIR, Mössbauer and infrared spectra, hence demonstrating that the delocalised electronic structure is retained, although an increase by two orders of magnitude is seen for the K_c value in

comparison to the diethynyl benzene derivative (**62A** K_c = 1.3 x 10^6) and (**62** 2.6 x 10^4).[14a] Changing the substituents on the benzene ring, either by increasing or decreasing the electronegativity of the benzene ring, has a similar (but more subtle), effect to increasing the aromaticity of the ring. This results in a delocalised electronic structure being retained.[20] Increasing the number of benzene rings at the core (a di-phenyl core) causes the NIR band to become broader and more solvatochromic in comparison to a single phenyl core, indicating it has a more localised electronic structure for the mixed valence complex (Figure 7).[21]

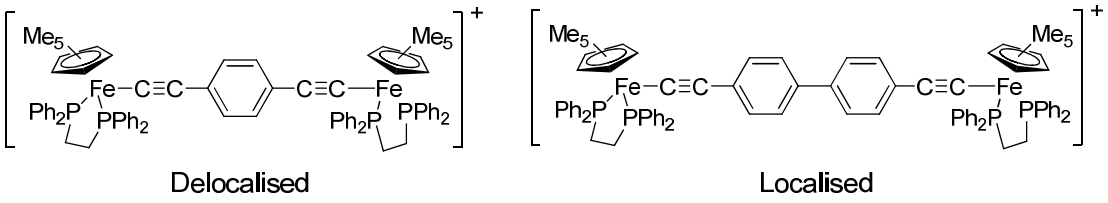

Figure 7: Successive inclusion of phenylene units to the bridging moiety to change the ground state from localised to delocalised.

Upon changing the linkage through the benzene from 1,4 to 1,3, the nature of the NIR band changes it gives rise to a more localised electronic structure, where the NIR band is generally deconvoluted into several bands dominated by a broad relatively low intensity band.[14b,22] This has important connotations in the development of dendrimer systems based around a benzene core where the localisation of charge is important in the development of redox active nano-magents.[23] Hetero-metallic complexes, such as [{Fe(dppe)(η^5-C_5Me_5)}(μ-C≡C(C_6H_4)C≡C){Ru(dppe)$_2$R}]PF_6 (R = Cl, C≡C$C_6H_4NO_2$-4) produces a high energy NIR band, centered around 8500 cm^{-1}. The assignment of the principal transitions are fraught with ambiguity owing to the mixing of the diethynylbenzene ring with the 18 and 17 electron fragments. However, infrared spectroscopic data point towards a largely delocalised electronic structure.[24]

6.2 Synthesis

The syntheses of [Mo{C≡C(C_6H_4)C≡CH}(dppe)(η^7-C_7H_7)] (**66**), and [{Mo(dppe)(η^7-C_7H_7)}$_2${μ-C≡C(C_6H_4)C≡CH}]$^{n+}$ (**67^{n+}**), (n = 0, 1 and 2) were both carried out by Dr. E.C. Fitzgerald at the University of Manchester, the details of which are briefly included here for completeness.

The reaction of **5** in the presence of a large excess of HC≡C(C_6H_4)C≡CH and KO^{t}Bu leads to the formation of the mono-metallic **66** in good yield as a brown solid. The formation of the bimetallic complex **67** was carried out in a two step process. Firstly, **5** and HC≡C(C_6H_4)C≡CH were reacted together in a 2:1 ratio to form a bis-vinylidene complex [{Mo(dppe)(η^7-C_7H_7)}$_2${μ-=C=CH(C_6H_4)HC=C=}][PF_6]$_2$, [**68**][PF_6]$_2$; subsequently the deprotonation of [**68**][PF_6]$_2$ with KO^{t}Bu in acetone and the purification using a Celite column yielded **67** (Scheme 2).

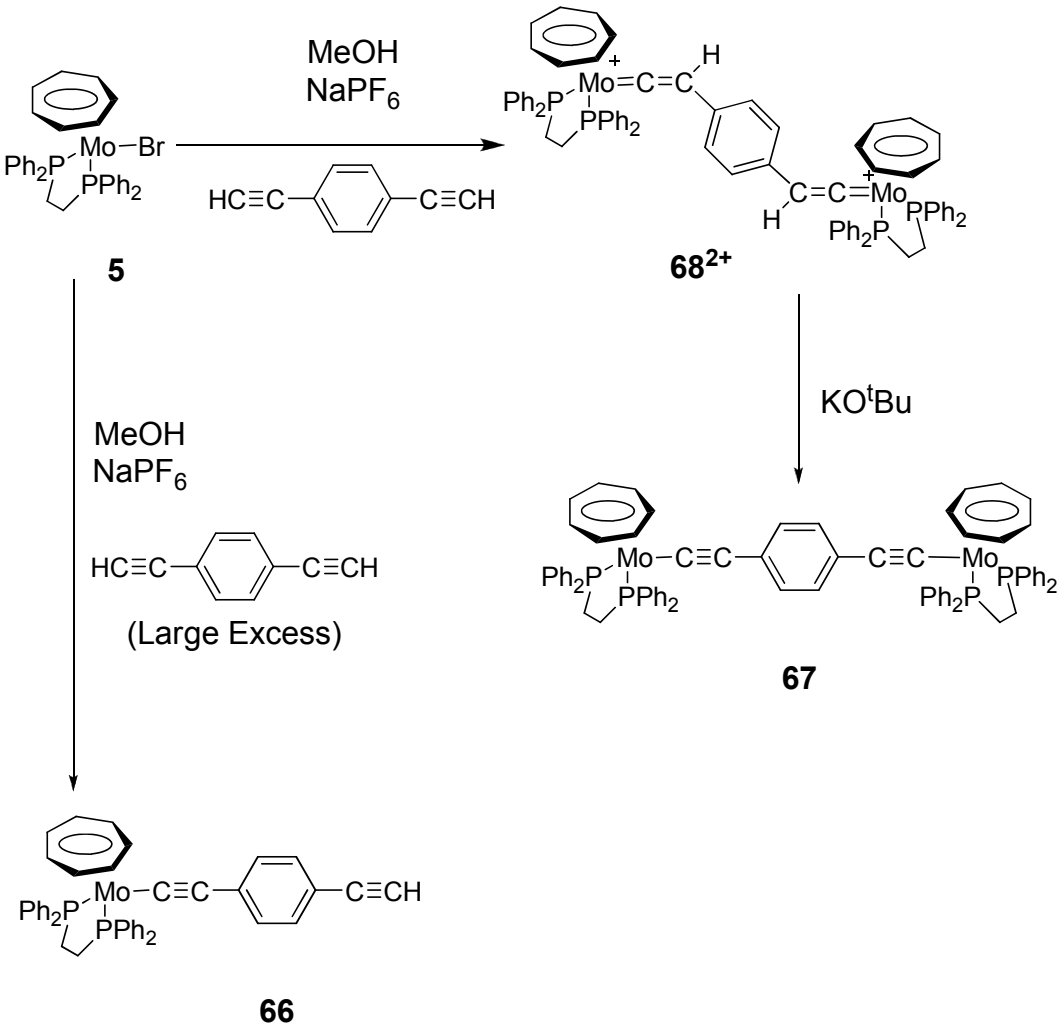

Scheme 2: Synthesis of 66 and 67.

As demonstrated in Chapters four and five, chemical oxidation of homo-bimetallic molybdenum complexes has been very successful, allowing the isolation of **67** in its various oxidation states. The reaction of **67** with one or two equivalents of $[Fe(\eta^5\text{-}C_5H_5)_2][PF_6]$ quantitatively forms [**67**]PF_6 and [**67**][$[PF_6]_2$ respectively.

6.3 Electrochemistry

The complexes **66** and **67** exhibit one (**66**) or two (**67**) diffusion controlled, chemically reversible, one electron oxidation processes under the conditions stated in Table 1, with the separation between the cathodic and anodic peak potentials comparable to that determined for the internal ferrocene standard.

Table 1: Cyclic voltammetry data, recorded at a Pt electrode in 0.1 M $^{n}Bu_4NPF_6$ /CH_2Cl_2. Referenced to FcH /FcH^+ = 0.00 V. (Where [Mo] = Mo(dppe)(η^7-C_7H_7))

Complex	$^1E_{1/2}$ /V	$^2E_{1/2}$ /V	ΔE^o /mV	K_c
[Mo]C≡CC_6H_5 (**1**)	-0.72	-	-	-
[Mo]C≡C($C_2B_{10}H_{10}$)C≡C[Mo] (**45**)	-0.71	-0.63	85	35
[Mo]C≡C($C_2B_{10}H_{10}$)C≡CH (**50**)	-0.64	-	-	-
[Mo]C≡CC≡C[Mo] (**57**)	-0.94	-0.51	430	2.5×10^7
[Mo]C≡C(C_6H_4)C≡CH (**66**)	-0.68	-	-	-
[Mo]C≡C(C_6H_4)C≡C[Mo] (**67**)	-0.84	-0.67	170	8.4×10^2

The monometallic complex **66** exhibits a single oxidation event at a similar potential to that of the most electron withdrawing aryl acetylide complexes, for example [Mo(C≡CCO_2Me)(dppe)(η^7-C_7H_7)] (**10**) ($^1E_{1/2}$ = -0.65 V). The first oxidation potential for **67** is 160 mV lower than the monometallic analogue **66**, this is in keeping with the observed first oxidation potential of the bimetallic analogues **57** and **45** (which are both lower than the mono-metallic analogues). A comparison of the $^1E_{1/2}$ potentials for **57** and **67**, reveals that **67** is 100 mV harder to oxidize than **57**. The analogous di-iron complex, **62**, is over 400 mV harder to oxidize than its butadiyndiyl bridged counterpart. [25]

6.4 Infrared Spectroelectrochemistry

Although the complexes can be chemically oxidised quite easily, for the simplicity of collecting a series of data, the oxidised forms of the mono, and especially the bi-metallic species **66** and **67** were generated *in situ* by spectroelectrochemical techniques. To confirm that the oxidised species were thr electrochemically generated complexes and not the product of a chemical reaction, each experiment was conducted in a cycle of oxidation and reduction. The recovery of the original spectrum demonstrates the chemical reversibility of the redox chemistry (Table 2).

Table 2: Infrared spectroelectrochemical data for 66^{n+} and 67^{n+} recorded in 0.1 M $^{n}Bu_4NPF_6$ /CH_2Cl_2.

Complex	ν(C≡C)		
	n = 0	n = 1	n = 2
$\mathbf{66}^{n+}$	2101, 2042, 2026	2106, 2038, 2016	-
$\mathbf{67}^{n+}$	2048	2025, 1967	2014, 1964

The infrared spectrum of mono-metallic complex **66** exhibits two sets of ν(C≡C) stretching modes, where the higher frequency mode corresponds to the uncoordinated alkynyl bond. The lower frequency mode, corresponds to the coordinated alkynyl bond, which is split into two bands. The splitting of the ν(C≡C) bands coordinated to the metal centre is a common feature for complexes which have frontier orbitals of largely metal character, such as iron phenyl acetylide [Fe(C≡CC_6H_5)(dppe)(η^5-C_5Me_5)] (**2**),[26] and the molybdenum butadiyndiyl complexes (**20** and **24**). Upon oxidation, $\mathbf{66}^{+}$, the lower energy bands shift to lower energy by 4 and 10 cm^{-1} respectively, whilst the higher frequency band increases by 5 cm^{-1}. Small shifts in the ν(C≡C) are indicative of metal centered oxidation, as seen for other [Mo(dppe)(η^7-C_7H_7)] containing complexes described in this thesis.[27]

The bimetallic complex **67** exhibits a single ν(C≡C) at a similar frequency to the mono-metallic complex **66** (Figure 8). The removal of one electron to form $\mathbf{67}^{+}$ produces two ν(C≡C) stretches, which is indicative of a valence-trapped complex on the infrared timescale. The two bands have different intensities, as the symmetric ν(C≡C) gains intensity from being coupled to the charge transfer transition.[28] The higher frequency ν(C≡C) band is at a similar position to the ν(C≡C) stretch in the [Mo(dppe)(η^7-C_7H_7)] acetylide complexes. The infrared spectrum of $\mathbf{67}^{+}$ therefore points towards a localised structure for the mixed valence complex. The tail of an electronic transition is obvious in the infrared spectrum of $\mathbf{67}^{+}$, the nature of which will be discussed in greater detail below.

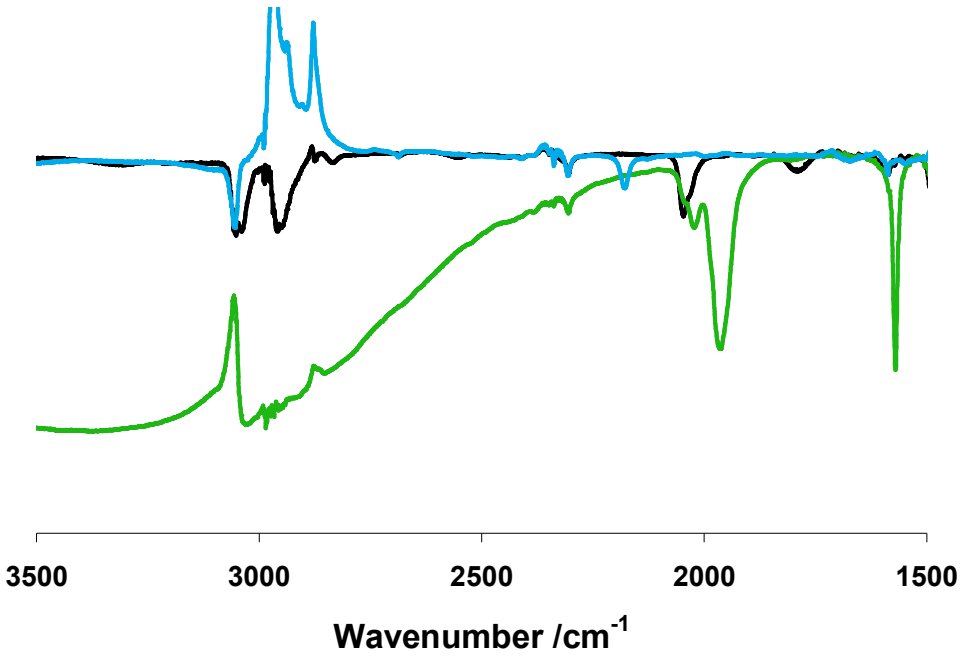

Figure 8: Infrared spectra of 67^{n+}, where n = 0 (Black), n = 1 (Green), n = 2 (Light blue) (Recorded in 0.1 M $^{n}Bu_4NPF_6$ /CH_2Cl_2).

6.5 Electronic Structure Calculations

The use of DFT and TD-DFT computations has provided valuable insight in the study of bimetallic molybdenum complexes their spectroscopic properties and elucidating the electron transfer process. In order to choose the appropriate level of theory, the mixed valence complex $[\{Mo(dHpe)(\eta^7\text{-}C_7H_7)\}_2\{\mu\text{-}C{\equiv}C(C_6H_4)C{\equiv}C\}]^+$ (**67H$^+$**), was first modeled to determine if a localised geometry could be generated, as the TD-DFT results from these models can be used to aid interpretion of the transitions in the NIR region.[29] After testing several combinations of functionals and basis sets, only the combinations MPW1K /LANL2DZ and CAM-B3LYP /LANL2DZ modeled **67H$^+$** with a localised electronic structure. To judge the suitability of the two models the TD-DFT calculations were compared to the experimental spectra, and these showed that the Coulomb attenuated functional (CAM-B3LYP) produced better agreement between the computed and observed data. For consistency the CAM-B3LYP /LANL2DZ model was used to compute $[\{Mo(dHpe)(\eta^7\text{-}C_7H_7)\}_2\{\mu\text{-}C{\equiv}C(C_6H_4)C{\equiv}C\}]$ (**67H**) and $[\{Mo(dHpe)(\eta^7\text{-}C_7H_7)\}_2\{\mu\text{-}C{\equiv}C(C_6H_4)C{\equiv}C\}]^{2+}$ (**67H^{2+}**).

6.5.1 Neutral Species Calculations

The two $[Mo(C{\equiv}C)(dppe)(\eta^7\text{-}C_7H_7)]$ moieties which are bonded to the benzene ring in **67H** have very similar geometries, with calculated Mo-C_1 and C_1-C_2 bond lengths comparable to those of **57H** and **45H** (Table 3). In addition, the calculated infrared spectrum, in terms of the relative intensities of the bands, were in good agreement with

the experimental data (although the calculated frequency was higher than the experimental value, 2189 cm^{-1} and 2048 cm^{-1} respectively).

Table 3: Calculated geometries of $67H^{n+}$ (where n = 0, 1, or 2).

Bond Length /Å	**67H**	**$67H^{+}$**		**$67H^{2+}$**
		Mo_1-C_1≡C_2	Mo_2-C_1≡C_2	
Mo_1-C_1	2.126	2.092	2.035	1.977
C_1-C_2	1.241	1.248	1.251	1.274
Mo_1-P_1 /Mo_1-P_2	2.531	2.537	2.566	2.560
	2.536	2.540	2.562	2.559
Bond Angle /^{o}				
Mo_{1A}-C_{1A}-C_{2A}	178.839	179.681	179.052	179.550
P_{1A}-Mo_{1A}-P_{2A}	178.560	177.421	178.427	176.939

Of central importance for this discussion is the composition of the filled molecular orbitals, as these allude to the degree of mixing between the metal centres, which are the primary sites of oxidation, and the bridge orbitals. The composition of the HOMO in **67H** reveals that it is evenly distributed between the [Mo(dppe)(η^7-C_7H_7)] fragments and the diethynylbenzene bridging moiety (51 % for [Mo(dppe)(η^7-C_7H_7)] and 49 % bridge fragment). To allow a full comparison of the calculations carried out on the carborane complex **45H** and the diynyl complex **57H**, the geometry of **67H** was also calculated at MPW1K /LANL2DZ. Upon changing the functional used, the composition of the HOMO changed slightly so that the Mo(dppe)(η^7-C_7H_7) fragment only contributes 48 %. This represents a progressive mixing between the bridging and metal moieties, whereby the bridge character of the HOMO gradually increases from 31 % (**45**) to 41 % (**57**) and finally to 52 % for the diethynylbenzene containing complex **67** (Figure 9). The mixing between these two components is also reflected in the changes in relative energies of metal d-orbitals. As expected, there is little difference between the lower lying orbitals comprising of the d_{x2-y2}, d_{xy}, d_{zy}, and d_{zx}, which is primarily due to the low

contribution of the bridge as a consequence of the strong δ- and π-interactions with the cycloheptatrienyl ring. However, the d_{z2} orbital (HOMO) of **67H** is further removed from the lower lying filled molecular orbitals, in comparison to **45** by 0.44 eV, but still 0.13 eV lower than **57**. If Koopman's theorem is evoked, such data can explain the electrochemical results, where the $^{1}E_{1/2}$ value for **57** is 100 mV easier to oxidize than **67**. The increased mixing shown in **67H** is a product of a better energy match between the diethynyl bridge and the [Mo(dppe)(η^{7}-C_7H_7)] d_{z2} metal d-orbital.

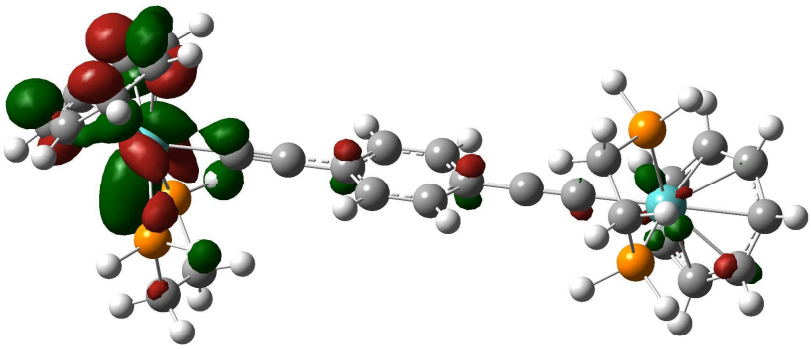

LUMO

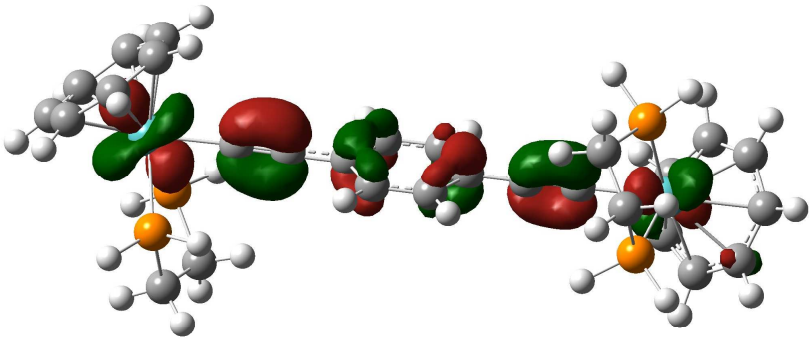

HOMO

Figure 9: HOMO and LUMO molecular orbital plots of 67H plotted as an isosurface at 0.04 au.

6.6 EPR Spectroscopy

The ease at which [**67**]PF_6 and [**67**][PF_6]$_2$ could be isolated permitted the examination of their X-band EPR spectra. This work was performed by Dr. E.C. Fitzgerald at the University of Manchester and is reproduced here to aid the discussion of these two complexes (Table 4).

Table 4: X-band EPR fluid solution (CH_2Cl_2, 243 K) of [67]PF_6 and [67][PF_6]$_2$.

Complex	a_{iso}(Mo)	a_{iso}(^{31}P)	a_{iso}(^{1}H)	g_{iso}
1^{+}	31.3	22.6	4.3	1.996
67^{+}	14.7	10	1.9	1.992
67^{2+}	31.3	22.7	4.3	1.993

The spectrum of [**67**]PF_6 is well resolved and has allowed the hyperfine coupling constants to be accurately simulated (this is in stark comparison to the spectra of **57**$^{+}$ for which no accurate hyperfines could be computed) (Figure 10). The a_{iso}Mo value for **67**$^{+}$ is less than half that of the monometallic **1**$^{+}$ and **45**$^{+}$, indicating that the electron is equally coupled to both molybdenum centres on the EPR timescale. The same is true for the associated a_{iso}^{1}H(C_7H_7) and a_{iso}^{31}P hyperfine coupling constants. As seen for the molybdenum acetylides, **1**$^{+}$, there is no evidence of the electron coupling to the protons on the benzene core of the bridge. These values show that the electron is coupled to both the molybdenum centres at the same time on this spectroscopic timescale, 10^{-9} s. Therefore, the rate of the electron transfer process in **67**$^{+}$ is faster than X-band EPR and therefore is faster than both the carboranyl **45**$^{+}$ (<10^{-9} s) and the butadiyndiyl **57**$^{+}$ (~ 10^{-9} s) bridged complexes.

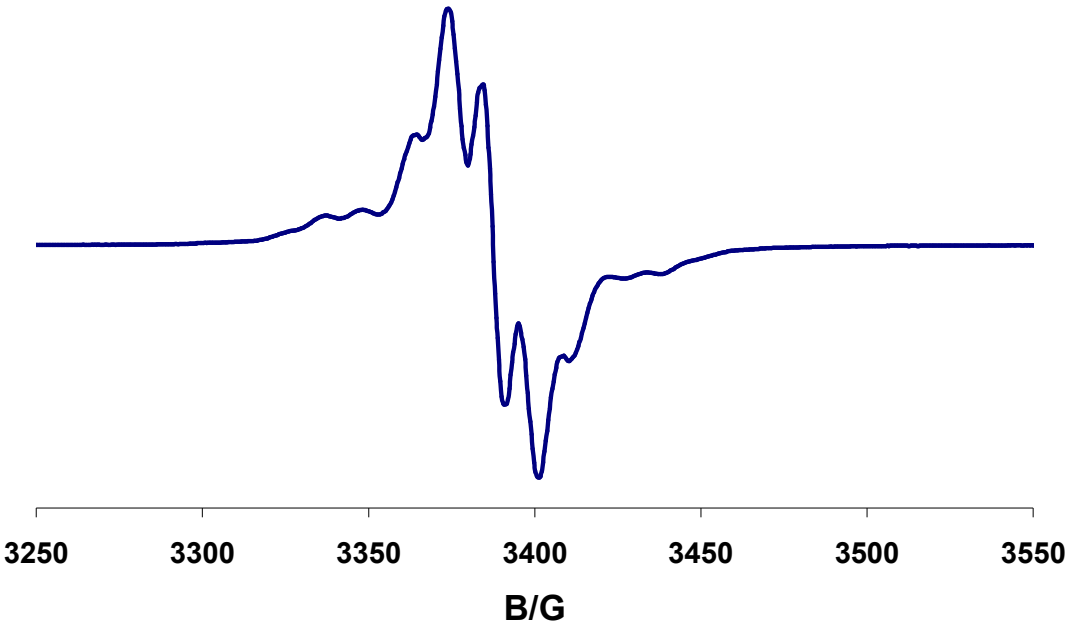

Figure 10: First derivative X-band EPR of [67]PF_6 recorded in CH_2Cl_2, 243 K.

Upon further oxidation to generate **67**$^{2+}$, the X-band EPR spectrum becomes similar to that of [Mo(C≡CR)(dppe)(η^7-C_7H_7)]$^+$, a feature that is seen for all the homo-bimetallic dications, [{Mo(dppe)(η^7-C_7H_7)}$_2$(μ-C≡CXC≡C)]$^{2+}$, studied in this thesis (Figure 11). Once again, this is an indication that **67**$^{2+}$ exists as a singlet biradical and is a consequence of the dominance of the metal d_{z2} orbital which causes the un-paired electrons to be trapped on the decoupled [Mo(dppe)(η^7-C_7H_7)]fragments.

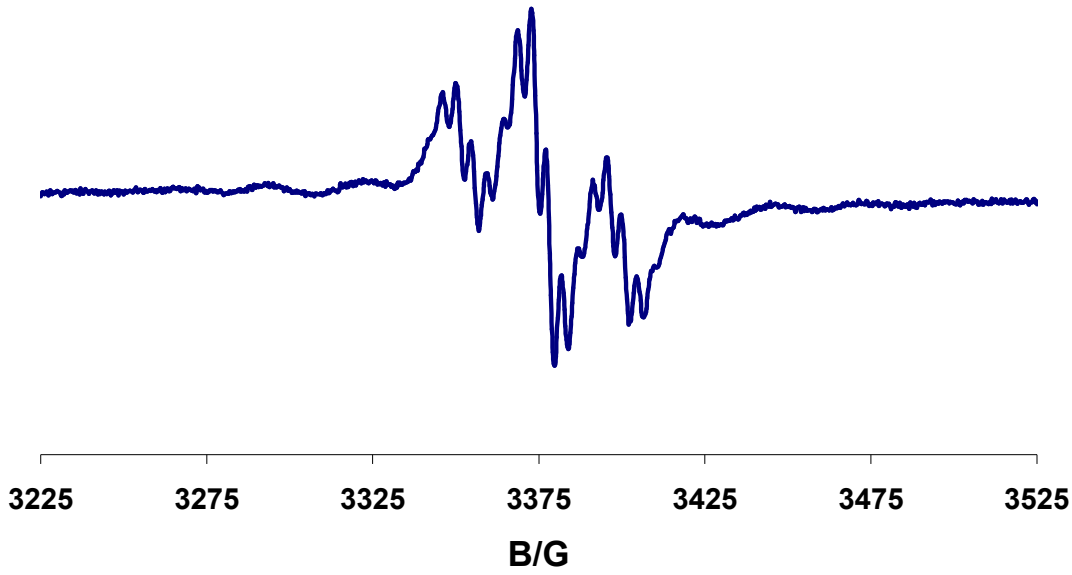

Figure 11: First derivative X-band EPR of [67][PF_6]$_2$ recorded in CH_2Cl_2, 243 K.

6.6.1 Monocation Species Calculations

At CAM-B3LYP /LANL2DZ, the geometry of **67H**$^+$ is calculated to have two distinct [Mo(dppe)(η^7-C_7H_7)] fragments, where the 17 electron fragment is distinguished from the other by an elongation of Mo-P bond lengths and a contraction of Mo-C_1 bond (Table 3). The localised structure is further defined by the calculated ν(C≡C) spectrum which shows two intense bands, in a 1:8 ratio, corresponding to the symmetric:asymmetric ν(C≡C) stretches.

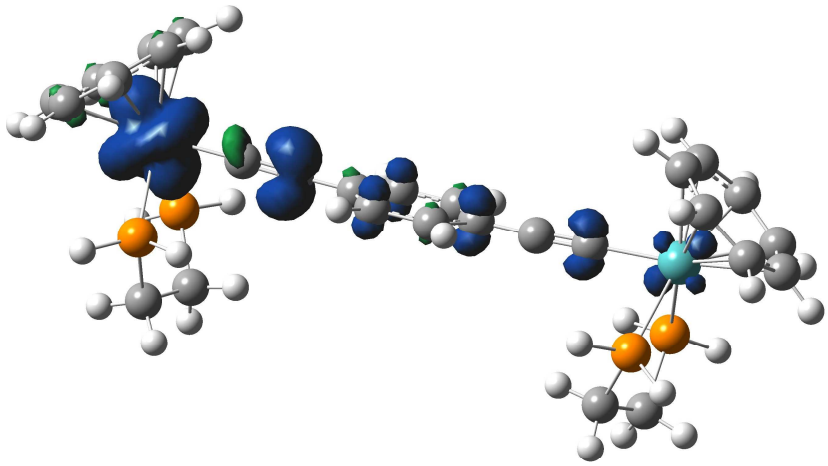

Figure 12: Spin density plot of $67H^+$.

Table 5: Mulliken spin denisty for $67H^+$ (Mo_1 and Mo_2 refer to each half of the compound).

Atom	$67H^+$ /Mo_1	$67H^+$ /Mo_2
Mo	0.814233	0.080643
C_1	-0.076048	-0.015187
C_2	0.238368	0.095893
$\Sigma(C_6H_4)$	0.086439	

To aid the interpretation of the EPR spectrum the Mulliken spin densities for **67H**$^+$ have been calculated, revealing that the spin density is distributed mainly on one [Mo(dppe)(η^7-C_7H_7)] fragment (Table 5, Figure 12). However, in comparison to the carborane complex **45**$^+$ the distribution of spin density between the two molybdenum atoms is more even for **67H**$^+$ (Mo_1 = 0.814233 /Mo_2 = 0.080643), whereas for **45**$^+$ (Mo_1 = 1.264462 /Mo_2 = -0.000809), with more of the spin residing on the diethynylbenzene bridging moiety.

6.6.2 Dication Species Calculations

The geometry of the singlet state of **67H**$^{2+}$ was calculated, based upon the results from EPR spectroscopy. The preference of the singlet state over the triplet state is a common trait for homobimetallic [Mo(dppe)(η^7-C_7H_7)] complexes, and is exemplified by the identical EPR spectra for **45**$^{2+}$ and **57**$^{2+}$. The calculated singlet geometry of **67H**$^{2+}$ gives two identical Mo(dHpe)(η^7-C_7H_7) fragments, with a further contraction of the Mo-C_1 and elongation of Mo-P bond lengths. The identical nature of the two Mo(dppe)(η^7-C_7H_7) is further shown by the calculated infrared spectrum revealing a single intense ν(C≡C) band (Table 3).

The electronic structure closely resembles that of **45**$^{2+}$, whereby the HOMO is dominated by the δ-interaction between the molybdenum centre and the cycloheptatrienyl ring system. However, owing to the increased mixing of the diethynylbenzene bridge with the [Mo(dppe)(η^7-C_7H_7)] moiety 60 % of the HOMO is comprised from contributions of the bridge, whereas for **45**$^{2+}$ only 25 % of the HOMO is comprised of the diethynylcarborane bridge. The even distribution of the HOMO across the complex, and more importantly over the [Mo(dppe)(η^7-C_7H_7)] fragments, goes some way to explain the EPR spectra of **67**$^{2+}$. However, despite the DFT model showing a larger contribution of bridge to the HOMO of the complex, there is still no evidence of the unpaired electrons being coupled to the protons on the bridging benzene ring in the experimental EPR spectrum.

The LUMO and HOMO are almost identical in character, both consisting of the metal d_{z2} orbital and large contributions form the bridging moiety. Overall, the sequence of oxidation events, from **67**, $\mathbf{67}^{+}$ to $\mathbf{67}^{2+}$, can be described in terms of the sequential depopulation of the HOMO of **67** (Figure 13).

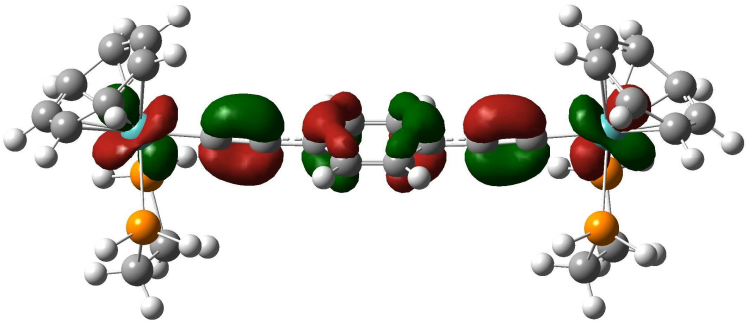

LUMO

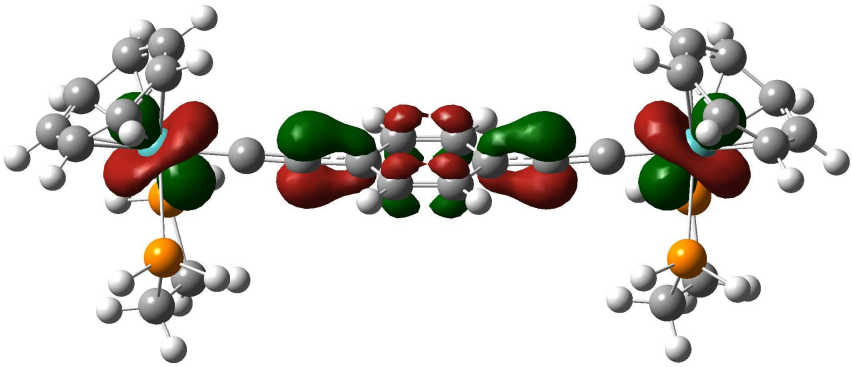

HOMO

Figure 13: HOMO and LUMO molecular orbital plots of $67H^{2+}$ plotted as an isosurface at 0.04 au.

6.7 UV /vis Spectroelectrochemistry and TD-DFT Calculations

As shown in previous Chapters, the combination of experimental spectra and TD-DFT calculations provide a powerful insight into the electronic structure of organometallic complexes. To aid the collection of information on each of the oxidation states, $\mathbf{67}^{n+}$ (n = 0, 1, 2) were generated *in situ* using spectroelectrochemical methods (Table 6, Figure 14).

Table 6: UV /vis spectroelectrochemical results of $[67]^{n+}$ (recorded in 0.1 M $^{n}Bu_4NPF_6$ /CH_2Cl_2) with TD-DFT assignments.

n	$\mathbf{67}^{n+}$	$\mathbf{67H}^{n+}$	
	Transition /cm^{-1} (ε /M^{-1} cm^{-3})	Transition /cm^{-1} (intensity)	Character of transition
0	17900 (1900)	19400 (0.0011)	Mo → C_7H_7
	23600 (21000)	19600 (0.0089)	Mo → C_7H_7
	31600 (21600)	30100 (0.1056)	Mo → dHpe
	38200 (33900)	31700 (1.1836)	Mo → C_6H_4
		42000 (0.3377)	Mo → C_6H_4
+1	15600 (3900)	21800 (0.1858)	MoC≡C → C_6H_4C≡CMo
	19900 (6700)	26700 (0.1932)	MoC≡C → C_6H_4C≡CMo
	26600 (10400)	28700 (0.3495)	MoC≡C → C_6H_4C≡CMo
	37200 (30700)	39500 (0.1488)	MoC_7H_7 → dHpe
+2	12200 (2050)	12900 (0.5511)	Mo → C≡C(C_6H_4)C≡C
	15300 (16200)	14400 (1.803)	Mo → C≡C(C_6H_4)C≡C
	21700 (11500)	27300 (0.0969)	Mo → C_7H_7
	27000 (11500)	32900 (0.1142)	C≡C → Mo
	31800 (21700)	42200 (0.2805)	C_7H_7 → Mo
	37500 (35400)	50300 (0.1224)	C≡C → Mo

The electronic spectrum of **67** is typical of all [Mo(dppe)(η^7-C_7H_7)] supported alkynyl complexes, where the majority of the transitions (17900 to 32000 cm^{-1}) are concerned with transitions between the cycloheptatrienyl and phosphine ligands and the molybdenum centre. Uniquely for **67**, the highest energy transitions (38200 cm^{-1}) involve transitions from the molybdenum centre to the benzene ring of the bridging moiety.

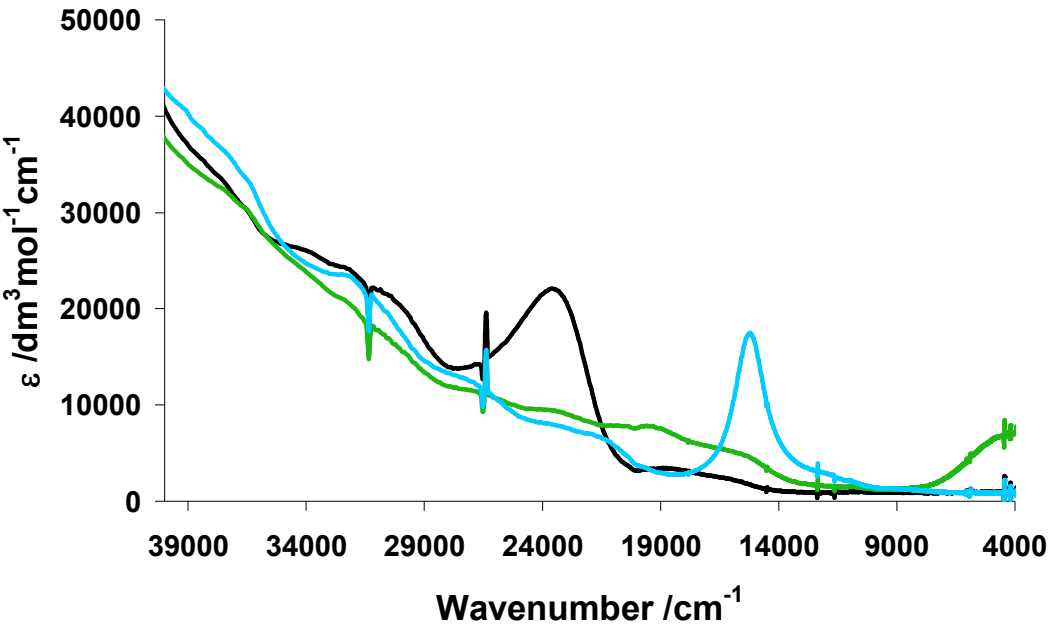

Figure 14: UV /vis spectra for 67^{n+}, where n = 0 (Black), n = 1 (Green), n = 2 (Light blue) (Recorded in 0.1 $M^nBu_4NPF_6$ /CH_2Cl_2).

Upon oxidation to **67**$^+$, a number of low energy electronic transitions are observed below 12000 cm^{-1}, the nature of which will be discussed later in this Chapter. The composition of the transitions between 30000 and 12000 cm^{-1} are more ambiguous than those found in **45**$^+$ and **57**$^+$ owing to the increased mixing between the bridging ligand and [Mo(dppe)(η^7-C_7H_7)] fragment. The mixing of metal and ligand character of these transitions are common in organometallic complexes, while the terms MLCT /LMCT are less accurate they are useful in summarising general trends. As such, the transitions (15600, 19900 and 26600 cm^{-1}, table 6) are assigned as transitions between the nominal 18 electron [Mo(C≡C-)(dppe)(η^7-C_7H_7)] moiety and the 17 electron [Mo(C≡CC_6H_5)(dppe)(η^7-C_7H_7)] moiety, admixed with bridge character. Transitions above 30000 cm^{-1} are more typical of complexes containing the 17 electron

$[Mo(dppe)(\eta^7\text{-}C_7H_7)]^+$ fragment, which are transitions between the cycloheptatrienyl ring /phosphines and the molybdenum centre.

The electronic spectra of $\mathbf{67}^{2+}$ is similar to the diynyl complex $\mathbf{57}^{2+}$, where there is an intense low energy transition at 15000 cm^{-1} which is calculated to be MLCT in character, as was predicted for $\mathbf{57}^{2+}$. The higher energy transitions (20000 – 30000 cm^{-1}) are also calculated to be MLCT in character, mirroring the diynyl complex $\mathbf{57}^{2+}$.

6.8 NIR Spectroscopy

An analysis of the NIR region for both **67** and $\mathbf{67}^{2+}$ contained no bands that were distinguishable from the baseline. However, for $\mathbf{67}^{+}$, an intense, broad band, asymmetric envelope is observed (centered at 5000 cm^{-1}) which is truncated at a lower energy. The ease at which [**67**]PF_6 could be isolated has allowed the thorough investigation of this region of the spectrum, using the methodology as described Chapters four and five.

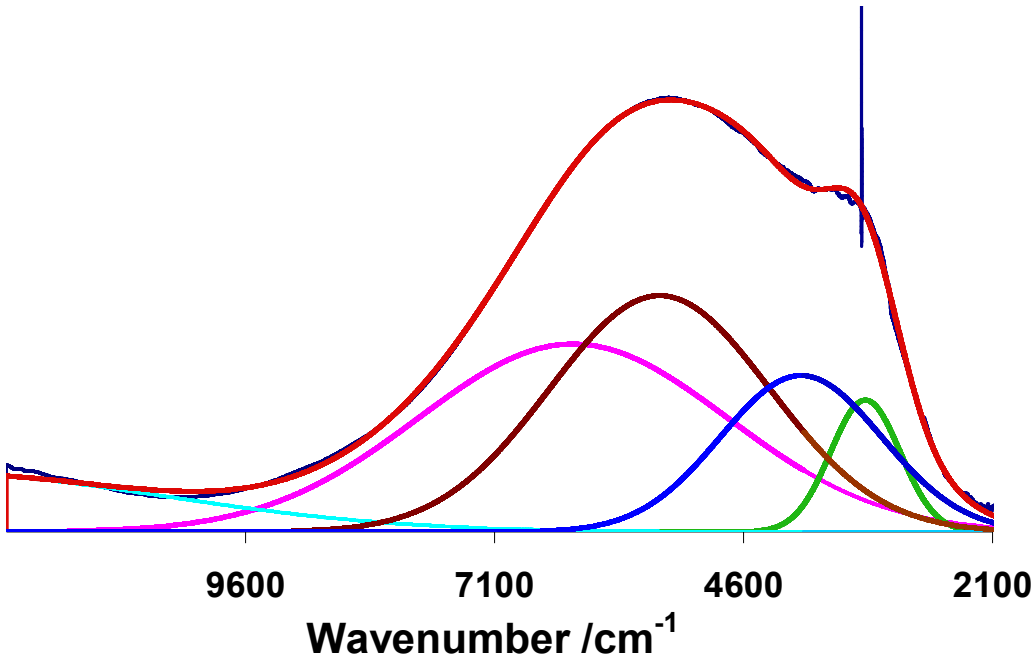

Figure 15: NIR spectrum of [67]PF_6 recorded in acetone.

Table 7: Deconvoluted band data for [67]PF_6 in acetone.

Acetone	IT (1)	IT (2)	IT (3)	LMCT
ν /cm^{-1}	3300	3900	5400	6200
$\Delta\nu_{1/2}$ /cm^{-1}	830	1900	2600	3700
A	0.15	0.18	0.27	0.21

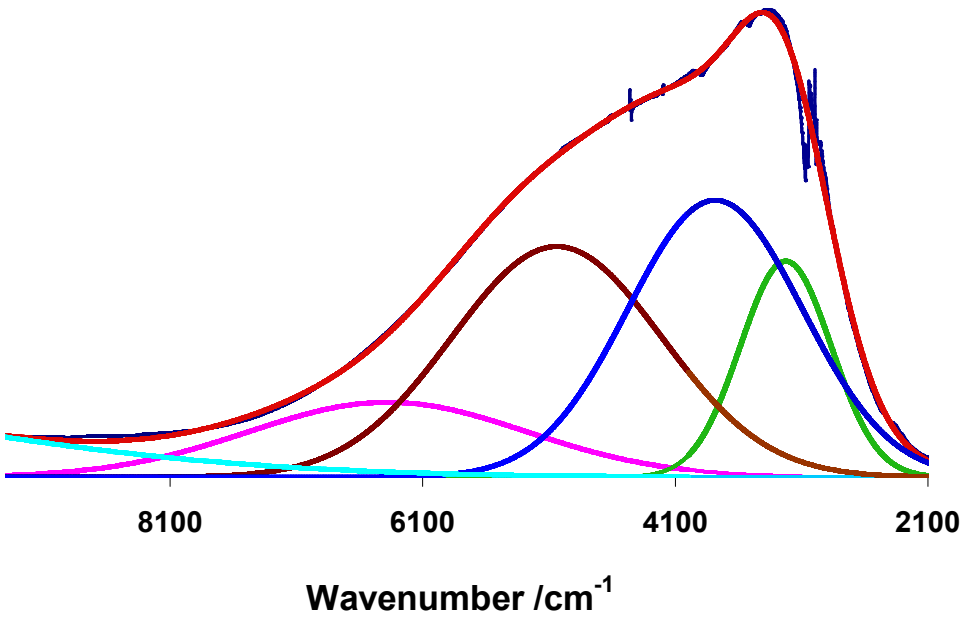

Figure 16: NIR spectrum of [67]PF_6 recorded in CH_2Cl_2.

Table 8: Deconvoluted band data for [67]PF_6 in CH_2Cl_2.

CH_2Cl_2	IT (1)	IT (2)	IT (3)	LMCT
ν /cm^{-1}	3200	3700	5000	6300
$\Delta\nu_{1/2}$ /cm^{-1}	820	1600	2000	2700
ε /$dm^3mol^{-1}cm^{-1}$	2000	2600	2200	700

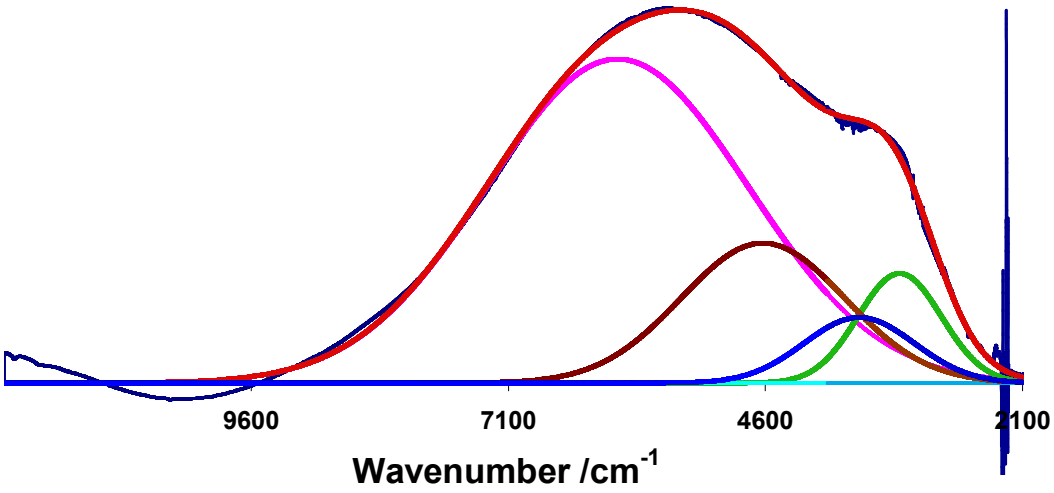

Figure 17: NIR psectrum of [67]PF_6 recorded in MeCN.

Table 9: Deconvoluted band data for [67]PF_6 in MeCN.

MeCN	IT (1)	IT (2)	IT (3)	LMCT
ν /cm^{-1}	3200	3600	4500	6000
$\Delta\nu_{1/2}$ /cm^{-1}	950	1400	2000	3100
A	0.12	0.07	0.15	0.35

The NIR spectrum of [**67**]PF_6 was recorded in a range of solvent media and the resulting band envelopes deconvoluted into four Gaussian bands, all of which were solvatochromic (Table 7-9, Figure 15-17). However, due to the limited solubility of **67**$^+$ in acetone and MeCN the extinction coefficients were only calculated for spectrum recorded in CH_2Cl_2. The solvatochromism of the bands is indicative of a localised ground state, which is a common feature for [Mo(dppe)(η^7-C_7H_7)] capped complexes owing to the unique electronic symmetry imposed on the complex by the molybdenum

d_{z2} orbital. Unlike the previous bimetallic complexes studied, the identities of the deconvoluted bands are much more difficult to assign, owing to similar intensities and the solvatochromic nature. In addition to the bands changing in energy, the relative intensities of the bands altered changed dramatically upon changing the dielectric constant of the solvent medium. Although the charge transfer transitions are expected to be solvatochromic, the LMCT-type transition is also solvatochromic. By increasing the polarity of the solvent medium, it acts to stabilise the polarised states involving the bridging ligand. This in turn causes both the energy the LMCT-type transition to lower, most likely through the stabilisation of the donor portion ([Mo(C≡CC_6H_5)(dppe)(η^7-C_7H_7)]) of the complex. Therefore, increasing the mixing between the [Mo(dppe)(η^7-C_7H_7)] fragment and the bridge serves to amplify this effect.

Owing to the increased mixing of the bis(ethynyl)benzene bridge with the [Mo(dppe)(η^7-C_7H_7)] moiety, the common two state interpretation is not sufficient to describe the electronic structure. This is emphasised by the predicted band widths of IT(1) being much wider than the experimentally obtained results (2700 cm^{-1} and 820 cm^{-1} respectively). Thus, a three state approximation is used. Using this model the mixing of three electronic states can be described as an adiabatic ground state and charge transfer state and a diabatic bridge state. The adiabatic ground state is confirmed by the solvatochromic nature of the NIR band and infrared spectroscopy. Moreover, the increased mixing of the states has been inferred by the DFT calculations. The increased mixing between these states serves to increase the intensity of the charge transfer transitions and the LMCT transitions in this region, causing further ambiguity to the assignment of the convoluted bands.

The generation of a localised geometry for **67H**$^{+}$ has allowed TD-DFT calculations to be used to aid the assignment of the complex NIR band. As seen in Chapter four, the TD-DFT calculation fails to accurately reproduce the spectroscopic data, however, it provides an intuitive visualisation of the molecular orbitals involved (Figure 18).

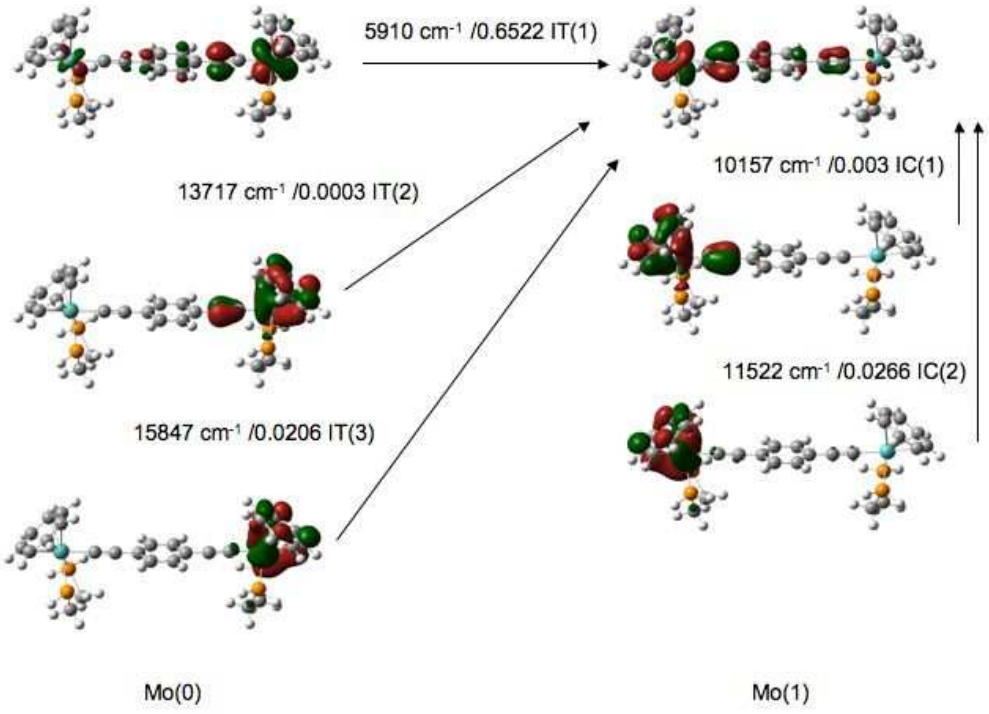

Figure 18: TD-DFT assignments for the first 5 electronic transitions of 67H^{+} (Molecular orbitals plotted as isosurfaces at 0.04 au) (Values displayed as calculated energy /oscillation strength).

Although, the calculation does not show the relative order of the NIR transitions, it is possible to see the increased involvement of the bridge in the composition of the intervalence transitions.

Although the inclusion of bridge and metal fragments in the charge transfer processes complicates the description of the NIR transitions, assignments of the spectroscopic data can still be made. The lowest energy bands 3200, 3800 cm^{-1} (in CH_2Cl_2) and the

band at 5000 cm^{-1} (in CH_2Cl_2) can be assigned to be charge transfer bands, IT(1), IT(2) and IT(3) respectively, as they exhibit the most solvatochromic behaviour. The band at 6300 cm^{-1} in CH_2Cl_2, has the most LMCT character, as such is more solvent independent. In comparison to $\mathbf{57}^+$, this transition is over 2000 cm^{-1} lower in energy than $\mathbf{67}^+$, which is similar in energy to that of the charge transfer transitions. The lowering of the LMCT-type transition mirrors the increased rate of electron transfer in comparison to $\mathbf{45}^+$ and $\mathbf{57}^+$ as determined by EPR spectroscopy. In addition, the solvatochromic behaviour of IT(1) becomes less pronounced as the bridging moiety becomes more heavily mixed with the [Mo(dppe)(η^7-C_7H_7)] fragment ($\mathbf{45}^+$ varies by 600 cm^{-1}, $\mathbf{57}^+$ varies by 700 cm^{-1} and $\mathbf{67}^+$ varies by 100 cm^{-1}), which indicates that the two redox sites are becoming more strongly coupled to one another. In addition, the intensities of the LMCT and IT transitions is indicative of bridge becoming increasingly implicit in the charge transfer process.

6.9 Conclusion

By changing the bridging moiety to 1,4-diethynylbenzene, the degree of mixing between the [Mo(dppe)(η^7-C_7H_7)] moiety and the bridge increases in comparison to the carborane analogue **45** and the diynyl analogue **57**. Despite this increased mixing, the phenylene bridged complex **67**$^+$ remains a true mixed valence complex owing to the unique electronic structure of the 17 electron [Mo(dppe)(η^7-C_7H_7)] fragment. A three state approximation of electronic states involved in the charge transfer process has been applied to **67**$^+$ in order to rationalise the NIR spectrum, revealing that the nominally LMCT-type transition is significantly lower in energy in comparison to **57**$^+$. This serves to increase the rate of electron transfer, and by using different spectroscopic timescales, this can be estimated to be between 10^{-10} – 10^{-12} s. As found for **45**$^{2+}$ and **57**$^{2+}$, EPR measurements and computational results show **67**$^{2+}$ is also a singlet bi-radical.

6.10 General Proccdures

General experimental procedures have been described in Chapter two.

6.10.1 Computational Details

All calculations were carried out using the Gaussian 03 package[30] and the Gaussian 09 package.[31] The model geometries **67H^{n+}** (n = 0, 1 or 2) discussed here were optimised using CAM-B3LYP and MPW1K[32], with no symmetry constraints. The pseudo-potential LANL2DZ[33] was used for all the atoms. Frequency calculations were carried out these optimised geometries at the corresponding levels and shown to have no imaginary frequencies. Molecular orbital and TD-DFT computations were carried out on these optimised geometries at the appropriate level of theory and the orbital contributions were generated with the aid of the GaussSum.[34]

6.11 References

[1] (a) M.S. Khan, M.R.A. Al-Mandhary, M.K. Al-Suti, T.C. Corcoran, Y. Al-Mahrooqi, J.P. Attfield, N. Feeder, W.I.F. David, K. Shamkland, R.H. Friend, A. Kohler, E.A. Marseglia, E. Tedesco, C.C. Tang, P.R. Raithby, J.C. Collings, K.P. Roscoe, A.S. Batsanov, L.M. Stimson, T.B. Marder, *New. J. Chem.,* 2003, **27**, 140. (b) S. Takahashi, Y. Kuroyama, K. Songashira, N. Hagihara, *Synthesis,* 1980, 627. (c) M.J. Plater, J.P. Sinclair, S. Aiken, T. Gelbrich, M.B. Hursthouse, *Tetrahedron,* 2004, **60**, 6385. (d) T.X. Neean, G.M. Whitesides, *J. Org. Chem.,* 1988, **53**, 2489. (e) G.T. Crisp, T.P. Bubner, *Tetrahedron,* 1997, **53**, 11899.

[2] (a) Y. Zhu, M.O. Wolf, *J. Am. Chem. Soc.,* 2000, **122**, 10121. (b) K.R.J. Thomas, J.T. Lin, Y.S. Wen, *Organometallics,* 2000, **19**, 1008. (c) S. Le Stang, F. Paul, C. Lapinte, *Organometallics,* 2000, **19**, 1035. (d) S. Roue, S. Le Stang, L. Toupet, C. Lapinte, *C.R. Chimie,* 2003, **6**, 353.

[3] (a) D. Beljonne, M.C.B. Colbert, P.R. Raithby, R.H. Friend, J.L. Bredas, *Synth. Met.,* 1996, **81**, 179. (b) M.C.B. Colbert, J. Lewis, N.J. Long, P.R. Raithby, M. Younus, A.J.P. White, D.J. Williams, N.N. Payne, L. Yellowlees, D. Beljonne, N. Chawdhury, R.H. Friend, *Organometallics,* 1998, **17**, 3034. (c) F. Paul, S. Goeb, F. Justaud, G. Argouarch, L. Toupet, R.F. Ziessel, C. Lapinte, *Inorg. Chem.,* 2007, **46**, 9036.

[4] (a) W-Y. Wong, G-L. Lu, K-F. Ng, C-K. Wong, K-H. Choi, *J. Organomet. Chem.,* 2001, **637-639**, 159. (b) W-Y. Wong, K-Y. Ho, K-H. Choi, *J. Organomet. Chem.,* 2003, **670**, 17.

[5] (a) S.K. Hurst, M.P. Cifuentes, M.G. Humphrey, *Organoemtallics,* 2002, **21**, 2353. (b) T. Weyland, C. Lapinte, G. Frapper, M.J. Calhorda, J-F. Halet, L. Toupet, *Organometallics,* 1997, **16**, 2024. (c) N.J. Long, A.J. Martin, F.F. de Biani, P. Zanello, *J. Chem. Soc., Dalton. Trans.,* 1998, 2017. (d) I. Cuadrado, M. Moran, C.M. Casado, B. Alonso, J. Losada, *Coord. Chem. Rev.,* 1999, **195**, 395. (e) C.E. Powell, S.K. Hurst, J.P. Morrall, M.P. Cifuentes, R.L. Roberts, M. Samoc, M.G. Humphreys, *Organometallics,* 2007, **26**, 4456. (f) T. Weyland, K. Costuas, L. Toupet, J-F. Halet, C. Lapinte, *Organometallics,* 2000, **19**, 4228.

[6] (a) G.M. Dykes, *J. Chem. Technol. Biotechnol.,* 2001, **76**, 903. (b) R.L. Roberts, T. Schwich, T.C. Corkery, M.P. Cifuentes, K.A. Green, J.D. Farmer, P.J. Low, T.B. Marder, M. Samoc, M.G. Humphrey, *Adv. Mater.,* 2009, **21**, 2318. (c) T. Weyland, I. Ledoux, S. Brasselet, J. Zyss, C. Lapinte, *Organometallics,* 2000, **19**, 5235.

[7] L. Medei, L. Orian, O.V. Semeikin, M.G. Peterleitner, N.A. Ustynyuk, S. Santi, C. Durante, A. Ricci, C. Lo Sterzo, *Eur. J. Inorg. Chem.,* 2006, 2582.

[8] S. Takahashi, H. Morimoto, E. Murata, S. Kataoka, K. Sonogashira, N. Hagihara, *J. Poly. Sci.,* 1092, **20**, 565.

[9] H.B. Fyfe, M. Mlekuz, D. Zargarian, N.J. Taylor, T.B. Marder, *J. Chem. Soc., Chem. Commun.,* 1991, 188.

[10] (a) O. Lavastre, M. Even, P.H. Dixneuf, *Organometallics,* 1996, **15**, 1530. (b) O. Lavastre, J. Plass, P. Bachmann, S. Guesmi, C. Mionet, P.H. Dixneuf, *Organometallics*, 1997, **16**, 184. (c) S. Takahashi, Y. Ohyama, E. Murata, K. Sonogashira, N. Hagihara, *J. Poly. Sci.,* 1980, **18**, 349.

[11] B. Kim, J.M. Beebe, C. Olivier, S. Rigaut, D. Touchard, J.G. Kushmerick, X-Y Zhu, C.D. Frisbie, *J. Phys. Chem. C.,* 2007, **111**, 7521.

[12] N. Chawdhury, N.J. Long, M.F. Mahon, L-L. Ooi, P.R. Raithby, S. Rooke, A.J.P. White, D.J. Williams, M. Younus, *J. Organomet. Chem.,* 2004, **689**, 840.

[13] M.S. Khan, M.K. Al-Suti, M.R.A. Al-Mandhary, B. Ahrens, J.K. Bjernemose, M.F. Mahon, L. Male, P.R. Raithby, R.H. Friend, A. Kohler, J.S. Wilson, *Dalton, Trans,* 2003, 65.
[14] (a) N. Le Narvor, C. Lapinte, *Organometallics,* 1995, **14**, 634. (b) M.A. Fox, J.D. Farmer, R.L. Roberts, M.G. Humphrey, P.J. Low, *Organometallics,* 2009, **28**, 5266.
[15] (a) M. Younus, N.J. Long, P.R. Raithby, J. Lewis, *J. Organomet. Chem.,* 1998, **570**, 55. (b) S.K. Hurst, M.P. Cifuentes, A.M. McDonagh, M.G. Humphrey, M. Samoc, B. Luther-Davies, I. Asselberghs, A. Persoons, *J. Organomet. Chem.,* 2002, **642**, 259. (c) G. Albertin, S. Antoniutti, E. Bordignon, M. Branzotto, *J. Organomet. Chem.,* 1999, **585**, 83.
[16] (a) K. M-C. Wong, S. C-F. Lam, C-C Ko, N. Zhu, V. W-W. Yam, S. Roue, C. Lapinte, S. Fathallah, K. Costuas, S. Kahlal, J-F. Halet, *Inorg. Chem.,* 2003, **42**, 7086. (b) N. Gauthier, C. Olivier, S. Rigaut, D. Touchard, T. Roisnel, M.G. Humphrey, F. Paul, *Organometallics,* 2008, **27**, 1063.
[17] F. de Montigny, G. Argouarch, K. Costuas, J-F. Halet, T. Roisnel, L. Toupet, C. Lapinte, *Organometallics,* 2005, **24**, 4558.
[18] (a) Y. Tanaka, J.A. Shaw-Taberlet, F. Justaud, O. Cador, T. Roisnel, M. Akita, J-R Hamon, C. Lapinte, *Organometallics,* 2009, **28**, 4656. (b) J.A. Shaw-Taberlet, S. Sinbandhit, T. Roisnel, J-R. Hamon, C. Lapinte, *Organometallics,* 2006, **25**, 5311.
[19] (a) A. Klein, O. Lavastre, J. Fiedler, *Organometallics,* 2006, **25**, 635. (b) S.I. Ghazala, F. Paul, L. Toupet, T. Roisnel, P. Hapiot, C. Lapinte, *J. Am. Chem. Soc.,* 2006, **128**, 2463.
[20] Y. Matsuura, Y. Tanaka, M. Akita, *J. Organomet. Chem.,* 2009, **694**, 1840.
[21] S.I. Ghazala, F. Paul, L. Toupet, T. Roisnel, P. Hapiot, C. Lapinte, *J. Am .Chem. Soc.,* 2006, **128**, 2463.
[22] T. Weyland, K. Costuas, L. Toupet, J-F. Halet, C. Lapinte, *Organometallics,* 2000, **19**, 4228.
[23] T. Weyland, K. Costuas, A. Mari, J-F. Halet, C. Lapinte, *Organometallics,* 1998, **17**, 5569.
[24] N. Gauthier, C. Olivier, S. Rigaut, D. Touchard, T. Roisnel, M.G. Humphrey, F. Paul, *Organometallics,* 2008, **27**, 1063.
[25] F. Coat, F. Paul, C. Lapinte, L. Toupet, K. Costuas, J-F. Halet, *J. Organomet. Chem.,* 2003, **683**, 368.
[26] F. Paul, J-Y. Mevellec, C. Lapinte, *Dalton. Trans.,* 2002, 1783.
[27] N.J. Brown, D. Collison, R. Edge, E.C. Fitzgerald, M. Hellowell, J.A.K. Howard, H.N. Lancashire, P.J. Low, J.J.W. McDouall, J. Raftery, C.A. Smith, D.S. Yufit, M.W. Whiteley, *Organometallics,* 2010, **29**, 1261.
[28] B.S. Brunsching, C. Creutz, N. Sutin, *Chem. Soc. Rev.,* 2002, **31**, 168.
[29] (a) M.A. Fox, R.L. Roberts, T.E. Baines, B. Le Guennic, J-F. Halet, F. Hartl, D.S. Yufit, D. Albesa-Jove, J.A.K. Howard, P.J. Low, *J. Am. Chem. Soc.,* 2008, **130**, 3566.
[30] M.J. Frisch, G.W. Trucks, H.B. Schlegel, G.E. Scuseria, M.A. Robb, J.R. Cheeseman, J.A. Montgomery Jr., T. Vreven, K.N. Kudin, J.C. Burant, J.M. Millam, S.S. Iyengar, J. Tomasi, V. Barone, B. Mennucci, M. Cossi, G. Scalmani, N. Rega, G.A. Petersson, H. Nakatsuji, M. Hada, M. Ehara, K. Toyota, R. Fukuda, J. Hasegawa, M. Ishida, T. Nakajima, Y. Honda, O. Kitao, H. Nakai, M. Klene, X. Li, J.E. Knox, H.P. Hratchian, J.B. Cross, C. Adamo, J. Jaramillo, R. Gomperts, R.E. Stratmann, O. Yazyev, A.J. Austin, R. Cammi, C. Pomelli, J.W. Ochterski, P.Y. Ayala, K. Morokuma, G.A. Voth, P. Salvador, J.J. Dannenberg, V.G. Zakrzewski, S. Dapprich, A.D. Daniels, M.C. Strain,

O. Farkas, D.K. Malick, A.D. Rabuck, K. Raghavachari, J.B. Foresman, J.V. Ortiz, Q. Cui, A.G. Baboul, S. Clifford, J. Cioslowski, B.B. Stefanov, G. Liu, A. Liashenko, P. Piskorz, I. Komaromi, R.L. Martin, D.J. Fox, T. Keith, M.A. Al-Laham, C.Y. Peng, A. Nanayakkara, M. Challa- combe, P.M.W. Gill, B. Johnson, W. Chen, M.W. Wong, C. Gonzalez, J.A. Pople, GAUSSIAN 03, Revision C.02, Gaussian Inc., Wallingford, CT, 2004.

[31] Gaussian 09, Revision **A.1**, M. J. Frisch, G. W. Trucks, H. B. Schlegel, G. E. Scuseria, M. A. Robb, J. R. Cheeseman, G. Scalmani, V. Barone, B. Mennucci, G. A. Petersson, H. Nakatsuji, M. Caricato, X. Li, H. P. Hratchian, A. F. Izmaylov, J. Bloino, G. Zheng, J. L. Sonnenberg, M. Hada, M. Ehara, K. Toyota, R. Fukuda, J. Hasegawa, M. Ishida, T. Nakajima, Y. Honda, O. Kitao, H. Nakai, T. Vreven, J. A. Montgomery, Jr., J. E. Peralta, F. Ogliaro, M. Bearpark, J. J. Heyd, E. Brothers, K. N. Kudin, V. N. Staroverov, R. Kobayashi, J. Normand, K. Raghavachari, A. Rendell, J. C. Burant, S. S. Iyengar, J. Tomasi, M. Cossi, N. Rega, J. M. Millam, M. Klene, J. E. Knox, J. B. Cross, V. Bakken, C. Adamo, J. Jaramillo, R. Gomperts, R. E. Stratmann, O. Yazyev, A. J. Austin, R. Cammi, C. Pomelli, J. W. Ochterski, R. L. Martin, K. Morokuma, V. G. Zakrzewski, G. A. Voth, P. Salvador, J. J. Dannenberg, S. Dapprich, A. D. Daniels, Ö. Farkas, J. B. Foresman, J. V. Ortiz, J. Cioslowski, and D. J. Fox, Gaussian, Inc., Wallingford CT, 2009.

[32] (a) B.J. Lynch, P.L. Fast, M. Harris, D.G. Truhlar, *J. Phys. Chem. A.,* 2000, **104**, 4811. (b) B.J. Lynch, Y. Zhao, D.G. Truhlar, *J. Phys. Chem. A.,* 2003, **107**, 1384. (c) G.A. Petersson, M.A. Al-Laham, *J. Chem. Phys.,* 1991, **94**, 6081. (d) G.A. Petersson, A. Bennett, T.G. Tensfeldt, M.A. Al-Laham, W.A. Shirley, J. Mantzaris, *J. Chem. Phys.,* 1988, **89**, 2193.

[33] (a) P.J. Hay, W.R. Wadt, *J. Chem. Phys.,* 1985, **82**, 270. (b) W.R. Wadt, P.J. Hay, *J. Chem. Phys.,* 1985, **82**, 284. (c) P.J. Hay, W.R. Wadt, *J. Chem. Phys.,* 1985, **82**, 299.

[34] N.M. O'Boyle, A.L. Tenderholt, K.M. Langner, *J. Computational. Chem.,* 2007, **5**, 839.

Chapter 7: An Adventure through Cyanocarbon Chemistry

7.1 Introduction

Previous Chapters have explored how the identity of the bridging moiety affects the electron transfer rate and description of the mixed valence state. As a common theme, all the bridges used have bonded to the metal fragment via a (formal) $C{\equiv}C^{-}$ moiety. The acetylide anion $RC{\equiv}C^{-}$ is isoelectronic with the nitrile group, $RC{\equiv}N$, whilst the acetylide dianion $[C{\equiv}C]^{2-}$ is related to cyanide $[C{\equiv}N]^{-}$. Although the chemistry of acetylide complexes is well developed, the cyano moiety was used in the "first" for many organometallic compounds, including being the first terminal vinylidene complex[1] (Figure 1) and the oldest known synthetic mixed-valence compound, Prussian Blue.[2]

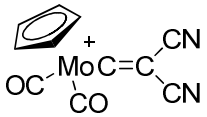

Figure 1: The first vinylidene complex.

Of more relevance to recent studies of mixed valency in organometallic complexes has been the development of cyanoacetylene chemistry ($RC{\equiv}CC{\equiv}N$) including the use of cyanoacetylide, $[C{\equiv}CC{\equiv}N]^{-}$, as a bridging moiety. Ready comparisons can be made between cyanoacetylide and the now common butadiyndiyl bridge, $[C{\equiv}CC{\equiv}C]^{2-}$, in that they are isoelectronic, and both possess a set of orthogonal, highly conjugated π-orbitals. The relationship between the cyanoacetylide ligand, $[C{\equiv}CC{\equiv}N]^{-}$ and the

ubiquitous cyanide ligand, $[C\equiv N]^-$, are also obvious, and metal complexes containing these ligands both allow the ready coordination of additional metal centres to the nitrogen terminus. This contrasts with the synthetic chemistry of the butadiyndiyl ligand, which despite some spectacular individual successes, is still something of a trial and error process in designing routes to M-C≡CC≡C-M' compounds. Despite the obvious advantages of cyanoacetylenes over butadiyndiyl bridges, synthetic methodologies towards it have remained comparatively undeveloped.

Cyanoacetylene has been detected in interstellar clouds[3] and has been shown to be luminescent in rare gas matrices.[4] However, its incorporation into organometallic complexes has been limited. A tin derivative of the cyanoacetylene, $Et_3SnC\equiv CC\equiv N$, was originally reported in 1964 as part of a study coordinating alkyl-tin derivatives to a range of acetylenes.[5] The first organometallic complex to contain the ligand was a square planar platinum compound, $[Pt(C\equiv N)(C\equiv CC\equiv N)(PPh_3)_2]$, formed by the novel photochemical isomerization reaction of $[Pt(\eta^2\text{-}NCC{=}CCN)(PPh_3)_2]$, (Scheme 1) rather than using the previous stannyl-derivative described earlier.[6]

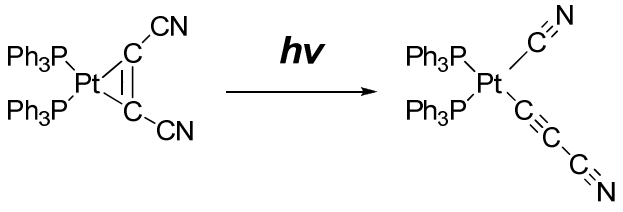

Scheme 1: Photochemical formation of the cyanoacetylide ligand.

It was another eighteen years before another complex containing the ligand was reported, $[Fe(C\equiv CC\equiv N)(CO)_2(\eta^5\text{-}C_5H_5)]$, as a product from the reaction of $[Fe(SCH_3)(CO)_2(\eta^5\text{-}C_5H_5)]$ and $HC\equiv CC\equiv N$.[7] Once again, cyanoacetylene containing

complexes were not examined for another 15 years, when a series of group ten tetra-cyanoacetylide complexes were synthesised. The use of stannyl-cyanoacetylene, $Me_3SnC{\equiv}CC{\equiv}N$, and the metal halides, $[NEt_4]_2[MCl_4]$ (M = Ni, Pt and Pd) facilitated in some cases by palladium catalysts, provided routes to the complexes $[M(C{\equiv}CC{\equiv}N)_4]$ (M = Ni, Pt Pd) (Figure 2).[8]

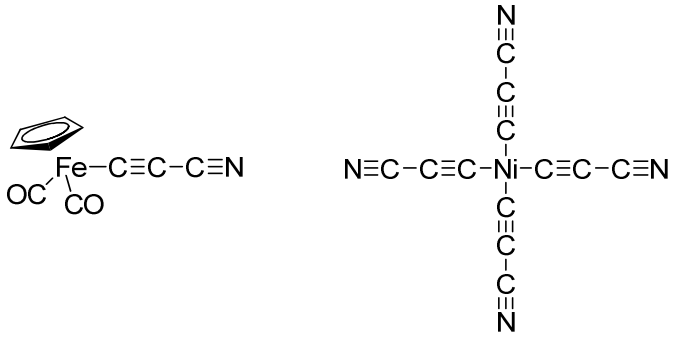

Figure 2: Examples of cyanoacetylide containing complexes.

More recently, group eight metal cyanoacetylide complexes $[M(C{\equiv}CC{\equiv}N)(L)_2(\eta^5\text{-}C_5R_5)]$ (M = Ru, L_2 = dppe R = Me (**69**), $L_2 = PPh_3$ R = H, (**70**), and M = Fe, L = dppe R = H, (**71**)), have been synthesised in high yields from reactions of $[M(C{\equiv}CLi)(dppe)(\eta^5\text{-}C_5R_5)]$ with phenyl cyanate, PhOCN (Scheme 2).[9]

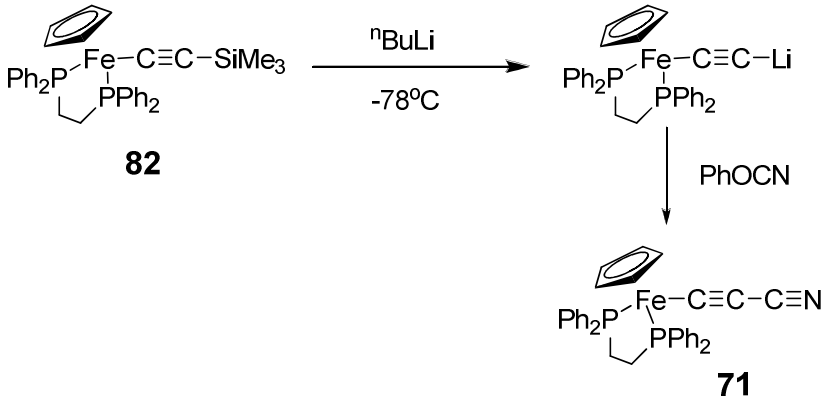

Scheme 2: Synthesis of 71 using phenyl cyanate.

The relative ease with which the monometallic complexes could be made allowed the development of cyanoacetylide bridged complexes via the reaction of the monometallic complex with a metal halide. A series of homo- and hetero-bimetallic complexes were synthesised using group eight metal moieties, such as [Ru(dppe)(η^5-C_5Me_5)], [Fe(dppe)(η^5-C_5H_5)], [Ru(PPh_3)$_2$(η^5-C_5H_5)], [$W(CO)_5$] and [$RhCl(CO)_2$]. Trimetallic complexes have also been synthesised where *cis*-[Ru(dppe)$_2$] (**71A**) is the central metal moiety with two cyanoacetylide complexes coordinated to it (Figure 3).

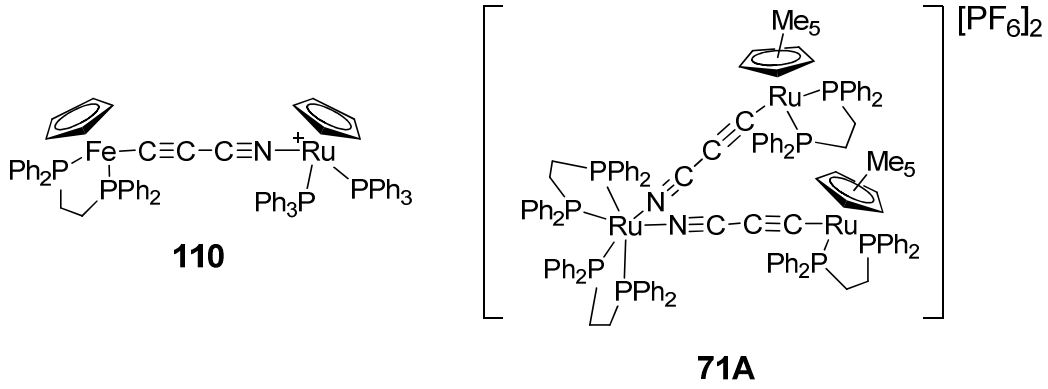

Figure 3: Tri- and Bi-metallic complexes containing the cyanoacetylide bridge, 71A and 110.

The coordination of **71** to the luminescent [Re(CO)$_3$(^{t}Bu-Bipy)] fragment produced a complex uniquely set up to directly monitor excited state behavior of the charge transfer between the complex and the bipyridine ligand.[10] The excitation of previously assigned MLCT transition was monitored by picosecond time resolved infrared (ps-TRIR) spectroscopy. This revealed that the transition is a fast electron transfer between a charge separated excited state, (between Fe-d and bpyπ*Re moieties) which is mediated by the cyanoacetylide bridge.

7.2 Chose of Cyanating Agent: Syntheses of bromo- and cyano-vinylidenes

Previous routes to the cyanoacetylide using lithiation techniques often led to the cyanation of the ancillary ligands on the metal moiety following the treatment with phenyl cyanate. Due to this, a new route was needed which did not require the use of strong basic conditions (Scheme 2).[9b]

Cyanogen bromide (BrCN) is ambinucleophilic therefore depending on the conditions, it can act as either a source of bromide or cyanogen. This is exemplified in the reaction of BrCN with acetyl-acetonates, where depending on the transition metal and the solvent conditions, early transition metals produced 3-bromo products and the late transition metals produced 3-cyano products. When vanadium and iron centres are used, increasing the dielectric constant of the solvent yields 3-bromo products, whereas solvents with a low dielectric constants yield 3-cyano products.[11]

In this work, $[Ru(C{\equiv}CC_6H_5)(PPh_3)_2(\eta^5\text{-}C_5H_5)]$ (**72**) first was reacted with BrCN in order to assess if the C_2 atom of the acetylide moiety was sufficiently nucleophilic to attack the cyanogen moiety and form either a cyanovinylidene, $[Ru\{=C=C(C_6H_5)CN\}(PPh_3)_2(\eta^5\text{-}C_5H_5)]PF_6$ ([**73**]PF_6) or a bromovinylidene species, $[Ru\{=C=C(C_6H_5)Br\}(PPh_3)_2(\eta^5\text{-}C_5H_5)]PF_6$ ([**74**]PF_6) (Figure 4).

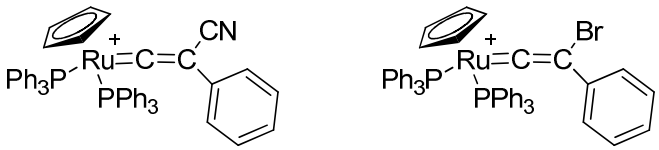

73 **74**

Figure 4: Diagram of 73 and 74.

The reaction was carried out in several solvent media, in order to polarise the BrCN, to be a better source of cyanogen. After stirring at room temperature for two hours, the solvent of choice was removed and precipitation of CH_2Cl_2 solution of the residue into Et_2O produced a green powder. An analysis of the powder by ^1H NMR showed it to be a mixture consisting of both **73** and **74**, which were identified by their unique resonance for the protons of the C_5H_5 ligand, and the composition being dependant on the solvent medium.[12] Changing the solvent from CH_2Cl_2 to toluene increased the proportion of **73** by 50 %, however attempts to separate the mixture by preparative TLC were unsuccessful leading to the decomposition of **74**. Pure samples of **72** could be synthesised by the reaction of the vinylidene $[Ru\{=C=C(H)C_6H_5\}(PPh_3)_2(\eta^5\text{-}C_5H_5)]PF_6$ ($[\mathbf{75}]PF_6$) with BrCN in the presence of NH_4PF_6 using CH_2Cl_2 as the solvent medium (Scheme 3). Similarly the reaction of $[Fe(C{\equiv}CC_6H_4R\text{-}4)(dppe)(\eta^5\text{-}C_5H_5)]$ (R = H (**76**), CH_3 (**77**)), and $[Ru(C{\equiv}CC_6H_4CH_3\text{-}4)(dppe)(\eta^5\text{-}C_5Me_5)]$ (**77A**) with BrCN and NH_4PF_6 in CH_2Cl_2, gives the corresponding mono-bromovinylidene complexes, $[Ru\{=C=C(C_6H_4CH_3\text{-}4)Br\}(dppe)(\eta^5\text{-}C_5Me_5)]PF_6$, ($[\mathbf{77B}]PF_6$) and $[Fe\{=C=C(C_6H_4R\text{-}4)Br\}(dppe)(\eta^5\text{-}C_5H_5)]PF_6$ (R = H ($[\mathbf{78}]PF_6$), CH_3 ($[\mathbf{79}]PF_6$)).

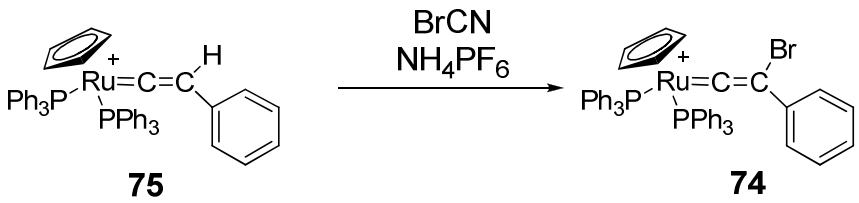

75 **74**

Scheme 3: Synthesis of 74.

To extend this serendipitous result, the reactions between BrCN and [Ru(C≡CSiMe$_3$)(L)$_2$(η^5-C$_5$R$_5$)], (where L$_2$ = PPh$_3$ R = H (**80**), L$_2$ = dppe R = Me (**81**)) and [Fe(C≡CSiMe$_3$)(dppe)(η^5-C$_5$H$_5$)] (**82**),were examined to provide a possible route to [M(C≡CBr)(dppe)(η^5-C$_5$R$_5$)], a potentially useful synthon for the synthesis of extended chain complexes using palladium based coupling strategies.[13] Instead the reaction yielded a series of novel di-bromovinylidenes, [Ru(=C=CBr$_2$)(L)$_2$(η^5-C$_5$R$_5$)]BF$_4$ (L$_2$ = PPh$_3$ R = H ([**83**]BF$_4$), L$_2$ = dppe R = Me ([**84**]BF$_4$)) and [Fe(=C=CBr$_2$)(dppe)(η^5-C$_5$H$_5$)]BF$_4$ ([**85**]BF$_4$), (**85** was synthesised by Dr. M.A. Fox) which were isolated in the form of purple air sensitive solids (Scheme 4).[11]

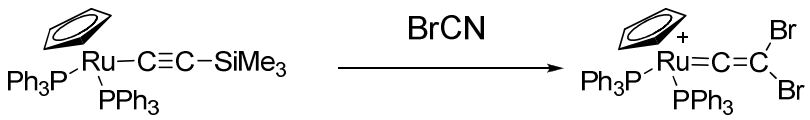

Scheme 4: Synthesis of dibromovinylidenes.

Another source of cyanogen is 1-cyano-4-dimethylaminopyridinium tetrafluoroborate, [CAP]BF$_4$ (**86**) (Figure 5), which has been used extensively in biochemical applications, including the cyanoation of cystine peptides,[14] the activation of polysaccarids[15] and cellulose membranes.[16]

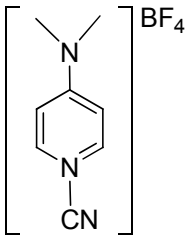

Figure 5: [CAP]BF_4 reagent 86.

However, the reactivity of **86** towards metal acetylides was un-tested prior to this work. The reaction between **72** and **86** in CH_2Cl_2 gave **73** in high yield (90 %) after purification by preparative TLC, where the driving force of the reaction was the formation of 4-dimethylaminopyridine leaving group (Scheme 5). In addition to **73** other examples of mono-cyanovinylidene were also synthesised using this methodology, [Fe{=C=C(C_6H_4R-4)CN}(dppe)(η^5-C_5H_5)]BF_4 (R = H ([**87**]BF_4), CH_3 ([**88**]BF_4)) and [Ru{=C=C($C_6H_4CH_3$-4)CN}(dppe)(η^5-C_5Me_5)]BF_4,[17] ([**89**]BF_4). Using similar methodologies, the compounds [Ru{=C=C(C_6H_4R-4)CN}(PPh_3)$_2$(η^5-C_5H_5)]BF_4 (R = OMe ([**90**]BF_4), Fe(η^5-C_5H_4)(η^5-C_5H_5) ([**91**]BF_4), CO_2Me ([**92**]BF_4), CN ([**93**]BF_4) were also synthesised by E.A. Strickson.[18]

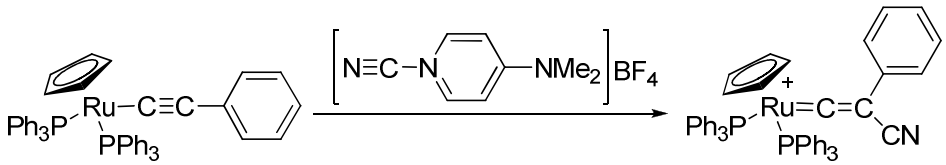

80 **73**

Scheme 5: Synthesis of mono-cyanovinylidene 73.

7.3 Syntheses of Cyanoacetylide Complexes

The previously published methodology for the preparation of [Ru(C≡CC≡N)(dppe)(η^5-C_5Me_5)] (**69**) using **86** as the source of cyanogen relied on the formation of [Ru(C≡CH)(dppe)(η^5-C_5Me_5)] (**94**).[9b] However, the storage and generation of C≡CH metal acetylides with a terminal hydrogen atom (**94**) can be difficult. An alternative approach is to use the more stable and easier to sysnthesise C≡CSiMe$_3$ derivatives.

Success was found for the reaction between trimethylsilyl acetylides **80** – **82** with the cyanating agent **86**, where the cyanoacetylide complexes **69**, **70** and **71** were synthesised, all in reasonably high yields with reaction times of less than 2 hours, which was a substantial improvement on the lithiation methodology (Scheme 6). The reaction of **69** with excess **86** led to the formation of [Ru{=C=C(CN)$_2$}(dppe)(η^5-C_5Me_5)]BF_4 ([**95**]BF_4), which could be isolated in modest yield (36 %).[18]

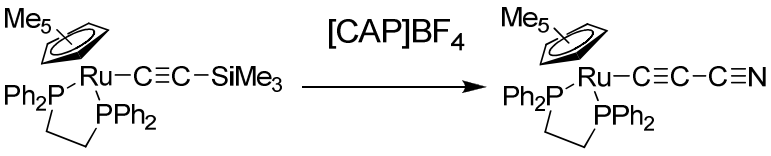

81 **69**

Scheme 6: Synthesis of 69 using 86.

However, when the same reaction was tried with [Fe(C≡CC≡N)(dppe)(η^5-C_5H_5)] (**71**), the dicyanovinylidene product was not isolated and instead a dimethylaminopyridine substituted dicyano containing product was formed, **96**. Complex **96** was also formed when an excess of **86** (even as low as 0.1 equivalents too much) was used in the formation of **71**, that led to a substantial reduction in yield (Scheme 7).

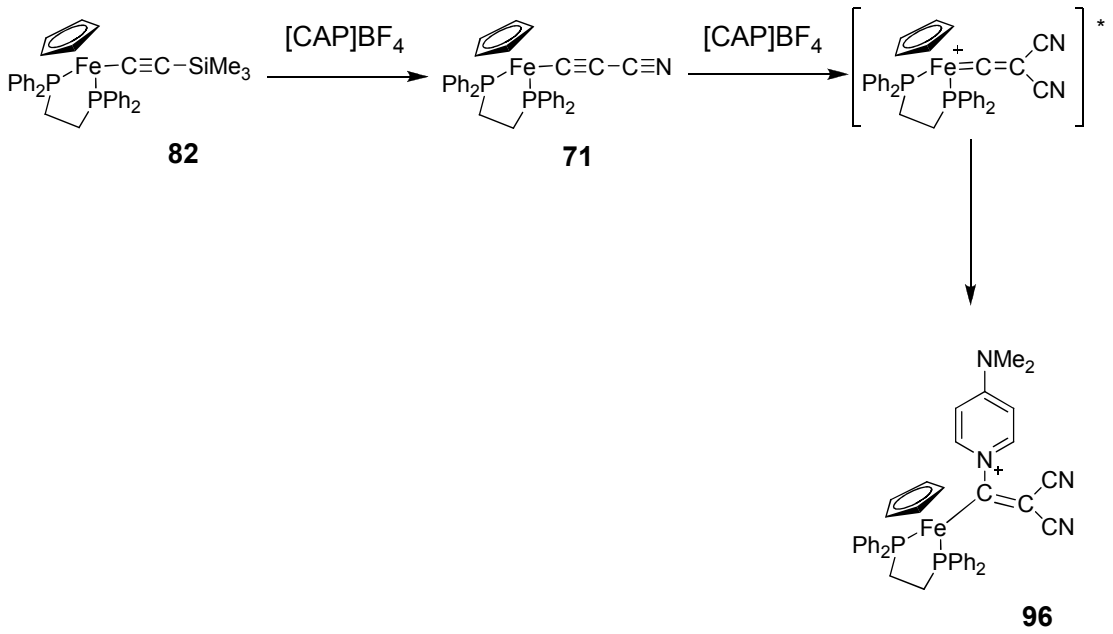

Scheme 7: Synthesis of 71 and associated side reaction.

The formation of the iron dicyanovinylidene complex is short lived, owing to the activation of the C_1 position, making it more susceptible to nucleophilic attack from the free dimethylamino pyridine.

The reaction between [Fe(C≡CSiMe$_3$)(dppe)(η^5-C$_5$Me$_5$)] (**97**), and **86** in CH_2Cl_2 yielded the cyanoacetylide complex [Fe(C≡CC≡N)(dppe)(η^5-C$_5$Me$_5$)] (**98**), in low yields (14 %) (Scheme 8). The low yield was not attributed to a dimethylaminopyridine substituted complex as for the cyclopentadiynyl analogues, but rather due to the formation of [{Fe(dppe)(η^5-C$_5$Me$_5$)}$_2$(μ-C≡CC≡C)]$^{0/1+}$ (**53**) which could be isolated by preparative TLC. This was presumably as a consequence of the coupling of **97** being promoted by oxidation in the presence of **86**, dimethylaminopyridine base, cyanogen or oxygen.

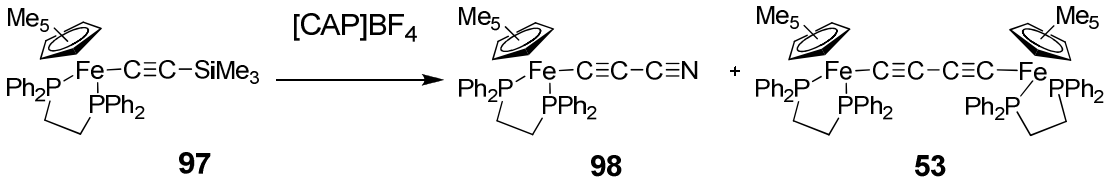

Scheme 8: Synthesis of 98 and associated side product.

The cyanating reagent **86** was also found to successfully cyanate other metal acetylides. The reaction of mono- and bis-acetylide complexes [RuCl(C≡CH)(dppe)$_2$] (**99**) and [Ru(C≡CH)$_2$(dppe)$_2$] (**100**) with the cyanating agent **86** in CH_2Cl_2 produced the desired cyanoacetylide complexes, [RuCl(C≡CC≡N)(dppe)$_2$] (**101**) and [Ru(C≡CC≡N)$_2$(dppe)$_2$] (**102**) (Scheme 9).

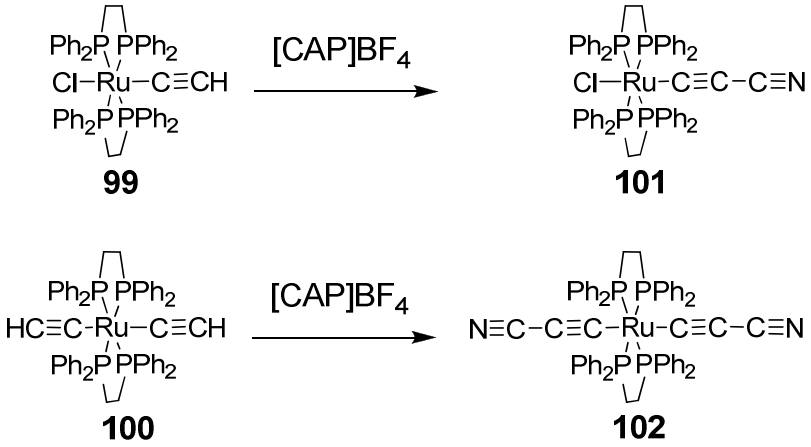

Scheme 9: Synthesis of 101 and 102.

Complex **101** could not be synthesised as a pure product, although very small amounts (< 2 mg) could be purified by re-crystallisation and as such an approximate X-ray structure could be determined. The other component of this mixture could not be accurately identified, but the data hints towards a pyridine containing complex, due to a ν(CN) stretch at 2239 cm^{-1} and a ^{31}P NMR resonance at 49.2 ppm. In addition, complex **102** could not be synthesised as a pure sample even after careful chromatography. Of the two contaminates (which were identified by ^{31}P NMR and

MALDI+ mass spectrometry), [Ru(C≡CH)(C≡CC≡N)(dppe)$_2$] could be identified, by a ^{31}P resonance at 54.1 ppm, and the other contaminate was the same as that found in the mixture of **101**.

The formation of the fluorescent complex [Re(C≡CC≡N)(CO)$_3$(^{t}Bu-bipy)] (**103**) was achieved in low yield (15 %) from the reaction of [Re(C≡CSiMe$_3$)(CO)$_3$(^{t}Bu-bipy)] (**104**) and the cyanating agent **86** in CH_2Cl_2. In addition, the novel complex [Fe(C≡CC≡N)(CO)$_2$(η^5-C_5H_5)] (**105**) could be synthesised by a similar procedure using [Fe(C≡CSiMe$_3$)(CO)$_2$(η^5-C_5H_5)] (**106**) as the starting material. However, pure samples of **105** were not obtained due to the complex being sensitive to chromatography methods.

In addition to the reaction of **86** with organometallic complexes, organic acetylenes were also tested as a convenient route to cyanoacetylenes. Unfortunately, even with the use of lithiated acetylene reagents, the reaction yielded no cyanoacetylene products.

7.3.1 Electrochemical and Spectroscopic Investigations of [Fe(C≡CC≡N)(dppe)(η^5-C_5Me_5)]

The [Fe(dppe)(η^5-C_5Me_5)] moiety has been used extensively in systems designed to study charge transfer in organometallic systems. Therefore, efforts were made to characterise **98** by spectroscopic, structural, electrochemical and spectroelectrochemical methods.

In comparison to the starting material **97**, the ^{13}C NMR resonance for C_1 shifts from 162.9 ppm[19] to 166.8 ppm upon the addition of the electron withdrawing cyano moiety to the alkynyl chain. This is also reflected in the decrease of the ^1H NMR resonance for the pentamethyl-cyclopentadienyl ring which increases by 0.16 ppm. In addition, the infrared stretch which can be attributed to ν(C≡C) is lowered in energy from 1981 cm^{-1} to 1979 cm^{-1}.

Both **97** (Figure 6) and **98** (Figure 7) were structurally characterised by X-ray crystallographic techniques. Compound **97** showed typical bond values for iron acetylides,[20] with the Fe-C_1 and Fe-P bond lengths being almost identical to **2**. The addition of the cyano moiety in **98** causes, relative to **97**, the contraction of the Fe-C_1 bond by 0.04 Å, and no significant change of the Fe-P bond lengths. The C≡CC≡N moiety itself, compound **98** retains the alternating triple /single /triple bond structure as seen for other Group eight analogues (Table 1).[9a,9b]

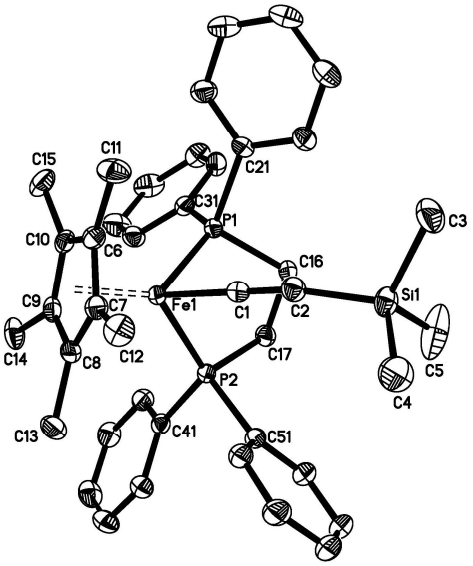

Figure 6: ORTEP diagram of 97 showing the labeling scheme. The hydrogen atoms omitted for clarity. The thermal ellipsoids are plotted at 50 % probability.

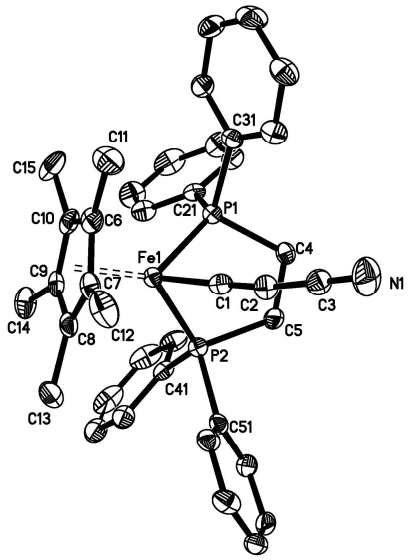

Figure 7: ORTEP diagram of 98 showing the labeling scheme. The hydrogen atoms omitted for clarity. The thermal ellipsoids are plotted at 50 % probability.

Table 1: Selected bond length and bond angle data for 97 and 98.

Bond Length /Å	**97**	**98**
Fe-C_1	1.8972(13)	1.851(2)
C_1-C_2	1.2329(19)	1.223(3)
C_2-C_3 /C_2-Si	1.8187(14)	1.368(3)
C_3-N	-	1.159(3)
Bond Angle /^{o}		
Fe-C_1-C_2	179.34(13)	176.7(2)
P-Fe-P	86.175(15)	84.85(3)
C_1-C_2-C_3 /C_1-C_2-Si	164.73(13)	172.5(3)

The oxidation of **98** using cyclic voltammetry techniques shows a diffusion controlled, chemically reversible, one electron oxidation process (at a platinum electrode, recorded in a 0.1 M $^nBu_4NPF_6$ /CH_2Cl_2 solution and referenced to FcH /FcH^+ = 0.00 V couple.) $E_{1/2}$ = -0.19 V. This makes **98** much harder to oxidise than the aryl acetylide analogues, for example [Fe(C≡C$C_6H_4NO_2$-4)(dppe)(η^5-C_5Me_5)] (**2**) ($E_{1/2}$ = -0.61 V) and [Fe(C≡CC_6H_4OMe-4)(dppe)(η^5-C_5Me_5)] ($E_{1/2}$ = -0.39 V).[21] This is a trend across all the cyanoacetylide complexes, where **69**, **70** and **71** are all more difficult to oxidise than their aryl acetylide counterparts.

Guided by the electrochemical results, spectroelectrochemical experiments were undertaken as a convenient method for rapidly generating and studying **98** and **98**$^+$. In comparison to the ruthenium **69** and the iron **71** cyclopentadienyl analogues infrared and UV /vis spectroelectrochemical experiments could be carried out at room temperature and **98**$^+$ showed good stability in solution for prolonged periods of time.

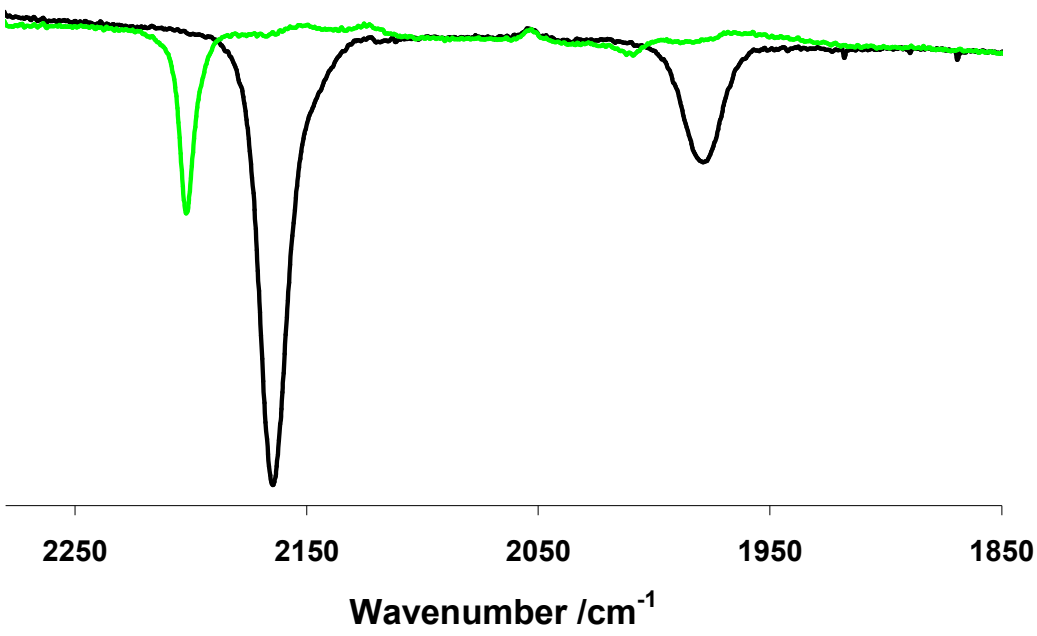

Figure 8: Infrared spectrum for 98^{n+}, where n = 0 (Black), n = 1 (Green) (Recorded in 0.1 M $^{n}Bu_4NPF_6$ /CH_2Cl_2).

Table 2: Infrared spectroelectrochemical data for 98^{n+}, recorded in 0.1 M $^{n}Bu_4NPF_6$ /CH_2Cl_2.

98^{n+}	ν(C≡CC≡N) /cm^{-1}	
n = 0	1979	2165
n = 1	2010	2201

Upon oxidation of **98** the overall band pattern is retained but is shifted to higher energy and both bands are reduced in intensity (Table 2, figure 8). The assigned ν(C≡C) band and the cyclopentadienyl analogue $\mathbf{71}^{+}$ exhibits a single band upon oxidation and compound $\mathbf{69}^{+}$ shows a splitting of the ν(C≡N) band, although the general trend is in keeping with $\mathbf{98}^{+}$. Assessing the character of the HOMO using methodologies with simpler aryl acetylides is difficult from these results due to the polyyne nature of the cyanoacetylide ligand. Due to this nature, the infrared stretches assigned will not consist solely of vibrations relating to that bond, but will be coupled to the neighbouring bond, therefore the change in energy is not directly related to the character of the HOMO.

The UV /vis spectra of **98** and **98**$^{+}$ closely resemble that of **69** and **71** (Table 3, figure 9). The generation of the 17 electron complex causes a shift of the higher energy transitions from 36200 cm^{-1} to 37600 cm^{-1}. At lower energy (around 20000 cm^{-1}) **98**$^{+}$ several broad transitions arise which have been assigned to be LMCT in character (this is similar to **69**$^{+}$ and **71**$^{+}$).

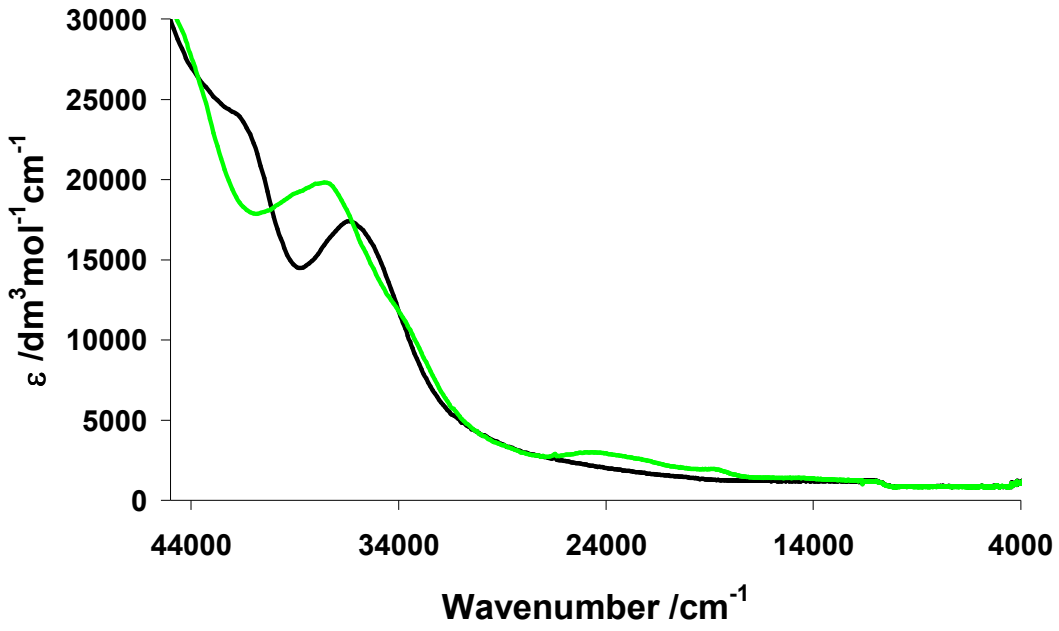

Figure 9: UV /vis /NIR spectra 98^{n+}, where n = 0 (Black), n = 1 (Green) (Recorded 0.1 M $^{n}Bu_4NPF_6$ /CH_2Cl_2).

Table 3: UV /vis /NIR spectroelectrochemical data of 98^{n+}, recorded in 0.1 M $^{n}Bu_4NPF_6$ /CH_2Cl_2. (where sh denotes a shoulder)

98^{n+}	Transition /cm^{-1} (ε /M^{-1} cm^{-3})
n = 0	36200 (16300) 41800 (23100)
n = 1	sh 15000 (390) 18900 (950) sh 24000 (1900) sh 34000 (10800) 37600 (18800) sh 44400 (28300)

7.4 Cyanoacetylide Bridged Complexes

The development of high yielding simple methodologies for cyanoacetylide containing complexes has allowed the discovery of a number of bimetallic complexes containing the ligand. Bimetallic complexes containing [Ru(dppe)(η^5-C_5Me_5)], [Ru(dppe)(η^5-C_5H_5)], [Fe(dppe)(η^5-C_5H_5)], [RhCl$(CO)_2$], [Ru$(dppe)_2$] and [W$(CO)_5$] have been synthesised in moderate to high yields from the reaction between the cyanoacetylide and a metal halide or solvated metal fragment.

The ruthenium acetylide [RuCl(C≡CC_6H_5)$(dppe)_2$] (**107**) was reacted with the ruthenium cyanoacetylide (**69**) to yield the bimetallic complex [{Ru(dppe)(η^5-C_5Me_5)}(μ-C≡CC≡N){Ru(C≡CC_6H_5)$(dppe)_2$}]PF_6 ([**109**]PF_6) in good yield (Scheme 10). The benefit of using **107** as a coordination partner is the presence of the extra alkynyl substituent, this adds an extra vibrational probe, which can be used to assess the effects of oxidation on the metal centre.

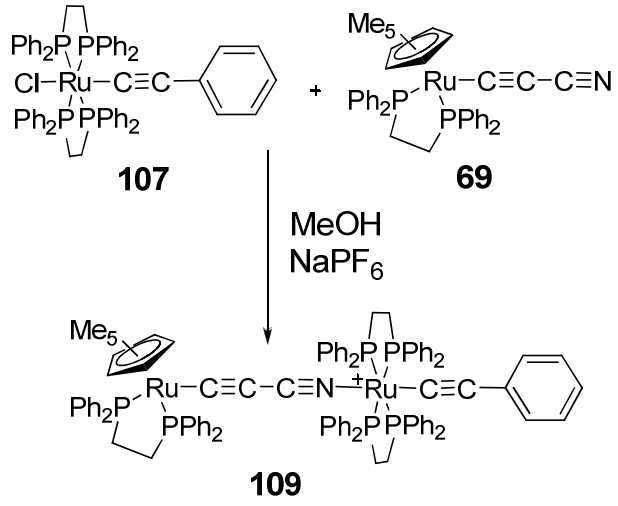

Scheme 10: Synthesis of 109.

In addition, [MoBr(dppe)(η^7-C_7H_7)] (**5**) was reacted, under similar conditions as described above, with the iron cyanoacetylide **71**, giving [{Fe(dppe)(η^5-C_5H_5)}(μ-C≡CC≡N){Mo(dppe)(η^7-C_7H_7)}]PF_6 ([**108**]PF_6) in good yield (Scheme 11).

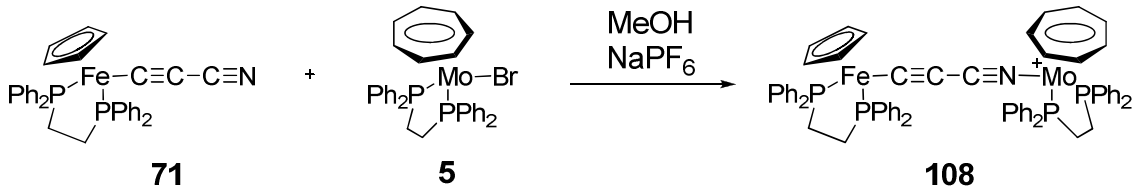

Scheme 11: Synthesis of 108.

The coordination of the [Mo(dppe)(η^7-C_7H_7)] fragment to **71** does little to alter the ν(C≡CC≡N) stretching features, with the highest energy band lowered in energy by 2 cm^{-1}. In comparison to [{Fe(dppe)(η^5-C_5H_5)}$_2$(μ-C≡CC≡N){Ru(PPh_3)$_2$(η^5-C_5H_5)}]PF_6, [**110**]PF_6, the lowest energy band does not change in energy, however the highest energy band, predominantly ν(C≡N) in character, is comparatively lower in energy by 21 cm^{-1}. More significant changes are seen for [**109**]PF_6, where the infrared spectra shows three clearly spaced bands for which the assignments can be made by comparison to the monometallic parts. The highest and lowest energy stretches (2180 and 1967 cm^{-1}) are attributable to ν(C≡CC≡N) based upon the bands seen for the mono-metalic precursor **69**. Therefore, the stretch at 2083 cm^{-1} corresponds to the ν(C≡C) of the [Ru(C≡CC_6H_5)(dppe)$_2$] moiety (where **107** ν(C≡C) = 2072 cm^{-1}).[22]

Limited NMR data (^{1}H and ^{31}P nuclei) was collected for [**109**]PF_6 due to the instability of the complex in solution. The complex was shown to be *trans*- rather than *cis*- due to the presence of a single ^{31}P resonance (48.4 ppm) corresponding to the [Ru(dppe)$_2$] moiety, another resonance at higher ppm (78.4 ppm) corresponding to the [Ru(dppe)(η^5-

C_5Me_5)] moiety. In comparison to the mono-metallic cyanoacetylide **69**, the ^{31}P NMR resonance is very similar (**69**, 80.22 ppm), indicating that the coordination of the [Ru(C≡CC_6H_5)(dppe)$_2$] moiety does not alter the bonding about the [Ru(dppe)(η^5-C_5Me_5)] fragment. This is further reflected in the ^1H NMR spectrum where the C_5Me_5 resonance is identical for both **69** and **109**.

The collection of NMR data for [**108**]PF_6 required a small amount of [Co(η^5-C_5H_5)$_2$] to be added to the sample, as employed for all the [Mo(dppe)(η^7-C_7H_7)] containing compounds. Limited NMR data (^1H and ^{31}P nuclei) were collected for the analogous hetero-bimetallic complex [**110**]PF_6. The coordination of the [Mo(dppe)(η^7-C_7H_7)] fragment to **71** has a similarly small effect on the ^1H NMR resonances associated with the [Fe(dppe)(η^5-C_5H_5)] moiety. In addition, ^{31}P NMR for the [Mo(dppe)(η^7-C_7H_7)] remains unchanged from **5**, but a small decrease (2 ppm) is noted for the resonance associated with the [Fe(dppe)(η^5-C_5H_5)] moiety from the parent complex **71**. In summary, coordination of the [Mo(dppe)(η^7-C_7H_7)] fragment has little spectroscopic effect on the iron cyanoacetylide moiety.

Electrochemical investigations on [**108**]PF_6 showed two diffusion controlled, chemically reversible, one electron oxidation processes (at a platinum electrode, recorded in a 0.1 M $^nBu_4NPF_6$ /CH_2Cl_2 solution and referenced to FcH /FcH^+ = 0.00 V couple) at -0.20 V and +0.48 V. The first oxidation takes place on the molybdenum centre, however, the potential is much higher than for complexes containing a Mo-C≡C moiety. To investigate this further, the simple nitrile complex, [Mo(N≡C$C_6H_4CH_3$-4)(dppe)(η^7-C_7H_7)]PF_6 ([**111**]PF_6) was synthesised, and was shown to have a similarly high oxidation potential (+0.07 V). The ΔE value for the molybdenum salt [**108**]PF_6 is

the same as the ruthenium salt [**110**]PF_6 (680 mV) from which a K_c value of 3.16 x 10^{11} could be calculated. Indicating a similar thermodynamic stability to the analogous homo-bimetallic butadiyndiyl bridged complexes, **53** (K_c = 1.6 x 10^{12})[23] and **52** (9.7 x 10^{10}).[24]

Guided by the electrochemical results, infrared spectroelectrochemical experiments were undertaken to generate [**108**]$^{n+}$ (n = 1, 2 and 3) (Table 4, figure 10). However, attempts to isolate the trication were unsuccessful. The removal of one electron to form the mixed valence species [**108**]$^{2+}$, results in a shift of the entire band envelope to lower energy, with the highest energy band moving by 65 cm^{-1} and the lowest energy band by 35 cm^{-1}. This is almost identical to the oxidation of [**110**]PF_6 (55 cm^{-1} and 44 cm^{-1} respectively),[9a] and such similarities indicate that the HOMO of the complex is of a comparable composition.

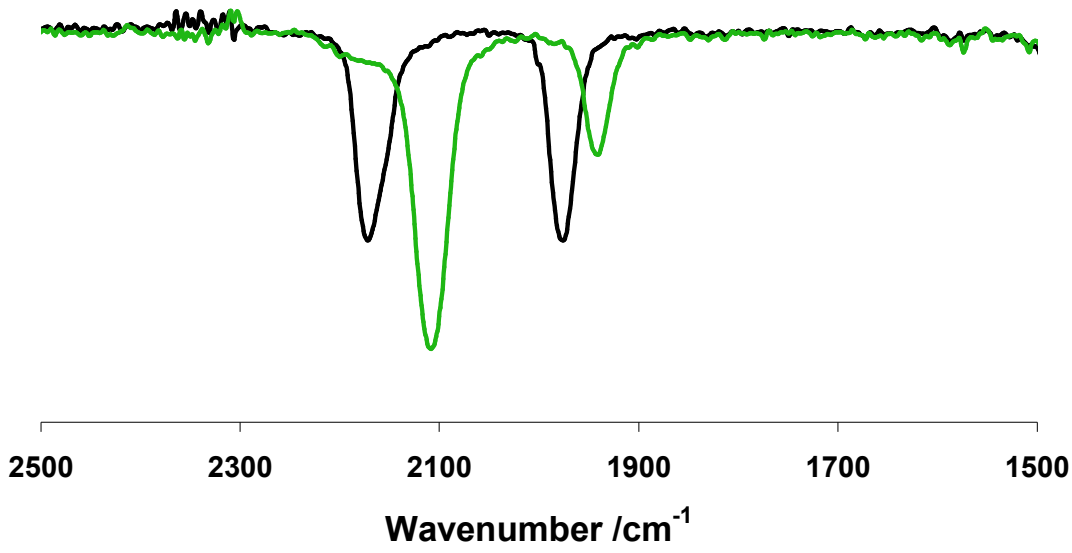

Figure 10: Infrared spectra of 108^{n+}, where n = 1 (Black), n = 2 (Green) (Recorded in 0.1 M $^{n}Bu_4NPF_6$ /CH_2Cl_2).

Table 4: Infrared spectroelectrochemical data for 108^{n+}, Recorded in 0.1 M $^{n}Bu_4NPF_6$ /CH_2Cl_2.

n	ν(C≡CC≡N) /cm^{-1}	
	$[\mathbf{108}]^{n+}$	$[\mathbf{110}]^{n+}$
1	2172, 1975	2191, 1976
2	2107, 1940	2136, 1932

To further investigate the electronic structure of $\mathbf{108}^{n+}$, UV /vis /NIR spectroelectrochemical investigations were undertaken (Table 5, figure 11). The 36 electron complex $\mathbf{108}^{+}$ showed only two high energy transitions, which have been tentatively assigned as metal /phosphine or metal /ring in character based upon previous TD-DFT calculations from earlier Chapters.

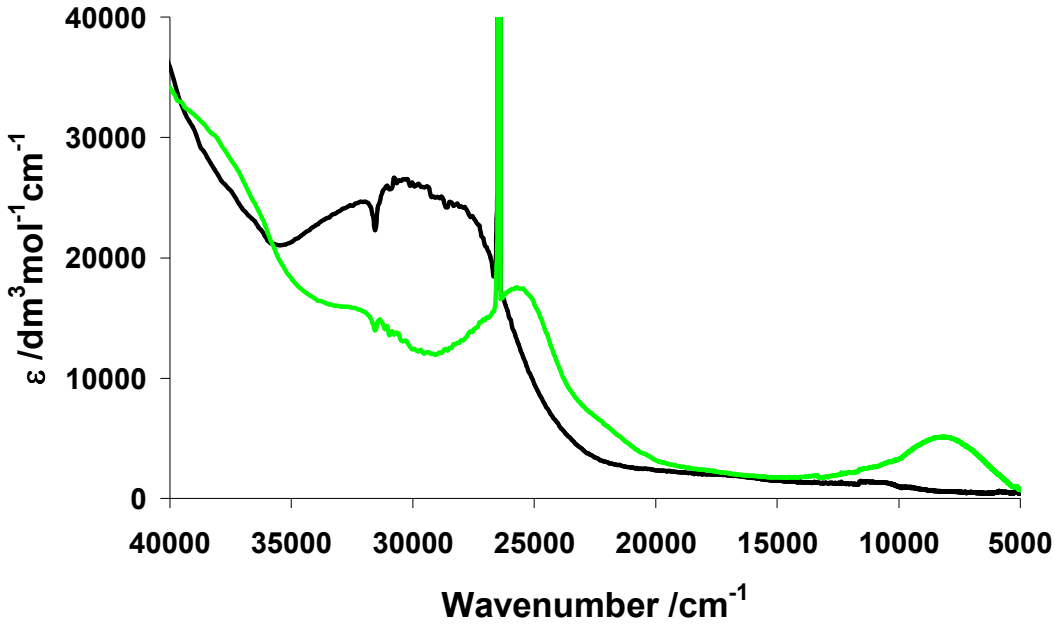

Figure 11: UV /vis spectra of 108^{n+}, where n = 1 (Black), n = 2 (Green) (Recorded 0.1 M $^{n}Bu_4NPF_6$ /CH_2Cl_2).

Table 5: UV /vis spectroelectrochemical data for 108^{n+}, recorded in 0.1 M $^{n}Bu_4NPF_6$ /CH_2Cl_2.

108^{n+}	ν /cm^{-1} (ε /$dm^3mol^{-1}cm^{-1}$)
n = 1	30700 (26600) 27700 (23700)
n = 2	37500 (28500) 32100 (15700) 25600 (17400) 8230 (5100)

Below 20000 cm^{-1} the cation $\mathbf{108}^{+}$ is spectroscopically transparent. The removal of an electron to generate the dication $\mathbf{108}^{2+}$ results in the splitting of the high energy band into two separate transitions (32100 and 25600 cm^{-1}). Of greater importance is the appearance of a broad complex band in the NIR region at 8230 cm^{-1} (which spans over 8000 cm^{-1}) and contains information precluding to the electronic structure of the potentially mixed valence complex.

The complex NIR band at 8230 cm^{-1} was deconvoluted using the summation of Gaussian bands, as demonstrated in previous Chapters, which revealed five distinct transitions (Table 6, figure 12).

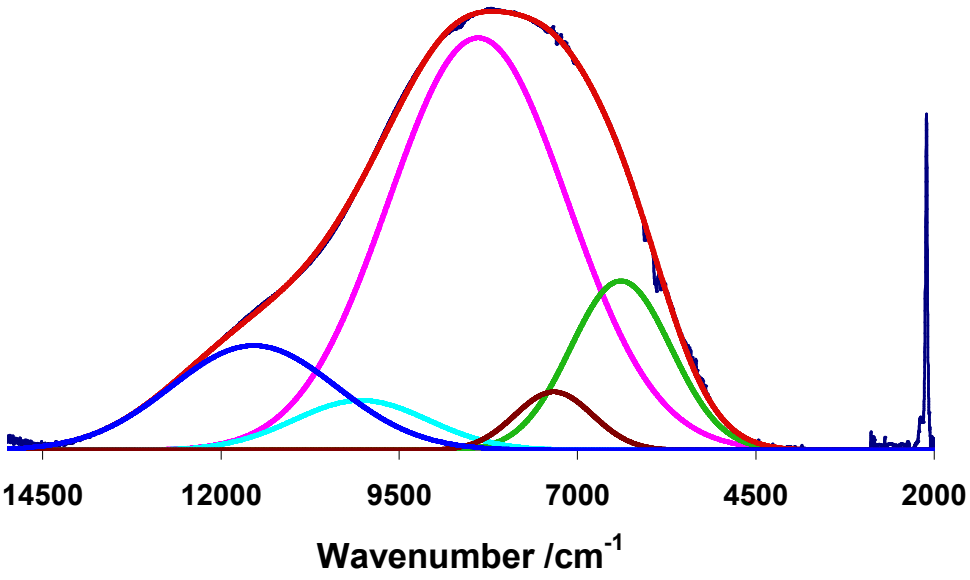

Figure 12: NIR deconvolution of 108^{+}, recorded in 0.1 M $^{n}Bu_4NPF_6$ /CH_2Cl_2.

Table 6: Deconvoluted NIR band data.

Band	ν /cm^{-1}	$\Delta\nu_{1/2}$ /cm^{-1}	ε /$dm^3mol^{-1}cm^{-1}$
1	6300	1700	3100
2	7200	1300	1100
3	8300	3000	7700
4	10000	2400	800
5	11400	2700	2000

Whilst the availability of chemically isolated samples of [**108**][PF_6]$_2$ would have greatly facilitated this study by allowing solvatochromic studies, resonance Raman and EPR experiments to be carried out, in their absence, several conclusions can be drawn, based on results collected in the previous Chapters. The band shape and deconvolution are similar to the phenylene bridged di-molybdenum cation **67**$^{+}$, where the band shape is asymmetric and truncated at low energy, however, the entire band is at much lower energy, around 3000 cm^{-1} (Figure 12, table 6). Although the linkage between the bridge and the molybdenum centre is different from the previous Chapters (Mo-C≡C compared to Mo-N≡C), in order to assign the character of each of the transitions, it is beneficial to draw comparion from all the molybdenum complexes studied. From the cyclic

voltammetry data it is clear that the first oxidation is molybdenum centered, therefore, the lowest intensity bands (at 7200 and 10000 cm^{-1}) correspond to interconfigurational transitions on the Mo(dppe)(η^7-C_7H_7) fragment, as transitions energies similar to this are prevalent on all the other bimetallic molybdenum complexes.

The two transitions at 11400 and 8300 cm^{-1} are common to all the hetero-bimetallic complexes that have been studied, albeit they are at slightly different energies because different metal moieties are involved, in addition, the transition at 6300 cm^{-1} is similar to that in [{Ru(dppe)(η^5-C_5Me_5)}$_2$(μ-C≡CC≡N)][PF_6]$_2$. The character of these transitions has not been fully elucidated in previous studies,[9c] nevertheless, the presence of these transitions in **108**$^{2+}$ indicates that they must be of a similar character. The most intense transition (8300 cm^{-1}) can be tentatively assigned as LMCT in character, between a cyanoacetylide bridge and the [Mo(dppe)(η^7-C_7H_7) moiety]. As the highest energy band (11400 cm^{-1}) is present in [**110**][PF_6]$_2$, its character must be due to transitions with the iron centre and cyanoacetylide ligand.

The lowest energy transition (6300 cm^{-1}) is consequently a transition which is more charge transfer in character, owing to the low energy and intensity of the band. However, it is not solely a transition between the 18 electron iron centre and the 17 electron molybdenum centre. Due to the heavy mixing between iron, molybdenum and cyanoacetylide moieties the character of the transition is more occluded and as such becomes less charge transfer in character. As discussed in the Chapter one hetero-bimetallic complexes (where the electrophores are no longer identical) have asymmetric electronic ground states, therefore the observed optical transition (E_{op}) (at 6300 cm^{-1}) is no longer directly related to the reorganisational energy (λ).

$$E_{op} = \lambda + \Delta G^o$$

The ΔG^o value can be approximated from the electrochemical results,

$$\Delta G^o = -RT \ln K_c$$

it must be noted that an approximation is all that can be made due to the sensitivity of K_c to the conditions the measurement is made in, which leads to a value ΔG^o = -65.6 kJmol^{-1} (5500 cm^{-1}).[25] A consequence is that the reorganisational energy (λ) is small (λ = 800 cm^{-1}) in comparison to the homo-bimetallic systems, indicating that the cyanoacetylide bridge is pre-organised to allow the electron transfer process to take place more easily. The implication of this and the assignment of the other bands are that the cyanoacetylide bridge promotes a more delocalised ground state.

7.5 Conclusion

The quest for a convenient facile route to synthesis and coordination of the cyanoacetylide moiety to metal fragments has led to the syntheses of a number of cyano and bromo containing organometallic complexes.[11,18] The reaction of metal aryl acetylides with cyanogen bromide preferentially produces bromovinylidene complexes. Moreover, when trimethylsilyl acetylides are used, novel di-bromovinylidene complexes are formed. The cyanating reagent **86** proved successful at cyanating a wide range of metal aryl acetylides resulting in mono-cyanovinylidene complexes, with trimethylsilyl metal acetylides yielding the target cyanoacetylide containing complexes. Easy access to iron cyanoceylide **71** allowed the synthesis of the hetero-bimetallic which contained the cyanoacetylide ligand as a bridging moiety [**108**]PF_6. Preliminary investigations on the di-cation of **108** using NIR, IR and UV /vis spectroelectrochemical techniques revealed that the cyanoacetylide bridge promotes a more delocalised electronic structure irrespective of the nature of the metal moieties supporting it, which is a marked difference to the common, analogous butadiyndiyl bridge.

7.7 Preparations

7.6.1 General Procedures

General experimental procedures have been described in Chapter two. The reagent BrCN was first sublimed under vacuum at ambient temperatures prior to use. The compounds **86**,[18] **72**,[26] **75**,[27] **76**,[28] **77**,[30] **77A**,[29] **82**,[9a] **94**,[30] **97**,[20] **99**,[24] **100**,[24] **104**,[31] **106**[32] and **107**[24] were prepared by standard methods.

7.6.1.1 Preparation of [Ru(C≡CC≡N)(PPh$_3$)$_2$(η^5-C$_5$H$_5$)], 70

A CH_2Cl_2 (20 cm^3) solution of **80** (0.100 g, 0.127 mmol) and **86** (0.044 g, 0.191 mmol) was stirred at room temperature for 1 hour. The solvent was removed *in vacuo* and the product was extracted from the residue into the minimum amount of CH_2Cl_2 and was then micro filtered through a small cotton wool plug into stirring hexane to give **70** a pale yellow precipitate, identified by comparison with an authentic sample (0.068 g, 72 %)

7.6.1.2 Preparation of [Fe(C≡CC≡N)(dppe)(η^5-C_5H_5)], 71.

A CH_2Cl_2 (20 cm^3) solution of **82** (0.1 g, 0.162 mmol) and **86** (36 g, 0.156 mmol) was stirred at room temperature for 10 minutes. The solvent was removed *in vacuo* and the mixture was separated using preparative TLC (acetone:hexane, 40:60). The yellow band was isolated and precipitation from addition of a CH_2Cl_2 solution of the complex into stirring hexane gave the product, identified as **71** by comparison with an authentic sample (0.033 g, 64 %).

7.6.1.3 Preparation of [Ru{=C=C(C_6H_5)Br}(PPh_3)$_2$(η^5-C_5H_5)]PF_6, 74.

A solution of [**75**]PF_6 (0.100 g, 0.107 mmol), NH_4PF_6 (0.0383 g, 0.235 mmol) and BrCN (0.310 g, 0.293 mmol) in CH_2Cl_2 (10 cm^3) was stirred for 14 hours. The resulting dark green solution was concentrated, and filtered into rapidly stirred Et_2O, causing precipitation of the product as a dark green solid, which was recrystallised from acetone and hexane (0.0066 g, 61 %). ^{1}H NMR (d^6-acetone) δ 5.62 (s, 5H, C_5H_5), 7.12 – 7.52 (m, 35H, Ph). ^{31}P NMR (d^6-acetone) δ 40.9 (s, PPh_3). ^{13}C NMR (d^6-acetone) δ 96.3 (s, C_5H_5), 123.9 (s, C_2), 128.4 (s, C1), 129.4 (overlapped C3, C4), 129.7 (s, C6), 128.9 (dd, J_{CP} = 5 Hz, Ph_m), 131.4 (s, Ph_p), 133.8 (s, Ph_i), 134.0 (dd, J_{CP} = 5 Hz, Ph_o), 340.7 (t, J_{CP} = 16 Hz, C_1). IR (CH_2Cl_2) ν(C=C) 1652 cm^{-1}. Elemental Anal. Calc. for $RuC_{49}H_{36}F_6P_3Br$: C; 57.87, H; 3.97 %. Found: C; 58.10, H; 4.29 %.

7.6.1.4 Preparation of [Ru{=C=C($C_6H_4CH_3$-4)Br}(dppe)(η^5-C_5Me_5)]PF_6, 77B.

A solution of **77A** (0.068 g, 0.0902 mmol), NH_4PF_6 (0.037 g, 0.227 mmol) and BrCN (0.037 g, 0.227 mmol) in CH_2Cl_2 was stirred for 2 hours. The solvent was removed *in vacuo*, extracted into CH_2Cl_2 and microfiltered into Et_2O. The solution is then taken to dryness to yield the green product (0.055g, 63 %). ^{1}H NMR δ 1.68 (s, 15H, C_5Me_5), 2.24 (s, 3H, Me), 2.74 (m, 2H, CH_2), 3.08 (m, 2H, CH_2), 6.60 (d, J_{HH} = 5.2 Hz, 2H, Ar_α), 6.73 (d, J_{HH} = 6.4 Hz, 2H, Ar_β), 7.02 – 7.54 (m, 20H, Ph). ^{31}P NMR δ ($CDCl_3$) 74.5 (s, dppe), 165.6 (septet, PF_6). ^{13}C NMR δ ($CDCl_3$) 10.4 (s, C_5Me_5), 21.4 (s, Me), 28.8 (m, CH_2), 104.7 (s, C_5Me_5), 104.8 (s, C_2), 122.4 (s, C1), 125.3 (s, C2), 129.1 (2 x dd, J_{CP} = 4.8 Hz, Ph_m), 129.6 (s, C3), 130.9 (m, Ph_i), 131.5 (s, Ph_p), 132.2 (s, Ph_p), 132.8 (dd, J_{CP} = 5.2 Hz, Ph_o), 133.2 (m, Ph_i), 133.3 (dd, J_{CP} = 5.2 Hz, Ph_o), 138.6 (s, C1), 332.4 (t, J_{CP} = 16.5 Hz, C_1). IR (CH_2Cl_2) ν(C=C) 1649 cm^{-1}. Found ES+ MS (m/z) : 829.13041. Needed $RuBrP_2C_{45}H_{46}$: 829.12961 amu.

7.6.1.5 Preparation of [Fe{=C=C(C_6H_5)Br}(dppe)(η^5-C_5H_5)]PF_6, 78.

To a solution of **2** (0.1 g, 0.161 mmol) and NH_4PF_6 (0.06 g, 0.403 mmol) in CH_2Cl_2 (15 cm^3), BrCN (0.043 g, 0.403 mmol) was added and stirred overnight under nitrogen. The solution was taken to dryness and redissovled in CH_2Cl_2 and filtered. Preparative TLC of the CH_2Cl_2 solution (80:20, acetone:hexane) gave a green band, which upon isolation, by precipitation from CH_2Cl_2/ Et_2O, gave a deep green solid (0.065 g, 58 %). ^{1}H NMR ($CDCl_3$) δ 3.10 (m, 2H, CH_2), 3.15 (m, 2H, CH_2), 4.77 (s, 5H, C_5H_5), 6.75 – 7.65 (m, 25H, Ph). ^{31}P NMR ($CDCl_3$) δ 93.6 (s, dppe), -143.1 (septet, PF_6). ^{13}C NMR ($CDCl_3$) δ 28.6 (s, dppe), 84.9 (s, C_2), 90.7 (s, C_5H_5), 127.4 – 137.9 (m, Ph/ dppe), 348.4 (t, J_{CP} = 33.4 Hz, C_1). IR (CH_2Cl_2) ν(C=C) 1614 cm^{-1}. Found ES+ MS (m/z) : 699.06761. Needed $FeBrP_2C_{39}H_{34}$: 699.06631 amu.

7.6.1.6 Preparation of [Fe{=C=C($C_6H_4CH_3$-4)Br}(dppe)(η^5-C_5H_5)]PF_6, 79.

To a solution of **77** (0.1 g, 0.158 mmol) and NH_4PF_6 (0.064 g, 0.394 mmol) in CH_2Cl_2 (15 cm^3), BrCN (0.041 g, 0.394 mmol) was added and stirred overnight under nitrogen. The solvent was removed *in vacuo* and the residue re-dissolved in CH_2Cl_2 and filtered. Preparative TLC of the CH_2Cl_2 solution (45:55, acetone:hexane) gave a green band, which upon isolation, by precipitation from CH_2Cl_2/ Et_2O, gave a deep green solid (0.067 g, 59 %). ^{1}H NMR ($CDCl_3$) δ 2.26 (s, 3H, CH_3) 2.65 (m, 2H, CH_2), 2.88 (m, 2H, CH_2), 4.81 (s, 5H, Cp), 6.66 (d, J_{HH} = 7.0 Hz, Tol), 6.80 (d, J_{HH} = 6.5 Hz, Tol) 7.04 – 7.63 (m, 20H, Ph). ^{31}P NMR ($CDCl_3$) δ 94.0 (s, dppe), -143.1 (septet, PF_6). ^{13}C NMR ($CDCl_3$) δ 21.5 (s, CH_2), 85.3 (s, C_2), 91.0 (s, C_5H_5), 125.2 – 138.7 (m, Ph/ dppe), 349.2 (s, C_1). IR (CH_2Cl_2) ν(C=C) 1609 cm^{-1}. Found ES+ MS (m/z) : 713.08313. Needed $FeBrP_2C_{40}H_{36}$: 713.08196 amu.

7.6.1.7 Preparation of [Ru(C≡CSiMe$_3$)(PPh$_3$)$_2$(η^5-C$_5$H$_5$)], 80.

A solution of RuCl(PPh$_3$)$_2$(η^5-C$_5$H$_5$) (1.00 g, 1.38 mmol), NaBPh$_4$ (0.567 g, 1.66 mmol) and H≡CSiMe$_3$ (1.66 g, 16.9 mmol) in a 50:50 THF /NEt$_3$ solution (75 cm^3 total volume) was heated at reflux for 3 hours. After this time, the solvent was removed *in vacuo*. The residue was extracted with hot hexane to give a yellow solution, from which the product was isolated by removal of the solvent (0.98 g, 90%). ^{1}H NMR (CDCl$_3$) δ -0.03 (s, 9H, SiMe3), 4.19 (s, 5H, C$_5$H$_5$), 7.02 – 7.53 (m, 60 H, Ph). ^{31}P NMR δ 51.2 (s, PPh$_3$). ^{13}C NMR (CDCl$_3$) δ 1.7 (s, SiMe$_3$), 85.4 (s, C$_5$H$_5$), 118.7 (s, C$_2$), 127.5 (dd, J_{CP} = 5 Hz, Ph$_m$), 128.3 (s, C$_5$H$_5$), 133.9 (dd, J_{CP} = 5 Hz, Ph$_o$), 138.9 (m, Ph$_i$); 139.6 (t, J_{CP} = 24 Hz, C$_1$). ^{31}P NMR (CDCl$_3$) δ 51.2 (s, PPh$_3$). IR (CH$_2$Cl$_2$) ν(C≡C) 1994 cm^{-1}. Found: ES(+)MS (m/z) 789.18110 [**M**]$^+$: calculated for RuSiP$_2$C$_{46}$H$_{44}$: 789.18362.

7.6.1.8 Preparation of [Ru(C≡CSiMe$_3$)(dppe)(η^5-C$_5$Me$_5$)], 81.

A solution of RuCl(dppe)(η^5-C$_5$Me$_5$) (0.100 g, 0.149 mmol), NaBPh$_4$ (0.061 g, 0.18 mmol) and HC≡CSiMe$_3$ (0.181 g, 1.84 mmol) in a 50:50 THF /NEt$_3$ (20 cm^3 total volume) solution was heated under reflux for 2 hours, after which time the solution is filtered and the solvent was removed *in vacuo*. The residue was extracted with hot hexane to give a yellow solution, from which the product could be isolated by removal of the solvent (0.049 g, 45%). Although the resulting yellow solid turns green upon prolonged exposure to air, NMR analysis reveals little change and the discoloured samples are suitable for further reaction. ^{1}H NMR ($CDCl_3$) δ -0.18 (s, 9H, SiMe$_3$), 1.52 (s, 15H, C$_5$Me$_5$), 2.05 (m, 2H, CH$_2$), 2.75 (m, 2H, CH$_2$), 7.12 – 7.78 (m, 20H, Ph). ^{31}P NMR ($CDCl_3$) δ 81.6 (s, dppe). ^{13}C NMR ($CDCl_3$) δ 1.4 (s, SiMe$_3$), 9.9 (s, C$_5$*Me$_5$*), 29.1 (m, CH$_2$), 92.4 (s, *C$_5$*Me$_5$), 112.1 (s, C$_2$), 126.9 and 127.3 (dd, $\boldsymbol{J}_{CP}$ = 5 Hz, Ph$_m$), 128.7 (s, Ph$_p$), 133.2 and 133.9 (dd, $\boldsymbol{J}_{CP}$ = 5 Hz, Ph$_o$), 136.9 (m, Ph$_i$), 152,5 (t, $\boldsymbol{J}_{CP}$ = 23 Hz, C$_1$). IR (CH_2Cl_2) ν(C≡C) 1996 cm^{-1}. ES(+)-MS (*m/z*) 733.1 [**M**+H]$^+$.

7.6.1.9 Preparation of [Fe(=C=CBr$_2$)(dppe)(η^5-C$_5$H$_5$)]BF$_4$, 85.

To a solution of **82** (0.0600 g, 0.097 mmol) in CH_2Cl_2 (6 cm^3) was treated with BrCN (0.007 g, 0.66 mmol) to immediately give a dark purple solution, which was stirred for 5 minutes before the solvent was removed *in vacuo*. The residue dissolved in acetone (5 cm^3) and treated with $NaBF_4$ (0.05 g, 0.455 mmol). After stirring for 2 hours, the crude product was treated with diethyl ether to afford a brown precipitate, which purified by preparative TLC (3:7 acetone /hexane). A dark coloured band was collected and recrystallised by slow diffusion of hexane into a CH_2Cl_2 solution to give yellow – orange crystals of the product suitable for X-ray crystallography (0.0056 g, 73 %). ^{1}H NMR ($CDCl_3$) δ 2.98 (m, 2H, CH_2), 3.26 (m, 2H, CH_2), 5.32 (s, 5H, C_5H_5), 7.10 – 7.41 (m, 20H, Ph). ^{31}P NMR ($CDCl_3$) δ 91.1 (s, dppe). ^{13}C NMR ($CDCl_3$) δ 29.0 (m, CH_2), 91.8 (s, C_5H_5), 111.2 (s, C_2), 129.4 and 129.7 (dd, J_{CP} = 5 Hz, Ph_m), 131.6 (s, Ph_p), 131.4 and 132.9 (dd, J_{CP} = 5 Hz, Ph_o), 132.9 and 134.3 (m, Ph_i), 341.6 (t, J_{CP} = 34 Hz, C_1). IR (CH_2Cl_2) ν(C=C) 1609 cm^{-1}. ES+-MS (*m/z*) 703.0 [**M**]$^+$.

7.6.1.10 Preparation of $[Ru(=C=CBr_2)(PPh_3)_2(\eta^5\text{-}C_5H_5)]BF_4$, 83.

A solution of **80** (0.100 g, 0.151 mmol), BrCN (0.048 g, 0.45 mmol) and $NaBF_4$ (0.003 g, 0.30 mmol) in CH_2Cl_2 (15 cm^3) was stirred for 4 hours, after which time the solvent was removed *in vacuo* and the product extracted into the minimum amount of CH_2Cl_2. The deep purple product was precipitated into rapidly stirring hexane, collected by filtration and dried (0.020 g, 15 %). ^1H NMR (CD_2Cl_2) δ 4.35 (s, 5H, C_5H_5), 7.05 – 7.80 (m, 30H, Ph). ^{31}P NMR (CD_2Cl_2) δ 38.5 (s, PPh_3). ^{13}C NMR δ (CD_2Cl_2) 96.5 (s, C_5H_5), 109.9 (s, C_2), 129.1 (dd, J_{CP} = 5 Hz, Ph_m), 131.7 (s, Ph_p), 133.0 (m, Ph_i), 133.8 (dd, J_{CP} = 5 Hz, Ph_o), 337.9 (t, J_{CP} = 15 Hz, C_1). Found ES+ MS (m/z) : 874.95885. Needed $RuBr_2P_2C_{43}H_{45}$: 874.95983 amu.

7.6.1.11 Preparation of $[Ru(=C=CBr_2)(dppe)(\eta^5\text{-}C_5Me_5)]BF_4$, 84.

A solution of **81** (0.100 g, 0.137 mmol), BrCN (0.043 g, 0.41 mmol), $NaBF_4$ (0.030 g, 0.27 mmol) in CH_2Cl_2 (15 cm^3) was stirred for 4 hours, after which the solvent was removed *in vacuo* and the product was extracted into the minimum amount of CH_2Cl_2. The deep purple product was precipitated into rapidly stirring hexane and collected by filtration (0.105 g, 94 %). ^1H NMR (CD_2Cl_2) δ 1.75 (s, 15H, $C_5\mathit{Me_5}$), 2.72 (m, 2H, CH_2), 2.86 (m, 2H, CH_2), 7.09 – 7.63 (m, 20H, Ph). ^{31}P NMR (CD_2Cl_2) δ 73.0 (s, dppe). ^{13}C NMR (CD_2Cl_2) δ 10.3 (m, $C_5\mathit{Me_5}$), 28.9 (m, CH_2), 80.2 (s, $\mathit{C_5}Me_5$), 105.7 (s, C_2), 129.2 and 128.6 (dd, J_{CP} = 5 Hz, Ph_m), 130.5 (m, Ph_i), 132.1 and 132.4 (s, Ph_p), 133.1 (m, Ph_o), 329.3 (t, J_{CP} = 17 Hz, C_1). Found ES+ MS (m/z) : 818.99261. Needed $RuBr_2P_2C_{38}H_{39}$: 818.99113 amu.

7.6.1.12 Preparation of [Fe{C($NC_5H_4NMe_2$-4)=C}(CN_2)(dppe)(η^5-C_5Me_5)]PF_6, 96.

To a solution of **71** (0.10 g, 0.181 mmol) in CH_2Cl_2 (15 cm^3), **86** (0.083 g, 0.361 mmol) was added and the solution stirred overnight. The resulting dark brown solution was taken to dryness and the mixture separated using preparative TLC (70:30, acetone:hexane). The middle orange band is isolated and the solid predicated from acetone/ Et_2O. Crystals suitable for X-ray diffraction analysis were subsequently formed from evaporation of a $CDCl_3$ solution (0.063 g, 48 %). ^{1}H NMR ($CDCl_3$) δ 2.01 (m, 2H, CH_2), 2.38 (m, 2H, CH_2), 3.15 (s, 6H, NMe_2), 4.66 (s, 5H, C_5H_5), 6.41 (d, 2H, J_{HH} = 8.0 Hz, DMAP), 7.22 – 7.52 (m, 17H, DMAP /Ph). ^{31}P NMR ($CDCl_3$) δ 84.0 (s, dppe). ES+-MS (*m/z*) 717.1 [**M**]$^+$.

7.6.1.13 Preparation of [Fe(C≡CC≡N)(dppe)(η^5-C_5Me_5)], 98.

A CH_2Cl_2 (20 cm^3) solution of **97** (0.100 g, 0.165 mmol) and **86** (0.038 g, 0.165 mmol) was stirred for 2 hours, giving a brown coloured solution. Reducing the solution to dryness and extraction with CH_2Cl_2 (5 cm^3) the mixture was separated using preparative TLC (45 /55 acetone /hexane) and the orange band was isolated. The product was extracted from the silica with CH_2Cl_2 (15 cm^3) and the product predicated the addition of hexane (30 cm^3) to yield the yellow product (0.014 g, 14 %). ^{1}H ($CDCl_3$) δ 1.22 (C_5Me_5), 1.90 (m, 2H, CH_2), 2.45 (m, 2H, CH_2), 7.09 – 7.55 (m, 20H, Ph). ^{31}P NMR ($CDCl_3$) δ 97.2 (s, dppe). ^{13}C NMR ($CDCl_3$) δ 9.78 (s, $C_5\mathit{Me}_5$), 30.3 (m, CH_2), 85.9 (s, C_2), 89.5 (s, C_5Me_5), 107.4 (s, C_3), 127.6 (dt, $\boldsymbol{J}_{CP}$ = 4.0 Hz, Ph_m), 129.6 (d, $\boldsymbol{J}_{CP}$ = 15.0 Hz, Ph_p), 133.7 (dt, $\boldsymbol{J}_{CP}$ = 15.7 Hz, Ph_o), 135.57 (d, Ph_i), 166.8 (t, $\boldsymbol{J}_{CP}$ = 34.7 Hz, C_1). IR (CH_2Cl_2) ν(C≡CC≡N) 2165, 1979 cm^{-1}. ES(+)-MS (*m/z*) 639.8 $[\mathbf{M}]^+$. Crystal data: M = 0.20 x 0.14 x 0.02 mm^3, , space group p b c a (No. 0), V = 6427.5(4) $Å^3$, Z = 8, F_{000} = 2688, T = 120(2) K, 48647 reflections collected, unique (R_{int} = 0.0948). Final *GooF* = 1.037, *R1* = 0.0892, *wR2* = 0.0806.

7.6.1.14 Preparation of [{Fe(dppe)(η^5-C_5H_5)}(μ-C≡CC≡N){Mo(dppe)(η^7-C_7H_7)}]PF_6, 108.

A mixture of **5** (117 mg, 0.176 mmol), **71** (100 mg, 0.176 mmol) and $NaPF_6$ (59 mg, 0.351 mmol) in MeOH (15 cm^3) was refluxed for 3 hours. After which the solution is cooled and the brown precipitate collected on a sinter. The brown solid was then extracted into CH_2Cl_2 (5 cm^3) and passed through a cotton plug into Et_2O (40 cm^3). The yellow /brown precipitate was then collect on a sinter and dried in air (150 mg, 76 %). ^1H NMR (CD_2Cl_2) δ 1.89-1.96 (m, 2H, CH_2), 2.03-2.34 (m, 6H, CH_2), 4.25 (s, 5H, C_5H_5), 4.82 (s, 7H, C_7H_7), 7.11-7.51 (m, 40H, Ph). ^{31}P NMR (CD_2Cl_2) δ 64.5 (s, Mo(dppe)), 102.6 (s, Fe(dppe)), 165.4 (m, PF_6). ^{13}C NMR (CD_2Cl_2) δ 25.6 (m, CH_2 {Fe}), 28.2 (m, CH_2 {Mo}), 81.4 (s, C_5H_5), 85.8 (s, C_3), 88.1 (s, C_7H_7), 118.8 (s, C_2), 128.1-129.1 (m, Ph_m), 130.1-130.6 (m, Ph_p), 131.3-133.2 (m, Ph_o), 135.6-139.5 (m, Ph_i), 171.8 (t, J_{CP} = 36 Hz, C_1). IR (CH_2Cl_2) ν(C≡CC≡N) 2172, 1976 cm^{-1}. MS ES+ (*m /z*): expected for $FeMoNP_4C_{67}H_{60}$: 1156.20981. Result: 1156.21108.

7.6.1.15 Preparation of [{Ru(dppe)(η^5-C_5Me_5)}(μ-C≡CC≡N){Ru(dppe)$_2$}]PF_6, 109.

A methanol solution (20 cm^3) containing Ru(C_3N)(dppe)(C_5Me_5) (0.066 g, 0.097 mmol), RuCl(C≡CPh)(dppe)$_2$ (0.10 g, 0.097 mmol) and $NaPF_6$ (0.019 g, 0.12 mmol) was heated at the point of reflux for 8 hours. The mixture was then allowed to cool and stir at room temperature for 5 days, resulting in white cloudy suspension. The precipitate was filtered and the methanol solution taken to dryness to yield a pale green/ yellow precipate (0.107 g, 66 %) ^{1}H NMR ($CDCl_3$) δ 1.51 (s, 15H, C_5Me_5), 2.39 (m, 2H, CH_2 of [Ru*]), 2.65 (m, 8H, 4 x CH_2 [Ru(dppe)$_2$]), 2.75 (m, 2H, CH_2 of [Ru*]), 6.68 – 7.55 (m, 65H, Ph/ Ar). ^{31}P NMR ($CDCl_3$) δ 48.4 (s, 2 x dppe), 78.4 (s, dppe). IR (CH_2Cl_2) ν(C≡CPh) 1967 cm^{-1}, ν(C≡CC≡N) 2083 2180 cm^{-1}. ES+ MS (m/z) expected for $Ru_2NP_6H_{92}C_{99}$: 1864.37845. Result: 1684.38185.

7.6.1.16 Preparation of [Mo(N≡CC$_6$H$_4$Me-4)(dppe)(η^7-C$_7$H$_7$)]PF$_6$, 111.

A mixture of **5** (100 mg, 0.150 mmol), N≡C(C$_6$H$_4$CH$_3$-4) (18 mg, 0.150 mmol) and $NaPF_6$ (38 mg, 0.225 mmol) in MeOH (20 cm^3) was heated at reflux for 90 minutes. The solvent was then removed *in vacuo*, the residues extracted into CH_2Cl_2 (5 cm^3) and passed through a cotton plug into Et_2O (40 cm^3). The brick red precipitate was then collect on a sinter and dried in air (89 mg, 84 %). IR (CH_2Cl_2) ν(C≡N) 2215 cm^{-1}. The purity of the compound was assessed by cyclic voltammetry giving a single wave $^1E_{1/2}$ = +0.07 V (at a platinum electrode, recorded in a 0.1 M $^nBu_4PF_6$ /CH_2Cl_2 solution and referenced to FcH /FcH^+ = 0.00 V couple).

7.7. References

[1] R.B. King, M.S. Saran, *Chem. Commun.,* 1972, 1053.
[2] A. Ludi, *J. Chem. Ed.,* 1981, **58**, 1013.
[3] (a) P. Thaddeus, C.A. Gottlieb, H. Gupta, S. Brunken, M.C. McCarthy, M. Agundez, M. Guelin, J. Cernicharo, *Astrophys. J.,* 2008, **677**, 1132. (b) M.C. McCarthy, C.A. Gottlieb, H. Gupta, P. Thaddeus, *Astrophys. J.,* 2006, **652**, L141.
[4] M. Turowski, M. Gronowski, S. Boye-Peronne, S. Douin, L. Moneron, C. Crepin, R. Kolos, *J. Phys. Chem.,* 2008, **128**, 164304.
[5] W.P. Neumann, F.G. Kleiner, *Tetrahedron Lett.,* 1964, **49**, 3779.
[6] W.H. Baddley, C. Panattoni, G. Bandoli, D.A. Clemente, U. Belluco, *J. Am. Chem. Soc.,* 1971, **21**, 5590.
[7] R. Kergoat, M.M. Kubicki, L.C. Comes de Lima, H. Scordia, J.E. Guerchais, *J. Organomet. Chem.,* 1989, **367**, 143.
[8] Y. Zhou, A.M. Arif, J.S. Miller, *Chem. Commun.,* 1996, 1881.
[9] (a) M.E. Smith, R.L. Cordiner, D. Albesa-Jove, D.S. Yufit, F. Hartl, J.A.K. Howard, P.J. Low, *Can. J. Chem.,* 2006, **84**, 154. (b) R.L. Cordiner, M.E. Smith A.S. Batsanov, D. Albesa-Jove, F. Hartl, J.A.K. Howard, P.J. Low, *Inorg. Chim. Acta.,* 2006, **359**, 946. (c) R.L. Cordiner, D. Corcoran, D.S. Yufit, A.E. Goeta, J.A.K. Howard, P.J. Low, *Dalton. Trans.,* 2003, 3541.
[10] M.E. Smith, E.L. Flynn, M.A. Fox, A. Trottier, E. Wrede, D.S. Yufit, J.A.K. Howard, K.L. Ronayne, M. Towrie, A.W. Parker, F. Hartl, P.J. Low, *Chem. Commun.,* 2008, 5845.
[11] S. Thambidurai, S.A. Samath, K. Jeyasubramanian, S.K. Ramalingam, *Polyhedron,* 1994, **13**, 2825.
[12] M.I. Bruce, M.G. Humphrey, G.A. Koutsantonis, B.K. Nicholson, *J. Organomet. Chem.,* 1985, **296**, C47.
[13] M.I. Bruce, M. Jervic, C.R. Parker, W. Patalinghug, B.W. Skelton, A.H. White, N.N. Zaitseva, *J. Organomet. Chem.,* 2008, **693**, 2915.
[14] (a) J.P. Whitten, J.R. McCarthy, D.P. Matthews, *Synthesis,* 1988, 470. (b) S. Bystricky, E. Machova, P. Bartek, N. Kolarova, G. Kogan, *Glycoconjugate J.,* 2000, **17**, 677. (c) J. Wu, J.T. Watson, *Protein Sci.,* 1997, **6**, 391. (d) J. Wu, J.T. Watson, *Anal. Biochem.,* 1998, **258**, 268.
[15] (a) D.E. Shafer, B. Toll, R.F. Schuman, B.L. Nelson, J.J. Mond, A. Lees, *Vaccine,* 2000, **18**, 1273. (b)A. Lees, B.L. Nelson, J.J. Mond, *Vaccine,* 1996, **14**, 190. (c) J. Kohn, M. Wilchek, *F. E. B. S. Lett.,* 1983, **154**, 209.
[16] D. S. Tollner, F.W. Scheller, A. Warsinke, *Anal. Biochem.,* 2002, **304**, 157.
[17] N.J. Brown, P.K. Eckert, M.A. Fox, D.S. Yufit, J.A.K. Howard, P.J. Low, *Dalton. Trans.,* 2008, 433.
[18] E.A. Strickson, MChem Thesis, 2008.
[19] J. Kiesewetter, G. Poignant, V. Guerchais, *J. Organomet. Chem.,* 2000, **595**, 81.
[20] K. Costuas, F. Paul, L. Toupet, J-F. Halet, C. Lapinte, *Organometallics,* 2004, **23**, 2053.
[21] R. Denis, L. Toupet, F. Paul, C. Lapinte, *Organometallics,* 2000, **19**, 4240.
[22] M.A. Fox, J.E. Harris, S. Heider, V. Perez-Gregorio, M.E. Zakrzewska, J.D. Farmer, D.S. Yufit, J.A.K. Howard, P.J. Low, *J. Organomet. Chem.,* 2009, **694**, 2350.

[23] M.I. Bruce, P.J. Low, K. Costuas, J-F. Halet, S.P. Best, G.A. Heath, *J. Am. Chem. Soc.,* 2000, **122**, 1949.
[24] N. Le Narvor, L. Toupet, C. Lapinte, *J. Am. Chem. Soc.,* 1995, **117**, 7129.
[25] (a) F. Barriere, N. Camire, W.E. Geiger, U.T. Mueller-Westerhoff, R. Sanders, *J. Am. Chem. Soc.,* 2002, **124**, 7262. (b) E.A. Fellow, F.R. Keene, *J. Phys. Chem. B.,* 2007, **111**, 6667.
[26] M.I. Bruce, R.C. Wallis, *J. Organomet. Chem.,* 1978, **161**, C1.
[27] M.I. Bruce, G.A. Koutsantonis, *Aust. J. Chem.,* 1991, **44**, 207.
[28] C. Bitcon, M.W. Whiteley, *J. Organomet. Chem.,* 1987, **336**, 385.
[29] M.A. Fox, R.L. Roberts, W.M. Khairul, F. Hartl, P.J. Low, *J. Organomet. Chem.,* 2007, **692**, 3277.
[30] M.I. Bruce, B.G. Ellis, P.J. Low, B.W. Skelton, A.H. White, *Organometallics,* 2003, **22**, 3184.
[31] V. W-W. Yam, V. C-Y. Lau, K-K. Cheung, *Organometallics,* 1995, **14**, 2749.
[32] M.P. Gamasa, J. Gimeno, E. Lastra, M. Lanfranchi, A. Tiripiochio, *J. Organomet. Chem.,* 1991, **405**, 333.

Chapter 8: Thesis Overview /Conclusions

This thesis has examined a series of mono- and bi-metallic organometallic complexes containing the Mo(dppe)(η^7-C_7H_7) fragment. Although the compounds containing this moiety had been known for many years, an in-depth analysis of the electronic structure had not been undertaken. A wide range of mono-metallic complexes supported by the the Mo(dppe)(η^7-C_7H_7) fragment and containing a series of acetylides (**12, 13**), aryl acetylides (**1**, **6-10**, **14**), diynyl (**20**, **24**) and triynyl (**26**) alkynyl based ligands were synthesised to permit thorough investigation of the electronic structure of the molybdenum moiety. It was found through the use of spectroelectrochemical and computational techniques that the cycloheptatrienyl ring imparts a unique ordering of the metal d-orbitals, which is not found in the analogous Group seven (Re(NO)(PPh_3)(η^5-C_5Me_5)) and eight metal fragments ([Fe(dppe)(η^5-C_5Me_5)] and [Ru(dppe)(η^5-C_5Me_5)]). The cycloheptatrienyl ring stabilises the metal d_{xz} and d_{yz} orbitals via a strong δ-interaction, this serves to destabilise the filled metal d_{z2} orbital to form the HOMO of the complex. The d_{z2} orbital is of the wrong symmetry to mix well with the π-system of the alkynyl fragments, leading to exceptional metal centred oxidation character for alkynyl complexes containing this metal moiety.

The metal centred oxidation character of the molybdenum moiety has allowed the synthesis of genuine mixed valence complexes, [{L_xM^n}(μ-C≡CXC≡C){$M^{n+1}L_x$}] (X = $C_2B_{10}H_{10}$ (**45**), bond (**57**), C_6H_4, (**67**)), in which the ability of the bridging moiety to promote or inhibit the electron transfer process has been examined. In all three complexes three intervalence charge transfer (IVCT or IT) bands could be identified

through the deconvolution of the NIR band a feature which is due to the electronic asymmetry of the complexes imposed by the cycloheptatrienyl ring.

The degree of mixing between the molybdenum fragment has a significant effect on the shape on the NIR band envelope and the rate of electron transfer. As the bridge character of the HOMO gradually increases from **45**, to **57** and **67**, the IT bands overlap, resulting in a more intense and less symmetric band envelope. In addition, a fourth LMCT-type transition becomes apparent in the NIR region once the bridge fragment is heavily mixed with the molybdenum moiety (**57** and **67**), the energy of which decreases in-line with the increased mixing. As the energy of this band is lowered the electron transfer rate (determined using spectroscopic techniques) is increased.

Despite the HOMO of the complexes becoming more bridge in character as the metal and bridging ligand mixes, oxidation still takes place primarily on a Mo(dppe)(η^7-C_7H_7) moiety. Therefore, the mixed valence complexes (**45**$^+$, **57**$^+$ and **67**$^+$) are all described as localised mixed valence systems, where the degree of electronic coupling between the molybdenum electrophores increases as a function of the bridge character of the HOMO. This is evidenced by the solvatochromic behaviour of the lowest energy IT(1) band, which becomes gradually less sensitive to the dielectric constant of the solvent medium as the bridge character increases. The trend for the higher energy IT(2) and IT(3) bands is less apparent, from TD-DFT models these bands involve orbtials which are high in C_7H_7 character, as such they are less rigorously shielded from effects of the solvent medium than the insulated d_{z^2} orbital.

Examination of these mixed valence systems **45**$^+$, **57**$^+$ and **67**$^+$ has also shown that the "one size fits all" approach in using the two-state model does not hold true. The carboranyl complex **45**$^+$ provides a model system which agrees with the two-state model for electron transfer, as the electrophores are significantly isolated from the bridge and the bridge serves only to act as a conduit through which electron transfer can take place. Thus, the complex can be described accurately using the equations developed by Hush and co-workers. However, upon increasing the mixing of the bridge and molybdenum moieties (**57**$^+$ and **67**$^+$) the two-state model is no longer sufficient and a three-state model proved more appropriate in describing these more heavily mixed complexes. This more complex model includes a third electronic state which describes the bridge fragment and accounts for the presence of a LMCT-type transition in the NIR region.

To compliment the series of carbon-based bridges studied in Chapters two to six, complexes containing the cyanoacetylide moiety $[C{\equiv}CC{\equiv}N]^-$ have been investigated. Essential to the development of this ligand as a bridging moiety was the ready inclusion of the ligand into mono-metallic complexes. These investigations lead to the serendipitous discovery of complexes containing mono- (**74, 77B, 78, 79**) and di-bromovinylidnene (**83** – **85**) and mono- (**73**, **87** – **93**) and di-cyanovinylidene (**95**) moieties. The cyanating agent 1-cyano 4-dimethylaminopyridine tetrafluoroborate ([CAP]BF_4) (**86**) readily produced the cyanoacetylide moiety from trimethylsilyl protected acetylide containing complexes. The [CAP]BF_4 reagent proved successful in cyanating a wide range of Group eight metal fragments, such as $Fe(C{\equiv}CSiMe_3)(dppe)(\eta^5\text{-}C_5Me_5)$ (**97**) and $Ru(C{\equiv}CSiMe_3)(dppe)(\eta^5\text{-}C_5Me_5)$ (**81**). The ease at which homo- and hetero-bimetallic complexes could be synthesised using the cyanoacetylide ligand was demonstrated by the coordination of $Ru(C{\equiv}CC{\equiv}N)(dppe)(\eta^5$-

C_5Me_5) (**69**) and Fe(C≡CC≡N)(dppe)(η^5-C_5H_5) (**71**) to Ru(C≡CC_6H_5)$(dppe)_2$ (**109**) and Mo(dppe)(η^7-C_7H_7) (**108**) respectively.